Development of Mechanically Robust Ultra-thin Polymer Films Using Covalent Layer by Layer Assembly of Epoxy Compounds

ISLAMABAD

A thesis submitted to Quaid-i-Azam University, Islamabad
in partial fulfillment of the requirements for the degree of

Doctor of Philosophy

(Inorganic/Analytical Chemistry)

by

SHAHID SAEED

Department of Chemistry
Quaid-i-Azam University
Islamabad, Pakistan
2011

This is to certify that this dissertation entitled, *"Development of Mechanically Robust Ultra-thin Polymer Films using Covalent Layer by Layer Assembly of Epoxy Compounds"* submitted by **Mr. Shahid Saeed** is accepted in its present form by the Department of Chemistry, Quaid-i-Azam University, Islamabad, Pakistan, as satisfying the partial requirement for the degree of *Doctor of Philosophy* in *Inorganic/Analytical Chemistry*.

External Examiner (1)

Prof. Dr. M. Aziz Choudhary
Chairman, Department of Chemistry
Mirpur University of Science & Technology
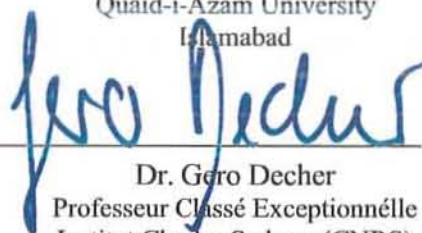Mirpur (AJK)

External Examiner (2)

Dr. Riaz Qadeer
Deputy Chief Scientist
PSO, DTC, PAEC
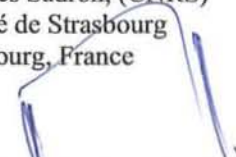P. O. Box 1611, Islamabad

Supervisor

Dr. Muhammad Ilyas Sarwar
Associate Professor
Quaid-i-Azam University
Islamabad

Co-supervisor

Dr. Gero Decher
Professeur Classé Exceptionnélle
Institut Charles Sadron, (CNRS)
Université de Strasbourg
Strasbourg, France

Head of Section

Prof. Dr. Amin Badshah
Department of Chemistry
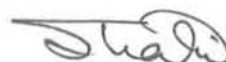Quaid-i-Azam University
Islamabad

Chairman

Prof. Dr. Saqib Ali (PoP)
Department of Chemistry
Quaid-i-Azam University
Islamabad

CERTIFICATE

It is certified that all the experimental work was performed at the Institut Charles Sadron (ICS), Université de Strasbourg (Formerly Université Louis Pasteur) *et Center National de la Recherche Scientifique* (C.N.R.S), Strasbourg, France, and a part of it was carried out in Polymer Chemistry Laboratory, Department of Chemistry, Quaid-i-Azam University, Islamabad, Pakistan. To the best of my knowledge, the work is original and has never been presented by any other person at any platform or for the evaluation of Ph.D. thesis.

Mr. Shahid Saeed
Department of Chemistry
Quaid-i-Azam University
Islamabad-45320, Pakistan
2011

Dedicated to my sweet daughter

Dua

Acknowledgements

All the praise and thanks are to Allah and blessed be His Prophet (PBUH) who is the key source of inspiration for true seekers of knowledge. Without Allah's help nothing could be achieved. HE made every impossible thing, possible during my doctoral studies.

*I would like to express my gratitude to my supervisor **Dr. Muhammad Ilyas Sarwar**, Associate Professor for his help, guidance and patronage throughout my PhD studies at the Department of Chemistry, QAU, Islamabad.*

*I owe a special debt of gratitude to my co-supervisor, and mentor **Prof. Dr. Gero DECHER**, Professeur Classé Exceptionnélle at the Institut Charles Sadron, Université de Strasbourg (Formerly Université Louis Pasteur) et Center National de la Recherche Scientifique (C.N.R.S), Strasbourg, France, for introducing me to fascinating LbL technique. Through his positive feedback and criticism, I have developed the scientific communication and personal skills that indubitably go along with rest of my professional life. I will always remain grateful to him for being a wonderful person and a conscientious man. These words may have shown their humility to the brilliance of him.*

Dr. Olivier Felix deserves my heartfelt appreciation for his ever co-operating attitude, pleasant personality and readiness to be with me in every hour of need. His amusing remarks and encouragement forces me to again say, Monsieur (I MISS you) Olivier! My acknowledgement may go incomplete without a mention of my collaborator and nice friend, Zhiqiang Zheng, a doctoral student in the Gero's research group. Together we protected the Au-NPs layers and enjoyed free coffee at the cafe of ICS. John Louis Tequert, technician in Gero Team deserves to be mentioned for providing every lab facility needed. My huge appreciation to group fellows, Emek, Rafael, Gabriela, Hemanti, Dasha, Lux Christelle, Cini and Ali for the good will and cooperation extended to me.

Dr. Martin Brinkmann deserves my sincere acknowledgment for providing me access to the rubbing machine in his laboratory. Christophe Contall deserves special mention and appreciation for conducting a number of AFM and valuable discussion during AFM analysis.

Dr. Rohama Gill and Dr. Kh. Ansar Yasin deserve special thanks for helping me immensely during my studies and also by sincere guidance and morale boosting support during the inevitable moments of despair.

I cannot forget a former colleague and friend Dr. Mazhar Ejaz Nasir, a postdoctoral fellow at Manchester University for not only conducting a number of AFM analyses, but encouraging me throughout by his regular "Monday Phone Calls".

I am grateful to the Higher Education Commission of Pakistan for their support through Indigenous Scholarship Program as well as International Research Support Initiative

Preface

The thesis consists of three chapters. Chapter one contains the literature review of the Layer by Layer (LbL) nanofabrication technique with special emphasis on covalent LbL assemblies, mechanical robustness of LbL assemblies and epoxy resins.

Chapter two include details of the experimental procedure for the optimization of various parameters for the film build up at nanometre scale and a brief introduction of various characterization techniques used.

While chapter three elaborates the results of the prepared ultrathin films via LbL multilayers growth on silicon wafer and quartz substrate as monitored with the help of an ellipsometer, UV-Visible spectrometer and their robustness studied with the help of an indigenously manufactured rubbing machine. Surface morphological studies using atomic force microscopy (AFM) technique of virgin and rubbed samples of neat epoxy-amine films and epoxy protected gold nanoparticle films is discussed in detail in this chapter. Finally, the epoxy-amine network used for the protection of Au-NPs films for their robustness is also described. Effect of catalysts and accelerators on curing of epoxy-amine LbL assemblies is also demonstrated in this chapter.

Contents   Page Number

Chapter 1   Literature Review

Chapter 2   Material and Method

Chapter 3   **Results and Discussion**

List of Figures

List of Tables

List of Schemes

<u>Glossary of the Terms, Acronyms and Symbols</u>

n	Number of layer pairs
Δ	Phase difference between p- and s-polarized reflections light
Ψ	Ratio of the modulus of amplitude of reflection
A	A-399 Catalyst
APD	Araldite My-720-PEI-Dipping
APDA	Araldite My-720-PEI-Dipping-A399
APDC	Araldite My-720-PEI-Dipping-Combined
APDE	Araldite My-720-PEI-Dipping- EEM
APDP	Araldite My-720-PEI-Dipping-Piperazine
ATD	Araldite My-720-TEPA-Dipping
ATDA	Araldite My-720-TEPA-Dipping-A399
ATDC	Araldite My-720-TEPA-Dipping-Combined
ATDE	Araldite My-720-TEPA-Dipping-EEM
ATDP	Araldite My-720-TEPA-Dipping_piperazine
Au-NPs	Gold Nanoparticles
AFM	Atomic Force Microscopy
C	Combined catalyst system (Piperazine-EEM-triethanolamine)
CAD	CNER-Ammonia-Dipping Technique
CDPS	CNER -Dipping-PEI-Spray
CNT	Carbon nano tubes
CPD	CNER -PEI-Dipping
CPDA	CNER -PEI-Dipping-A399
CPDC	CNER -PEI-Dipping-Combined Catalysts
CPDE	CNER -PEI-Dipping-EEM
CPDC	CNER -PEI-Dipping-Combined Catalysts

XVI

CPDP	CNER -PEI-Dipping-Piperazine
CTD	CNER -TEPA-Dipping
CTDA	CNER -TEPA-Dipping-A399
CTDC	CNER -TEPA-Dipping-Combined Catalyst
CTDE	CNER -TEPA-Dipping-EEM
CTDP	CNER -TEPA-Dipping-Piperazine
EEM	2,4,6-tris(dimethylaminomethyl)phenol, (Epoxy embedding medium accelerator)
EEW	Epoxy equivalent weight
ER	Epoxy Resins
DAR	Di-azo resin
DGEBA	Diglycidyl ether of Bisphenol-A
DGEBF	Diglycidyl ether of Bisphenol-F
HA	Hyaluronic acid
IR	Infra Red
LB	Langmuir Blodgett
LbL	Layer by Layer
Lupasol-HF®	Lupasol-Half Free (50% Aqueous Solution PEI)
P	Piperazine
PAA	Poly(acrylic acid)
PAH	Poly(allylamine hydrochloride)
PB	Polybetaine
PEI	Poly(ethylenimine)
PEI_{dia}	Dialysed Poly(ethylenimine)
PEO	Polyethylene oxide
PGA	Poly(L-glutamic acid)
PLL	Poly(L-lysine)

PNER	Phenol Novolac Epoxy Resin, DEN®-438®
PDPS	PNER -Dipping-PEI-Spray
PPD	PNER -PEI-Dipping
PPDA	PNER -PEI-Dipping-A399
PPDC	PNER -PEI-Dipping-Combined Catalysts
PPDE	PNER -PEI-Dipping-EEM
PPDP	PNER -PEI-Dipping-Piperazine
PSS	Poly(sodium 4-styrenesulphonate)
PTD	PNER -TEPA-Dipping
PTDA	PNER -TEPA-Dipping-A399
PTDC	PNER -TEPA-Dipping-Combined Catalyst
PTDE	PNER -TEPA-Dipping-EEM
PTDP	PNER -TEPA-Dipping-Piperazine
PUs	Polyurethanes
QCM	Quartz crystal microbalance
SEM	Scanning electron microscopy
STM	Scanning tunnelling microscopy
SAMs	Self assembled monolayers
SAXR	Small angle X-ray reflectivity
SLD	Scattering length density
TEPA	Tetraethylenepentamine
TGDDM	Tetraglycidyldiaminophenylmethane
UHV	Ultra high vacuum
UV	Ultra violet
UV-NIR	Ultraviolet-Near Infra-Red Spectrometer

Abstract

Nanofabrication of two component epoxy adhesives *via* covalent linkage was carried out using Layer by Layer (LbL) multilayer assemblies, adopting a dipping as well as alternate spraying-dipping technique for the deposition onto pre-activated silicon or quartz substrates and gold nanoparticles (Au-NPs). Dipping technique was employed for the curing of cresol novolac epoxy resin (CNER), phenol epoxy novolac resin DEN-438$^{®}$ (PNER) and Araldite MY-720 with poly(ethylenimine) (PEI) and tetraethylenepentamine (TEPA) on silicon and quartz surfaces. Thus the LbL film architectures obtained for various adsorption times and polymer concentrations were (PEI/CNER)$_n$, (PEI/PNER)$_n$, (PEI/MY-720)$_n$, PEI(CNER/TEPA)$_n$/CNER, PEI(PNER/TEPA)$_n$/PNER and PEI(MY-720/TEPA)$_n$/MY-720 (where n = number of layer pairs deposited). The classical conditions of polyelectrolyte multilayer build-up for covalent LbL assembly were optimized for the construction of multilayers having linear growth increment with respect to the number of layers chemisorbed. The thickness of each layer pair was measured using an ellipsometer and found in the range of 10 to 40 nm depending on the epoxy compound used. The multilayer films so prepared were quite homogeneous and highly reproducible. UV-Visible spectroscopy was also employed to monitor the chemisorption of UV active chromophores.

The optimised epoxy-amine network layers thus formed by covalent LbL assembly of epoxy resins were then applied onto Au-NPs films of the architecture (PAH/Au-NPs)$_5$. These epoxy protected Au-NPs films having architecture (PAH/Au-NPs)$_5$/(PEI/CNER)$_{10}$ and (PAH/Au-NPs)$_5$/(PEI/PNER)$_{10}$ were tested for their mechanical robustness with the help of a rubbing machine. The surface morphology of the rubbed samples was studied by AFM, although certain grooves appeared, but there is no significant difference in overall film thickness before and after rubbing test. So, epoxy protected Au-NPs film proved to be quite strong to endure 60 rubbing cycles as compared to virgin Au-NPs film which were mechanically much weak.

The adsorption process was further optimised to get fast curing process by employing various accelerators, increasing the polymer concentration, decreasing the adsorption time and also by reducing the number of layer pairs. Lupasol-HF, proved to be an exceptional curing agent after dialysis (to get narrow but high molar mass PEI$_{dia}$), for the

curing of various epoxy resins at room temperature. The spraying of PEI_{dia} (40 mg mL^{-1}) for 10 s followed by dipping for 10 min in epoxy solution (100 mg mL^{-1}) greatly enhanced the speed of covalent LbL adsorption process. Although curing of these films at elevated temperature resulted in ultimate robustness with no loss in thickness after 20 rubbing cycles, yet room temperature curing was also employed for a specified time period by storing the films in air tight containers. The epoxy-amine film thickness for the protection of Au-NPs was found to be 10 nm for CNER and 6 nm for PNER. The ellipsometer data revealed that after more than 60 rubbing cycles, the epoxy protected Au-NPs film lost ca. 6% of initial film thickness.

Moreover, the study has proved to be an economical preparation of more effective covalent LbL assemblies, both in terms of cost and time. Therefore, the epoxy-amine network has great potential to protect the underlying weak Au-NPs films and many such future applications.

Chapter 1

Literature Review

In the present work, various surfaces were functionalized with molecularly thin films *via* covalent LbL assembly. Individual layers of such multilayer architectures typically have a thickness in the nanometre range and a surface roughness of the order of a certain percentage of their thickness. The chemisorption of each individual layer must be controlled in a way that the molecules in each layer do not adsorb with all their functional groups binding to the surface below. This would be catastrophic, if all the functional groups were utilised in one layer build-up and would not lead to a regular film growth. Instead conditions must be found at which molecules chemisorb onto the surface with only some of their functional groups bound to the surface while exposing the remaining functional groups to the solution interface. This field of research is situated in the nanosciences and more precisely in the area of nanomaterials. Herein, these fields and the area of organic monolayers and films including the so-called LbL assembly technique which is a simple yet powerful method for the preparation of nanoscale multi-material films are briefly introduced.

1.1 Nano-science and Technology

The idea of nanotechnology was aired by Feynman, (a noble laureate) in his lecture entitled, "There's Plenty of Room at the Bottom" at annual meeting of American Physical Society in Caltech[1]. He presented the idea of manipulation of extremely small objects by taking one atom of matter at a time. He amazed his audience by announcing how all the 24 volumes of Encyclopaedia Britannica can be written on a paper pin head by reducing the letters by 1/25,000 of their normal size[2]. Feynman discussed how this could be done without loss of resolution and read using an electron microscope.

The term nanotechnology was first used by Taniguchi[3], as it mainly consisted of processing, separation, consolidation, and deformation of materials by one atom or by one molecule. Generally, more acknowledged definition of nanotechnology is the manufacture and study of objects with dimensions less than 100 nm. According to Drexler[4], existence of life is enough proof that machines could be designed and built atom by atom. Consequently with the invention of the scanning tunnelling microscope (STM), nanoscience and nanotechnology were realized enormously in the scientific world.

While nature plays with the full range of objects on the length scale from femtometres to parsecs, mankind is somewhat limited to the length scale between subatomic

particles and the size of our planet for instance. Functionality of an object on any length scale depends on the intricate interplay of its constituents. Complex systems had new properties which may be different from their constituents. Electrons and nuclei form atoms in the sub-angstrom scale, while atoms form molecules in the angstrom scale[5] (Figure 1.1). In material science, polymers could be prepared from monomers which represent the early nanometre scale. Although the range accessible to man is already limited, yet we hardly master more than a fraction of what is available to us.
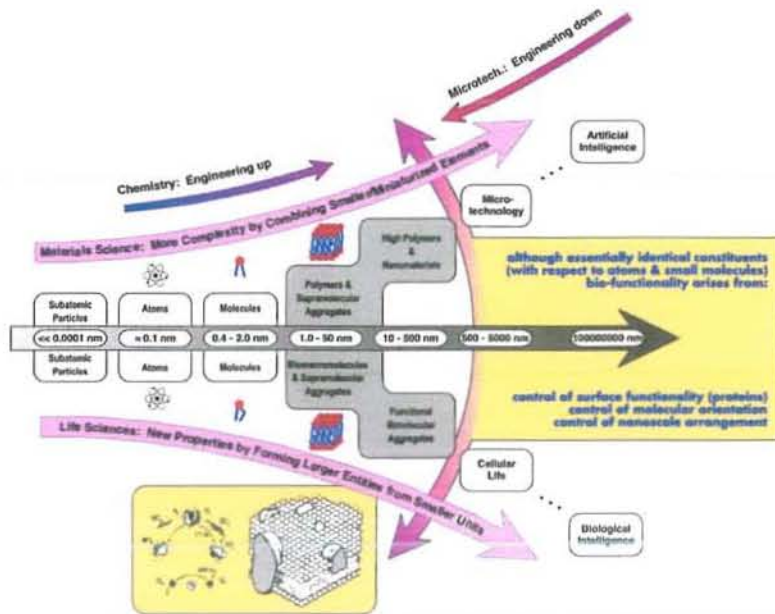
Figure: 1.1 Length scale of complexity[5]

An interesting length scale is provided by the organization of matter in nanometre level. Life is the most fascinating but complex property of matter. Nature clearly shows that the minimum size of a life form is nanoscopic to microscopic in dimension e.g. viruses are 75-100 nm, ribosome 25 nm, proteins 5-50 nm and DNA 2 nm[6]. This is the length scale that is just being touched but not mastered yet by either bottom up (chemical synthesis) or top down (miniaturization) approaches.

1.1.1 Nanofabrication

Nanofabrication involves the manipulation of matter at the nanoscopic length scale to provide design structures and patterns with purposeful functions. Matter can be shaped, positioned and organized at the nanoscale using either top down or bottom up nanofabrication[7]. The top down approach sculpts matter from macroscopic to

nanoscopic dimension in a serial process to form functional constructs with purposeful utility. In bottom up self-assemblies, the macroscopic objects construction takes place in a parallel manner from nanoscale building blocks like electrons, protons, atoms and ions etc. The concept of self-assembly has matured scientifically in chemistry, physics, materials science, engineering, biology and medicine over the past few decades. These concepts are now largely exploited in nanofabrication of a number of applications. The constantly increasing potential of nanofabrication is much appreciated in self-assembly of alkanethiol monolayers on gold for a myriad of soft-lithographies[8,9]. LbL electrostatic assembly of polyelectrolytes for smart drug delivery vehicles[10,11], bio-conjugated self-assembled nanocrystals for medical diagnostics[12,13] self-assembled semiconductor nanowires for flexible electronics[14] and microphase separated block copolymers as nanolithographic masks for silicon-based flash memories[13]. These are a few high profile examples of how self-assembly has enabled nanofabrication and a facilitated nanotechnology.

1.2 Thin Films

Surface science has become a very important part of material science as interaction of an object with its environment is always through its surface. An ever-increasing segment of materials science is revolving around particles (nano- and microparticle), thin films and layered materials. The fabrication, patterning and structural characterization of hybrid multilayer films on nanometre length scale is both crucial as well as imperative to the field of material science.

Thin films have enabled progress in numerous advanced technological and industrial fields[15] such as protective thin films for prevention of wear and tear, contact damage, and also to protect the underlying substrate from thermal degradation, corrosion etc. They are also used as antistatic coatings, antireflection coatings[16], electro-optics[17] and non-linear optics, optical switches and filters[18] optical data storage[19] and light emitters[20,21], chemical[22] and biochemical sensors[23,24], conductive films[25], bio compatibilization of surfaces[26,27] self-cleaning hydrophobic surfaces[28] and many other explorable sectors. A number of parameters have to be optimised before the thin films find various real world applications, e.g. in optical devices, they need to have very precise and uniform thicknesses and refractive indices. These parameters are usually met in inorganic coatings deposited by rather expensive vacuum instruments. Organic

materials are now finding their due share in the preparation of ultra-thin films. The organic or polymeric thin films are much soft; and offer specific advantages over inorganic thin films for particular applications, for example fluid like coatings can provide scratch resistance to plastic lenses. The processability of such films is much easier and cheaper as compared to inorganic materials, as they can be created at room temperatures. Another advantage of organic thin film coatings is that they can be applied to surface of any shape and kind, in addition to large surface areas. Organic thin films can be deposited on a solid substrate by various techniques such as: thermal evaporation, chemical vapour deposition, sputtering, electro-deposition, Langmuir-Blodgett (LB) technique, self-assembly, forced solvent removal techniques etc.

The so-called LbL assembly method, introduced by Decher *et al.* in the early 90's[29] has proven successful for the fabrication of nanoscale hybrid films. In the following section, LB, self assembled monolayers (SAMs) and LbL technique for ultrathin film formation, their methods and basic principles involved therein are elaborated.

1.2.1 Langmuir-Blodgett (LB) Monolayers

The effect of oily films on an aqueous surface was first documented by Francklin[30] in 1774. Later, Pockels[31] described a method to manoeuvre oily films at the air-water interface by means of movable barriers. Raleigh [30,32,33] explained that the films reported by Pockels at the air-water interface were one molecule thick (15 A°).

Thin organic films, ranging in thickness from about sub nanometres to 100 nanometres with molecular ordered structure; show a considerable scientific and technical promise. LB technique is one of the conventional methods of ultrathin film fabrication in which well-organized systems of moieties are efficiently built to one monolayer at a time (Figure 1.2). The procedure involves the transfer of monolayer of a particular substance, originally adsorbed at the gas-liquid interface, to a substrate. The thickness of these LB multilayers films depend on the molecular structure of the compound and the number of layers deposited [34]. Blodgett reported multiple deposition of long aliphatic carboxylic acids onto a solid substrate[35,36]. The apparatus used for the formation of LB films include a Langmuir trough with a dipping device to manipulate the substrate through the gas-liquid interface, an automated movable barrier, which

moves during the deposition process in order to maintain a controlled surface pressure, and a surface pressure sensor that controls the movable barrier[37].

Unlike the traditional LB films of amphiphiles having poor thermal and mechanical stability, robust monolayer fabrication of ligand-stabilized gold nanoclusters[38,39] semiconducting quantum dots[40,41] and polymeric films[42,43] was also reported. Huang *et al*[39] described a long range hexagonal close packed order of alkanethiol encapsulated Au-NPs. Films were not completely devoid of defects. In fact, it was discovered that, at lower particle concentrations (0.06-0.3 mg ml^{-1}), the level of orderliness increases, as shown by the fast Fourier Transformation images.

Chen[38] modified that work by using bifunctional linkers as encapsulating ligands on the surface of Au-NPs. By the use of rigid aryl dithiols as the chemical cross-linkers to the neighbouring particles, the mechanical stability of the monolayer film was further improved. The LB technique provided long range ordering of monolayers and multilayers [44] of species that self-assemble at the liquid surface. Functional units can be formed from systems of monomolecular layers having properties not shown by individual layers[45]. Upon UV irradiation, an energy transfer takes place from a sensitizer layer to an acceptor layer and results in fluorescence of former. Cyanine dyes as acceptor and sensitizer were used in the experiment. The energy transfer model can be used to ascertain whether the required structure has in fact been produced. Kuhn *et. al*[46] demonstrated that planned structures showing order dependent properties were assembled by nanomanipulation of successive deposition of compressed monolayers formed at the water-air interface. Traditionally, LB films were prepared from low molar mass compounds, like fatty acids but have poor mechanical, thermal and chemical stability, which reduced their application in practical devices. This problem was solved by the use of polymeric LB films, that enhanced the thermal, mechanical and chemical stability of these films[47,48].
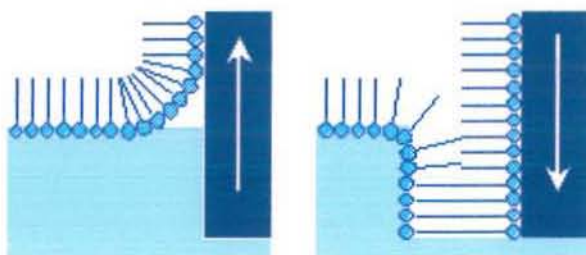
Figure 1.2: Formation of LB films by immersing the substrate into the solution[49].

Although, LB method is an elegant way to build-up multilayer assemblies, but it requires rather expensive instruments with tedious maintenance and it is also not applicable to many kinds of non-amphiphilic material[50]. The LB technique is also limited by the choice of solvent and requirement of very smooth and homogenous surfaces for deposition[51]. Moreover, LB films have low stability towards solvent and temperature changes[52]. Although, early investigations were related to the interfacial phenomena, but now the interest is shifted to functional LB films with potential applications[47] in thin film optics, sensors and transducers, protective layers, patternable materials, for surface preparation and modification, for chemically modified electrodes and biological membranes.

1.2.2 Self Assembled Monolayers (SAMs)

In the light of nanofabrication by bottom-up approach, self-assembly has provided a powerful tool for making materials and organizing them into functional blocks designed for a specific purpose. Matter of all kinds, e.g. atoms, molecules, colloids and polymers, can undergo spontaneous self association to get advanced level of structural complexity. The self-assembly idea seems to be from the work of Langmuir and Blodgett[53] and observations of Bigelow *et al*[54] that long chain alkylamines form a heavily crowded monolayer on the platinum surface.

Sagiv[55] pointed out that homogeneously mixed monolayers containing components with different properties and molecular shape may be easily formed on various solid polar substrates by adsorption from organic solutions. There was irreversible adsorption *via* covalent bonding of active silane molecules to the surface of the substrate. Monolayers covered surfaces become inert to further binding of molecules from the fluid phase due to nonpolar moieties (like methyl groups), thus preventing formation of ordered multilayers as well. In his later research work, he[56,57] proposed a multilayer assembling procedure aimed at circumventing this difficulty. In the two step strategy, first monolayer adsorption was followed by chemical activation of the exposed surface, to provide polar adsorption sites for the adsorption of the coming monolayer. This was achieved by means of a bifunctional surfactant possessing a polar and a non-polar terminal functional group convertible to a suitable polar group after completion of the first adsorption step.

Nuzzo and Allara coated gold surfaces with alkyl disulfides and discovered that they formed closely packed monolayers of chemisorbed alkanethiolate molecules, called self-assembled monolayers (SAMs)[58]. In these SAMs, there was evidence of strong S-S attachment of alkyl disulfides with polycrystalline gold substrate. Their structures were characterized by IR and photoelectron spectroscopy that possessed chemical and thermal stability[59]. Same group also reported the adsorption of dimethyl disulfide and methanediol under ultra high vacuum (UHV) conditions on Au (III) substrate surface. Although, both adhered strongly but the adsorption of disulfide was more favoured[60]. Monolayers of alkanethiols on gold were stable indefinitely at ambient temperature but desorption of constituents took place in hexadecane at 80°C[61].

Self assembled monolayers provided a convenient way to adsorb specific organic molecules having –SH, –COOH, –NH$_2$, and silane functional groups onto noble metals and nanocluster surfaces (Figure 1.3). The hydrophobic or hydrophilic behaviour of metal surface can be guided by the choice of the terminal functional groups of organic molecules. Organic inorganic nano hybrid materials so prepared were used to construct electronic devices, sensors, super capacitors, catalytic reagents, rechargeable power supplies etc.
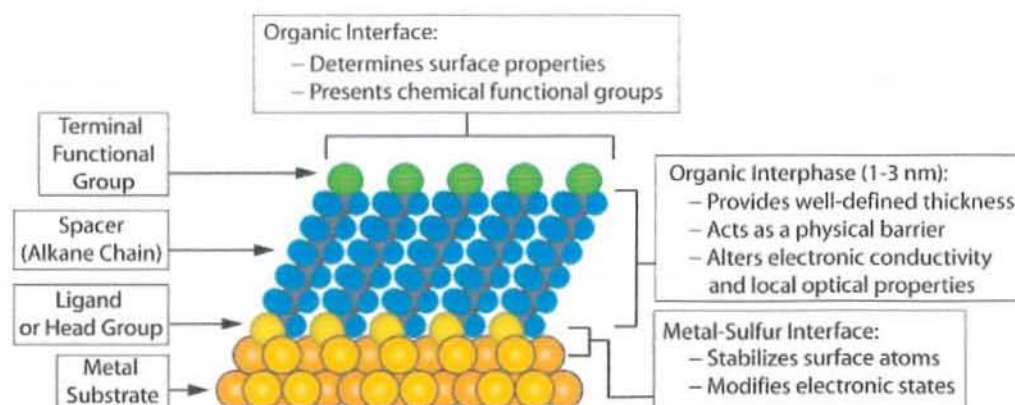
Figure 1.3: Representation of self assembled monolayers (SAMs)[8]

The adsorbates organize spontaneously and sometimes epitaxially into crystalline or semicrystalline structures. The molecules or ligands forming SAMs have a chemical functionality, called "headgroup", which have a specific affinity for a particular substrate. In many cases, the headgroup has a high affinity for the surface and displaces the already adsorbed adventitious organic materials from the surface. There are a number of headgroups that bind to specific metals, metal oxides, and semiconductors.

The most extensively studied class of SAMs is derived from the adsorption of alkanethiols on gold[62,63] silver[64,65] copper[62,66] palladium[67] platinum[68] and mercury[69].

The experiments established many of the basic structural characteristics of these systems (surface structure, chain organization, orientation), practical protocols for preparing SAMs (concentrations, length of time for immersion, solvents, temperature) and some details of the thermodynamics and kinetics governing the process of self assembly[70,71]. Since early 1990s, a major portion of the research was focused on the expansion of types of substrates used to support SAMs and to some degree, on the types of molecules used. However, the variety of ligands studied is still limited to functionalities formed from a small set of elements in a narrow range of oxidation states and much of the work has continued to focus on SAMs formed from thiols. The SAMs technique can be applied to a wider range of substances, but it is not a useful method for multilayer fabrication.

1.2.3 Layer by Layer Self Assembly: - An Overview

Iler in 1966[72] mentioned the alternate deposition of oppositely charged mineral particles onto smooth surfaces such as glass. His work was later improved by Gaines[73] but was completely discontinued afterwards in the whole community.

The LbL assembly of organic and polymeric compounds was pioneered by Decher starting in early 1990s[74,29,75,76,77]. Since then, research in this novel field of material science had attracted the attention of scientists, all over the world, across the academic and industrial fields. The LbL technique is based on the alternating exposure of a substrate or a solid support in oppositely charged polyelectrolyte solutions either through dipping or spraying (Figure 1.4). There are several rinse steps after each exposure to remove any un-adsorbed or loosely bound material on the surface[78]. So, one can build as many layers as needed, with any desired thickness, depending on the particular type or requirements of the experiment. Therefore, the LbL nanofabrication technique offers very precise control over the thickness and uniformity of the coating or the ultrathin films built, down to the sub nanometre scale.

In LbL assembly process, each corresponding component is adsorbed in a single step, and after whole assembly construction, films have a defined sequence. Therefore, LbL assembly can be considered as a sort of multifunctional synthesis using mostly weak interactions. LbL has a great analogy to a classical chemical synthesis process. While in

a chemical synthesis, different reacting species through a series of reaction steps yield a product often accompanied by a co-product. So purity and overall yield are always a compromise in chemical synthesis. In LbL process, through a series of deposition steps, a multilayer film of defined architecture is obtained, which is highly pure and reproducible with high device yield[79]. The fabrication of multi-composite films by the LbL procedure means literally the nanoscopic assembly of hundreds of different materials in a single device using environment friendly, ultra low cost technique operated at room temperature. The materials can be small organic molecules or inorganic compounds[80,81] macromolecules[11,82] biomacromolecules such as proteins[83] or DNA[84,85,86,87,88], carbon nanotubes[89], clay[90], nanoparticles[91] or even colloids (metallic or oxide colloids or latex particles[92,93]. The technique can be applied to solvent accessible surfaces of almost any kind and shape, the more exotic ones being microcapsules, colloids or biological cells[94,95] and a surface coating even for objects with a surface of several square meters is also possible.
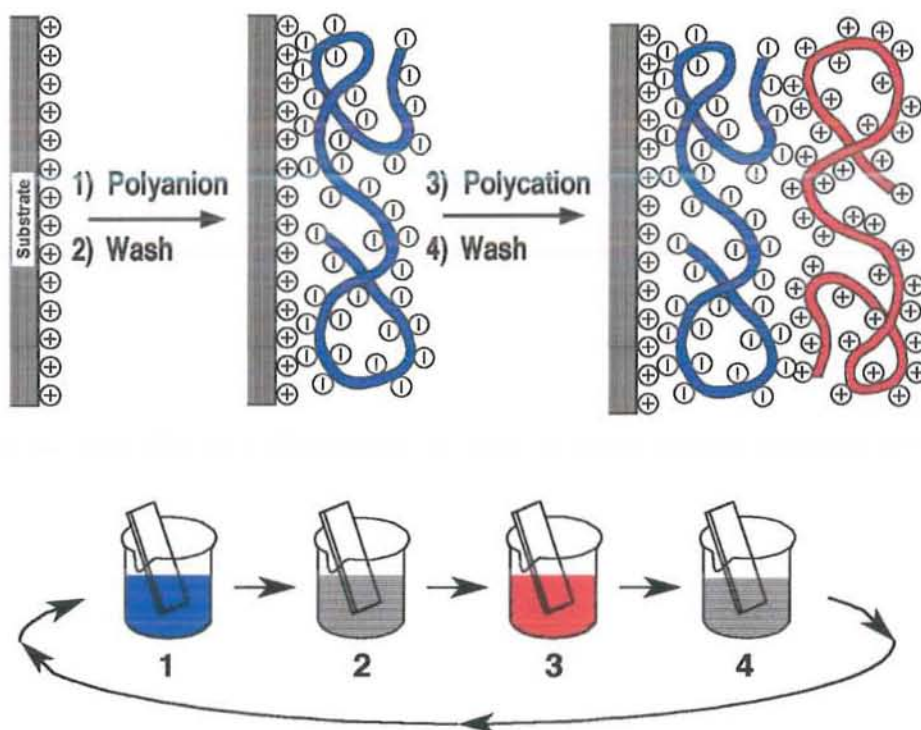
Figure 1.4: Top: Simplified molecular concept of the first two adsorption steps depicting film deposition starting with a positively charged substrate. **Bottom:** Steps 1 and 3 represent the adsorption of a polyanion and polycation respectively, and steps 2 and 4 are washing steps.

On contrary, other thin film making techniques have a serious limitation as they work on special kinds of materials. However, by this technique, thin film can be coated on a

number of different substrates such as silicon, gold, platinum, plastic, glass, quartz, stainless steel, clay, nanoparticles, blood cells and colloidal particles[96]. The whole process can be automated using robots, making the coating procedure less time consuming and applicable for commercial applications where productivity and labour are the major problems. The LbL deposition technique is categorised as a template assisted assembly which is much faster as compared to self-assembly or chemical modification. The result of self-assembly is mostly uncertain or difficult to predict. The LbL nanofabrication allows multimaterial assembly of several compounds, thus giving access to multilayer films whose complex functionality fall into either of the two categories:

The properties of an object depend on the interaction of its surface with environment. So surface can be tailored for specific purposes like corrosion protection[97], antireflective coatings[98], stickiness or non-stickiness[99], surface induced nucleation[100,101], antifouling[102], hydrophillicity or hydrophobicity[103,104], biocompatibility[105,106], chemical sensing or biosensing[107,108], biomaterial coatings[109] and microchannel flow control[110].

The sequence of adsorption of different substances on a substrate defines the architecture of multilayers and thus the overall device properties. Therefore, it is wisely called a knowledge based or programmed assembly. In contrast to self-assembly, it leads to property engineering by controlling mostly one-dimensional spatial arrangement of functionalities in multimaterial layered nanocomposite membrane reactors[111], optoelectronics[112], photonic devices such as light emitting diodes[94,113] or complex waveguides, compartmentalized films with barrier layers or separation membranes[114,115,116].

There are several techniques to carry out adsorption of materials for LbL nanofabrication assemblies. The most common preparation method introduced by Decher initially was dipping[75] which is still the mostly used deposition method. Winterton[117] patented spray deposition of oppositely charged polyelectrolytes onto ophthalmic lenses which was later reported by Schlenoff[118]. Spin-coating[107,119] is also widely used in LbL deposition technique now-a-days. Both spraying and spin-coating adsorption techniques require a very small volume of liquid for surface coating as compared to dipping deposition. The structure and properties of LbL assembled films

are influenced by the preparation methods. Various analytical instruments can be used to monitor film build-up process during LbL nanofabrication, such as UV-Visible spectroscopy can efficiently monitor multilayer build-up if at least one chromophore group is present in the constituent polymers. Film thickness can be measured with the help of an ellipsometer, whereas film growth mechanism can be studied *in-situ* with Quartz Crystal Microbalance (QCM), while surface Plasmon spectroscopy was used to study various interactions in LbL films[120,121].

1.3 Multilayer Structure

1.3.1 Layered or Amorphous

Does polyelectrolyte multilayer have a real layered structure or polyelectrolyte chains interpenetrate giving rise to a perfectly homogeneous structure? To answer this question, X-ray reflectivity and neutron reflectivity measurements were carried out to characterize polyelectrolyte multilayer structure. Both instruments are widely used in the characterization of polyelectrolyte multilayer films[121,122]. In X-ray reflectivity experiment, electron density in the normal direction will be analyzed. Kiessig fringes, derived from the destructive interference between reflected beam from air/film interface and film/substrate interface, can be observed[123,124,125] in smooth films. However, X-ray reflectivity measurement can not reveal the internal layered structure of polyelectrolyte multilayer, represented by Bragg peaks. The absence of Bragg's peaks in X-ray reflectivity measurement may be either due to the fact that the stratification in multilayers is not sufficient for adjacent layers to inter-digitate or the electron density contrast of individual layers is not large enough.

On contrary, in neutron reflectometry, the scattering length density (SLD) profile perpendicular to the surface will be analyzed. This SLD profile can be interpreted by a "box" model with a specific value for thickness, roughness and density attributed to each box. Besides Kiessig fringes, Bragg peaks have also been observed by several groups[126,127,112,113] for films containing individual layers of deuterated polymers. These Bragg peaks indicate a well-defined stratified multilayer structure, corresponding to a super lattice structure in normal direction, with more or less interpenetration of adjacent layers not only in different zones border but also in the whole film. (Figure 1.5)
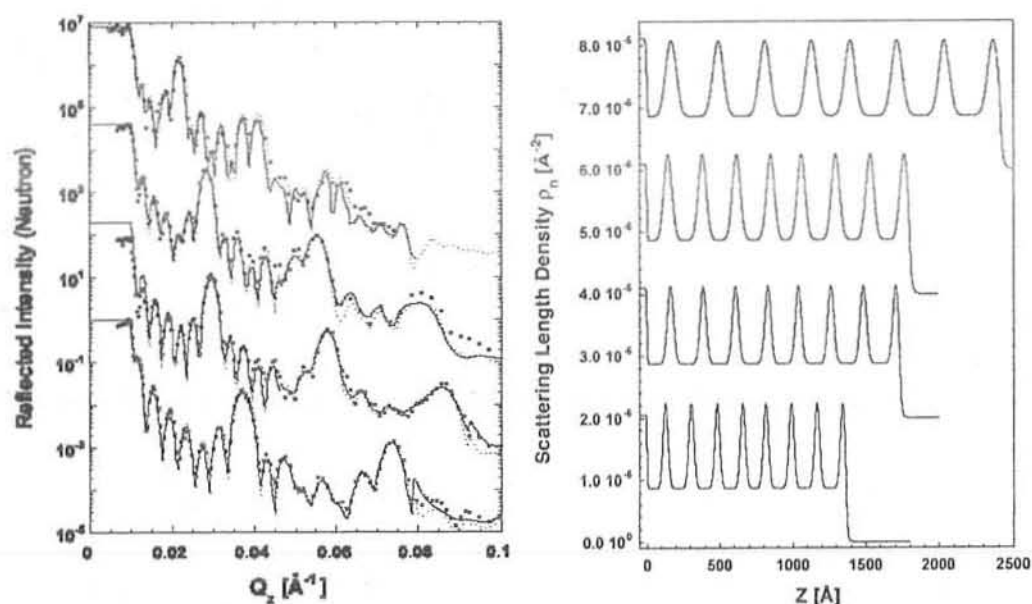
Figure 1.5: Neutron reflectivity scans and layer profiles of 4 multilayer samples with different film structure[97] **Left:** Neutron reflectivity scans and numerical fits leading to the layer profiles shown on the right. **Right:** Scattering length density profiles of the 4 reflectometry scans on the left. Each of the eight deuterated layers is clearly picked up in every multilayer sample. Bottom two have 80 layers with architecture ((PSS-h7/PAH)$_4$/PSS-d7/PAH)$_8$ while upper two 64 layers with architecture ((PSS-h7/PAH)$_3$/PSSd7/PAH)$_8$.

1.3.2 Polyelectrolyte Multilayer Formation: - Three Zone Model

A three zone-model described by Decher *et al*[128,129] for the formation of polyelectrolyte multilayer is shown in Figure 1.6. Zone I is composed of one or few polyelectrolyte layers close to the substrate surface. Zone III is also composed of one or few polyelectrolyte layers close to the outer surface of the film. Zone II is the "bulk" film between zone I and zone III. Properties of this zone are not influenced by either substrate or air. In most cases, chemical composition and structure of these three zones are different. Zone II is globally neutral while zone I and III are normally charged by different numbers of extrinsic charge sites. Although zone II is neutral, some counterions may be found there. As a result, even polyelectrolytes with 1:1 stochiometric ratio might not be able to realize 1:1 charge overcompensation. Charge density in zone III is more important than in zone I because zone III is responsible for further polyelectrolyte adsorption, charge overcompensation and film growth. This means that counterions are found everywhere in zone III. The very presence of counterions indicates that the border between different zones is not sharp. Individual polymer layers are rather strongly intermingled with neighbouring layers, even layers further away from the surface will contribute to the surface charge excess. This is the

12

"fuzzy" notion introduced by Decher[75]. The structure of polyelectrolyte multilayer is not perfectly defined as crystalline, but it is not completely disordered as well. There is positional order between molecules, but not between atoms.
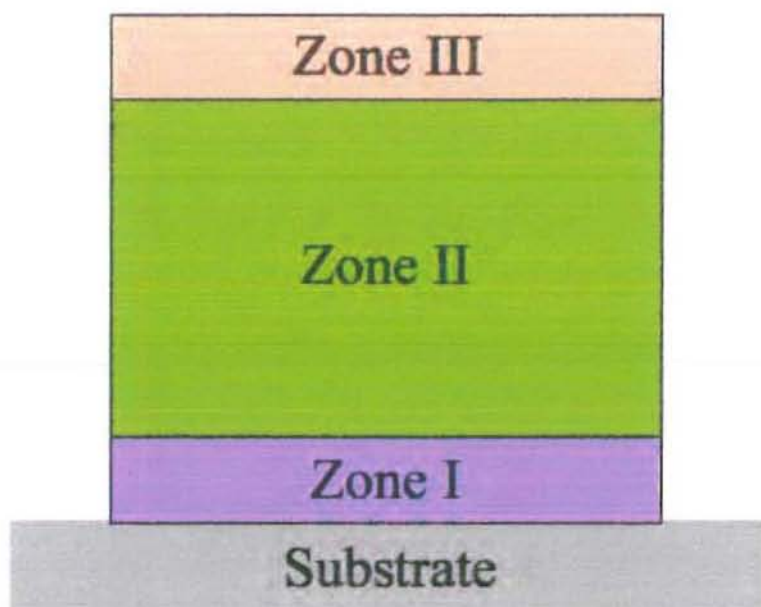
Figure 1.6: Three zones model for polyelectrolyte multilayer. Interfaces between different zones are diffuse rather than a sharp plane[130].

The number of layers belonging to zone I and III respectively, depend on a number of parameters, including nature of substrate, chemical structures of polyions complex and deposition method and/or conditions, but the exact condition remains still unknown. The three zone model is only valid in polyelectrolyte multilayers with a sufficient number of layers deposited. Detailed film formation is presented in Figure 1.7.

In the three zones model, zone II will be formed when both zone I and III have reached their final chemical composition and thickness and more polyelectrolyte deposition and polyions formation will not change the thickness of zone I and III. Only then the thickness of zone II will increase. As mentioned before, the borders of these three zones is not sharp but gradual and there is probably chain inter-diffusion between different zones interfaces. When more polyelectrolytes have been deposited on the surface, newly created polyions complex will increase the distance between polymers at the interface of zone II/III and the surface. Influences of these polymers at the interface to the outmost surface will be decreased as well. These polymers will now be considered more likely to be a part of zone II instead of formerly interface situated

13

polymers. These polymers will successively embed in zone II when more layers are added, so keeping the thickness of zone III almost constant.

increasing numbers of layers
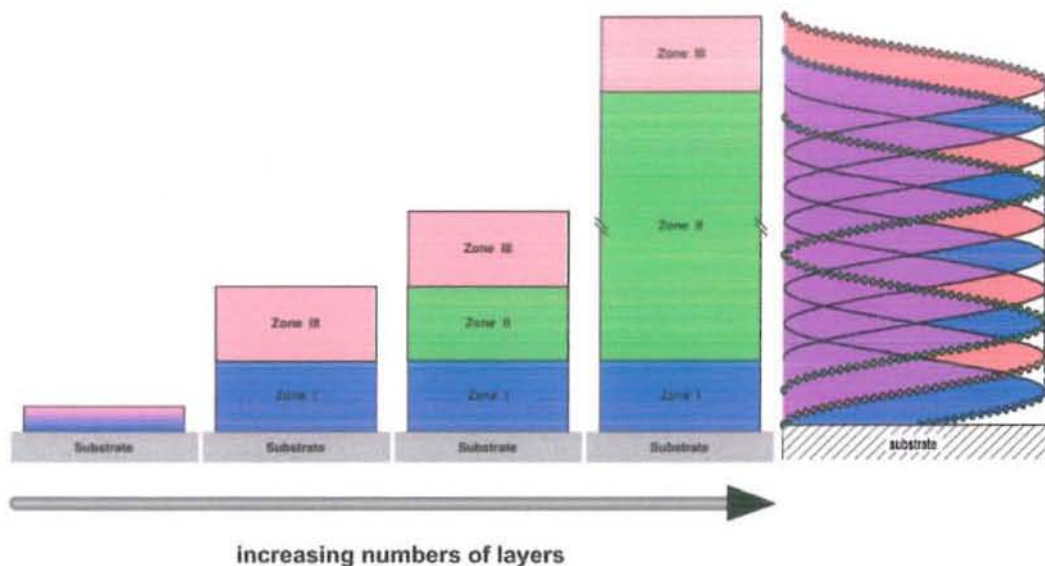
Figure 1.7: The zone model for polyelectrolyte multilayer[129]. On the very right is depicted how the three zones can be correlated with model consisting of individual but strongly overlapping layers[131,129].

Infact, the polyelectrolyte multilayer thickness increase depends on the film growth of zone II. This "transition" character during multilayers assembly also defines the notion of "fuzzy" and makes borders between each zone gradual. Polymer chains inter-diffusion at each zone interface level, presented on the very right part of Figure 1.7, is possible. Even though the exact structure and composition of these three zones are not clear, the difference between charged zone I/III and "neutral" zone II influences the physiochemical behaviour of the whole polyelectrolyte multilayer. Charged zones, especially zone III where film growth occurs only on the top, acts more like individual polyelectrolyte during a film build-up process while "neutral" zone II is not so active in film construction. An attention should be paid here; the inactivity of zone II is only valid for linear growth film. In super linear growth film, polymers can diffuse into zone II, and in this case, zone II is a "reservoir" for these mobile polymer chains. Even zone II is "neutral" and inactive in a global way; many different chemical compounds can diffuse "into" a film at high "outside" concentrations. The swell/deswell tendency of certain polyelectrolyte multilayer in the presence of salt in the solution was observed by Decher[132].

14

1.3.3 Deviation from Linear Growth Behaviour

However, it is noted[133,134,135,136] that a linear regime is never reached or only after the deposition of a large number of layers. The groups of Schaaf, Voegel, and Decher have reported multilayers composed of weak polyelectrolytes showing strong super linear growth[137,138].

Many combinations of strong polyelectrolytes yield a growth behaviour that becomes linear after the first few layer pairs, a typical example is shown in Figure 1.7. However, it was discovered that this linear growth regime has not been observed in certain polyelectrolyte systems[137,139,140]. During LbL deposition, after a few layer pairs, film shows a super-linear growth behaviour which has been frequently observed in weakly charged polyelectrolytes self-assemblies such as poly(L-glutamic acid) (PGA), poly(L-lysine) (PLL), hyaluronic acid (HA), polysaccharide etc. Schaaf[141,142,143] suggested "in" and "out" theory of "free" polyelectrolyte chains in the multilayer to explain the mechanism of this super-linear growth regime. A model is proposed in which polyions are not kinetically trapped in the position where they were originally deposited, but diffuse inside the film[138]. Laugel *et al*[144] suggested a semi-theoretical model for the prediction of which polyelectrolyte couples will have a linear or super-linear growth regime during the multilayer construction. The super-linear growth regime is frequently observed in normally less than 10 layer pairs. If deposition cycle continues, a linear growth regime will be observed after 15 or 20 layer pairs, or even more[145,146,147]. However, the mechanism of this super-linear/linear transition is not clear yet.

1.4 Adsorption Techniques for LbL Assemblies

1.4.1 Dipping, Spraying and Spin Coating

The conventional technique to prepare multilayers is solution dipping (Figure 1.4), while spraying and spin coating are the other major adsorption methods used in LbL assembly. The use of spin coating is limited due to substrate size and planarity, therefore, dipping and spraying are the two most frequently used adsorption techniques. In dipping adsorption technique for the multilayer formation, the substrate is brought into contact with polyelectrolyte solutions. During adsorption, polymer chains will diffuse from bulk solution to the surface and get adsorbed. The adsorption time for a single layer pair construction varies from few minutes up to an hour depending upon nature of polymers used and other experimental considerations.
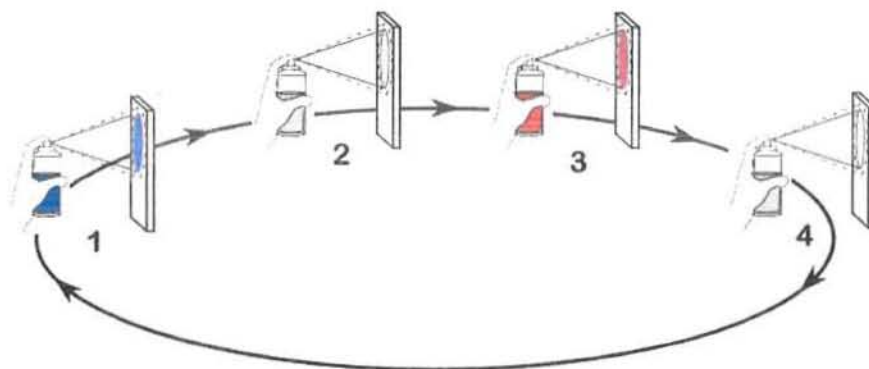
Figure 1.8: Spraying deposition technique for multilayer build-up.

Winterton[117,148] and Schlenoff[118] introduced spraying deposition in the last decade. The spraying technique decreases the adsorption time with a factor of 25-150[149] as compared to conventional dipping method. Spraying is a very efficient technique to produce a homogeneous film at the surface placed at a certain distance. It is thus extremely well suited for LbL multilayer assemblies, especially for the homogeneous wetting of large and/or uneven surfaces. In the spraying process, a substrate is held up vertically and liquid is horizontally sprayed onto the substrate. Once polymer solution strikes substrate surface, drainage caused by gravity will ensure the liquid coverage on the surface (Figure 1.8/1). So polymer is dispersed and adsorbed uniformly onto the substrate. Because of the vertically installed substrate and the gravity induced drainage, some polymer chains are much weakly adsorbed than the others. A specified wait period is necessary to allow maximum adsorption of the polyelectrolyte chains on to the substrate. Rinsing is done after the wait period to remove weakly adsorbed polyelectrolytes from the substrate surface. Rinse solution is sprayed onto the substrate for a specified time period and an additional waiting time is necessary for the drainage of rinse solution containing some of the un-adsorbed polyelectrolytes (Figure 1.8/2). After the rinse step, oppositely charged polymer solution is sprayed onto the substrate surface (Figure 1.8/3), followed by another rinsing step (Figure 1.8/4).

Recently, Kolasinska *et al*[150] compared the properties of polyelectrolyte multilayer films prepared using the dipping and spraying techniques. The purpose was to establish whether the dipping LbL process could be replaced by spraying technique without compromising the quality. Films obtained using spraying techniques are thinner than those prepared by dipping having the same number of layers pairs. Although spraying

technique offer great advantage of short time of preparation, yet cannot provide some features provided by polyelectrolyte multilayers prepared by dipping technique such as stability and uniformity. Generally, confirmed by X-ray reflectometry and AFM analysis, sprayed polyelectrolyte multilayer is thinner but smoother than dipped ones[149]. As explained before, different physiochemical conditions will influence the structure and properties of polyelectrolyte multilayer. One of the factor in obtaining thinner films from spraying deposition was the relatively lesser contact time (typically few seconds)[149] between polymer and substrate surface.

Some controllable and uncontrollable parameters in spraying LbL assembly[149] can explain this phenomenon. Examples of controllable parameters include spray distance, spray volume, concentrations of polyelectrolyte while uncontrollable parameters include droplet size, droplet speed and speed distribution during spraying process and concentrations of polyelectrolytes in droplets. The use of spin-coaters was demonstrated by Hong *et al.*[151,152] and Wang and co-workers[153]. Both spraying and spin coating have the advantage that only small amounts of liquids are needed to coat large surface areas.

1.4.2 Simultaneous "one-step" Spraying

A simultaneous spraying method for the polyelectrolyte film formation was described by Hubbell *et al*[154]. However, no further detail of film deposition mechanism and structure was provided. Hiorth *et al*[155] developed simultaneous spraying method on a rotating cylinder for polyelectrolyte film construction. The films formed by simultaneous spraying technique were dry and salt or other substances present in aqueous solution could not escaped from the films as there were no washing steps involved in between deposition cycles. However, spraying procedure using polycation and polyanion at the same time is a promising method to perform a single step functionalization process. Porcel *et al*[156] proposed a new simultaneous spraying method, in which traditional spraying instruments was used (Figure 1.9). A linearly grown (PGA/PAH)$_n$ film was obtained with simultaneous spraying process[156], although a typical super-linear growth regime for such film was observed in LbL self-assembly. In simultaneous spraying process, important controlling parameters are polyelectrolyte concentrations, spraying rate, spraying time, adsorption time and rinse time.
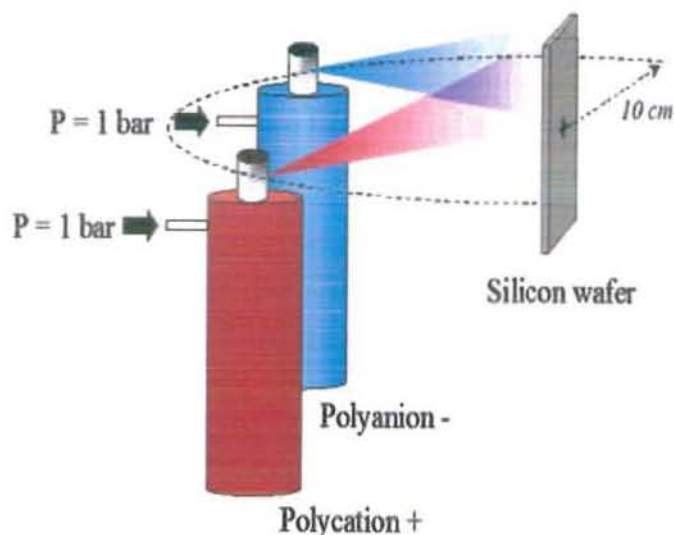
Figure 1.9: Experimental set up for simultaneous spraying process[156].

They also proposed a film formation mechanism for simultaneous spraying process. In polyions complexation, there exists a characteristic time τ when all charged functional groups of a polyelectrolyte interact thoroughly with functional groups of the oppositely charged polyelectrolyte. When a polycation is sprayed onto a surface covered with negatively charged groups, it will interact immediately with polyanion on the surface. After this characteristic time τ, polyions complexation may be considered as complete. But on the other hand, if during the time τ another polyanion is sprayed again onto the surface, it will also interact immediately with polycations already present on the surface, even though the complexation between polycation and former adsorbed polyanion is not yet completely finished. If polyelectrolyte spraying time interval is within this characteristic time τ, the film formation process should be continuous and simultaneous.

The unusual linear growth regime of (PGA/PAH)$_n$ film was due to the steady-state conditions caused by constant spraying and deposition of sprayed LbL film was totally possible on the top of such simultaneous sprayed film. However, difficulties in simultaneous spraying process are the lack of precisely controlled parameters in film formation and the possibility to apply this method to other polyelectrolyte pairs. But simultaneous spraying is a promising method in one step functionalization by combing different components.

1.5 Monitoring Multilayer Build-up

1.5.1 *Ex-situ* Characterisation Techniques

Ex-situ characterization techniques for LbL build up studies are non-destructive and highly accurate. UV-Visible spectroscopy is the simplest and easiest way to follow multilayer build-up process. $(PSS/PAH)_n$ films is probably the best characterised system so far (Figure 1.10). UV-Vis spectroscopy is used to measure the optical absorbance due to the presence of chromophore groups in both the polymers.
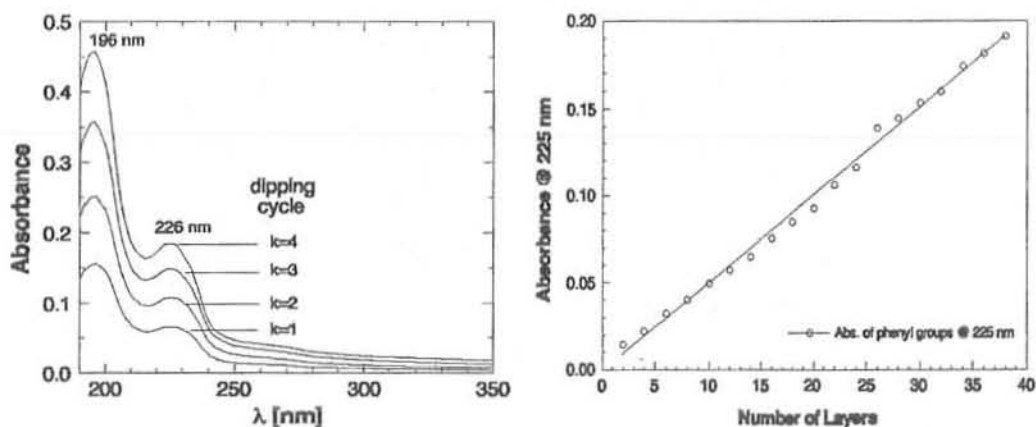
Figure 1.10: Left: UV-Visible spectra taken after different adsorption cycles (k) during the preparation of a PSS/PAH multilayer. The bands at 195 nm and 226 nm originate from the aromatic chromophore of the styrene monomer unit of PSS. The absorbance increases regularly with the number of PSS layers. **Right:** Plot of the absorbance of the PSS band at 225 nm versus the number of layers deposited. The numerical fit to the data (solid line) shows that the increase of absorbance per layer is constant.

The film thickness can also be determined by ellipsometry and X-ray reflectometry studies as shown in Figure 1.11. The reflectivity traces were taken on a dry specimen at various stages of multilayer build-up. Each reflectivity trace corresponds to a single data point in the ellipsometric data curve. Salt concentration greatly affects the multilayer build-up process[157]. In case of weak polyelectrolytes, layer thickness can be precisely controlled by pH[158]. *Ex-situ* methods are simple and provide sufficient information on the deposition behaviour.

Very recently, nuclear magnetic resonance (NMR) was added to the "toolbox" of multilayer research[159,160] and this deserves special attention as it gives access to structural data.
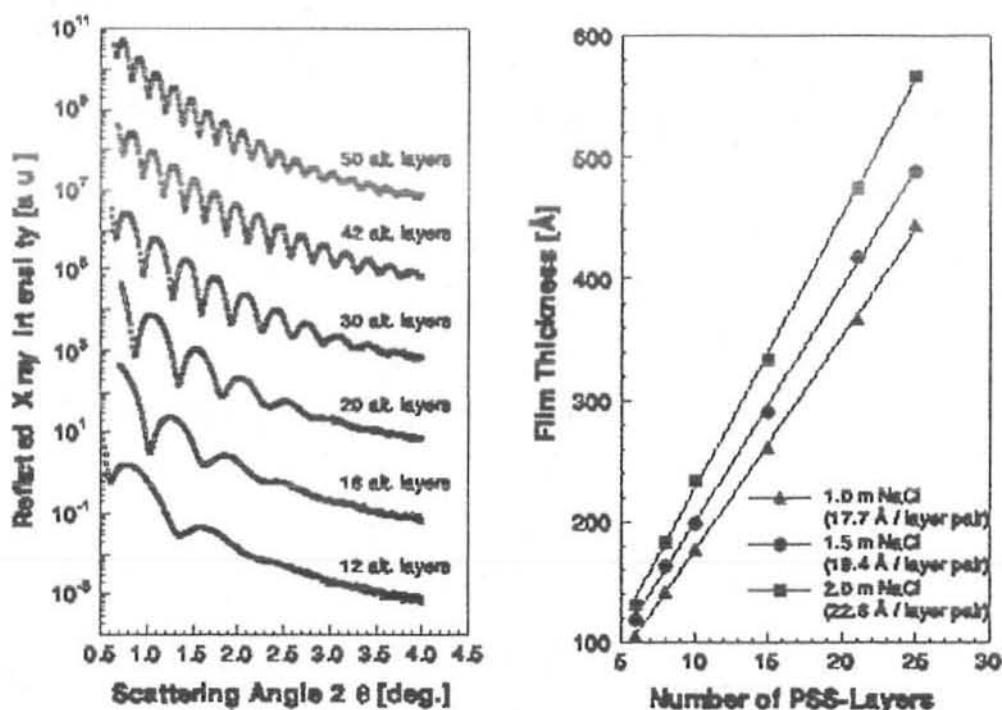
Figure 1.11: X-ray reflectometry of multilayer films of the architecture (PSS/PAH)*n*, *n* ranging from 6 to 25. **Left:** raw data obtained from a single specimen at different *n* in the dry state. **Right:** plot of film thickness versus number of layers for three sets of curves as the one on the left.

1.5.2 *In-situ* Characterisation Techniques

The *ex-situ* characterization techniques for multilayers build-up are simple and widely used but one of the major drawbacks is that the deposition process has to be interrupted to make the measurement. The *ex-situ* measurements not only disrupt the adsorption process but they have to be taken in the dry state, which may not be desirable in some cases. One of the consequences of deposition under different conditions is, for example, that the film thicknesses are different for identical numbers of layers. It is usually observed, that films deposited from identical solutions with identical adsorption times at same temperature show a different film thickness for the same number of layers depending on whether they have intermittently been dried and characterized or not.

In-situ characterization methods are, therefore, necessary in order to obtain results for samples that need not be dried during the course of measurements. These methods may allow one to follow the adsorption kinetics and/or multilayer reorganisation depending on time resolution as shown in Figure 1.12. During the adsorption of a polyanion, the surface charge changes from positive to negative, leading to electrostatic repulsion and

hence to self limitation of the adsorbed amount. In most cases the adsorption of polyelectrolytes is irreversible and rinsing helps to remove the weakly adsorbed polyelectrolyte molecules. The adsorption, thus leads to a surface charge reversal that allows adsorbing a polyelectrolyte of opposite charge and thus continuing the growth process[128].
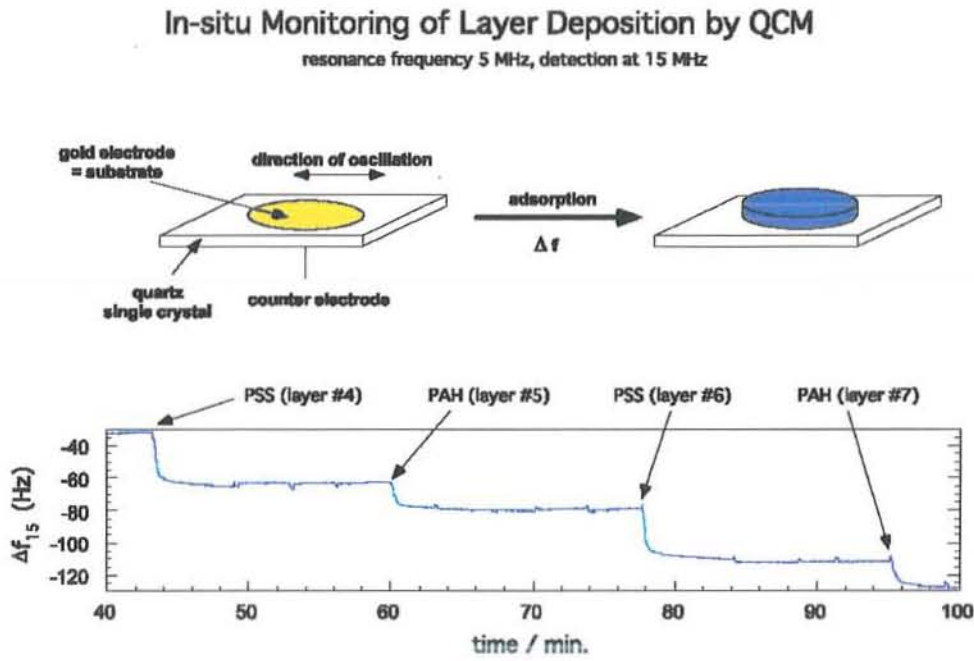
Figure 1.12: Continuous QCM trace of the third harmonic at 15 MHz (raw data) during the deposition of PSS (large displacements) and PAH (small displacements) during 11 adsorption steps.

Besides measurements of the zeta potential and results obtained by quartz crystal microbalance (QCM) (Figure 1.13), typical *in-situ* methods include surface Plasmon spectroscopy[161,162] optical waveguide light mode spectroscopy (OWLS)[138,163] optical reflectometry in stagnation point flow cells[164] scanning angle reflectometry (SAR)[165] ellipsometry[166,167] in situ atomic force microscopy (AFM)[168] attenuated total reflection Fourier transform infrared spectroscopy (ATR-FTIR)[169,] surface forces measurements[170,171] X-ray and neutron reflectometry[172,173] or second harmonic generation (SHG) but the latter are not widely available.

21
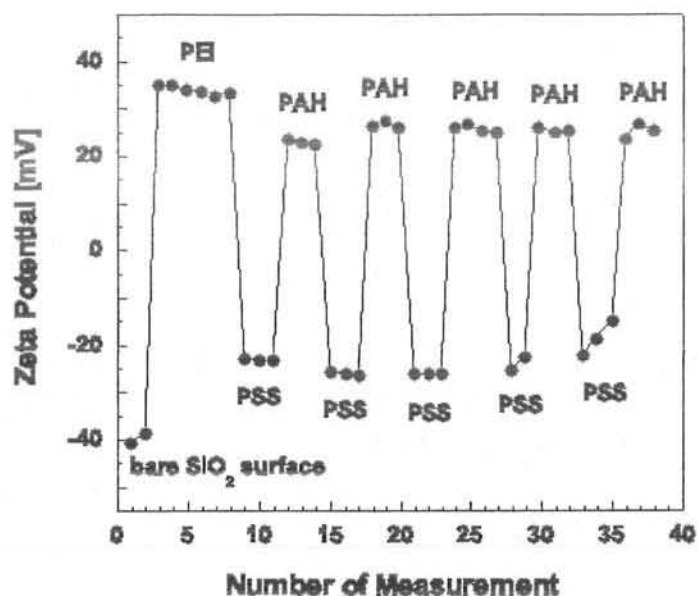
Figure 1.13: Streaming potential measurement showing the surface charge reversal during multilayer build-up *in situ*. The first layer (PEI) was followed by 5 deposition cycles of PSS and PAH.

1.6 Driving Force for LBL Assemblies

1.6.1 Polyelectrolytes and Polyelectrolyte Multilayers

A macromolecular species that dissociates into a highly charged polymeric molecule when placed in some solvent like H_2O is termed as polyelectrolyte or polyions. Counter ions are an additional product of dissociation which are small oppositely charged ions that tend to neutralize the charge on the repeat units of the polyelectrolyte, thus maintaining the electro neutrality. Polyelectrolytes are classified on the basis of their origin into natural and synthetic. Examples of naturally occurring polyelectrolytes are biopolymers like proteins and DNA while PAH and PSS are categorised as synthetic polymers. At higher ionic strength, a polyelectrolyte tends to become thicker and more coiled due to the screening effects of polymer charges by the presence of excessive salt counter-ions in solution. At low ionic strength, polyelectrolytes tend to be in its extended and uncoiled form. The factor responsible for the extended form of polyelectrolytes is the presence of intramolecular repulsion of the unscreened charges on each monomer unit.

Polyelectrolytes have found a number of applications in chemistry, largely at the interface of polymer, materials, colloids, surface and analytical chemistry. They have been used in the health and personal care industry as thickening reagents[174], rheology

modifiers[175] and viscosity enhancers for shampoos, conditioners, deodorants and body lotions[176,177]. They have also been used for water treatment[178], waste treatment[179] sludge dewatering[180] and the paper and pulp industry as retention aids as well as flocculating and coagulating agents for solid-liquid separations. Recently Shiratori and Sato have designed a thin film coating of polyelectrolytes assembled from chitosan and another polyelectrolyte containing an enzyme extracted from bamboo[51]. The thin film wrap prepared was effective in preventing decomposition and ripening of fresh fruits by suppressing the emission of ethylene gas, and thus keeping these fruits fresh for longer periods of time. In addition, these polyelectrolytes were assembled into ultra-thin film composite membranes and has received significant attention and interest in the field of technology and industry[176,181,182,183,184,185,186]. Other applications include the coagulation of colloidal dispersions,[187] biocompatible coatings for hemo-sorbents and other medical devices in contact with blood[188,189], dialysis membranes[190,191], ultra filtration[192], concrete stabilization, and enzyme mimics[193,194]. Another recent application of the polyelectrolyte complexes is their ability to form complexes with biomacromolecules. For example, polyelectrolyte complexes between DNA and a polycation is used to compact DNA, thus protecting it from digestive enzymes in the blood stream and living tissues and increasing the efficiency of *in vivo* gene transfection[195,196].

1.6.2 LbL Assemblies Based on Hydrogen Bonding

One of the most commonly studied, non-electrostatic intermolecular interactions used in LbL assembly technique is hydrogen bonding. By utilising this interaction, many uncharged materials have been successfully integrated into multilayer films. This is due to the presence of various moieties that can provide hydrogen bonding among individual polymers chains. For example, the highly electronegative oxygen atoms present on polyethylene oxide (PEO) polymer backbone provides hydrogen bonding site. Chen *et al.*[197] reported that covalently attached di-azo resin (DAR)/poly(acrylic acid) (PAA) multilayers were fabricated by the LbL self assembly of DAR/PAA in aqueous solution followed by UV irradiation[198]. The reaction between DAR/PAA in the film is shown in Figure 1.14. UV radiation turns the interaction between the films from ionic to covalent, thus the stability of the DAR/PAA is greatly improved as compared to unexposed film[1984].
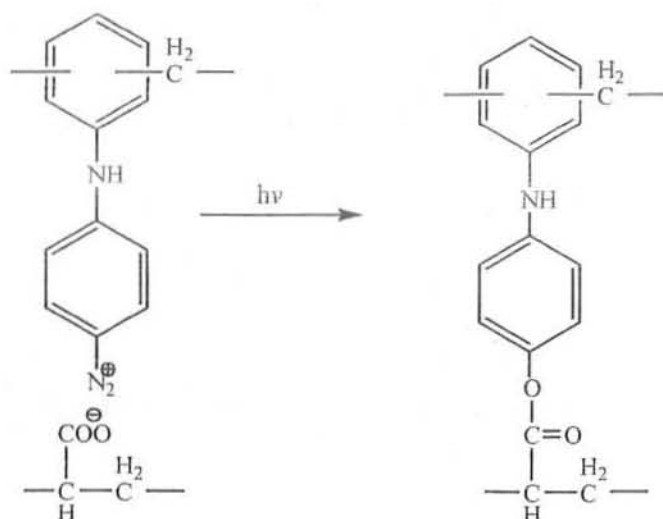
Figure 1.14: The reaction between DAR/PAA[198].

Stockton and Rubner[199] conducted seminal studies in LbL multilayer assembly based on hydrogen bonding. Polyaniline was used in alternation with a variety of water soluble macromolecules, such as poly(vinylpyrrolidone), poly(vinyl alcohol), polyacrylamide (PAA), and PEO. Infrared spectroscopy[199] verified that the multilayer build-up was driven by hydrogen bonding due to the appearance of the N–H stretching peaks at ca. 3300 cm^{-1}. Zhang and co-workers[200] used PAA and poly(4-vinylpyridine) for the build-up of multilayers[200]. Earlier attempts to assemble positively charged polyelectrolytes resulted in very limited film growth if hydrogen bonding was not involved in the assembly[201].

Sukhishvili *et al*[202,203] established that water soluble uncharged molecules capable of hydrogen bonding interactions were self-assembled at various surfaces using the LbL approach. The multilayers so fabricated were dissolved at high pH value. Routes to stabilize hydrogen-bonded self-assembly via thermal, photochemical[204] or chemical cross-linking[205,206] as well as the ability to deposit and stabilize hydrogen-bonded LbL assemblies on spherical substrates[205,207,208] have been recently reported by several groups. Stabilized hydrogen-bonded assemblies were explored for encapsulating various chemicals and controlled release of encapsulated cargo[207]. Caruso *et al*.[209] mentioned LbL adsorption of negatively charged polynucleotides at surfaces based on DNA hybridization driven by hydrogen bonding. Schlenoff and co-workers[210] studied LbL deposition of similarly charged hydrogen-bonding homopolynucleotides (poly-(adenylic acid) and poly(uridylic acid)) and found that these two molecules failed to

24

produce films, unless they were co-assembled into films with a polycation. Sukhishvili *et al*[211] explored hydrogen-bonded LbL self-assembly of a weak zwitterion polybetaine (PB) with a neutral polymer in aqueous environment (Figure 1.15). Interest to incorporate PBs into thin layers was greatly due to PBs' improved biocompatibility[212], antibacterial properties[213] and their utility for building bioinert coatings[214,215]. As a diazonium containing polycations is photosensitive, it would provide an alternative method for fabricating patterned surfaces[216].
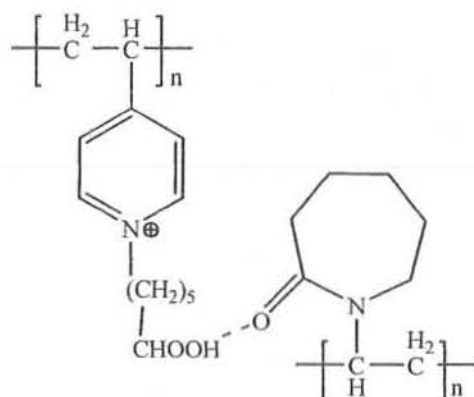
Figure 1.15: Hydrogen bonding between PB and PVCL units[211].

1.6.3 Covalent Layer by Layer Assemblies

To make grafts through covalent LbL is a new approach of surface modification having ancient roots. The preparation of oriental lacquer-ware started in 4000 BC in China and Japan is analogous to covalent multilayer assembly processes[217,218]. The sap used for the lacquer-ware coatings was an aqueous emulsion of phenolic lipids and polysaccharide-glycoprotein complexes derived from lacquer trees. The process that generates the product's high gloss and durable coating was an LbL process involving around 40 repeated *coating-drying-polishing-rubbing-drying* cycles. Enzymatic radical dimerization or polymerization of phenolics leads to covalent bonds during the drying cycle of that covalent LbL process.

Although ionic or hydrogen bonded self-assembly processes are experimentally simple and broadly useful, yet they have some drawbacks. In particular, ionic or hydrogen bonded LbL assemblies can disassemble under conditions where the ionic or hydrogen bonds are unstable e.g., strongly acidic, strongly basic or high ionic strength solutions can influence the multilayers stability. In still other cases, this tender disassembly of a multilayer grafts even provides advantages (e.g. in drug release applications[11]).

25

Nevertheless, some applications are better served by chemically more robust multilayer assemblies that withstand harsh conditions. Covalent LbL assembly process was patented by Decher group[219]. Since then, formation of covalent LbL assembled films has been an area of enormous investigation.

Earlier literature about the covalent LbL assembly concerns the condensation reactions between electrophillic polyfunctional or polymeric carbonyl compounds and a number of nucleophiles like amine, amide, ester, urea, urethanes, oxime, and imine etc. Owing to the extra stability of amide bonds, the most commonly employed LbL reaction is between amine and an activated carboxylic acid. Crooks and co-workers[220] performed sequential covalent assembly of polymers, using a copolymer of maleic anhydride reacted in alternation with a polyamidoamine dendrimer. After four reaction cycles, the film reached a thickness of 40–50 nm[220].

Bruening et al.[221] coated three layer pairs of Gantrez/PAH film to obtain a thickness of 27 nm on Al surface. The impedance of Al electrodes increased to 10 times after imidization of the covalent LbL assembly at 150°C. Grunlan and co-workers[222] developed covalent and ionic LbL assembly on functionalized polyethylene (PE) powder that results in conductive thin films. Li and colleagues[223] prepared fluorescent nanotubes with PEI and 3,4,9,10-perylenetetracarboxylic dianhydride and dianhydride inside the pores of alumina membranes. Alumina membrane was dissolved after 10 layer pairs to get 350 nm diameter nanotubes. Lynn et al.[224] demonstrated click route to the synthesis of covalent LbL assemblies of PEI and carbonyl group of poly(2- vinyl-4,4-dimethylazlactone) *via* a diamide of 2,2-dimethylglycine. The thickness of layer pair was 6 nm. Covalent LbL assembly method was applied on glass and gold substrates using polymer containing an aldehyde and an alkoxyamine to form oximes[225].

Gao and colleagues prepared covalent LbL assemblies of glutaraldehyde and PAH on MnCO$_3$ particles[226]. The template was dissolved to get stable microcapsules which indicate the successful cross linking of multilayers. Yang et al.[227] reported thiols containing a boronic acid group assembled on gold nanoparticles by covalent assemblies between polyvinyl alcohol and boronic acid. Electrophilic substitution by a polymeric aryl diazonium salt and an electron rich polymer formed from formaldehyde and *m*-cresol has successfully assembled grafts on quartz and sulfonated polystyrene

latex[228,229]. These were stable to solvents like dimethylformamide (DMF) and tetrahydrofuron (THF). Bergbreiter and co-workers used water as solvent for nucleophillic aromatic substitution of PEI and cyanuric chloride LbL grafts on silica[230].

Kohli and Blanchard[231,232] investigated various approaches to prepare multilayer films using a sequential covalent LbL scheme. Unlike the use of preformed polymers to form multilayer films, in these studies, the polymer is effectively grown in stepwise fashion, adding one molecular subunit per cycle utilising urea interlayer linking interfacial chemistry. Their first paper[231] investigated two variations in this theme: firstly the alternate reaction of diisocyanates and diamines (Figure 1.16) and secondly, reaction of isocyanate in the presence of small amount of water. In another approach, hydrolysis of isocyanate groups to get amine moieties followed by reaction with other isocyanate groups to form urea linkages.
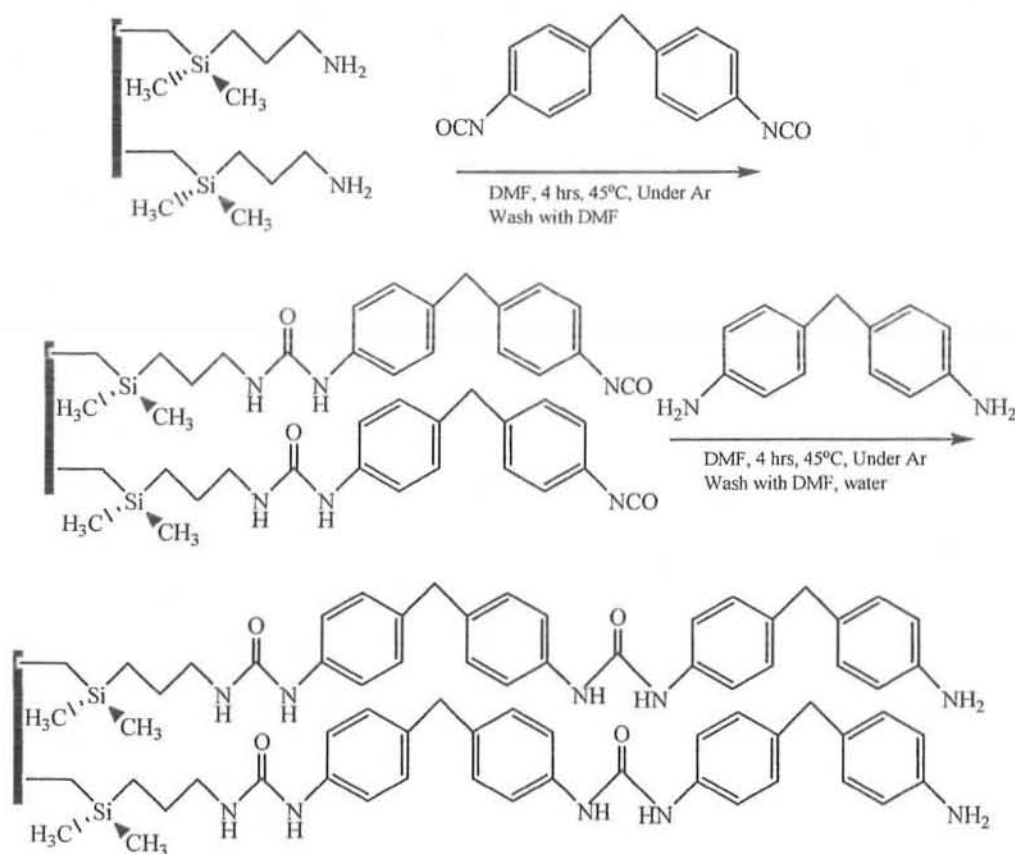
Figure 1.16: Multilayer film formations via urea linkages[231].

Linear growth of films assembled using the first approach was monitored by ellipsometry, with a total thickness of 9.8 nm for 7 layer pairs. Some deviations from

27

linearity were observed for the films assembled *via* the second approach, although the films obtained were considerably thicker (62.5 nm for 7 layer pairs). The thicknesses of these films were comparable to the polyelectrolyte multilayers prepared with conventional electrostatic LbL processes.

Further investigations were made in assembling an alternating hydroxyl phenyl maleimide and vinyl ether polymer with adipoyl chloride[233]. The adipoyl chloride reacts with the hydroxyl functionality to form covalently bonded layers. Linear film build-up was studied by using several techniques, with a thickness of 1.6 nm per layer pair.

The sequential covalent approach has been used to build poly(*p*-phenylenevinylene) polymers, which have potential application as conducting materials[234]. This was achieved by synthesizing two poly(*p*-phenylenevinylene) derivatives with amino and activated ester side chains. The LbL assemblies were formed by the alternation of the two materials which facilitated a condensation reaction between the two functional groups. Linear film build-up was observed using both UV-Visible absorption and ellipsometry, the later revealing layer pair thickness of approximately 0.8 nm. The stability of these films was demonstrated by sonication in THF for several hours without loss of any material.

Caruso *et al.*[235] reported click chemistry approach for the formation of covalent multilayers. The covalent linking methodology has generated significant research interest in the last few years due to its efficiency, inertness to functional groups, and mild reaction conditions. 1, 2, 3-triazole linkage was formed by the reaction between an alkyne and azide group at the interface. The linear growth of covalent layers was achieved using alternate PAA polymers with a 14% component of azide and alkyne functionality (Figure 1.17). These systems were assembled in aqueous conditions and were stable to a wide range of pH and various organic solvents.
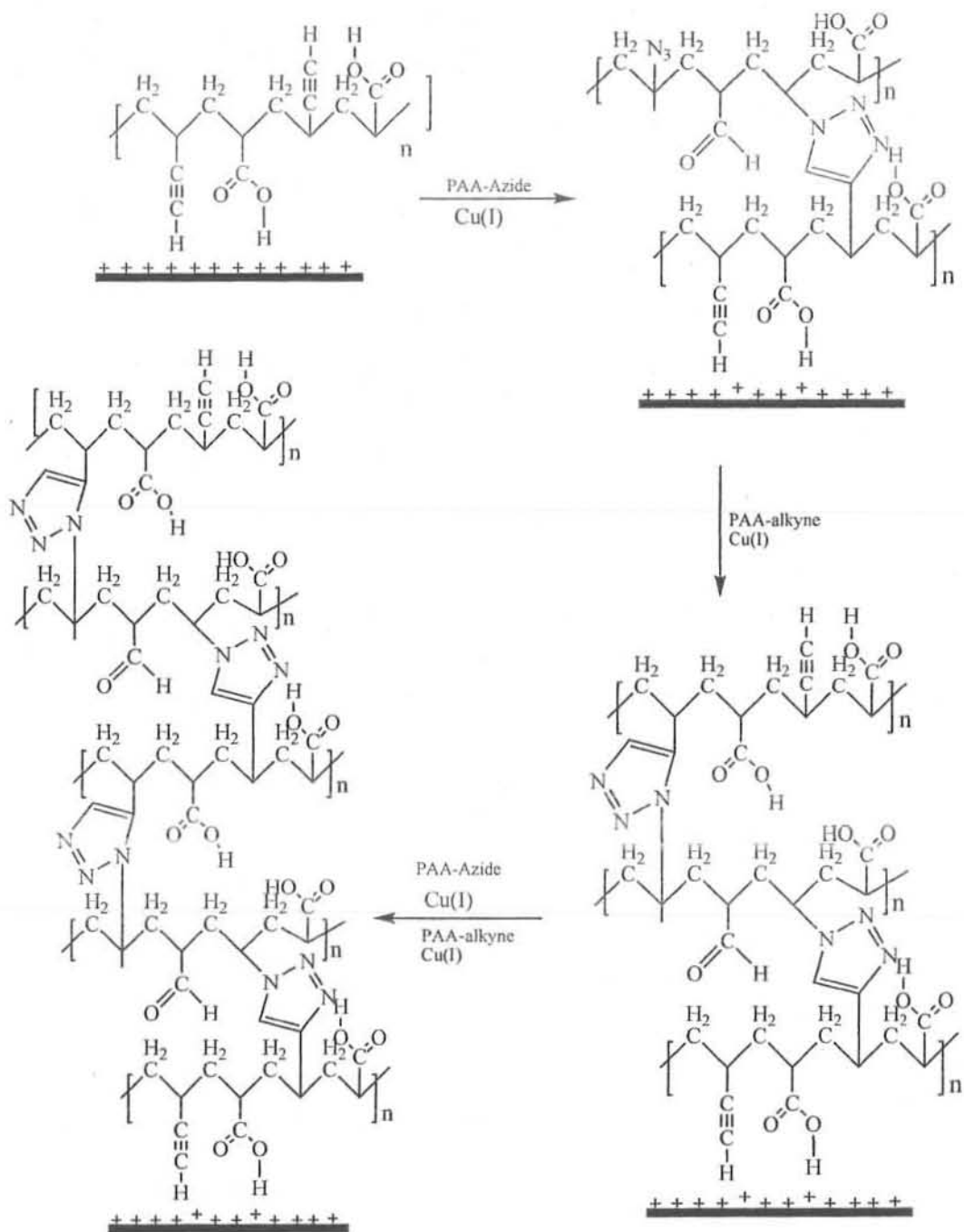
Figure 1.17: LbL assembly via stepwise triazole formation (click reaction). The initial layer was adsorbed electrostatically[235].

Covalent LbL assembly differs from ionic LbL assembly in a number of aspects.

- Ionic LbL assembly is the alternative adsorption of oppositely charged polyelectrolytes while polymers to be used in covalent LbL assembly

possess complementary functional groups that can form *in situ* stable covalent bonds.

- Ideally, such reactions occur under mild conditions and ambient atmosphere.
- Side products should be easily separated from the films so as to avoid film contamination.

Reactions that Sharpless has described as 'click' chemistry are ideal candidates for this sort of chemistry[236]. For applications that require functional robust thin films or nanocomposites, covalent LbL assembly has many advantages over traditional electrostatic LbL assembly methods [237]

- Covalently assembled LbL thin films are highly stable against harsh conditions such as extreme pH or extreme ionic strength.
- *In situ* covalent bond formation avoids the need for post assembly cross-linking.
- A large number of functional groups are available in polymers; so a number of reactions occurred during multilayer graft.
- The process can be carried out in either aqueous or organic solutions depending on the type of reactions. This can be advantageous if it is desirable to incorporate materials that do not dissolve or that cannot be used in the aqueous solutions.
- Covalent bond formation is spontaneous and energetically favourable process. So a newly deposited layer cannot readily disassemble from the previous layer. This makes it possible to incorporate low functionality molecules during the LbL process.

A covalent LbL assembly process leaves behind excess reactive groups inside the multilayer matrix that can further react with other molecules to tailor the product. This can all be done by using various combinations of small molecules with polymers, polymers with polymers, or polymers with nanoparticles to form products of varying composition. Click chemistry has provided a novel route for the formation of covalent LbL assemblies for nanocomposites and robust ultrathin formation. In the coming days, the scope of this particular chemistry for the formation of covalent LbL assemblies will be much attractive for nanotechnology and biomedicine.

1.7 Mechanical Robustness Studies of Multilayers

First and foremost among the motivations for fabricating robust multilayers is the desire to exploit them for applications that require a stable structure under harsh environment. Methods for fabricating robust multilayer assemblies have been developed by Zhang *et al.*[200], Bruening and colleagues[185] and Rubner and co-workers[199]. The concept of improving the stability of multilayer assemblies was further extended to hydrogen bonding assemblies[197]. Sun *et al.* fabricated robust multilayers *via* LbL to produce chemically modified electrodes[238]. The electrodes exhibit a high mechanical stability in a solution of high ionic strength. Mechanical properties of the electrostatic self assembled (ESA) films have been investigated using "tape peel tests"[239]. Scanning force microscopy (SFM) technique was employed for the study of surface mechanical properties with a submicron resolution. In a SFM experiment, the tip acts as a model single-asperity contact, combining careful control of the applied force with *in situ* microscopic analysis of the modified region.

Surface mechanical properties of polyelectrolyte multilayer films have been studied by AFM as force to distance measurement experiments. A few investigations were also conducted to determine dynamic interactions and friction in single layer polyelectrolyte film[240,241,242]. Elasticity measurements for a series of PAH/P-Azo polyelectrolyte LbL films manufactured at various pH values was conducted to determine the mechanical nature at various charge densities[243].

The physical and chemical stability of a nano-structured device are key parameters in its potential applications. Mechanical properties of LbL assembled films have been extensively studied by several groups. Donath *et al*[244] determined the Young's modulus of LbL assembled $(PSS/PAH)_n$ capsules around 700MPa. Vinogradova *et al.*[245,246,247] investigated the Young's modulus of LbL assembled polyelectrolyte films around 100-200MPa. He further suggested that the Young's modulus of LbL assembled polymer films was related to thickness of films and also proposed the theory of ionic strength to explain the Young's modulus difference in different polymer couples. The mechanical properties of fully charged strong polyelectrolyte (PSS) are better than partially charged weak polyelectrolyte (PAH). Cohen *et al.*[248,249] suggested that the wear property of the $(PAH/PAA)_n$ films is also strongly associated with films thickness. In nano-indentation experiment, a $(PAH/PAA)_n$ film with 70 nm thickness can protect efficiently the steel substrate[248]. Kotov and co-workers[250,251] observed LbL assembled films with

nanometric metallic or inorganic compounds demonstrate a considerable increase in mechanical properties and pointed out that phase separation was responsible for mechanical failure in hybrid materials. Free standing poly(diallydimethylammonium) chloride (PDDA) / montmorillonite clay films, have a Young's modulus of the order of 11GPa, compared to those of plywood bones 6-16GPa[250] and natural nacre (64GPa)[250]. Fery *et al.*[252] studied the Young's modulus of sprayed LbL assemblies of Au-NPs and different polyelectrolytes, a chemical covalent cross-linking treatment has been done after film formation. The Young's modulus of such films varies from 0.4GPa to 2.3GPa. With excellent mechanical properties of LbL assembled films, fabrication of free-standing polymer or hybrid membrane becomes possible[250,253].

Most of the LbL films studied so far can be considered in general as nonductile structures, while many applications, such as flexible electronics or biomedical coatings, need enhanced ductility and toughness. Nearly all LbL films show elastic moduli typically of a few GPa[250,254, 255 256, 257,258] (as high as 106 GPa[259]) and only a few percentiles of ultimate strain. Two recent examples of hydrated multilayers and LbL nanotubes were shown to be much "softer" in nature, with elastic moduli of only tens to a few hundreds of MPa; however, no strain data were provided[260,261]. Lutkenhaus *et al.*[262] pointed out that hydrogen bonded multilayers of PEO and PAA have tensile modulus of 2MPa and ultimate tensile strain of 360%.

Schönhoff *et al.*[263] proposed a theoretical model to explain mechanical behaviour based on residual water content in multilayer thin films. In a freshly prepared (PSS/PAH)$_n$ films, this immobilized water volume fraction can be up to 56%. A polyions complex can associate 6-8 water molecules[263,264] and multilayer are capable to swell and deswell after formation. A high percentage of hydrated films are supposed to have weak mechanical properties. In hybrid LbL assembled materials; the incorporated materials will fill the void place, resulting in the expulsion of trapped water. So a decrease in the percentage of hydration water in films matrix leads to improved mechanical properties.

Podsiadlo *et al*[265] prepared LbL composites using water-soluble polyurethanes (PUs). The preparation of millimetre thick composites by hierarchical stacking of "exponential" LbL films composed of cationic PU (Cat PU) and PAA is shown in Figure 1.18. Individual 70 μm thick films showed ultimate tensile strain of approx. 250%, ultimate tensile strength of approximately 30 MPa. These LbL films were highly

robust and ductile with ultimate strains reaching as high as 680%. This result is more than 2 orders of magnitude greater than most LbL assemblies prepared thus far.
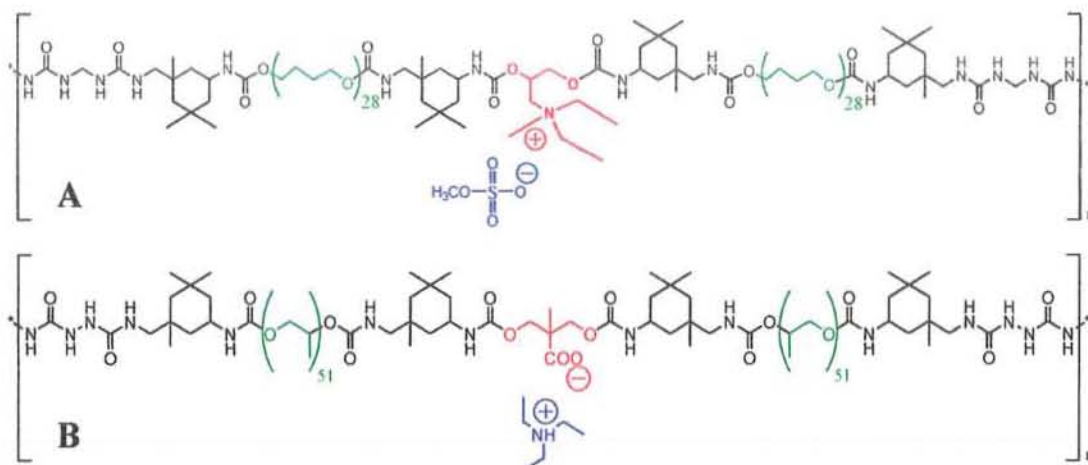
Figure 1.18: Chemical structures of (A) Cat and (B) An-PUs. Charged groups are highlighted in Red, counterions in Blue, and soft segments in Green[265].

Most of the studies so far focused on mechanical properties of LbL assembled multilayer films including tensile strength, stretch or elastic properties etc. Very few have focused on wear properties of films[266]. Nanoindentation is a powerful investigation technique in wear property study of multilayer films, and has been widely used. However, this technique provides limited information about a localised region. So far, no wear behaviour on macroscopic scale is available. For real applications, the homogeneity of the mechanical response of a material should be investigated as well.

1.8. Commercial Applications of LbL Assembled Films

The use of both LB and SAMs ultra-thin film formation technique was limited due to lack of their commercial applications. The versatility of LbL multilayer technique, in terms of ease of fabrication, surface functionalization by combining a large number of polymeric and macromolecular species, nanoparticles, colloids, biological materials etc. on any substrates surface regardless of its shape and size and speed of surface modification offers the accessibility of this technique to a growing number of real world commercial applications. The LbL multilayer technique requires minute quantities of the polymeric materials and the formation of no byproducts, may rightly be called, environmental friendly technique.

Derived originally from "Bola" molecules, the LbL self-assembly technique has been offering solutions to a number of problems in many different fields. For example,

catalytic membranes can be fabricated by alternate LbL adsorption of polyelectrolytes and metal nanoparticles on porous supports[267]. Besides traditional planar substrate, polyelectrolyte multilayer can be assembled on spherical substrate by using nanoparticle template, which makes the fabrication of hollow capsule possible. These hollow capsules are frequently used for drug delivery purpose in addition to dye dispersion industries and catalysis reported by several groups[268,269]. After many years of laboratory research activities, a few commercial products based on LbL self assembly technique have now been marketed.

An important real world application of the LbL assembly is the Yasa-Sheet, which was developed by Shiratori from Keio University Japan (Figure 1.19).

Figure 1.19: Yasa Sheet marketed by Shiratori from Keio University Japan[51].

The Yasa sheets have a multilayer film containing an enzyme extracted from bamboo that controls the ethylene concentration and thus extends the shelf-life of fruits and vegetables[51]. The Yasa Sheets has achieved excellent product award from Nikkei in 2001.

The LbL coated contact lens gave very accurate measurement of contact angle as compared to non-coated contact lenses. This property was utilised by Ciba-Vision to market their first commercial contact lens coated with a multilayer (Figure 1.20).

Figure 1.20: Photographic image of CIBA-Vision's Focus contact lens based on LbL films.

Looking back at the history of LbL technique, many questions were frequently heard in its early years like, "pre-adsorbed layers should desorb upon deposition of the next layer "; "LbL multilayer coating are not stable"; "LB technique did not work for any applications so why should LbL" ? But marketing of all these commercial products contradicts all initial worries associated with this technology. This is just a beginning of a number of real world applications of LbL.

1.9 Epoxy Resins

The term epoxy, epoxy resin, or epoxide refers to a broad group of reactive compounds that are characterized by the presence of at least two oxirane[270] or epoxy rings as shown in Figure 1.21.
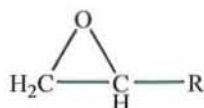
Figure 1.21: Structure of oxirane ring.

Oxirane is a three-member ring with an oxygen atom linked to two already bonded carbon atoms[271,272] Epoxy groups are capable of reacting either with suitable curing agents or catalytically homopolymerized to form high molecular weight polymers. Once cured, the epoxy polymers have a densely cross linked, thermosetting structure with high cohesive strength and adhesion properties[273]. However, the term epoxy can also be used to indicate an epoxy resin in the thermoplastic or uncured state. A general formula for an epoxy resin can be represented by a linear polyether with terminal epoxy groups and secondary hydroxyl groups occurring at regular intervals along the length of the chain (Figure 1.22).
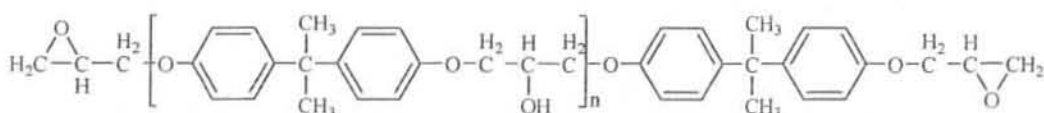
Figure 1.22: Structure of diglycidyl ether of bisphenol-A (DGEBA)

The synthesis of epoxy resins began in the late 1890s[274]. Schlack[275] patented reaction products of amines with epoxies, including one epoxy based on bisphenol-A and epichlorohydrin. Castan[276] and Greenlee[277] documented the commercial importance of epoxy resins. Castan produced a low melting epoxy resin from bisphenol-A and epichlorohydrin that yielded a thermosets composition with phthalic anhydride[276].

The major use of epoxy resins was as protective surface coatings and still this is the major consumption sector. Swern synthesised epoxy resins by the epoxidation of polyolefins with peroxy acids[278]. Dow developed the phenol novolac epoxy resins[279] while Shell introduced polyglycidyl ethers of tetrafunctional phenols, and Union Carbide developed a triglycidyl p-aminophenol resin. These products proved their commercial importance in highly demanding applications such as semiconductor encapsulants and aerospace composites where their performance justifies their higher costs relative to bisphenol-A based epoxies. Several important statements can be made relative to the structure of the epoxy molecule[280]:

- The epoxy groups at terminals of the molecule and many hydroxyl groups at the backbone of the molecule are highly reactive. The outstanding adhesion of epoxy resins is largely due to the secondary hydroxyl groups located along the molecular chain (Figure 1.22) as epoxy groups are generally consumed during curing process.

- Aromatic rings on epoxy resin backbone, provides a high degree of heat and chemical resistance.

- The presence of aliphatic groups confers chemical resistance and flexibility.

- The epoxy resin can be of different molecular weight, viscosity, liquid or hard solids. Low viscosity is helpful in good penetration and wetting.

- Based on the curing agents used and curing conditions, an epoxy resin can cure slowly or very quickly at room or at elevated temperatures.

- Epoxies exhibit low shrinkage as there is no by-product of curing and they can be cured under very low pressure. This provides an adhesive joint with a very low degree of internal stress when cured.

The epoxy resins are used widely as adhesives, high performance coatings[281] including paints, varnishes[282,283], dyes and also encapsulating materials[284]. Epoxies have excellent electrical properties[285,286], low shrinkage, good adhesion to many metals, flame retardancy[287], resistance to moisture[288] and thermal and mechanical shock[289]. Epoxy resins are characterised by many parameters like viscosity[290], epoxide equivalent weight[291, 292] and molecular weight. In spite of many favourable properties and extensive use in many industrial applications, one major drawback is their high brittleness[293].

Commercially produced epoxy resins are not necessarily completely linear or terminated with oxirane rings. Sometimes branching may occurs, with the end groups being either epoxy or hydroxyl. Various end groups can be introduced as a result of the manufacturing process. The extent and degree of branching vary from resin to resin and from supplier to supplier. Functionality of an epoxy depends on number of epoxy groups in a molecule[273]. In addition to bifunctional epoxy resins, tri-, tetra-, and polyfunctional epoxies are also available. The ratio of the main ingredients used in the synthesis of epoxy resins (epichlorohydrin, bisphenol-A, phenol novolac etc.) determines the extent of the reaction and the molecular weight (or value of n i.e. repeat units). As the number of repeat unit increases, the physical properties like viscosity and melting point also increases. The number of hydroxyl groups also increases for higher value of n, while the number of epoxy groups remains constant. An important term that is used in formulating epoxy adhesive compositions is epoxy equivalent weight (EEW)[273]. This may be defined as the weight of resin in grams that contains one equivalent of epoxy. As the molecular weight of resin increases, the EEW will also increases.

1.10 Types of Epoxy Resins

There are innumerous types of epoxy resins, but only a few of these are discussed here;

1.10.1 Diglycidyl Ether of Bisphenol-A (DGEBA)

Epoxy resins were first marketed by Ciba-Geigy in 1946, although their development began decades earlier. The most common commercial epoxy resin is formed from the

reaction of bisphenol-A and epichlorohydrin. This resin is known as the diglycidyl ether of bisphenol-A or DGEBA (Figure 1.22).

1.10.2 Epoxy Novolac Resins

Epoxy novolac resins are polyglycidyl ethers of a novolac resin[294]. Polyhydric alcohols having more than two hydroxyl groups per molecule (e.g. phenol novolac resins and *o*-cresol novolac resins) can be reacted with epichlorohydrin to produce epoxy novolac resins with structure shown in Figures 1.23 and 1.24. The epoxide functionality depends on the number of hydroxyl groups in the phenol novolac molecule and also to the extent to which they are reacted. Thus, selective epoxidation is usually practiced as complete epoxidation limits the useful size of the cured polymer. The epoxy novolacs are high-viscosity liquids or semisolids, and they are often mixed with other epoxy resins to improve handling and formulation properties. The thermal stability of most epoxy novolac systems is affected by the length of the cure cycle. Epoxy novolacs usually produce a product with improved elevated-temperature performance[295], chemical resistance, adhesion and mechanical properties, superior electrical properties, and heat and humidity resistance when cured with any of the conventional epoxy curing agents as compared to those of the bisphenol-A based cured resins[296]. Thus, epoxy novolacs are used in structural adhesive systems that require high-temperature performance. A high temperature cure is performed to get the maximum properties of an epoxy novolac. While at room temperature cures, the properties of the final product are similar to those of conventional DGEBA systems.

1.10.2.1 Phenol Novolac Epoxy Resins (PNER)

Phenol novolac epoxy resins (PNER) are multifunctional commercially important epoxies obtained by the epoxidation of phenol formaldehyde novolacs (Figure 1.23). With increase in the functionality, molar mass of the resin also increases. The epoxy functionality in PNER is between 2.2 and 3.8[296]. When cured with polyamide or aliphatic polyamines and their adducts, epoxy novolac show improvement over bisphenol-A epoxies, but the critical performance of each cure is limited by the performance of the curing agent. The improved thermal stability of PNER based thermosets is useful at elevated temperature performances, such as aerospace composites. Chemical process equipment and corrosion-resistant coatings are typical applications taking advantage of the chemical resistant properties of PNER resins. PNER based systems cure more rapidly than DGEBA epoxy resins with higher

exotherms. However, epoxy novolac form very rigid and brittle polymers when fully cured because of their high crosslink density. So they are often used as modifiers in epoxy adhesive systems rather than as the base polymer.
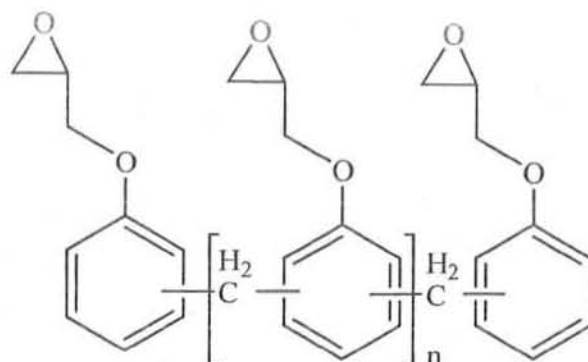
Figure 1.23: Structure of phenol novolac epoxy resin (PNER).

1.10.2.2 Cresol Novolac Epoxy Resins (CNER)

The *o*-cresol novolac epoxy resins (CNER) are analogous to phenol novolac epoxy resins. The only differences being the presence of methyl functional groups at ortho position of the aromatic ring in CNER epoxy (Figure 1.24). The CNERs have greater functionality (generally 2.3 to 6.0) as compared to conventional DGEBA resins, and the increased crosslink density results in greater temperature and chemical resistance[296].
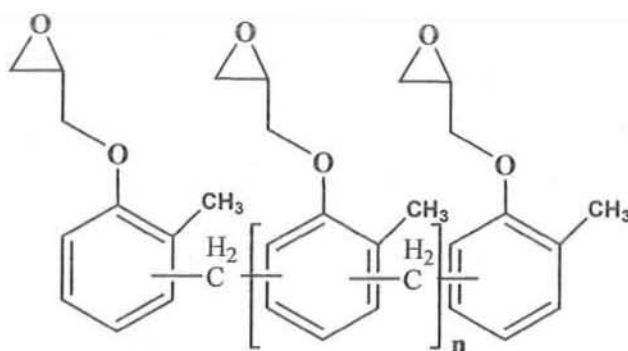
Figure 1.24: Structure of cresol novolac epoxy resin (CNER).

CNER exhibits better formulated stability and lower moisture adsorption than PNERs, but they have higher costs. Cresol based epoxy resins are widely used as base components in high performance electronic (semiconductors) and structural moulding compounds, high temperature adhesives, castings and laminating systems, tooling, and powder coatings.

1.10.3 Bisphenol-F Resins (DGEBF)

Diglycidyl ether resins based on bisphenol-F (DGEBF) have been synthesized to provide cured epoxy resins with greater flexibility and lower softening temperatures as compared to conventional DGEBA epoxy resins. These are prepared by the condensation of phenol to formaldehyde ratio in large excess[286]. Three isomers are possible depending upon the pH of the reaction medium as substitution can occur at the ortho-, meta-, or para- positions. The DGEBF resins have much lower viscosity than their DGEBA counterparts for the same *n* value. The lower viscosity of DGEBF resins provides far greater latitude in formulation. The major disadvantage of bisphenol-F epoxy resins is their higher cost as compared to DGEBA resins. Bisphenol-F based epoxy resins (Figure 1.25) are analogous to DGEBA based epoxy resins in most respects as they can be cured using similar curing agents and reaction mechanisms as do DGEBA epoxies. Bisphenol-F epoxies are often used in blends with DGEBA resins to lower the viscosity or to modify some other properties.
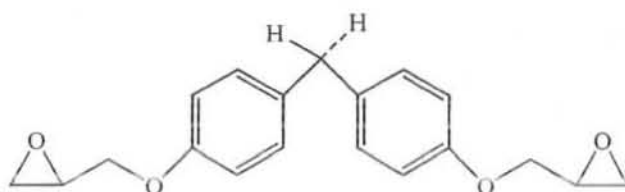
Figure 1.25: Structure of diglycidyl ether of bisphenol F.

1.10.4 Tetraglycidyl Ether of Tetraphenolethane

Tetraglycidyl ether of tetraphenolethane is an epoxy resin having high temperature and high-humidity resistance. It has a functionality of 3.5 and thus exhibits a very dense crosslink structure (Figure 1.26). It is used in the preparation of high-temperature adhesives. The resin is commercially available as a solid (e.g., EPON Resin 1031, Resolution Performance Polymers). It can be cross linked with aromatic amines or a catalytic curing agent to induce epoxy-to-epoxy homopolymerization at high temperature.
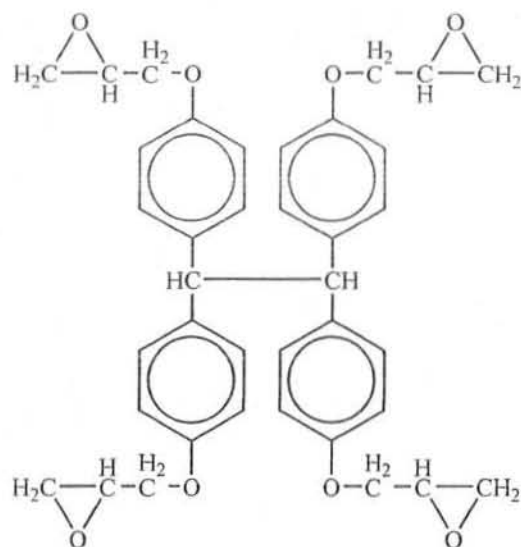
Figure 1.26: Structure of tetra glycidyl ether of tetraphenolethane.

1.10.5 Glycidyl Amine Epoxy Resins

Glycidylamine based epoxy resin are reaction products of aromatic amines and epichlorohydrin. They have high modulus and high glass transition temperature. These resins have been used in aerospace composites and high-temperature adhesive formulations. The most important resin in this class is tetraglycidyl diaminophenylmethane (TGDDM) with trade name Araldite MY-720, as shown in Figure 1.27. This resin is used widely in advanced composites for aerospace applications due to its outstanding high temperature properties. These resins are more costly than either the bifunctional bisphenols or the various novolacs. Advantages of TGDDM resins include excellent mechanical properties and high glass transition temperatures. Glycidyl amines are high viscosity liquids or semisolids at room temperature. Large amounts of epichlorohydrin produces lower molecular weight resins[297,298].
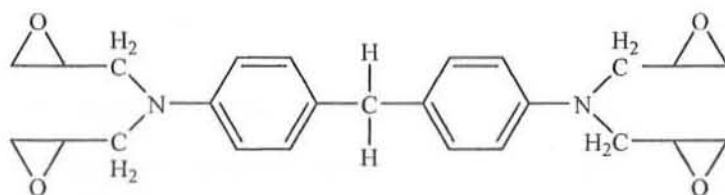
Figure 1.27: Structure of Araldite MY-720.

1.11 Curing of Epoxy Resins

The epoxy resins are capable of reacting with a variety of curing agents or with themselves in the presence of a catalyst to form solid, cross linked materials with considerable strength and adhesion. This transformation is generally referred to as curing or hardening. Curing is carried out by the addition of a chemically active compound known as a curing or hardening agent. Depending on the nature of epoxy formulation, curing may be accomplished at room temperature with the application of external heat, or with the application of an external source of energy other than heat such as ultraviolet[299] , TG-FTIR[300] or microwave[301]. Two primary types of epoxy curing reactions are possible:

- Polyaddition reactions
- Homopolymerization reactions

Both polyaddition and homopolymerization reactions can result in increased molecular weight and cross linking. The curing reactions occur without the formation of byproducts and are exothermic, and the rates of reaction increases with temperature. Since the epoxy resin cures primarily by a ring-opening mechanism, it exhibits a smaller degree of cure shrinkage than other thermosetting resins. The homopolymerization reactions in general require higher temperature cure as compared to polyaddition. However, most curing agents or catalysts will react, at least partially, with the resin at room temperature if given a long enough time.

1.11.1 Polyaddition Reactions

Polyaddition is the most commonly used type of reaction for the cure of epoxy resins. When curing takes place by the reaction of epoxy molecule and other kinds of reactive molecules with or without the help of a catalyst, the reaction is called polyaddition reaction. The resulting cured structure is a heteropolymer that is composed essentially of epoxy resin molecules linked together through the reactive sites of the curing agents. The polyfunctional curing agent makes up a significant portion of the epoxy formulation. The curing agents used in this type of reaction have active hydrogen like amines, amides, and mercaptans. For polyaddition curing, the most important curing agents for adhesives are primary and secondary amines containing at least three active hydrogen atoms and various di- or polyfunctional carboxylic acids and their anhydrides. A generalized polyaddition reaction of an active hydrogen compound and

an epoxy molecule is represented in Scheme 1.1. Hydroxyl groups, especially phenolic hydroxyls, and tertiary amines catalyze this reaction.
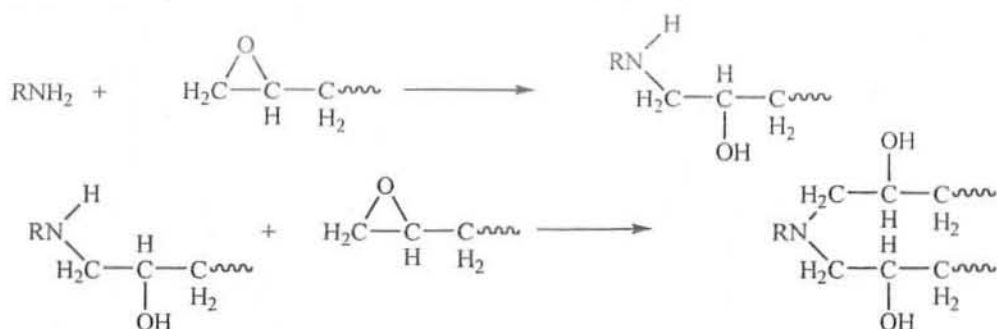
Scheme 1.1: Polyaddition reaction of an epoxy resin with an active hydrogen compound.

1.11.2 Homopolymerization Reactions

This is the self curing process among the reactive epoxy molecules (Scheme 1.2). The cured network is essentially made up only of the original epoxy molecules linked together through their own reactive sites. Thus, the properties of cured epoxy system are mainly due to the nature of epoxy resin alone. Homopolymerization provides better heat and environmental resistance as compared to polyaddition reactions. Homopolymerization requires the presence of both catalysts and high temperatures for the reaction to proceed. Like the polyaddition reaction, the homopolymerization reaction is also accelerated by hydroxyl groups or tertiary amines.
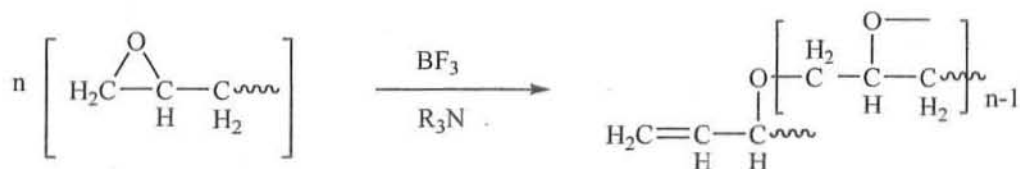
Scheme 1.2: Homopolymerization reaction of an epoxy resin compound.

1.12 Epoxy Curing Agents

1.12.1 Amine Curing Agents

Amines are one of the most common types of epoxy curing agents for multifunctional epoxy compounds[302]. The amines can be categorised as primary, secondary and tertiary. Aliphatic amines, such as diethylenetriamine or triethylenetetramine (TETA), were the first curing agents used for epoxy resins. The functionality of an amine hardener depends on the availability of active hydrogen atom bonded to nitrogen atom.

Thus two active hydrogen atoms are available for curing in case of primary amine while one in secondary and none in tertiary amine hardeners. Epoxy curing by a primary amine hardener is shown in Scheme 1.1[303]. Primary amine hardeners react rapidly at room temperature as compared to secondary amine curing agents[304,305]. The curing mechanism of epoxy with primary amine results in secondary amine and secondary alcohol. The secondary amine in turn reacts to give tertiary amine and two secondary alcohol groups (Scheme 1.1). Tertiary amine catalyses the reaction between excess epoxy and the hydroxyl groups so produced[306].

In general, reactivity of amines toward aromatic glycidyl ethers follows their nucleophilicity: aliphatic amines > cycloaliphatic amines > aromatic amines. Aliphatic amines can cure aromatic glycidyl ether resins even at room temperature without accelerators, whereas aromatic amines require higher temperatures.

Epoxy resins cured with aliphatic amines will blush and produces an oily surface under humid conditions. This is due to the reaction of the primary hydrogen atom of amine with carbon dioxide. A tertiary amine is often used as an accelerator in primary amine systems to correct for the problem of blushing[307]. Tertiary amines are also used as catalysts for homopolymerization of epoxy resins and as accelerators with other curing agents.

TETA, tetraethylenepentamine (TEPA)[308] diethylaminopropylamine (DEAPA), *m*-phenylenediamine (MPDA), and diaminodiphenyl sulfone (DDS) are the most commonly used primary amines. These give ambient or elevated temperature cure near stoichiometric ratios. Ethylenediamine is too reactive to be used in most practical adhesive formulations. Polyoxypropyleneamines (amine-terminated polypropylene glycols) give superior flexibility and adhesion. Some aromatic and aliphatic amines are shown in Figure 1.28.

Diaminodiphenylmethane

Diaminodiphenyl sulfone

triethylenetetramine

tetraethylenepentamine

Poly(oxypropylene triamine)
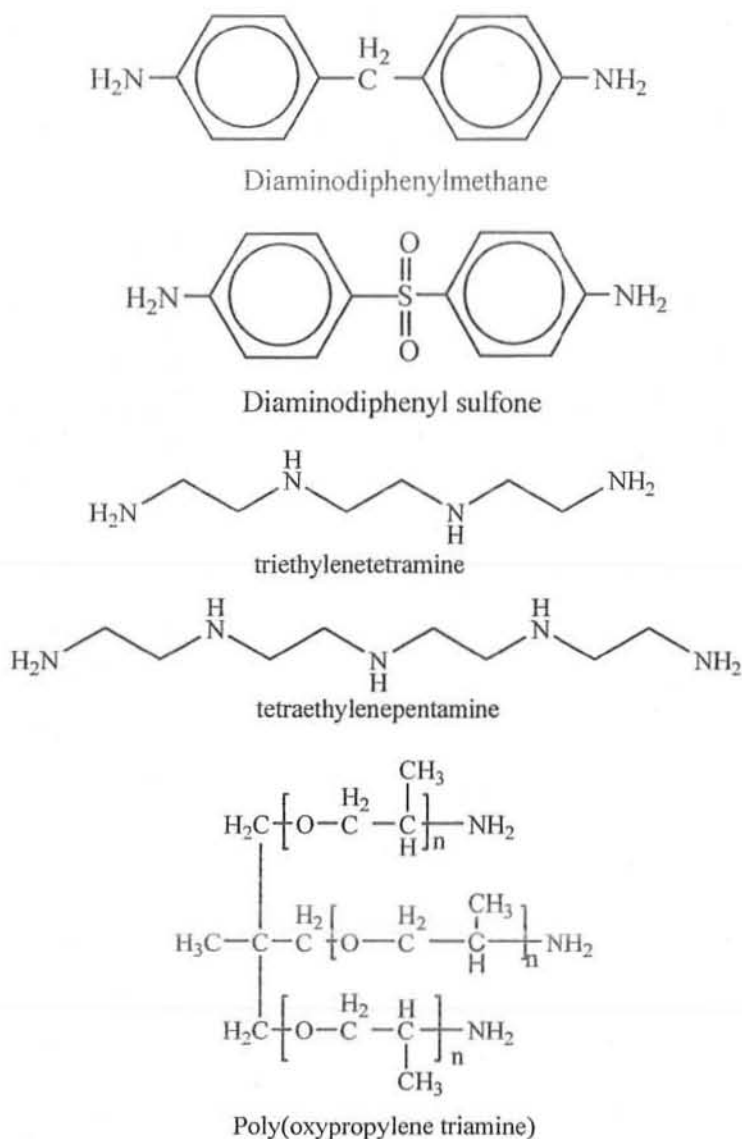
Figure 1.28: Structure of some aromatic and aliphatic amines used for epoxy curing reactions.

1.12.2 Polyamide Curing Agents

Polyamide curing agents are the reaction products of dimerized fatty acids and aliphatic amines like diethylenetriamine. This introduces a bulky, oil compatible, C36 carbon group between the amine sites. These are prepared by adding the fatty acid to an excess of amine. Polyamides are available in a wide range of viscosities that can be achieved by varying the amine/acid molar ratio in the reaction. The reactive functional groups are the terminal primary and internal secondary amine groups along the backbone of the polyamide. Commonly, polyamides are used as room temperature curing agents. These products have higher molecular weight than primary amines and, therefore, exhibit lower vapour pressure and resulting in lower irritation potential.

45

Higher concentrations of the curing agent yields increased flexibility and adhesion but reduces heat distortion temperature and chemical resistance. Polyamide cured DGEBA epoxies provide improved flexibility, moisture resistance, and adhesion over aliphatic amines alone. However, polyamide cured epoxy resins are generally inferior in thermal resistance and shear strength due to the reduction in crosslink density. Polyamide cured epoxy resins lose structural strength rapidly with increasing temperatures.

1.12.3 Anhydride Curing Agents

Besides primary amines, acid anhydrides are the next most important class of epoxy curing agents, although these are not commonly used in adhesive systems. The most common types of anhydrides are hexahydrophthalic anhydride (HHPA), phthalic anhydride (PA), nadic methyl anhydride (NMA), and pyromellitic dianhydride (PMDA). Anhydrides do not readily react with epoxy resins except in the presence of water, alcohol, or some other base, called an accelerator. Tertiary amines, imidazoles, and metallic salts often act as accelerators for epoxy curing of anhydride. The reaction of anhydrides with epoxy groups is complex, however, their use in adhesive formulations is limited except for high temperature applications because of the rather slow reactivity, long and elevated-temperature cure requirement and inferior adhesion compared to amine cured epoxies. The most important anhydride in epoxy adhesive formulations is PMDA (Figure 1.29), which provides very high temperature resistance properties.

Pyromellitic dianhydride
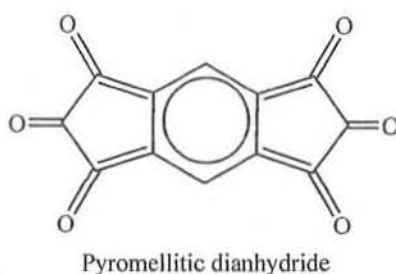
Figure 1.29: Structure of pyromellitic dianhydride.

1.13 LbL Assembly of Gold Nanoparticles

Colloidal gold also known as "nanogold" is an aqueous suspension of micrometre to nanometre sized gold particles. As one of the stable noble metal nanoparticles, the use of colourful aqueous solution of gold colloids can be dated back to Roman times[309]. The notation of gold nanoparticle was first introduced by Michael Faraday[310] in 1857

for "activated gold". Astruc[311] reviewed synthesis of Au-NPs as well as their functionalization by using a number of methods. Properties of Au-NPs were also discussed in detail. Michael Faraday introduced a method for the reduction of a solution of gold chloride by phosphorus. At present, the most commonly used method for the synthesis of Au-NPs is by the citrate reduction of $HAuCl_4$ in aqueous solution, reported by Natan *et al.*[312]. Synthesized Au-NPs are stabilized and surrounded by negatively charged citrate ions as shown in Figure 2.2. Most of the previously described work was related to the chemical coupling reactions on the gold surface but there was no general method for the functionalization of Au-NPs.

Most of the nanoparticles have relatively low dispersion stability except gold. Therefore, Au-NPs were used in the fabrication of a large number of multifunctional materials[313,314]. Au-NPs are finding important applications in a large number of fields based on LbL self-assembly. Decher *et al.*[315] fabricated Au-NPs/polyelectrolyte LbL assembled multilayer showing linear growth. One characteristic property of Au-NPs is their strong surface plasmon interactions, caused by electronic clouds of free electrons on the surface. This strong surface plasmon interaction between two adjacent Au-NPs layers causes a 120 nm red shift in plasmon absorption band. However, such interactions can be minimized either by increasing the distance between the two adjacent Au-NPs layers[315], by changing the environment of adsorbed Au-NPs[316], or by applying proper post-treatment, such as annealing[317].

Covalent multilayer film formed by the UV irradiation of DAR and Au-NPs was introduced by Zhang *et al*[318]. Schneider and Decher[319] claimed that core/ shell nanoparticles prepared *via* LbL were so stable that they can be centrifuged. Till the deposition of 20 layer pairs, there was little aggregation of Au-NPs. LbL approach demonstrated a novel method for the functionalization of nanoparticles in aqueous media, thus limiting the risk of ligand exchange reactions. UV-Visible spectroscopy and TEM confirm that fluorescent labelled core/shell Au-NPs were stable at all stages of their formation[320]. Various parameters for the build-up of LbL Au-NPs assemblies were optimised later on to discover that best yield of functional nanoparticles was obtained at higher polyions concentrations[321].

Labbe and co-workers[322] and Natan and colleagues[323] independently observed redox and conductive behaviour of Au-NPs films respectively. Natan measured the resistivity

of Au-NPs films as 5×10^{-4} Ω cm which was in good agreement to that of pure gold $(2.4\times10^{-6}$ Ω cm). Au-NPs/polyelectrolyte multilayers described so far were assembled *via* dipping process with typical Au-NPs adsorption time of around 4-6 hrs[315]. This adsorption time can be greatly reduced with the help of spraying technique. Fery *et al.*[324] demonstrated the use of spraying LbL technique for the construction of Au-NPs multilayer films. Spraying LbL technique is much faster as compared to dipping for the construction of Au-NPs.

Since their discovery, Au-NPs are finding increased utility as hybrid organic inorganic and bio-inorganic applications in various fields as diverse as optical, electronic, magnetic, catalytic and biomedical. Particularly, their extra-ordinary stability, complete biocompatibility, variety in modes of synthesis (like bio- and template synthesis), and a number of benign properties paved the way for their future role in nano-science, nanotechnology, bio-sensing, bio-nanotechnology and materials science. Another fascination of Au-NPs is their optoelectronic property related to surface plasmon absorption reflecting the collective oscillation of electrons of Au core. The combination of photonic property of Au-NPs with medicine and biology has paved the way for bio-molecular manipulation of DNA labelling, detection and genetic disorders. Biosensors and environmental sensors utilise the fluorescence, luminescence and electrochemical characteristics of Au-NPs with DNA, sugars and bio-molecules.

In a nutshell, a number of structures based properties and applications of Au-NPs in interdisciplinary research involving chemistry, physics and biology are to be explored in coming future. But for a number of surface based applications, mechanically strong and/ or protected Au-NPs are required. For this purpose the electrostatically assembled Au-NPs are being coated with mechanically strong protective layer to be used in future applications in present research work.

1.14. Mechanically Robust Ultra-thin Films Using Epoxy Oligomers

Multifunctional polymers in LbL self-assembly can be linked not only by electrostatic interaction but also by Van der Waals interactions, hydrogen bonding and covalent interactions to form a 3-D network. Among such polymeric substances, epoxy is an interesting class of compounds which can be cured *via* the formation of numerous covalent linkages with curing agents. Generally epoxy resins can be cured or cross-linked with a number of reagents to form structural adhesives. Epoxy novolac resins are

known for their excellent adhesion, chemical and thermal stability[325] and excellent mechanical properties as well as flame retardant[326] behaviour.

A major drawback of epoxy resins, however, is their high brittleness and notch sensitivity. A number of efforts were made to improve the toughness of the epoxy compounds[327,328]. Gleason et al.[329] prepared a mechanically strong nano-adhesive film using poly(glycidyl methacrylate) (PGM) and PAH polymers. A number of substrate can be used for the deposition of (PGM/PAH)$_n$ film including silicon, glass, quartz, poly(ethylene terephthalate), poly(carbonate) and poly(tetrafluoro ethylene). In order to modify the behaviour of epoxy resins, carbon nanotubes (CNT) were also used which provides reinforcement in composites so formed. Grujicic et al.[330] showed the excellent mechanical behaviour of multilayer prepared with poly(vinyl-ester-epoxy) reinforced with multi-walled carbon nanotubes (MWCNT). Although, epoxy resins are usually soluble in organic solvents; the application of epoxy based materials in biological field has also been indicated in areas such as in enzyme immobilization[331]. The amino epoxy films allow a rapid enzyme immobilization process to be carried out at a relatively low ion strength concentration and hydrophilic substrate surfaces. Gurumurthy et al.[332] explained the excellent adhesive and mechanical properties of epoxy films. During epoxy-polyimide cross-linking reaction, the epoxy molecules penetrate into polyimide layer, thus increasing the entanglement among the polymer chains. Number of covalent bonds formed between epoxy and polyimide also increases during curing process.

However, Tsukruk et al.[333] pointed out that, some epoxies containing silane functional groups form a chemically heterogeneous and disordered molecular layer due to the hydrolysis-adsorption-reactivity competition of the head end epoxy groups with the hydroxyl terminated silicon oxide surfaces. A thorough investigation of epoxy/silane monolayer formation at various concentrations and different adsorption times was carried out as well as the corresponding mechanical properties were also accomplished. It was observed that a smooth uniform film with rare surface aggregates can be formed at relatively high concentration (1% volume ratio), while loosely packed film with many bi- or tri-layer molecular aggregates will be formed at relatively low concentrations (0.1-0.5%, volume ratio). So, in order to ensure a uniform epoxy layers formation, preparation conditions had to be optimised, like epoxy concentration, adsorption time etc. The homogeneously formed epoxy film is extremely stable and

well attached onto the substrate surface. However, it is difficult to mechanically remove the layer without damaging underlying silicon substrate.

The epoxysilane SAMs formed are highly robust and extremely stable. The SAMs cannot be mechanically removed without damaging the silicon substrate. An optimal combination of self-assembly parameters allows fabrication of truly monomolecular and complete films. Epoxysilane molecules forming monolayer of 0.85 nm thickness are predominantly oriented along the surface in their extended conformation. The terminal epoxy groups are generally located on the surface of the SAMs. The presence of epoxy groups at the SAMs surface results in higher adhesive forces and strong reactivity of these functional SAMs. The organic epoxysilane monolayers chemically attached to the silicon surface significantly reduces the shear strength and dissipation of mechanical energy at the interface in such a way which is comparable with the behaviour of other functional SAMs. The epoxysilane SAMs may also serves as a molecularly smooth template for chemical tethering of composite polymer layers. It was noted that a grafted polystyrene layer completely screens the SAMs substrate by very strong attachment, and was difficult to be removed by very long contact to a good solvent accompanied by ultrasonic treatment. The epoxysilane polymer layer was mechanically stable and sustains significant shear stresses produced by the SPM tip at high loads. Fabrication of long embedded micro channels through LbL assemblies was indicated by Raptis *et al.*[334]. The process was based on fabricating two epoxy based layers having varying photo acid generator concentration.

1.15 Objectives of Present Work

Although the polyelectrolyte multilayers prepared by the alternate adsorption of polyanions and polycations have found numerous uses in the real world, yet the mechanical stability of such assemblies is uncertain. Thus there is a limitation to their potential applications in hostile environments. If it is possible to assemble together different complex thin film devices in a modular production line, the assembly of mechanically robust multilayers would, therefore, proves to be an extremely interesting objective for various industrial applications. As a covalent bond is more stable than an electrostatic bond, therefore, in the present work covalent LbL approach was selected for the preparation of ultrathin films. The covalently assembled multilayers may also be extremely effective as coating material for the protection of polyelectrolytes and nanoparticles. To achieve these objectives, primarily very strong joint between the two

surfaces by a two component epoxy adhesive was studied. Very fast click reaction between the polyamine and epoxy components, may be used to prepare covalently bonded multilayer thin films.

Following optimizations to be established are;

- To construct mechanically robust ultra-thin covalent LbL multilayers, commercially available epoxy resins were selected.

- Whether the covalent LbL assemblies follow the classical rules of polyelectrolyte multilayer formation like linear increase in thickness as a function of number of layer pairs, effect of polymers concentration and adsorption time on multilayer growth.

- Reproducibility of the results and optical homogeneity of the multilayer films.

- Minimum concentration of the epoxy-amine network required to achieve mechanical robustness as well as the speed of deposition process, without any compromise on the quality of covalent multilayer films.

- The effect of accelerators or catalysts on thickness increment, speed of the deposition process and mechanical strength will also be investigated.

- The thickness increment of the covalent multilayer films to be monitored with the help of an ellipsometer and UV-Visible spectroscopy.

- The mechanical robustness of the covalent LbL assemblies will be studied with the help of a rubbing machine.

- Another important investigation to be conducted is the construction of a desired thickness of epoxy-amine covalently bonded multilayers in minimum number of layer pairs by utilising either higher concentration of polymer solutions or by employing longer adsorption times. This may result in reduction of the processing time, consumption of polymer solutions, lesser waste and ultimately minimum processing cost.

- Finally, the optimized parameters will be applied to protect the weak Au nanoparticles films.

- The minimum thickness of the epoxy-amine network required to improve the mechanical strength of the weak Au-NPs film will be determined.

- The surface morphology of the epoxy amine and epoxy protected Au colloid nanoparticles films will be studied with the help of AFM.

- A comparison of thermal and ambient temperature time curing will be carried out, in order to apply these thin films in various types of other applications.

1.16 References:

1 Feynman, R. P., *There's plenty of room at the bottom, Eng. Sci.*, **1960**, 23, 22.

2 Feynman, R. P.; Leighton, R., *Surely you're joking Dr. Feynman: Adventures of a Curious Character*, W.W. Norton and Company, **1985**.

3 Taniguchi, N., On the Basic Concept of Nano-Technology. *Proc. Intl. Conf. Prod.London, Part II British Society of Precision Engineering*, **1974**.

4 Drexler, K. E., *Proc. Natl. Acad. Sci.* USA, **1981**, 78, 5275.

5 Decher, G.; Schlenoff, J. B., *Multilayer Thin Films: Sequential Assembly of Nanocomposite Materials*, Wiley-VCH: Weinheim, **2003**.

6 Edwards, S. A., *The Nanotech Pioneers*, Wiley-VCH: Weinheim, **2006**.

7 Young, T. S.; Fu, E., *Tappi Journal*, **1991**, 74, 197.

8 Love, J. C.; *et al.*, *Chem. Rev.* **2005**, 105, 1103.

9 Xia, Y. N.; Whitesides, G. M., *Ann. Rev. Mater. Sci.*, **1998**, 28, 153.

10 Keller, S. W.; *et al.*, *J. Am. Chem. Soc.*, **1994**, 116, 8817.

11 Lvov, Y.; Decher, G.; Möhwald, H., *Langmuir*, **1993**, 9, 481.

12 Chan, W. C. W.; Nie, S., *Science*, **1998**, 281, 2016.

13 Bruchez, Jr. M.; *et al.*, *Science*, **1998**, 281, 2013.

14 Friedman, R. S.; *et al.*, *Nature*, **2005**, 434, 1085.

15 Lopez, C., *et al.*, *Adv. Mater.* **2003**, 15, 1679.

16 Zakhidov, A. A., *et al.*, *Science*, **1998**, 282, 897.

17 Tang, C. B., *et al.*, *Science*, **2008**, 322, 429.

18 Freund, L. B.; Suresh, S., *Thin Film Materials* Cambridge University Press, Cambridge: U. K., **2003.**

19 Hattori, H., *Adv. Mater.*, **2001**, 13, 51.

20 Lee, J.-K.; Yoo, D. S.; Handy E. S.; Rubner M. F., *Appl. Phys. Lett.* **1996**, 69,1686.

21 Eckle, M.; Decher, G., *Nano Lett.*, **2001**, 1, 45.

22 Advincula R.C.; Inaoka S.; Roitman D.; Frank C.; Knoll W.; Baba A.; Kaneko F., (a). *MRS Proceedings*, Spring, **1999**, (b). *Flat Panel Displays and Sensors Principles, Materials, and Processes, Materials Research Society*, Warrendale, **1999**.

23 Keply, L. J.; Crooks, R. M.; Ricco, A., *Anal. Chem.*, **1992**, 64, 3191.

24 Voegel, J. C.; Decher, G.; Schaaf, P., *Actualite Chimique*, **2003**, 30.

25 Caruso, F.; Niikura, K.; Furlong, D.N.; Okahata, Y., *Langmuir*, **1997**, 13, 3427.

26 Swanson, B., Johnson, S., Shi, J., Yang, X., *ACS Symp. Ser.*, **1998**, 690, 130.

27 Chen, T., *Anal. Chem.*, **2000**, 72, 3757.

28 Hoshi, T., Saiki, H., Kuwazawa, S., Kobayashi, Y., Anzai, J., *Anal. Sci.*, **2000**, 16, 1009.

29 Decher, G.; Hong, J. D.; Schmitt, J., *Thin Solid Films*, **1992**, 210/211, 83.

30 Gaines, G. L. Jr. , *Insoluble monolayers at liquid-gas interfaces*, Interscience, New York, **1996**.

31 Pockels, A., *Nature*, **1891**, 43, 473.

32 Roberts, G., *Langmuir-Blodgett films*, Plenum Press, New York and London, **1990**.

33 Ulman, U., *An introduction to ultrathin organic films: from Langmuir-Blodgett to selfassembly*, Academic Press, Inc., Boston, **1991**.

34 Blodgett, K. B.; Langmuir I., *Phys. Rev.* **1937**, 51, 964.

35 Blodgett, K.B., *J. Am. Chem. Soc.* **1935**, 57, 1007.

36 Blodgett, K.B., *J. Phys. Chem.* **1937**, 41, 975.

37 Evans, D. F.; Wennerstrom, H., *The Colloidal Domain:Where Physics, Chemistry, Biology and Technology Meet*, 2nd edn.(New York: Wiley–VCH), **1999**.

38 Chen, S., *Langmuir*, **2001**, 17, 2878.

39 Huang, S.; Tsutsui, G.; Sakaue, H.; Shingubara, S.;Takahagi, T., *J. Vac. Sci. Technol. B*, **2001**, 19, 2045.

40 Tian, Y.; Fendler, J. H., *Chem. Mater.*, **1996**, 8, 969.

41 Ping, G. C.; Du, B. Y.; Wang, L. Y.; Cui, H, N.; He, T. B.; Zeng, G. F.; Xi, S. Q., *Mol. Cryst. Liq. Cryst.*, **1999**, 337, 189.

42 Feng, F.; Miyashita, T.; Amao, Y.; Asai, K., *Thin Solid Films*, **2000**, 366, 255.

43 Son, E. M.; Lee, B. J.; Kwon, Y. S., *Colloids Surf. A*, **2002**, 198, 367.

44 Cha, J.; See, Y. K.; Lee, J.; Chang, T., *Synth. Met.*, **2001**, 117, 149.

45 Kuhn, H.; Möbius, D., *Angew. Chem. Int. Ed.*, **1971**, 10, 620.

46 Inacker, O.; Kuhn, H.; Möbius, D.; Debuch, G., Z., *physik. Chem. Neue Folge*, **1976**, 101, 1-6, 337.

47 Swalen, J. D.; Allara, D. L.; Andrade, J. D.; Chandross, E. A.; Garoff, S.; Israelachvili, J.; McCarthy, T. J.; Murray, R.; Pease, R. F.; Rabolt, J. F.; Wynne, K. J.; Yu, H., *Langmuir*, **1987**, 3, 932.

48 Miyashita, T., *Prog. Polym. Sci.*, **1993**, *18*, 263. 11.

49 Image extracted from *http://scitech.ksc.kwansei.ac.jp/~ozaki/e_lb.htm*

50 Ariga, K.; Hill, J. P.; Ji, Q., *Phys. Chem. Chem. Phys.*, **2007**, 9, 2319.

51 Shiratori, S.; Sato, T., *Polym. Mater. Sci. Eng.*, **2003**, 88, 117.

52 Blodgett, K. B.; Langmuir, I., *J. Am. Chem. Soc.*, **1932**, 54, 3781.

53 Langmuir, I.; Blodgett, K. B., *Kolloid-Zeitschrift.*, **1935**, 73, 257.

54 Bigelow, W. C.; *et al.*, *J. Coll. Sci.*, **1946**, 1, 513.

55 Sagiv, J.; *J. Am. Chem. Soc.*, **1980**, 102, 1, 92.

56 Netzer, L.; Sagiv, J., *J. Am. Chem. Soc.*, **1983**, 105, 3, 675.

57 Netzer, L.; Iscovici, R.; Sagiv, J., *Thin Solid Films*, **1983**, 99, 235.

58 Nuzzo, R. G.; Allara, D. L., *J. Am. Chem. Soc.*, **1983**, 105, 4481.

59 Nuzzo, R. G.; Fusco, A. F.; Allara, D. L., *J. Am. Chem. Soc.*, **1987**, 109, 2358.

60 Nuzzo, R. G.; Zegarski, B. R.; Dubois, L. H., *J. Am. Chem. Soc.*, **1987**, 109, 733.

61 Bain, C. D.; Troughton, E. B.; Whitesides, G. M.; Yu-Tai, T.; Evall, J.; Nuzzo, R. G.; *J. Am. Chem. Soc.*, **1989**, 111, 321.

62 Bain, C. D.; Evall, J.; Whitesides, G. M., *J. Am. Chem. Soc.*, **1989**, 111, 7155.

63 Laibinis, P. E.; Whitesides, G. M.; Allara, D. L.; Tao, Y. T.; Parikh, A. N.; Nuzzo, R. G. *J. Am. Chem. Soc.*, **1991**, 113, 7152.

64 Walczak, M. M.; Chung, C.; Stole, S. M.; Widrig, C. A.; Porter, M. D., *J. Am. Chem. Soc.*, **1991**, 113, 2370.

65 Fenter, P.; Eisenberger, P.; Li, J.; Camillone, N., III; Bernasek, S.; Scoles, G.; Ramanarayanan, T. A.; Liang, K. S. *Langmuir*, **1991**, 7, 2013.

66 Love, J. C.; Wolfe, D. B.; Haasch, R.; Chabinyc, M. L.; Paul, K. E.; Whitesides, G. M.; Nuzzo, R. G., *J. Am. Chem. Soc.*, **2003**, 125, 2597.

67 Carvalho, A.; Geissler, M.; Schmid, H.; Micel, B.; Delamarche, E., *Langmuir*, **2002**, 18, 2406.

68 Li, Z.; Chang, S.-C.; Williams, R. S., *Langmuir*, **2003**, 19, 6744.

69 Muskal, N.; Turyan, I.; Mandler, D., *J. Electroanal. Chem.*, **1996**, 409, 131.

70 Ulman, A., *Chem. Rev.*, **1996**, 96, 1533.

71 Whitesides, G. M.; Laibinis, P. E., *Langmuir*, **1990**, 6, 87.

72 Iler, R. K.; Colloid, J., *Interface Sci.*, **1966**, 21, 569.

73 Gaines, G. L., *Thin Solid Films*, **1983**, 99, 1-3, 243.

74 Decher, G.; Hong, J. D., *Germ. Pat.*, DE 402 6978, **1990**.

75 Decher, G., *Science*, **1997**, 277, 1232.

76 Decher, G.; Hong, J. D., *Makromolekulare Chemie-Macromolecular Symposia*,

1991, 46, 321.

77 Decher, G.; Schmitt, J.; Siegmund, H. U.; Heiliger, L., *Eur. Pat.*, EP 647 477 A1, 1995.

78 Farhat, T. R.; Schlenoff, J. B., *Langmuir*, **2001**, 17, 1184.

79 Hao, E. C.; Lian, T. Q., *Chem. Mater.*, **2000**, 12, 3392.

80 Decher, G.; Hong, J. D., *Ber. Bunsen-Ges. Phys. Chem.*, **1991**, 95, 1430.

81 Mao, G.; Tsao, Y.; Tirrell, M.; Davis, H.T.; Hessel, V.; Ringsdorf, H., *Langmuir*, **1993**, 9, 3461.

82 Lvov, Y.; Haas, H.; Decher, G.; Möhwald, H.; Kalachev, A., *J. Phys. Chem.*, **1993**, 97, 12835.

83 Lvov, Y.; Ariga, K.; Kunitake, T., *J. Am. Chem. Soc.*, **1995**, 117, 22, 6117.

84 Sukhorukov, G. B.; Möhwald, H.; Decher, G.; Lvov, Y. M., *Thin Solid Films*, **1996**, 284/285, 220.

85 Lvov, Y.; Decher, G.; Sukhorukov, G., *Macromolecules*, **1993**, 26, 20, 5396.

86 Pei, R. J.; Cui, X. Q.; Yang, X. R.; Wang, E. K., *Biomacromolecules*, **2001**, 2, 2, 463.

87 Johnston, A. P. R.; Read, E. S.; Caruso, F., *Nano Lett.*, **2005**, 5, 5, 953.

88 Jessel, N.; Oulad-Abdeighani, M.; Meyer, F.; Lavalle, P.; Haikel, Y.; Schaaf, P.; Voegel, J. C., *Proceedings of The National Academy of Sciences of The United States of America*, **2006**, 103, 23, 8618.

89 Carrillo, A.; Swartz, J. A.; Gamba, J. M.; Kane, R. S.; Chakrapani, N.; Wei, B.; Ajayan, P. M., *Nano Letters*, **2003**, 3, 1437.

90 Vuillaume, P. Y.; Glinel, K.; Jonas, A. M.; Laschewsky, A., *Chem. Mater.*, **2003**, 15, 3625.

91 Crisp, M. T.; Kotov, N. A., *Nano Lett.*, **2003**, 3, 173.

92 Mamedov, A. A.; Kotov, N. A., *Langmuir*, **2000**, 16, 5530.

93 Rhodes, K. H.; Davis, S. A.; Caruso, F.; Zhang, B. J.; Mann, S., *Chem. Mater.*, **2000**, 12, 2832.

94 Caruso, F.; Caruso, R. A.; Möhwald, H., *Science*, **1998**, *282*, 1111.

95 Moya, S.; Dahne, L.; Voigt, A.; Leporatti, S.; Donath, E.; Möhwald, H., *Colloids Surf. A.*, **2001**, 183, 27.

96 Hammond, P. T., *Current Opinion in Colloid & Interface Science*, **2000**, 4, 430.

97 Farhat, T.; Schlenoff, J.; *Electrochem. Solid State Lett.*, **2002**, 5, B13.

98 Graul, T. W.; Schlenoff, J. B., *Anal. Chem.*, **1999**, 71, 4007.

99 Ngankam, P. A.; Lavalle, P.; Voegel, J. C.; Szyk, L.; Decher, G.; Schaaf, P.;
    Cuisinier, F. J. G., *J. Am. Chem. Soc.*, **2000**, 122, 8998.

100 Dutta, A. K.; Ho, T.T.; Zhang, L. Q.; Stroeve, P., *Chem. Mater.*, **2000**, 12, 1042.

101 Zhang, L. Q.; Dutta, A. K.; Jarero, G.; Stroeve, P., *Langmuir*, **2000**, 16, 7095.

102 Muller, M.; Rieser, T.; Lunkwitz, K.; Meierhaack, J., *Macromol. Rapid Commun.*,
     1999, 20, 607.

103 Kotov, N. A., *Nano Structured Materials*, **1999**, 12, 789.

104 Quinn, J. F.; Caruso, F., *Macromolecules*, **2005**, 38, 3414.

105 Elbert, D. L.; Herbert, C. B.; Hubbell, J. A., *Langmuir*, **1998**, 15, 5355.

106 Hwang, J. J.; Jaeger, K.; Hancock, J.; Stupp, S. I., *J. Biomed. Mater. Res.*, **1999**,
     47, 504.

107 Lee, S. H, *Polym. J.*, 2000, 32, 716.

108 Tidswell, I. M.; Ocko, B. M.; Pershan, P.S.; Wasserman, S. R.; Whitesides, G. M.;
     Axe, J. D., *Phys. Rev., B*, **1990**, 41, 1111.

109 Decher, G.; Lvov, Y.; Schmitt, J., *Thin Solid Films*, **1994**, 244, 772.

110 Barker, S. L. R.; Ross, D.; Tarlov, M. J.; Gaitan, M.; Locascio, L. E., *Anal. Chem.*,
     2000, 72, 5925.

111 Mecking, S.; Thomann, R., *Adv. Mater.*, **2000**, 12, 953.

112 Tarabia, M.; Hong, H.; Davidov, D.; Kirstein, S.; Steitz, R.; Neumann, R.; Avny,
     Y., *J. Appl. Phys.*, **1998**, 83, 725.

113 Kirstein, S.; Hong, H.; Steitz, R.; Davidov, D., *Synthetic Metals*, **1999**, 102, 1067.

114 Chen, T.; Friedman, K. A.; Lei, I.; Heller, A., *Anal. Chem.*, **2000**, 72, 3757.

115 Dai, J. H.; Jensen, A.W.; Mohanty, D.K.; Erndt, J.; Bruening, M.L., *Langmuir*,
     2001, 17, 931.

116 Farhat, T. R.; Schlenoff, J. B., *Langmuir*, **2001**, 17, 1184.

117 Winterton, L.; Vogt, J.; Lally, J.; Stockinger, F., *Novartis*, **1999**, WO9935520.

118 Schlenoff, J. B.; Dubas, S.T.; Farhat, T., *Langmuir*, **2000**, 16, 9968.

119 Pookrod, P.; Haller, K. J.; Scamehorn, J. F., *Sep. Sci. Technol.*, **2004**, 39, 811.

120 Russell, T.P., *Mater. Sci. Rep.*, **1990**, 5, 171.

121 Anastasiadis, S. H.; Russell, T. P.; *J. Chem. Phys.*, **1990**, 92, 5677.

122 Russell, T. P.; Karim, A.; Mansour, A.; Felcher, G. P., *Macromolecules*, **1988**, 21,

1890. 48.

123 Hong, H.; Steitz, R.; Kirstein, S.; Davidov, D., *Adv. Mater.*, **1998**, 10, 1104.

124 Lvov, Y.; Essler, F.; Decher, G., *J. Chem. Phys.*, **1993**, 97, 13773.

125 Arys, X.; Jonas, A. M.; Laguitton, B.; Laschewsky, A.; Legras, R.; Wischerhoff, E., *Thin Solid Films*, **1998**, 327, 734.

126 Decher, G.; Eckle, M.; Schmitt, J.; Struth, B.,*Curr. Opin. Colloid Interface Sci.*, **1998**, 3, 32.

127 Hong, H.; Steitz, R.; Kirstein, S.; Davidov, D., *Adv. Mater.*, **1998**, 10, 1104.

128 Ladam, G.; Schaad, P.; Voegel, J. C.; Schaaf, P.; Decher, G.; Cuisinier, F., *Langmuir*, **2000**, 16, 1249.

129 Pointu, D.; Decher, G., *Actualites GFP*, **2000**, 88, 3.

130 Tieke, B.; Van Ackern, F.; Krasemann, L.; Toutianoush, A., *European Physical Journal E: Soft Matter.*, **2001**, 5, 29.

131 Yonezawa, T.; Onoue, S.; Kunitake, T., *Adv. Mater.*, **1998**, 10, 414.

132 Sukhorukov, G. B.; Schmitt, J.; Decher, G., *Berichte Der Bunsen-Gesellschaft-Physical Chemistry Chemical Physics*, **1996**, 100, 948.

133 Cassier, T.; Lowack, K.; Decher, G.,*Supramol. Sci.*, **1998**, 5, 309.

134 Ruths, J.; Essler, F.; Decher, G.; Riegler, H., *Langmuir*, **2000**, 16, 8871.

135 Pardoyissar, V.; Katz, E.; Lioubashevski, O.; Willner, I., *Langmuir*, **2001**, 17, 1110.

136 Kolarik, L.; Furlong, D. N.; Joy, H.; Struijk, C.; Rowe, R., *Langmuir*, **1999**, 15, 8265.

137 Picart, C.; Lavalle, P.; Hubert, P.; Cuisinier, F. J. G.; Decher, G.; Schaaf, P.; Voegel, J. C., *Langmuir*, **2001**, 17, 7414.

138 Lavalle, P.; Gergely, C.; Cuisinier, F. J. G.; Decher, G.; Schaaf, P.; Voegel, J. C.; Picart, C., *Macromolecules*, **2002**, 35, 4458.

139 Picart, C.; Mutterer, J.; Richert, L.; Luo, Y.; Prestwich, G. D.; Schaaf, P.; Vogel, J. C.; Lavalle, P., *Proc. Natl. Acad. Sci. U.S.A.*, **2002**, 99, 12, 531.

140 Boulmedais, F.; Ball, V.; Schwinte, P.; Frisch, B.; Schaaf, P.; Voegel, J. C., *Langmuir*, **2003**, 19, 440.

141 Lavalle, P.; Vivet, V.; Jessel, N.; Decher, G.; Voegel, J. C.; Mesini, P. J.; Schaaf, P.; *Macromolecules*, **2004**, 37, 1159.

142 Richert, L.; Lavalle, P.; Payan, E.; Shu, X. Z.; Prestwich, G. D.; Stoltz, J. F.;

Schaaf, P.; Voegel, J. C.; Picart, C., *Langmuir*, **2004**, 20, 448.

143 Lavalle, P.; Picart, C.; Mutterer, J.; Gergely, C.; Reiss, H.; Voegel, J. C.; Senger, B.; Schaaf, P.; *J. Phys.Chem., B*, **2004**, 108, 635.

144 Laugel, N.; Betscha, C.; Winterhalter, M.; Voegel, J. C.; Schaaf, P.; Ball, V.; *J. Phys. Chem., B*, **2006**, 110, 19443.

145 Hubsch, E.; Ball, V.; Senger, B.; Decher, G.; Voegel, J. C.; Schaaf, P.; *Langmuir*, **2004**, 20, 1980.

146 Michel, M.; Izquierdo, A.; Decher, G.; Voegel, J. C.; Schaaf, P.; Ball, V., *Langmuir*, **2005**, 21, 7854.

147 Salomaki, M.; Vinokurov, I. A.; Kankare, J., *Langmuir*, **2005**, 21, 11232.

148 Gilliard, A.; Winterton, L. C.; Andino, R. V.; Lally, J., *US Patent*, **2004**, No. 6811805.

149 Izquierdo, A.; Ono, S. S.; Voegel, J. C.; Schaaf, P.; Decher, G., *Langmuir*, **2005**, 21, 7558.

150 Kolasinska, M.; Krastev, R.; Gutberlet, T.; Warszynski P., *Langmuir*, 25, 2, **2009**, 1225.

151 Cho, J.; Char, K.; Hong, J. D.; Lee, K. B., *Adv. Mater.*, **2001**, 13, 1076.

152 Lee, S. S.; Hong, J. D.; Kim, C. H.; Kim, K.; Koo, J. P.; Lee, K. B., *Macromolecules*, **2001**, 34.

153 Chiarelli, P. A.; Johal, M. S.; Casson, J. L.; Roberts, J. B.; Robinson, J. M.; Wang, H. L., *Adv. Mater.*, **2001**, 13, 1167.

154 Hubbell, J. A.; Elbert, D. L.; Herbert, C. B., *US patent*, 6, 743, 521, **2004**.

155 Hiorth, M.; Tho, I.; Sande, S. A., *Eu. J. Pharm.Biopharm.*, **2003**, 56, 175.

156 Porcel, C. H.; Izquierdo, A.; Ball, V.; Decher, G.; Voegel, J. C.; Schaaf, P., *Langmuir*, **2005**, 21, 800.

157 Bungenberg de Jong, H. G., *Colloid Science*, Elsevier, Amsterdam, New York. **1949**, 2, 10, 335.

158 Shiratori, S. S.; Rubner, M. F., *Macromolecules*, **2000**, 33, 4213.

159 Rodriguez, L. N. J.; Depaul, S. M.; Barrett, C. J.; Reven, L.; Spiess, H. W., *Adv. Mater.*, **2000**, 12, 1934.

160 Schwarz, B.; Schönhoff, M., *Colloids Surf., A* **2002**, 198-200, 293.

161 Advincula, R.; Aust, E.; Meyer, W.; Knoll, W., *Langmuir*, **1996**, 12, 3536.

162 Kurth, D. G.; Osterhout, R., *Langmuir*, **1999**, 15, 4842.

163 Ramsden, J. J.; Lvov, Y. M.; Decher, G.; *Thin Solid Films,* **1995**, 254, 246; erratum: idem, **1995**, 1261, 1343.

164 Hoogeveen, N. G.; Stuart, M. A. C.; Fleer, G.; Böhmer, M. R., *Langmuir,* **1996**, 12, 3675.

165 Ngankam, P. A.; Lavalle, P.; Voegel, J. C.; Szyk, L.; Decher, G.; Schaaf, P.; Cuisinier, F. J. G., *J. Am. Chem., Soc.,* **2000**, 122, 8998.

166 Auer, F.; Scotti, M.; Ulman, A.; Jordan, R.; Sellergren, B.; Garno, J.; Liu, G. Y.; *Langmuir,* **2000**, 16, 7554.

167 Mendelsohn, J. D.; Barrett, C. J.; Chan, V. V.; Pal, A. J.; Mayes, A. M.; Rubner, M. F., *Langmuir,* **2000**, 16, 5017.

168 Dubas, S. T.; Schlenoff, J. B., *Langmuir,* **2001**, 17, 7725.

169 Muller, M.; Rieser, T.; Lunkwitz, K.; Meierhaack, J., *Macromol. Rapid Commun.,* **1999**, 20, 607.

170 Lowack, K.; Helm, C. A., *Macromolecules,* **1995**, 28, 2912.

171 Lowack, K.; Helm, C. A., *Macromolecules,* **1998**, 31, 823.

172 Plech, A.; Salditt, T.; Munster, C.; Peisl, J., *J. Colloid Interface Sci.,* **2000**, 223, 74.

173 Steitz, R.; Leiner, V.; Siebrecht, R.; von Klitzing, R., *Colloids Surf. A.,* **2000**, 163, 63.

174 Young, T. S.; Fu, E., *Tappi Journal,* **1991**, 74, 197.

175 Vaynberg, K. A.; Berta, A. T.; Dunckley, P. M., *Journal of Adhesion,* **2001**, 77, 275.

176 Vandenberg, E. J.; Diveley, W. R.; Filar, L. J.; Patel, S. R.; Barth, H. G., *J. of Polym. Sc., Part A: Poly. Chem.,* **1989**, 27, 3745.

177 Modi, J. J., (Hercules Incorporated, USA). Application: EP, **1998**, 34.

178 Natarajan, R.; Deshpande, K. V., *Corrosion & Maintenance,* **1985**, 8, 205.

179 Radoiu, M. T.; Martin, D. I.; Calinescu, I.; Iovu, H., *Journal of Hazardous Materials,* **2004**, 106, 19.

180 Von Homeyer, A.; Krentz, D. O.; Kulicke, W. M.; Lerche, D., *Colloid and Polymer Science,* **1999**, 277, 637.

181 Sharp, K. A., *Biopolymers,* **1995**, 36, 227.

182 Jaber, J. A.; Schlenoff, J. B., *Current Opinion in Colloid & Interface Science,* **2006**, 11, 324.

183 Jisr, R. M.; Rmaile, H. H.; Schlenoff, J. B., *Angew. Chem., Int. Ed.,* **2005**, 44, 782.

184 Rmaile, H. H.; Schlenoff, J. B., *J. Am. Chem. Soc.,* **2003**, 125, 6602.

185 Sullivan, D. M.; Bruening, M. L., *Chemistry of Materials,* **2003**, 15, 281.

186 Krasemann, L.; Tieke, B., *Journal of Membrane Science,* **1998**, 150, 23.

187 Schatz, C.; Domard, A.; Viton, C.; Pichot, C.; Delair, T., *Biomacromolecules,* **2004**, 5, 1882.

188 Chellat, F.; Tabrizian, M.; Dumitriu, S.; Chornet, E.; Magny, P.; Rivard, C. H.; Yahia, L. H., *J. Biomed. Mater. Res.,* **2000**, 51, 107.

189 Cross, R. A., *Polyelectrolytes,* **1976**, 134.

190 Lin, W. C.; Liu, T. Y.; Yang, M. C., *Biomaterials,* **2004**, 25, 1947.

191 Schwarz, H. H.; Lukas, J.; Richau, K., *J. Membr. Sci.,* **2003**, 218, 1.

192 Uchiyama, H.; Christian, S. D.; Tucker, E. E.; Scamehorn, J. F., *J. Colloid Interface Sci.,* **1994**, 163, 493.

193 Gladilin, A. K.; Kudryashova, E. V.; Vakurov, A. V.; Izumrudov, V. A.; Mozhaev, V. V.; Levashov, A. V., *Biotechnol. Lett.,* **1995**, 17, 1329.

194 Kokufuta, E.; Shimizu, N.; Tanaka, H.; Nakamura, I., *Biotechnol. Bioeng.,* **1988**, 32, 756.

195 Kircheis, R.; Wagner, E., *Gene Ther. Regul.,* **2000**, 1, 95.

196 Kabanov, A. V.; Kabanov, V. A., *Bioconjugate Chem.,* **1995**, 6, 7.

197 Chen, K.; Caldwell, W. B.; Mirkin, C. A., *J. Am. Chem. Soc.,* **1993**, 115, 1193.

198 Shi, X.; Caldwell, W. B.; Chen, K.; Mirkin, C. A., *J. Am. Chem. Soc.,* **1994**, 116, 11598.

199 Stockton, W. B.; Rubner, M. F., *Macromolecules,* **1997**, 30, 2717.

200 Wang, L.; Wang, Z. Q.; Zhang, X.; Shen, J. C.; Chi, L. F.; Fuchs, H., *Macromol. Rapid Commun.,* **1997**, 18, 509.

201 Fischer, P.; Laschewsky, A., *Macromolecules,* **2000**, 33, 1100.

202 Sukhishvili, S. A.; Granick, S., *Macromolecules,* **2002**, 35, 301.

203 Kharlampieva, E.; Kozlovskaya, V.; Tyutina, J.; Sukhishvili, S. A., *Macromolecules,* **2005**, 38, 10523.

204 Yang, S. Y.; Rubner, M. F., *J. Am. Chem. Soc.,* **2002**, 124, 2100.

205 Kozlovskaya, V.; Ok, S.; Sousa, A.; Libera, M.; Sukhishvili, S. A., *Macromolecules,* **2003**, 36, 8590.

206 Yang, S. Y.; Lee, D.; Cohen, R. E.; Rubner, M. F., *Langmuir,* **2004**, 20, 5978.

207 Zelikin, A. N; Quinn, J. F.; Caruso, F., *Biomacromolecules*, **2006**, 7, 27.

208 Li, Z.; Lee, D.; Rubner, M. F.; Cohen, R. E., *Macromolecules*, **2005**, 38, 7876.

209 Johnston, A. P. R.; Read, E. S.; Caruso, F., *Nano Lett.*, **2005**, 5, 953.

210 Markarian, M. Z.; Moussallem, M. D.; Jomaa, H. W.; Schlenoff, J. B., *Biomacromolecules*, **2007**, 8, 59.

211 Kharlampieva, E.; Pristinski, D.; Sukhishvili; S. A., *Macromolecules*, **2007**, 40, 19.

212 Stenzel, M. H.; Barner-Kowollok, C.; Davis, T. P.; Dalton, H. M., *Macromol. Biosci.*, **2004**, 4, 445.

213 Lewis, A. L.; Cumming, Z. L.; Goreish, H. H.; Kirkwood, L. C.; Tolhurst, L. A.; Stratford, P. W., *Biomaterials*, **2001**, 22, 99.

214 Lowe, A. B.; Vamvakaki, M.; Wassall, M. A.; Wong, L.; Billingham, N. C.; Armes, S. P.; Lloyd, A. W., *J. Biomed. Mater. Res.*, **2000**, 52, 88.

215 Salloum, D. S.; Olenych, S. G.; Keller, T. C. S.; Schlenoff, J. B., *Biomacromolecules*, **2005**, 6, 161.

216 Bastide, S.; Gal, D.; Cahen, D.; Kronik, L., *Rev. Sci. Instrum.*, **1999**, 70, 4032.

217 Kumanotani, J., Prog. *Org. Coat.*, **1997**, 34, 135.

218 Otto, V., *J. Polym. Sci., Part A: Polym. Chem.*, **2000**, 38, 4327.

219 Decher, G.; Schmitt, J.; Siegmund, J. H. U.; Heiliger, L., *German Patent*: DE 433 310, **1993**, *Europ. Patent*, No. EP 647 477 A1, **1995**.

220 Liu, Y. L.; Bruening, M. L.; Bergbreiter D. E.; Crooks, R. M., *Angew. Chem., Int. Ed.* Engl., **1997**, 36, 2114.

221 Dai, J.; Sullivan, D. M.; Bruening, M. L., *Ind. Eng. Chem. Res.*, **2000**, 39, 3528.

222 Kim, Y. S.; Liao, K. S.; Jan, C. J.; Bergbreiter, D. E.; Grunlan, J. C., *Chem. Mater.*, **2006**, 18, 2997.

223 Tian, Y.; He, Q.; Tao, C.; Li, J., *Langmuir*, **2006**, 22, 360.

224 Buck, M. E.; Zhang, J.; Lynn, D. M., *Adv. Mater.*, **2007**, 19, 3951.

225 Chan, E. W. L.; Lee, D. C.; Ng, M. K.; Wu, G.; Lee K. Y. C.; Yu, L., *J. Am. Chem. Soc.*, **2002**, 124, 12238.

226 Tong, W.; Gao, C.; Mohwald, H., *Macromol. Rapid Commun.*, **2006**, 27, 2078.

227 Ma, Y.; Qian, L.; Huang, H.; Yang, X., *J. Colloid Interface Sci.*, **2006**, 295, 583.

228 Chen, J.; Luo, G.; Cao, W., *Macromol. Rapid Commun.*, **2001**, 22, 311.

229 Zhang, Y.; Yang, S.; Guan, Y.; Cao, W.; Xu, J., *Macromolecules*, **2003**, 36, 4238.

230 Bergbreiter, D. E.; Simanek E. E.; Owsik, I., *J. Polym. Sci., Part A: Polym. Chem.*, **2005**, 43, 4654.

231 Kohli, P.; Blanchard, G. J., *Langmuir*, **2000**, 16, 4655.

232 Kohli, P.; Blanchard, G. J., *Langmuir*, **2000**, 16, 8518.

233 Major J. S.; Blanchard, G. J., *Langmuir*, **2001**, 17, 1163.

234 Liang, Z.; Wang, Q., *Langmuir*, **2004**, 20, 9600.

235 Such, G. K.; Quinn, J. F.; Quinn, A.; Tjipto, E.; Caruso, F., *J. Am. Chem. Soc.*, **2006**, 128, 9318.

236 Kolb, H. C.; Finn, M. G.; Sharpless, K. B., *Angew. Chem., Int. Ed.*, **2001**, 40, 2004.

237 Bergbreiter, D. E.; Liao, K.S., *Soft Matter*, **2009**, 5, 23.

238 Shi, F.; Dong, B.; D. Sun, Q. J. I.; Wu, T.; Zhang, X., *Adv. Mater.*, **2002**, 14, 805

239 Bertrand, P.; Jonas, A.; Laschewsky, A.; Legras, R., *Macromol. Rapid Commun.*, 21, **2000**, 31.

240 Notley, S. M.; Biggs, S.; Craig, V. S., *Macromolecules*, **2003**, 36, 2903.

241 Feiler, A.; Plunkett, M. A.; Rutland, M. W., *Langmuir*, **2003**, 19, 4173.

242 Plunkett, M. A.; Feiler, A.; Ruthland, M. W., *Langmuir*, **2003**, 19, 4180.

243 Mermut, O.; Lefebvre, J.; Gray, D. G.; Barrett, C. J., *Macromolecules*, **2003**, 36, 8819.

244 Gao, C.; Donath, E.; Moya, S.; Dudnik, V.; Möhwald, H., *Eur. Phys. J. E.*, **2001**, 5, 21.

245 Kim, B. S.; Lebedeva, O. V.; Kim, D. H.; Caminade, A. M.; Majoral, J. P.; Knoll, W.; Vinogradova, O. I., *Langmuir*, **2005**, 21, 7200.

246 Vinogradova, O. I., *J. Phys.: Condens. Matter.*, **2004**, 16, R1105.

247 Vinogradova, O. I.; Andrienko, D.; Lulevich, V. V.; Nordschild, S.; Sukhorukov, G. B., *Macromolecules*, **2004**, 37, 1113.

248 Pavoor, P.V.; Gearing, B. P.; Gorga, R. E.; Bellare, A.; Cohen, R. E., *J. Appli. Poly. Sci.*, **2004**, 92, 439.

249 Pavoor, P. V.; Gearing, B. P.; Bellare, A.; Cohen, R. E., *Wear*, **2004**, 256, 1196.

250 Tang, Z.; Kotov, N. A.; Magonov, S.; Ozturk, B., *Nat. Mater.*, **2003**, 2, 413.

251 Mamedov, A. A.; Kotov, N. A.; Prato, M.; Guldi, D. M.; Wicksted, J. P.; Hirsch, A., *Nat. Mater.*, **2002**, 1,190.

252 Lu, C.; Dönch, I.; Nolte, M.; Fery, A., *Chem. Mater.*, **2006**, 18, 6204.

253 Ono, S. S.; Decher, G., *Nano Letters,* **2006**, 6, 592.

254 Jiang, C. Y.; Markutsya, S.; Pikus, Y.; Tsukruk, V. V., *Nat. Mater.* **2004**, 3, 721.

255 Ko, H.; Jiang, C. Y.; Shulha, H.; Tsukruk, V. V., *Chem. Mater.* **2005**, 17, 2490.

256 Gunawidjaja, R.; Jiang, C. Y.; Peleshanko, S.; Ornatska, M.; Singamaneni, S.;
     Tsukruk, V. V., *Adv. Funct. Mater.* **2006**, 16, 2024.

257 Lin, Y. H.; Jiang, C.; Xu, J.; Lin, Z. Q.; Tsukruk, V. V., *Adv. Mater.* **2007**, 19,
     3827.

258 Nolte, A. J.; Rubner, M. F.; Cohen, R. E., *Macromolecules,* **2005**, 38, 5367.

259 Podsiadlo, P.; Kaushik, A. K.; Arruda, E. M.; Waas, A. M.; Shim, B. S.; Xu, J. D.;
     Nandivada, H.; Pumplin, B. G.; Lahann, J.; Ramamoorthy, A.; Kotov, N. A.,
     Science **2007**, 318, 80.

260 Schoeler, B.; Delorme, N.; Doench, I.; Sukhorukov, G. B.; Fery, A.; Glinel, K.,
     Biomacromolecules, **2006**, 7, 2065.

261 Cuenot, S.; Alem, H.; Louarn, G.; Demoustier-Champagne, S.; Jonas, A. M., *Eur.
     Phys. J. E.,* **2008**, 25, 343.

262 Lutkenhaus, J. L.; Hrabak, K. D.; McEnnis, K.; Hammond, P. T., *J. Am. Chem.
     Soc.,* **2005**, 127, 17228.

263 Schönhoff, M.; Ball, V.; Bausch, A. R.; Dejugnat, C.; Delorme, N.; Glinel, K.;
     Klitzing, R.V.; Steitz, R., *Colloids and Surfaces A: Physicochem.Eng. Aspects,*
     2007, 303, 14.

264 Jaber, J. A.; Schlenoff, J. B., *Langmuir,* **2007**, 23, 896.

265 Podsiadlo, P.; Arruda, E. M.; Kheng, E.; Waas, A. M.; Lee, J.; Critchley, K.; Qin,
     M.; Chuang, E.; Kaushik, A. K.; Kim, H. S.; Qi, Y.; Noh, S. T.; Kotov, N. A., *ACS
     Nano,* **2009**, 3, 1564.

266 Lu, C.; Dönch, I.; Nolte, M.; Fery, A., *Chem. Mater.,* **2006**, 18, 6204.

267 Dotzauer, D. M.; Dai, J.; Sun, L.; Bruening, M. L., *Nano Letters,* **2006**, 6, 2268.

268 Gittins, D. I.; Caruso, F., *Adv. Mater.,* **2000**, 12, 1947.

269 Schneider, G.; Decher, G., *Nano Letters,* **2004**, 4, 1833.

270 Ellis, B., *"Chemistry and Technology of Epoxy Resins"*, 1st edition, Chapman &
     Hall, New York, **1993**, 1-36.

271 Hamerton, I., *"Recent Developments in Epoxy Resins"*, Rapra Review Report 91.

272 May, C. A., *Introduction to Epoxy Resins*, Chapter 1, Marcel Dekker, Inc. New
     York, **1988**.

273   Pertrie, E. M., *Epoxy Adhesive Formulations*, Mc-Grawhill, Chemical Engineering, **2006**.

274   Lee, H.; Neville, K., *Handbook of Epoxy Resins*, McGraw-Hill, Inc., New York, **1967**, reprinted **1982**.

275   Schlack, P., *Ger. Pat.* 676,117, 1938 and *U.S. Pat.* 2,136,928, **1938**.

276   Castan, P., *U.S. Pat.* 2,324,483, **1943**.

277   Greenlee, S. O., *U.S. Pat.* 2,456,408, **1948**.

278   D. Swern, *Chem. Rev.* **1949**, 45, 1.

279   *Technical Bulletin*, Dow Epoxy Resin, DEN, 439.

280   Osumi, Y., "*One-Part Epoxy Resin*," *Three Bond Technical News*, *Three Bond*, October 1, **1987**.

281   Lee H.; Neville, K.,"*Handbook of Epoxy Resins*", McGraw-Hill, **1967**.

282   Gorezyk, J.;Bogdal, D., "*Determination of Chain Branching in solid Epoxy resin*" Cracow Poland, Warszawska, *ECSOC-6*, **2002**, 24,31.

283   Brojer, Z.; Hertz, P. P., "*Zywice Epoksydowe*", Warszawa, WNT, **1982**.

284   Luo, S.; Wong C. P., *8th International Symposium on Advanced Packaging Materials*, **2002**.

285   Potter, W. G., "*Epoxide Resins*", Springer-Verlag, New York, **1970**.

286   Lee, H.; Neville, K., *Handbook of Epoxy Resins*, McGraw-Hill, Inc., New York, **1967**.

287   Shieh, J. -Y.; Wang, C. -S., *Polymer*, **2001**, 42, 7617.

288   ASM Compendium "Tactix 556 Datasheet," Vantico **Moisture**

289   ASM International, "*Engineered Materials Handbook*", USA, **1998**,1.

290   Conley, R. T., "*Thermal Stability of Polymers*", Marcel Dekker, New York, **1970**.

291   Garcia, G. F.; Soares, G. B., *Polymer Testing*, **2003**, 22, 51.

292   Dobinson, B.; Hoffman, W.; Stark, B. P., "*The Determination of Epoxide Group*", Pergamon Press, Oxford, **1969**.

293   Garea, S.; Corbu, A.; Deleanu, C.; Iovu, H., *Polymer Testing*, **2006**, 25, 107.

294   "Chemical Resistance Guide for Protective Coatings," Technical Bulletin SC: 2298, Shell Chemical Company, **1995**.

295   Sunshine, N.B., "*Flame Retardancy of Phenolic Resins and Urea and Melamine-formaldehyde Resins*", Marcel Dekker, Inc.New York, Vol. 2, **1973**.

296   *Technical Bulleti*n, Dow epoxy novolac resins.

297 Dobinson.; Bryan.; Thoseby.; Michael, R. *U.S. Patent*, 4, 540,769, **1985**.

298 Dobinson.; Bryan.; Thoseby.; Michael, R. *U.S. Patent*, 4, 280,069, **1994**.

299 Bajpai, M.; Shukla, V.; Kumar, A.; *Progress in Organic Coatings*, **2002**, 44, 271.

300 Boschel, D.; Fedtke, M.; Geyer, W., *Polymer*, **1997**, 38, 6, 1291.

301 Boey, F. Y. C.; Yap, B. H., *Polymer Testing*, **2001**, 20, 837.

302 Pham, H. Q.; Marks, M. J., *Encyclopaedia of Polymer Science and Technology*, 3rd ed.; Kroschwitz, J. I., Ed.; John Wiley & Sons, Inc.: Hoboken, NJ, **2003**; 9.

303 Shechter, L.; Wynstra, J.; Kurkjy, R. P., *Ind. Eng. Chem.*, **1956**, 48, 94.

304 Rondan, N. G.; Marks, M. J.; Hoyles, S.; Pham, H., paper presented at the *225th ACS National Meeting*, New Orleans, La., **2003**.

305 Horie, K.; Hiura, H.; Sawada, M.; Mita, I.; Kambe, H., *J. Polym. Sci.*, A–1 **8**, 1357, **1970**.

306 Dusek, K.; Ilavsky, M.; Lunak, S., *J. Polym. Sci., Polym. Symp.*, **1975**, 53, 29

307   Burton. B. L.; Fall **2001** Epoxy Resin Formulators Meeting of "The Society of the Plastics Industry".

308 Watanabe, O.; Murakami, S., *U.S. Patent.*, 5, 317,068, **1994**.

309 Mellor, J.W., *A comprehensive Treatise on Inorganic and Theoretical Chemistry*, 1923, Longmans, Green and Co., London.

310 Faraday, M., *Philos. Trans. R. Soc. London*, 1857, 147, 145.

311 Daniel, M. C.; Astruc, D., *Chem. Rev.*, **2004**, 104, 293.

312 Grabar, K .C.; Freeman, R.G.; Hommer, M. B.; Natan, M. J., *Anal. Chem.*, **1995**, 67, 735.

313 Schmid, G.; *Clusters and Colloids*, VCH, Weinheim, **1994**.

314 Schmid, G.; Lehnert, A., *Angew. Chem., Int. Ed.*, **1989**, 28, 780.

315 Schmitt, J.; Decher, G.; Dressick, W. J.; Brandow, S. L.; Geer, R. E.; Shashidhar, R.; Calvert, J. M., *Adv. Mater.*, **1997**, 9, 61.

316 Schmitt, J.; Machtle, P.; Eck, D.; Möhwald, H.; Helm, C. A., *Langmuir*, **1999**, 15, 3256.

317 Lu, C.; Möhwald, H.; Fery, A., *J. Phys. Chem. C*, **2007**, 111, 10082.

318 Fu, Y.; Xu, H.; Bai, S.; Qiu, D.; Sun, J.; Wang, Z.; Zhang, X., *Macromol. Rapid Commun.*, **2002**, 23, 256.

319 Schneider, G.; Decher, G., *Nano Lett.*, 2004, 4, 10.

320 Schneider, G.; Decher, G., *Nano Lett.*, **2006**, 6, 3.

321 Schneider, G.; Decher, G., *Langmuir*, **2008**, 24, 1778.

322 Ferreyra, N.; Coche-Guérente, L.; Fatisson, J.; Teijelo, M. L.; Labbé, P., *Chem. Commun.*, **2003**, 2056.

323 Musick, M. D.; Keating, C. D.; Keefe, M. H.; Natan, M. J., *Chem. Mater.*, **1997**, 9, 1499.

324 Lu, C.; Dönch, I.; Nolte, M.; Fery, A., *Chem. Mater.*, **2006**, 18, 6204.

325 Knop, A.; Scheib, W., *Chemistry and application of phenolic resins*. New York: Springer; **1979**.

326 Hsieh, F.; Beeson, H. D., *Fire Mater*, **1997**; 21,41.

327 McGarry, F. J., *In Polymer Toughening*, Arends, C. B., ed., Marcel Dekker, Inc.: New York, **1996**, 175.

328 Shaw, S. J., In *Rubber Toughened Engineering Plastics*, Collyer, A. A., ed., Chapman & Hall: London, **1994**, 165.

329 Im, S. G.; Bong, K. W.; Lee, C. H.; Doyle, P.S.; Gleason, K. K, *Lab on a Chip*, **2009**, 9, 411.

330 Grujicic, M.; Angstadt, D. C.; Sun, Y. P.; Koudela, K. L., *J. Mater. Sci.*, **2007**, 42, 4609.

331 Mateo, C.; Torres, R.; Fernandez-Lorente, G.; Ortiz, C.; Fuentes, M.; Hidalgo, A.; Lopez-Gallego, F.; Abian, O.; Palomo, J. M.; Betancor, L.; Pessela, B. C. C.; Guisan, J. M.; Fernandez-Lafuente, R., *Biomacromolecules*, **2003**, 4, 772.

332 Gurumurthy, C.; Kramer, E. J.; Hui, C. Y., *Journal of Adhesion*, **2006**, 82, 239.

333 Luzinov, I.; Julthongpiput, D.; Liebmann-Vinson, A.; Cregger, T.; Foster, M. D.; Tsukruk, V. V., *Langmuir*, **2000**, 16, 504.

334 Kitsara, M.; Chatzichristidi, M.; Niakoula, D.; Goustouridis, D.; Beltsios, K.; Argitis, P.; Raptis, I., *Microelectronic Engineering*, **2006**, 83, 1298.
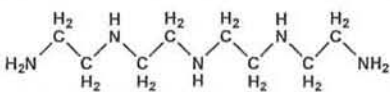
Chapter 2

Experimental

2.1 Materials and Methods

2.1.1 Polymers and Reagents

Various polyelectrolytes and epoxy resins used for the construction of epoxy-amine LbL assembly, Au-NPs multilayers and the protection of Au-NPs using epoxy-amine covalent LbL assemblies are summarized in Table 2.1. Polyethylenimine (PEI) was obtained from two sources; one from Sigma Aldrich (PEI) and the other with trade name LUPASOL-HF® from BASF SE (Germany) and used after dialysis (PEI$_{dia}$).

Table 2.1: Polyelectrolytes and polymers used for the construction of multilayers.

Polymers	$\overline{M_w}$ (g/mol)	Supplier
Poly(ethylenimine) **PEI**	25,000	Sigma-Aldrich
Poly(ethylenimine) **(LUPASOL-HF®)**	25,000	BASF Germany
Poly(allylamine hydrochloride) **PAH**	70,000	Sigma-Aldrich
Poly(styrene sulphonate) **PSS**	70,000	Sigma-Aldrich
Poly[(*o*-cresyl glycidyl ether) -*co*-formaldehyde] **CNER**	1270	Sigma-Aldrich
Poly[(phenyl glycidyl ether)-*co*-formaldehyde] **PNER (DEN 438)**[1]	580	Dow Chemicals
Tetraglycidyl-4, 4'-diamino-diphenylmethane **Araldite MY-720**	-	Huntsman
Tetraethylene pentamine **TEPA**	189.30	TCI, Japan
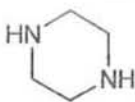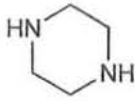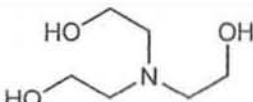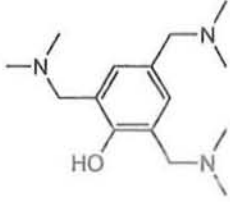
Dialysis was carried out with "SPECTRA/PRO-DIALYSIS MEMBRANE" (MWCO: 3500) obtained from Spectrum Laboratories Inc. USA. High purity solvents were used during this research work. Percentage purity and supplier names of the solvents and chemicals are summarized in Table 2.2.

Table 2.2: Solvents and chemicals used for the build-up of multilayers.

Solvent and Reagents	Percentage Purity	Supplier
Sodium citrate dihydrate	99.0	Sigma-Aldrich
Gold (III) chloride trihydrate	>49.0	Sigma-Aldrich
Acetone	99.8	Carl Roth
Methanol	99	Carl Roth
Sulfuric acid	98	Carl Roth
Hydrochloric acid	37	Carl Roth
Ethanol	99.9	Merck
Sodium chloride	99.5	Sigma

Various catalysts and accelerators were employed to speed up the curing process of epoxy with amines. The catalysts/accelerators were always added to polyamine solution in the concentrations as reported in Table 2.3. The addition of accelerators in the polyamine solution also avoided the self polymerization of epoxy molecules. All the accelerators used were in liquid state to ensure complete miscibility with the polyamine solution. All the accelerators/ catalysts, their structures and suppliers are summarized in Table 2.3.

Table 2.3: Catalysts and accelerators for the curing of epoxies in multilayers.

Accelerators	Structure	Molar Mass	Supplier
Accelerator A-399[2] (contains piperazine)		-	Huntsman
Piperazine[3] (99%)		86.14	Sigma
Triethanolamine (98%)		149.19	Sigma
2,4,6-tris(dimethylamino methyl)phenol (>95%) EEM		265.2	Fluka

Structural formulae of various multifunctional epoxies used during this research work are shown in Figure 2.1. One of the most important considerations behind the selection of a particular molecule for LbL synthesis is its functionality. In a multifunctional molecule, it is expected that some of the functional groups might react with the functional groups of molecule of the underlying layer while some remain un-reacted to accommodate the molecules of in-coming layer.

The multifunctional poly[(*o*-cresyl glycidyl ether)-*co*-formaldehyde] also known as cresol novolac epoxy resin (CNER), n=3 was purchased from Aldrich (Figure 2.1A). Relatively viscous and low molar mass epoxy poly[(phenyl glycidyl ether)-*co*-formaldehyde] also called phenol novolac epoxy resin (PNER), n=1.6 was gifted by Dow Chemical Company (DEN 438) (Figure 2.1B). N, N, N′, N′- tetraglycidyl-4, 4′-diamino-diphenylmethane gifted by Huntsman with trade name Araldite MY-720 is a low viscosity and low molar mass tetra functional epoxy resin (Figure 2.1C)

(A)

(B)

(C)
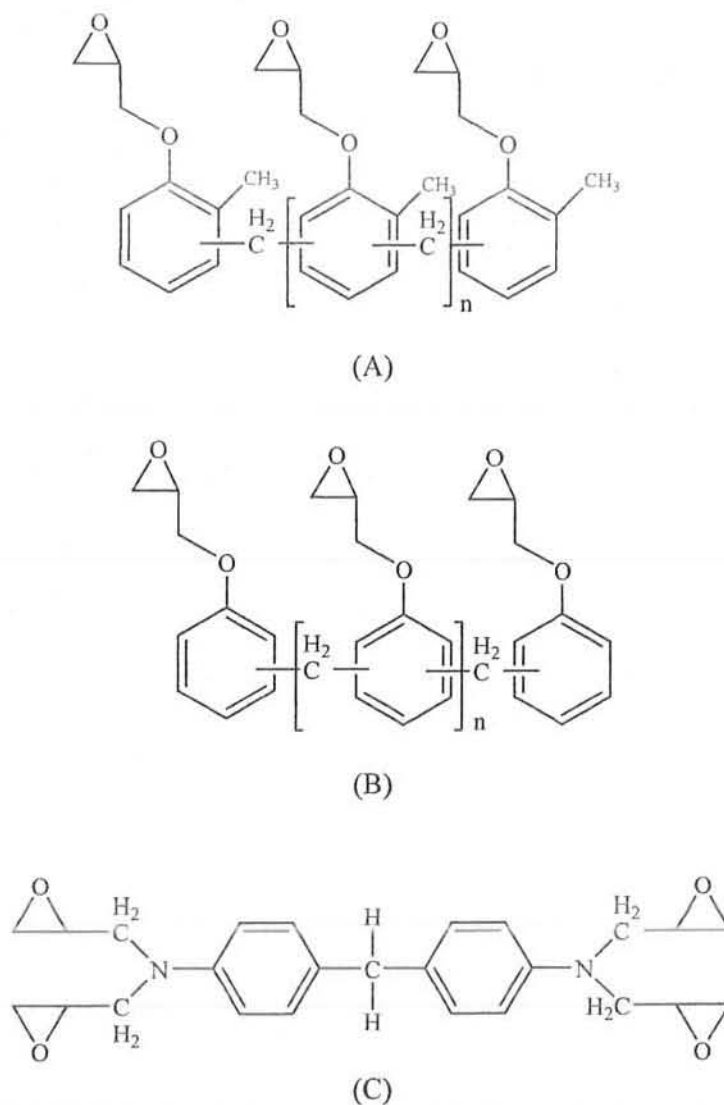
Figure 2.1: Structural formulae of epoxies; CNER (A), PNER (B) and Araldite MY-720 (C)

2.1.2 Polymer Solutions Preparation

All the epoxy solutions were prepared in acetone and kept in caped glass bottles, while PEI solution was prepared by using ultrapure water (Milli-Q plus system, Millipore) with a resistivity of at least 18.2 MΩ·cm in polystyrene bottles. Polyelectrolyte solutions were always freshly prepared by direct dissolution of their respective adequate amounts. Thus, PEI at 1.0 mg mL^{-1}, PSS at 0.6 mg mL^{-1} and PAH at 0.27 mg mL^{-1} were prepared respectively for the buildup of polyelectrolyte multilayers and Au-NPs multilayer. Each polyelectrolyte, except PEI, was dissolved in 0.5 M sodium chloride solution prepared in Milli-Q water. All final

polyelectrolyte concentrations correspond to about 3×10^{-3} monomol L^{-1} in which monomol corresponds to moles of the respective monomer repeat unit.

2.1.3 Gold Nanoparticles Synthesis

Au-NPs may be synthesized by reducing the tetrachloroauric acid ($HAuCl_4 \cdot 3H_2O$) in aqueous solution[4], in the presence of different reducers such as sodium citrate, sodium borohydrate or even some polymers with amine groups, like poly(ethylenimine). The experimental conditions for the synthesis of Au-NPs, such as heating or ambient, depends on the nature of reducing agents used. In this work, Au-NPs were synthesized by reducing $HAuCl_4$ with sodium citrate at 90°C.
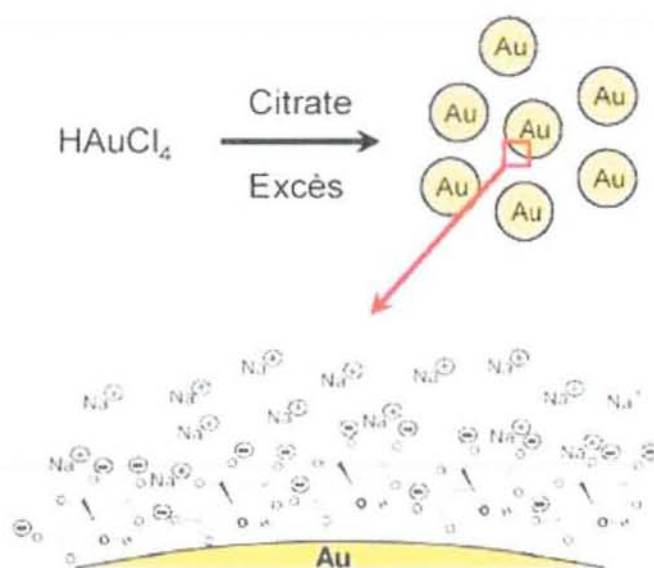
Figure 2.2: Representation of citrate based Au-NPs

$HAuCl_4$ solution (1.0 mM) was heated at 90°C with vigorous stirring followed by the addition of 150 ml of 38.8 mM sodium citrate solution which resulted in the formation of Au-NPs. These Au-NPs having excess of sodium citrate (Figure 2.2) were used without further purification. The mean diameter of the synthesized Au-NPs was approximately 13.6 nm[4].

2.1.4 Dialysis of LUPASOL-HF®

The polyethylenimine (PEI) supplied by BASF specialty chemicals, with trade name Lupasol-HF® was highly branched with molar ratios of primary to secondary to

tertiary amino groups of 34:40:26[5,6] respectively. The polydispersity of BASF Lupasol-HF® having $\overline{M_w}$ = 25,000 is very high as it contains polymer chains of varying molecular weight along with traces of ammonia. To get the molecular chains with a narrow molar mass distribution, dialysis of Lupasol-HF® was carried out with SPECTRA/PRO-DIALYSIS MEMBRANE (MWCO: 3500) obtained from Spectrum Laboratories Inc. USA. A pre-weighed quantity of Lupasol-HF was diluted ten times with Milli Q water in a polystyrene bottle and stirred for 30 min. The dialysis membrane was cut and washed thoroughly with osmosed water and then placed in a 10 L beaker and agitated for further half an hour (Figure 2.3).
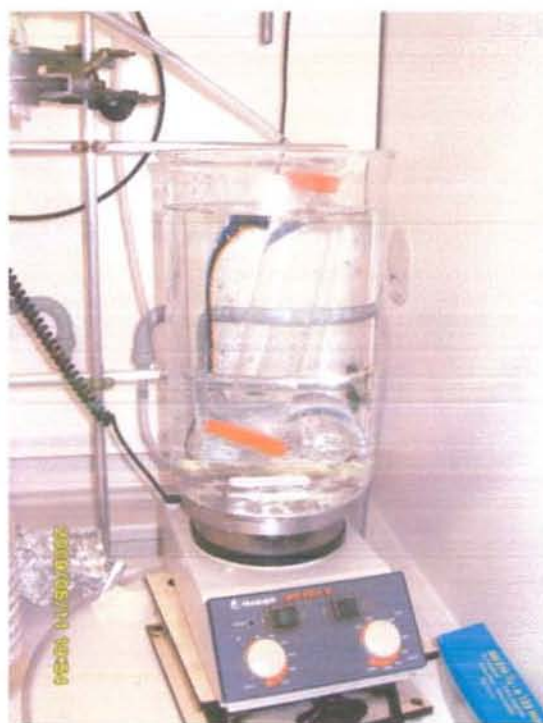
Figure 2.3: Dialysis set up of Lupasol-HF®.

It was removed from the beaker and washed again before sealing one end with a plastic clip. The dilute solution of Lupasol-HF® was poured into the dialysis membrane carefully and then its receiving end was also carefully clipped and placed back in a 10 L beaker filled with osmosed water. The stirring was continued for 8 to 10 days while water of the system was changed twice daily. The low molar mass polyamines emerging out of the dialysis membrane were monitored with the help of litmus paper after every 24 hr till neutral solution was obtained. More than 70 percent

of water was removed from the Lupasol-HF$^®$ using rotary evaporator. The remaining traces of water were removed using freeze drying process with liquid nitrogen. The PEI$_{dia}$ obtained was less than half of the original mass of Lupasol-HF$^®$ taken before dialysis.

2.1.5 Substrate Preparation

Silicon wafers with an orientation (100) were purchased from Wafernet Inc. UK. All wafers were cut to a size of about 12 mm × 45 mm for film construction and 25 mm × 75 mm for rubbing machine tests. Standard cut edge quartz slides were purchased from Geschnitten, Zu 100 ST. Neutral Verpacket Mikro. Quartz slides Thvet B France, Lames en QZS, UV, (32 x 12 x 1mm) and also from Hellma, Germany.

Before the film deposition, all Si wafers and quartz slides were cleaned by immersing in a mixture of methanol and hydrochloric acid (1:1, v/v ratio) for 30 min to remove any dirt and grease and then stored in concentrated sulfuric acid solution for overnight. All wafers were extensively rinsed with Milli-Q water and dried under a stream of nitrogen gas and used within a few hours for the deposition of multilayer films.

2.2 Film Build-up

2.2.1 Epoxy Film Build-up *via* Dipping Technique[7]

For all (PEI/ER)$_n$ multilayer films, the pre-cleaned substrate (Silicon wafer or Quartz slide) was first dipped in PEI solution for a specified times (t$_1$), followed by 2 min subsequent rinsing (t$_2$) with Milli-Q water in three different washing steps. After drying the substrate with nitrogen or compressed air, the substrate with PEI layer was then dipped in the epoxy resin solution prepared in acetone. This dipping time (t$_3$) for epoxy solution was kept the same as that of PEI solution (t$_1$ = t$_3$), followed by the rinsing in pure acetone for 2 min (t$_4$), in three different washing steps. The volumes of all solutions for dipping and rinsing steps were 15-20 mL.

Subsequently rinsing in three different solvent baths ensures the removal of weakly adsorbed material and reduces cross-contamination of the solutions in comparison with rinsing in a single wash beaker. After drying the film under a stream of pure nitrogen or compressed air, ellipsometric measurements were made to determine the

thickness of the layer pair. Typically, for the multilayer architectures (PEI/ER)$_n$, the total number of deposited layer pairs "n" was between 4 and 12. The outermost layer is always an epoxy layer. So, for a single layer pair, the total deposition time is $T = t_1 + t_2 + t_3 + t_4$.

The w/v concentrations of the epoxy solutions were the same as the concentration of PEI solution, so that (PEI conc.) = (ER conc.). Six concentrations of 1, 10, 20, 40, 80 and 100 mg mL^{-1} for both PEI and epoxy solutions were used for the buildup of epoxy-amine multilayers. The effect of time course was studied by changing dipping time of the substrate in PEI and epoxy solutions. Five different dipping time, $t_1 = t_3 = 25, 50, 120, 180$ and 240 min were chosen initially. In subsequent experiments, the adsorption time was reduced by using PEI$_{dia}$ and the paint brush spray system to spray the PEI$_{dia}$ (40 mg mL^{-1}) solution for time as low as 10s while dipping time in ER (100 mg mL^{-1}) was reduced to 10 min, thus speeding up the deposition process.

For all concentrations and dipping times, the rinse time was kept the same i.e. three rinse cycles for 2 min each ($t_2 = t_4$). After the deposition of each layer pair, the film thickness was measured by ellipsometry. For the films which were deposited on quartz substrates, UV-Visible measurements were also taken after deposition of each layer pair to ensure whether film growth was taking place by observing increase in absorption at the λ_{max} of UV active chromophore.

2.2.2 Accelerators Used for the Curing of Epoxy Resins

A number of accelerators and catalysts were also used to effectively cure the epoxy-amine LbL assemblies. Accelerators along with their structure and source are summarized in Table 2.3. The accelerators were used in order to get rapid curing of epoxy compounds as well as to get thicker layer pairs of epoxy-amine network as compared to un-catalysed systems. The accelerators used were in liquid state and completely miscible with the aqueous polyamine solution in the concentrations reported. Piperazine (P), accelerator 399[2] (A-399) and 2, 4, 6-tris(dimethylaminomethyl)phenol, also called epoxy embedding medium accelerator (EEM) was added in 10 mg mL^{-1} based on polyamine solution. Another catalyst system used was a combination of EEM ($\sim$10 mg mL^{-1}), piperazine ($\sim$10 mg mL^{-1}) and triethanolamine ($\sim$24 mg mL^{-1}) as reported by Waddill[8].

2.2.3 Au-Colloid Film Buildup by Spray Technique

The (PAH/Au-NPs)$_n$ colloid film was deposited on silicon wafer or quartz slide by spray; a technique discovered by Schlenoff and his team[9]. This technique allows us to fabricate a layer pair in 1 or 2 min, an acceleration of 50-150 times[10] in term of working time compare to the traditional dipped film. In addition, the sprayed film keeps the stratified structure the same as given by the dipped film[11]. A former paper[12] has described in details the fabrication and characterization of sprayed (PAH/Au-NPs)$_n$ films. The procedure is described briefly.

PEI layer was deposited onto a substrate by dipping followed by a PSS layer deposited by spray technique, followed by the consecutive PAH and Au-NPs spray. The spray conditions for polymer and Au-NPs were, spray time t_1=5s, adsorption or waiting time t_2 = 15 s, rinse solution NaCl (0.5 M) for PAH or Milli-Q water for Au-NPs spray time t_3 = 5 s, waiting time t_4 = 15 s. It should be noted here that, in order to ensure a full surface coverage by Au-NPs layer, the spray and rinse cycle for Au-NPs were repeated 5 times. So, for the deposition of a single PAH layer, the total working time is 40 s, and for Au-NPs layer, the working time is 200 s. After the (PAH/Au-NPs)$_n$ colloid film deposition, an additional (PAH/PSS) layer has been sprayed on the colloid film in order to cover the colloid film and make a connection to the next sequential PEI/ER film deposition.

The film growth was measured by ellipsometry. Prior to the ellipsometric measurement, all samples were rinsed by the particular solvent thoroughly based on the last layer and dried under a stream of nitrogen gas.

2.3 Mechanical Protection of Au Colloid Film

2.3.1 Protection of Au Colloid Film *via* Dipping Process

Two epoxy resins (CNER and PNER) were chosen for the protection of Au-NPs. The epoxy architecture of (PAH/Au-NPs)$_5$/(PEI/ER)$_{10}$ was obtained following the optimised adsorption conditions selecting PEI and epoxy resin concentration as 40 mg mL^{-1}. The dipping time for both polymer solutions (t_1 and t_3) were 50 min each. Thus it was ensured that the epoxy layer was always an outer layer. The samples were then stored in the polystyrene containers to allow time cure process at room temperature before being subjected to rubbing machine test.

2.3.2 Fast Epoxy Protection of Au Colloid Film *via* Alternate Spray-Dipping Process[13]

On the other hand in order to fasten the deposition process, PEI_{dia} with narrow molecular weight range was selected as polyamine curing agent for the two epoxies. PEI_{dia} (40 mg mL^{-1}) was sprayed with the help of paint spray brush for $t_1 = 10s$ followed by adsorption time of 30 s. Washing was done with the help of Milli-Q water using "AIR-BOY" spray cans for three times with $t_2 = 10$ s wash time. The substrate was then dipped into the epoxy resin solution made in acetone (100 mg mL^{-1}) for t_3 =10 min. Three equal time wash with $t_4 = 2$ min were then applied followed by drying with the help of compressed air. After obtaining the desired epoxy-amine film thickness onto the Au colloid film, the samples were stored for time curing process followed by rubbing analysis and AFM measurements.

2.4 Instruments Used

2.4.1 Manually Operated Sprayer Cans: "Air Boy"

All polyelectrolyte multilayer films or polymer Au-NPs films were deposited on a PEI precursor layer. The PEI layer was obtained by dipping a pre-cleaned Si wafer or quartz slide for 5 min in aqueous PEI solution. This was followed by rinsing with abundant Milli-Q water and drying with the help of nitrogen flux before further spray or dipping deposition.

The Au nanoparticles films were deposited on the substrate by spray with a commercial manual sprayer "AIR-BOY" purchased from Carl Roth. The spray bottle is made up of polypropylene and polyethylene (Figure 2.4). For each multilayer film formation experiment, four spray cans were needed: one for polyanion, one for polycation, one each for the rinsing solution of polycation and polyanion.

Figure 2.4: Photograph of manual sprayer "AIR-BOY".

2.4.2 Paint Brush Spray System

Paint brush spray system (Aerographe double action) obtained from PAASCHE Millennium-Wood was used to spray PEI_{dia} onto substrate in order to speed up the adsorption process (Figure 2.5).
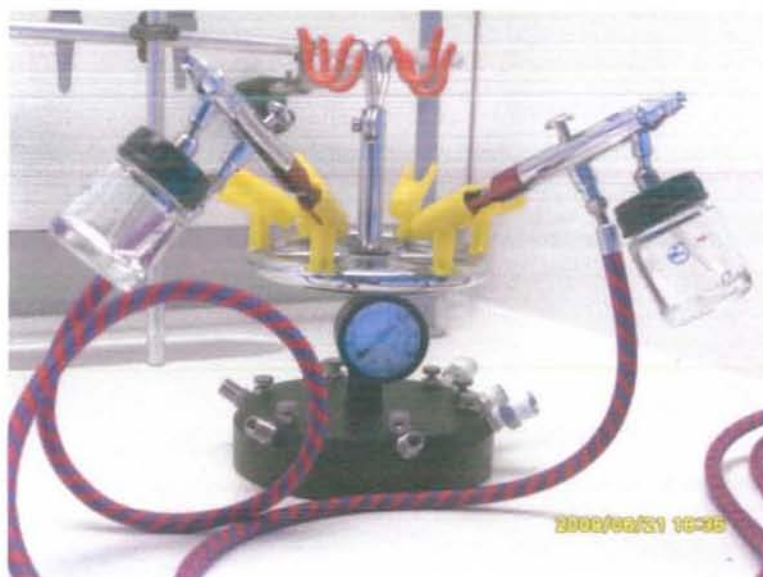

Figure 2.5: Photographic image of paint brush spray system.

The paint brush spray is advantageous in terms of polymer solution consumption and accuracy of spraying area. In addition compressed air is used to make a fine jet of the spray solution. During time of flight of the spray to the substrate, some of the solvent

might dried up due to evaporation, thus more concentrated polymer solution adsorbed on the substrate.

2.4.3 Ellipsometry

Ellipsometry[14] is an absolute non-contact and non-destructive optical technique for the measurement of thickness in the nm to micrometer scale with an angstrom resolution. It is highly accurate and reproducible technique for the measurement of surface roughness, crystallinity, anisotropy and refractive index of ultrathin transparent absorbing films on opaque absorbing substrates. Basically, it uses a polarized light as the investigation source and measures the polarization changes of reflected or transmitted light beam in the UV and IR region of the electromagnetic spectrum. In terms of sample preparation, the sample should be covered by optically homogeneous and well-defined isotopic layers to get the best dielectric properties of these layers.

The ellipsometer measures change in polarization of light reflected from a sample in terms of two parameters Δ and Ψ. These values are related to the ratio of Fresnel amplitude reflection coefficients for p- and s- polarised light through the equation;

$$R_p/R_s = \tan\Psi \exp(j\,\Delta)$$

$\tan\Psi$ measures the ratio of the modulus of the amplitude of reflection. The phase difference between p- and s-polarized reflections light is given by Δ. The ellipsometer measures the ratio of these two values so accurately that it does not need a reference sample and also it is not susceptible to light source fluctuations.
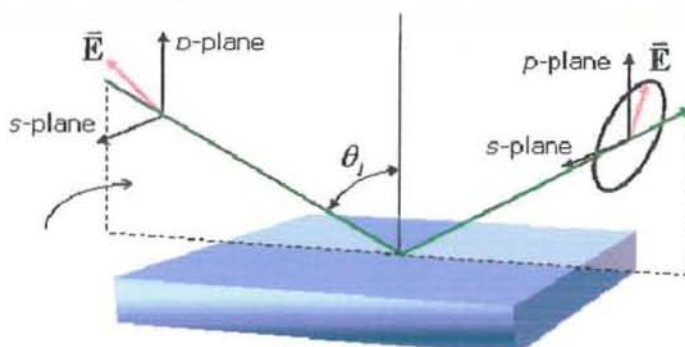

Figure 2.6: Block diagram of an ellipsometer[15].

Since it measures phase changes, it is highly sensitive to the presence of ultrathin films down to sub monolayer coverage. The *s*- plane is perpendicular to the plane of

incidence while the *p-* plane is parallel to the plane of incidence as shown in the Figure 2.6.

Measurement of the film thickness after every layer pair was carried out with a PLASMOS SD-2300 instrument operating with a He/Ne laser source at the single wavelength of 632.8 nm and a constant incident angle of 70° (Figure 2.7). The refractive indices of all polymer films was assumed to be constant at n = 1.465. While this procedure leads to a slightly incorrect values with respect to the absolute film thickness, but it allows for a quick determination of the relative film thickness. During the thickness measurement of each layer pair, ten different points were taken to obtain an average value and homogeneity.

The film thickness values mentioned in this study were obtained using the following assumption. For a polymer, the imaginary part of the refractive index is negligible because most polymers have no measurable absorbance in the range of the operating laser wavelength, which is around 632.8 nm. As a result, there is no Kramers-Kronig restriction for the measurement of thickness of most polymer films[16]. However, attention needed for the polymer/nanoparticle films, especially polymer/gold nanoparticle films. Au-NPs have strong plasmon absorption in the wavelength range 550-600 nm, which is close to operating laser wavelength of PLASMOS SD-2300 ellipsometer. So, during this measurement, there is a measurable light absorption by the Au-NPs present within the polymer films. As a consequence, the imaginary part of the refractive index should not be negligible any more corresponding to a Kramers-Kronig restriction.

However, qualitative interpretation of the film thickness is possible even when neglecting the absorbance of the film. For PLASMOS SD-2300 ellipsometer, there is no imaginary part in the refractive index settings, the thickness of polymer/Au-NPs film measured by such ellipsometer will be an indicative value other than a true value. However, these thickness measurement values give us a rapid estimation for the film growth mechanism. The linear growth of such polymer/Au-NPs film was also monitored with the help of UV-Visible spectroscopic studies.

Figure 2.7: Photographic image of the PLASMOS SD-2300 ellipsometer.

2.4.4 Ultraviolet-Visible Spectroscopy

For the monitoring of LbL build-up, UV-Visible spectroscopy has proved to be a primary tool as with increase in number of layer pairs, the absorption increases linearly. UV-Visible studies were performed by a Varian CARY 500 Scan UV-Vis-NIR spectrometer version 8.01 with a wavelength range of 190-800 nm. Source changeover takes place at 350 nm. All the samples were analysed at a scan rate of 50 nm min^{-1} with data interval 0.083 nm. The substrate for this purpose was always a quartz slide with particular dimensions to fit in the UV sample chamber.

Ultraviolet Visible NIR spectroscopy refers to absorption spectroscopy in the UV-Visible and near infra red region of the electromagnetic spectrum (190-3300 nm). This means it uses light in the visible and adjacent (near-UV and near-infrared (NIR)) ranges. In this region of the electromagnetic spectrum, molecules undergo electronic transitions. This method is quantitative for determining the concentration of an absorbing species in solution using Beer-Lambert Law.

According to Beer-Lambert law, the absorbance of a solution is directly proportional to the concentration of the absorbing species in the solution and the path length of the cell containing it. Thus, for a fixed path length, UV-Visible spectroscopy can be used to determine the concentration of the absorbing species in a solution. It is important to

know dependence of absorbance with change in concentration of the absorbing species. This can be taken from literature or more accurately, determined from a calibration curve. The mathematical form of the Beer-Lambert Law is given as;

$$A = -\log_{10}(I/I_0) = \varepsilon . c . L$$

where A is the absorbance to be measured, I_0 is the intensity of incident light at a particular wavelength, I is the intensity of the transmitted light, L is the path length of the cell containing sample solution and c is the concentration of the absorbing species (chromophore) in the solution. ε is a constant known as the molar absorptivity or extinction coefficient. For each species at a specific wavelength, this constant is a fundamental molecular property in a given solvent, at a particular temperature and pressure.

2.4.4.1 Instrumental Setup of UV-Visible Spectrometer

UV-Visible spectrophotometer measures the intensity of light passing through a sample (I), and compares this intensity to its original intensity (I_0). The ratio I/I_0 is called transmittance, usually expressed as a percentage (%T). The absorbance, A, is based on the transmittance as well:

$$A = -\log_{10}(\%T/100\%)$$

The basic set up of a UV-Visible NIR spectrophotometer consists of a light source, a sample holder, a diffraction grating or monochromator to separate the different wavelengths of light and a detector. A deuterium discharge lamp is usually used as light source for UV measurements and a tungsten-halogen lamp for visible and near infra red (NIR) measurements. The instruments automatically swap lamps when scanning between the UV, visible and NIR regions.

The wavelengths of these continuous light sources are typically dispersed by a holographic grating in a single or double monochromator or spectrograph. The spectral bandpass is determined by the monochromator slit width or by the array-element width in array-detector spectrometers. A combination of a PMT and a Peltier-cooled PbS IR detector is used in UV-Vis-NIR spectrometer. The light beam is

redirected automatically to the appropriate detector while scanning between the visible and NIR regions.

2.4.4.2 Applications of UV-Visible Spectroscopy

UV-Visible spectroscopy is usually used in the determination of materials containing metal ions and highly conjugated organic molecules. The d electrons of the metal ions or organic compounds, especially those with a high degree of un-saturation can be excited by the incident light from one electronic state to another, resulting in an absorption peak in the spectrum. Every substance has its unique absorption peak (absorption maximum, Abs_{max}) at a certain wavelength (wavelength maximum, λ_{max}), which makes the UV-Visible spectroscopy a quantitative and qualitative technique to characterize the presence of absorbing substances.

2.4.5 Atomic Force Microscopy (AFM)

AFM is a major tool for visualizing the surface morphological studies of ultra-thin samples. So, most of the AFM measurements were performed on MULTIMODE AFM supplied by Veeco USA with a controller Nanoscope IIIa (formerly called Digital Instruments) at the Institut Charles Sadron, Strasbourg, France. For surface topology studies, AFM was operated in tapping mode with a noncoated Silicon cantilever (Veeco, model TAP150, typical frequency is about 68-132 kHz). Inner morphology of the epoxy-amine network was also studied in the contact mode by gradually raising the cantilever force upto 400 nN. AFM images of some sample were analysed using AFM Omicron ultra high Vacuum (UHV) scanning probe microscopy (SPM) system at University of Manchester while some other AFM images were taken using Nanoscope 3, Multimode SPM supplied by Veeco, at Bath University. The AFM images of those samples which were subjected to rubbing analysis were scanned in two different scan sizes 5-6 μm and 10-12 μm.

Binnig, Quate and Gerber invented the first atomic force microscope (AFM) in 1986[17]. Scanning electronic microscope (SEM) visualize the sample surface while AFM feels the sample surface with a mechanical probe by measuring the variations in interaction between the scanning probe and the sample surface[18]. AFM is similar to the high-resolution scanning tunnelling microscope (STM). The piezoelectric elements helps in the movements of the scanning probe on the sample surface, which

makes AFM one of the best analytical instruments for imaging, measuring and manipulating small objects on the surface with a nanometre scale resolution.

2.4.5.1 Principle and Basic Set up of AFM

A typical AFM instrument is composed of a cantilever with a sharp tip at its end to scan surfaces, a piezoelectric element as mechanical movement unit; a laser source and a photodiode detector as analytical unit. A basic set up of an AFM unit is shown in Figure 2.8. The cantilever is usually made up of silicon or silicon nitride. The curvature radius of the tip is of the order of nanometres and the tip is ideally terminated by a single atom in order to ensure the best resolution. When the tip is brought into the proximity of a sample surface, forces between the tip and the sample lead to deflection of the cantilever according to Hooke's law.
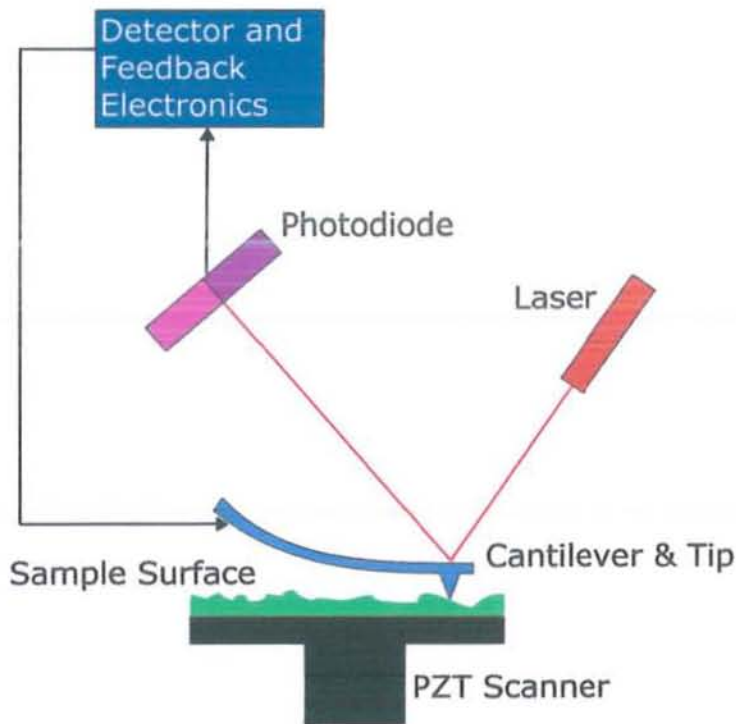
Figure 2.8: Block diagram of AFM[19].

If the tip of the cantilever scanned the sample surface at a constant height, a risk would exist that the tip collides with the surface, causing damage to the tip. Therefore, in most cases a feedback mechanism is employed to adjust the tip-to-sample distance to maintain a constant force between the tip and the sample. The sample is mounted

84

on a piezoelectric tube, which move the sample in the z direction for maintaining a constant force, while the x and y directions for scanning the sample.

When the cantilever tip is brought into the proximity of a sample surface, interaction energy between the tip and the sample is shown in the Figure 2.9. The interaction energy between the AFM tip and atoms on the sample surface has two components, one is repulsive component, indicating that the tip is very close to the surface and the other one attractive, indicating that the tip is not too close to the surface.
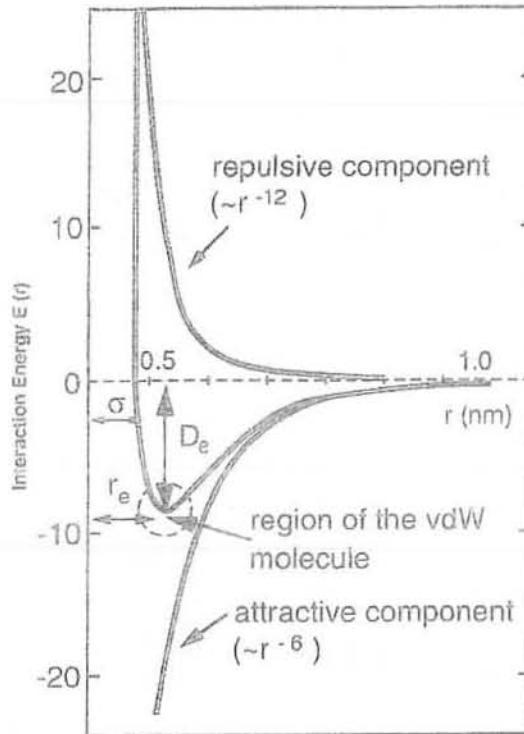
Figure 2.9: Surface/AFM tip interaction energy variation as a function of distance.

Typically, in an AFM imaging, interactions like capillary interactions, chemical bonding, electrostatic interactions etc could be excluded except the Van der Waals interactions, which correspond to the minimum level of interaction energy in the above figure. It is the region where AFM tip can detect the interacting energy changes, for example, from repulsive to attractive. According to the strength of these interaction energies, there will be a deflection of the AFM cantilever tip and this deflection is governed by the Hooke's law. The deflection of the cantilever is measured using a laser spot reflected from the top surface of the cantilever into an

array of photodiode. The movement of this laser spot plus the computational simulation will provide information about the topology of the sample surface.

2.4.5.2 Imaging Modes

The AFM instrument can be operated in various imaging modes, such as static (also called contact) mode or dynamic (tapping) mode. In contact mode, the tip deflection is used as feedback signal. A low stiffness cantilever is used in order to minimize the influence of acoustic. However, when the tip is approaching the surface, the attractive forces may become quite strong thus causing the tip to "snap-in" to the sample surface. Therefore, the contact mode AFM is always done in contact with the sample where the overall force is repulsive, and hence it is given the name "contact mode". In this mode, the force between the tip and the surface is kept constant during scan by maintaining a constant deflection. In the contact mode, interactions between AFM tip and the surface is repulsive, Figure 2.9 (repulsive component).

In the dynamic mode (tapping mode), the cantilever is externally oscillated at or close to its fundamental resonance frequency. The resonance frequency amplitude, phase and oscillation are customized by tip to sample interaction forces. The changes in oscillation with respect to the external reference oscillation provide information about the samples features. In this mode, the interactions between AFM tip and the surface is attractive, Figure 2.9 (attractive component).

However, at ambient condition, most of the samples develop a liquid meniscus layer on the surface, which may stick the tip to the surface during the scan for a short-range forces investigation, the dynamic imaging mode has by-passed this problem very well but the resolution is better in contact mode.

Tapping mode inherently prevents the tip from sticking to the surface and thus preventing damage during scanning. Tapping mode provides three types of data i.e. height mode, phase mode and amplitude mode. Another benefit of the tapping mode technique is its large, linear operating range. This makes the vertical feedback system highly stable, allowing routine reproducible sample measurements. In this imaging mode, the variation in amplitude of oscillation gives direct information about surface morphology of the sample while the phase oscillation variation provide information

about chemical contrast of the sample surface. During this research work, the dynamic (tapping) imaging mode was mostly employed to record the height images.

2.4.5.3 Advantages of AFM Imaging

AFM has a number of advantages as it provides a true 3-D topological imaging of the sample surface. Also, samples subjected to AFM do not require any special pretreatment (such as metal/carbon coatings) that would irreversibly change or damage the sample surface. Most of the AFM can work flawlessly well in ambient air or even in a liquid environment. This makes it possible to study bio-macromolecules and even living micro-organisms. The AFM can scan a maximum height up to micrometers and a maximum scanning area of around 150 x 150 micrometers.

2.4.6 Rubbing Machine

A rubbing machine was used for testing the mechanical robustness of the prepared epoxy-amine LbL films as well as epoxy-amine protected and unprotected Au nanoparticles multilayers at room temperature. This rubbing machine was built by the Atelier Mechanique Department of Institut Charles Sadron, Strasbourg, France. The working pressure of rubbing machine is 2 bars. The working of the rubbing machine consists of brushing the sample surface with the help of cotton velvet cloth held by a pneumatic vacuum pump[20] (Figure 2.10). The brushing/rubbing cycles are automated and controlled by an electropneumatic way. This rubbing machine is not a quantitative apparatus, so there are no exact values for applied force, but for each rubbing cycle, the applied force was kept always constant, which means, for all rubbing test, the operating conditions are the same.

The thickness of the sample before and after rubbing test was always measured with an ellipsometer to observe any loss of material caused by the rolling cylinder of the rubbing machine. The surface morphologicaly studies were performed with AFM in tapping mode.

Figure 2.10: Photographic image of the rubbing machine.
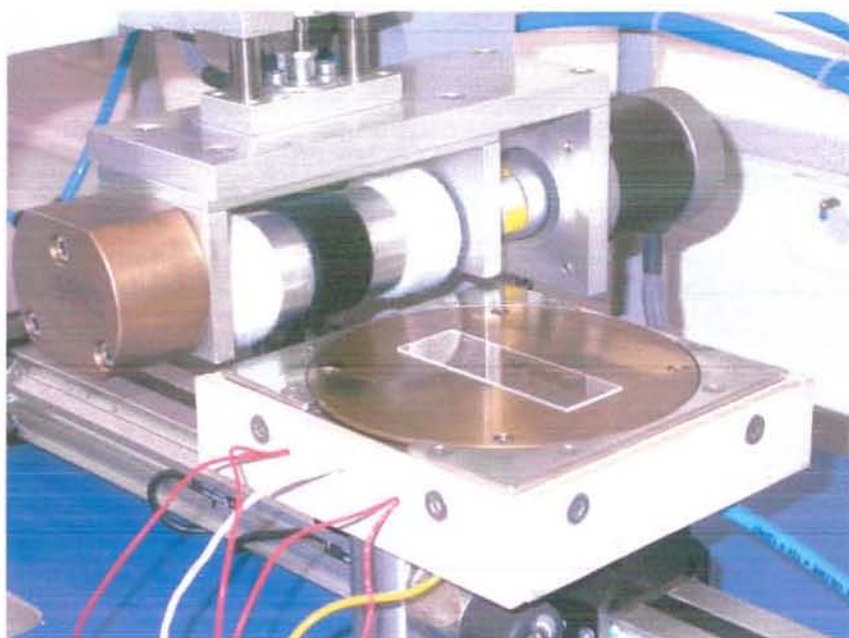
All the prepared samples were subjected to 1, 5, 15 and 20 rubbing cycles initially to observe the mechanical strength of the prepared films. After establishing the mechanical robustness of the epoxy-amine multilayer films upto 20 rubbing cycles, the number of rubbing cycles was increased to observe the maximum number of rubbing cycles endured by a particular sample.

2.5 References:

1- Technical Bulletin, DEN® 438®, Dow Chemical Company.

2- Accelerator 399, Technical Bulletin, Huntsman Corporation.

3- Ribera, D.; Manteco, A.; Serra, N. A., *Liquid-Crystalline Thermosets*, **2002**, 40, 3916.

4- Schneider, G.; Decher, G., *Nano Letters*, **2004**, 4, 1833.

5- Andreas, F.; Thunemann, J. B., *Macromolecules*, **2003**, 33, 6878.

6- Information by manufacturer BASF, specialty chemicals, Ludwigshafen, Germany.

7- Shahid *et al.*, Covalent layer-by-layer assembly with components from epoxy glue: Toward mechanically robust multimaterial thin film devices (under preparation)

8- Waddill, H. G., US, Patent, 4, 800, 222, **1989.**

9- Schlenoff, J. B.; Dubas, S. T.; Farhat, T., *Langmuir*, **2000**, 16, 9968.

10- Izquierdo, A.; Ono, S. S.; Voegel, J. C.; Schaaff, P.; Decher, G., *Langmuir*, **2005**, 21, 7558.

11- Felix, O.; Zheng, Z.; Cousin, F.; Decher, G., *Comptes Rendu Chimie*, **2009**, 12, 225.

12- Zheng, Z.; Felix, O.; Decher, G., *Chemical Communications*, **2008**, submitted.

13- Shahid *et al.*, Optimisation and speed up of deposition conditions for covalent LBL assemblies of epoxy components for producing robust multilayer films (manuscript under preparation).

14- Piel, J. P.; Castellon, B.; Lecat, J. H.; Boher, P.; Stehle, J. L., *Ellipsométrie: Théorie, Bernoux*, R6490, **2003**, Edit. Techniques de l'Ingénieur.

15- www.uta.edu/optics/research/ellipsometry/ellipsometry.htm

16- Lucarini, V.; Saarinen, J. J.; Peiponen, K. E.; Vartiainen, E. M., *Kramers-Kronig Relations in Optical materials Research, Series: Springer Series in Optical Sciences*, **2005**, 110 Edit. Springer.

17a- Binnig, G.; Rohrer, H.; Gerber, Ch.; Weibel, E. *Phys. Rev. Lett.* **1982**, 49, 57.
b- Binnig, G.; Quate, C. F.; Gerber, Ch. *Phys. Rev. Lett.* **1986**, 56, 930.

18- MultiMode SPM Instruction Manual, Version 4.31ce, Digital Instruments Veeco Metrology Group, **1997.**

19- http://en.wikipedia.org/wiki/atomic_force_microscopy

20- Brinkman, M.; Pratontep, S.; Chaumont, C.; Wittmann, J. C., *Macromolecules*, **2007**, 40, 9420.

Chapter 3

Results and Discussion

3.1 Covalent LbL Nanofabrication using Epoxy Compounds

The polyelectrolyte/epoxy films prepared by covalent LbL assembly were extremely robust and capable of protecting the weak polyelectrolyte/Au-NPs film assembled by pure electrostatic interactions using LbL technique. The virgin polyelectrolyte/Au-NPs films were very easily removed by wiping the film softly with a tissue paper. Appropriate protection film was needed for the weak underlying multilayers so as to provide them the desired mechanical strength for various applications.

The chemisorption of each individual layer must be controlled in a way that the molecules in each layer do not adsorb with all their functional groups binding to the surface below. This would be catastrophic, if all the functional groups were utilised in one layer build-up and would not lead to a regular film growth. Instead conditions must be found at which molecules chemisorb onto the surface with only some of their functional groups bound to the surface while exposing the remaining functional groups to the solution interface as depicted in Figure 3.1.

An obvious choice for the formation of mechanically strong polymer films was the two components of epoxy adhesive. An additional advantage of choosing this combination was that polyamine can be used as intermediate layer between the gold nanoparticles electrostatic assemblies and the protective epoxy covalent LbL assemblies.

After screening a number of different commercially available compounds, a branched poly(ethylenimine) (PEI) and a linear tetraethylpentamine (TEPA) were chosen as polyamine component while poly(o-cresylglycidyl ether)-co-formaldehyde also known as cresol novolac epoxy resin (CNER), poly(phenylglycidyl ether)-co-formaldehyde called phenol novolac epoxy resin (PNER) and Araldite MY-720 were selected as epoxy component to build covalent LbL assemblies for the protection of weak Au colloid layers. The molecules so selected were capable of forming 4 to 12 consecutive multilayers at room temperature for various adsorption times using different polymer concentrations without compromise on optical homogeneity and linear growth.
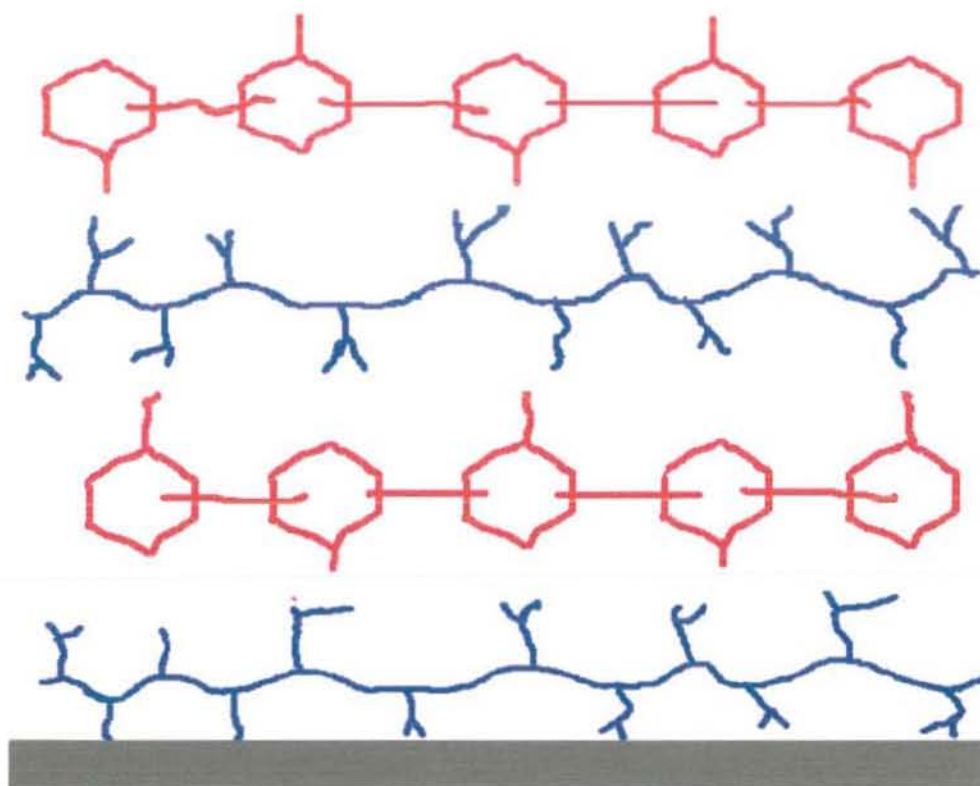
Figure 3.1: Schematic of adsorption of epoxy (Red) and polyamine (Blue) on Si substrate (Grey). Some of the functional groups remained un-adsorbed at each step of LbL build-up.

3.1.1 Optimisation of Concentration and Adsorption Time for (PEI/CNER)$_n$ System

Whether the covalent LbL assemblies follow the classical rules of polyelectrolyte multilayers, like linear growth, concentration course, adsorption time effect, homogeneity and reproducibility etc. Various concentrations of these polymers were used along with different adsorption times to observe whether there is linear growth of the covalent LbL as a function of concentration of polymers and adsorption times. The concentrations of PEI and epoxy were kept the same throughout the optimisation stage except stated otherwise. Thus 1, 10, 20, 40, 60, 80, 100 mg mL^{-1} w/v polymer concentrations were employed for the construction of covalent multilayers during the optimisation stage. In addition, effect of deposition time on the growth of layer pairs for PEI and epoxy resins was also studied. Five different dipping times 50, 100, 240,

360 and 480 min per layer pair were employed. PEI was always dissolved in ultra-pure Milli-Q water while epoxy solutions were prepared in acetone.

For the construction of $(PEI/CNER)_n$ covalent multilayers, the pre-activated substrate (silicon wafer or quartz slide) was dipped in aqueous solution of PEI for a specific time (t_1) followed by subsequent 2 min washing with Milli-Q water in three equal wash baths (t_2). During each washing sequence, substrate was given slight manual agitation to ensure the removal of un-adsorbed polymers chains. The substrate was dried with a stream of nitrogen or compressed air before it was placed in epoxy solution for the same time (t_3) as it was dipped previously in PEI solution so that $t_1 = t_3 = 25$, 50, 120, 180, 240 min. The substrate was then washed with pure acetone for 2 min in three equal wash (t_4). For a single layer pair, the total processing time was, $T = t_1 + t_2 + t_3 + t_4$.

The polyamines solutions were always kept in polystyrene bottles while epoxy solutions in well caped glass bottles. All the dipping and rinsing solutions had a volume of at least 20 mL. Consecutive rinsing in three different solvent baths ensured the removal of loosely bound and un-adsorbed polymeric material and also reduced cross-contamination of the solutions in comparison with rinsing in a single bath. After drying the film under a stream of pure nitrogen gas, ellipsometry measurements were carried out to determine the thickness of the multilayer. For the multilayer architectures $(PEI/CNER)_n$, the total number of deposited layer pairs "n" was between 4 and 12. The outermost layer was always an epoxy layer.

Figure 3.2 shows a linear build-up of $(PEI/CNER)_{10}$ film as a function of different polymer concentrations. During this experiment, the concentration of PEI and CNER solutions were kept the same and the dipping time for each polymer layer was 50 min. The choice of this dipping time will be explained later. The film thickness of $(PEI/CNER)_{10}$ increases linearly as a function of number of layer pairs deposited on the surface. The data correlation coefficient was quite high as evident from the statistics reported by the Kaleidagraph. Error in each individual measurement is represented by error bars which also provide information about the surface roughness of the multilayers so formed. Very low value of error bars for $(PEI/CNER)_{10}$ system confirmed the homogeneity of these covalently bonded LbL assemblies (Figure 3.2).
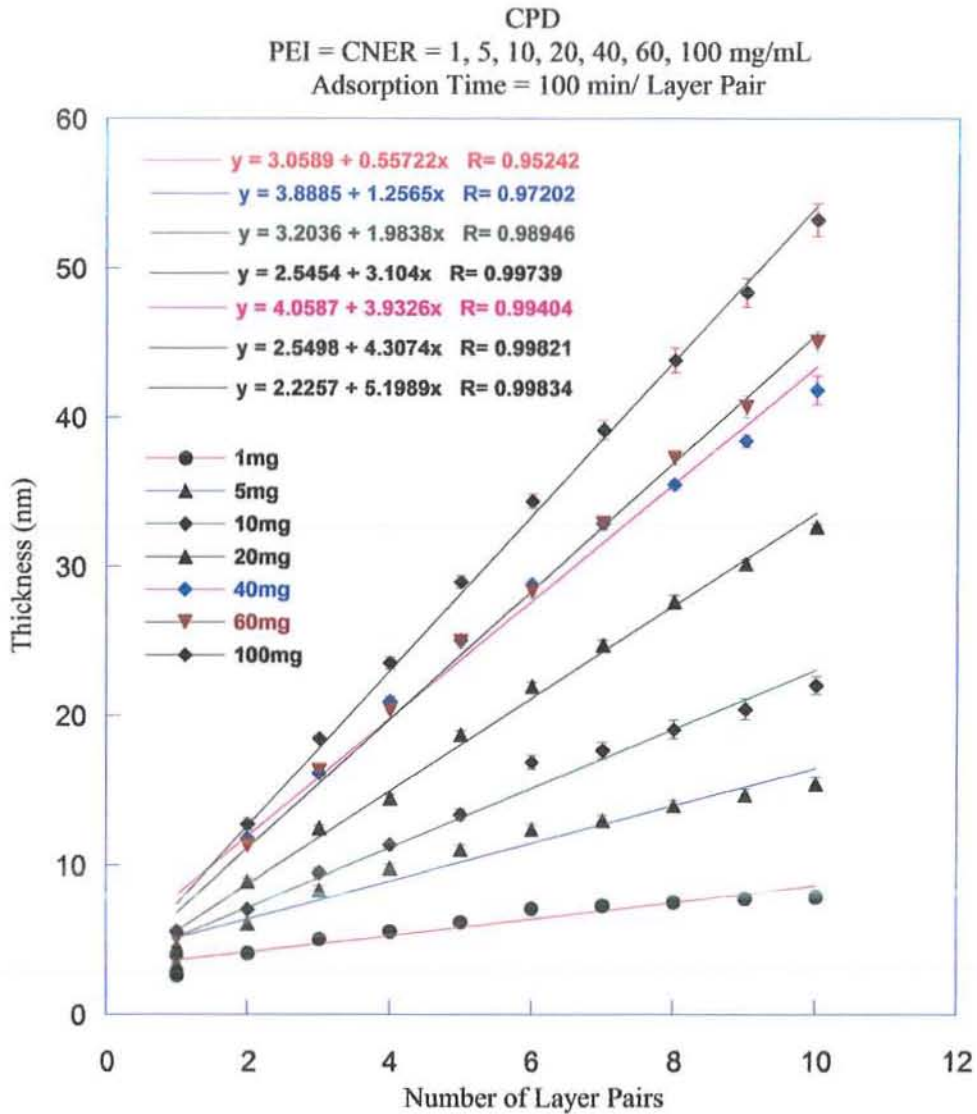
92

Figure 3.2: Thickness of (PEI/CNER)$_n$ films for different polymers concentrations as a function of the number of layer pairs at 100 min per layer pair adsorption time.

The thickness of the epoxy-amine film was measured with the help of an ellipsometer after every layer pair and plotted against number of layer pairs. The single layer pair increment "R" in case of all the concentrations provides information about the average increase in thickness of each layer pair were obtained from the graph of thickness vs number of layer pairs (Figure 3.2). The single layer pair increment was calculated for a series of experiments using 1, 10, 20, 40, 80 and 100 mg mL^{-1} concentrations for both the epoxy and polyamine solutions using 50, 100, 240, 360 and 480 min per layer pair

adsorption times. The results show a linear increase in thickness as a function of both number of layer pairs and concentration of polymers. The experiments were repeated to ensure their reproducibility.
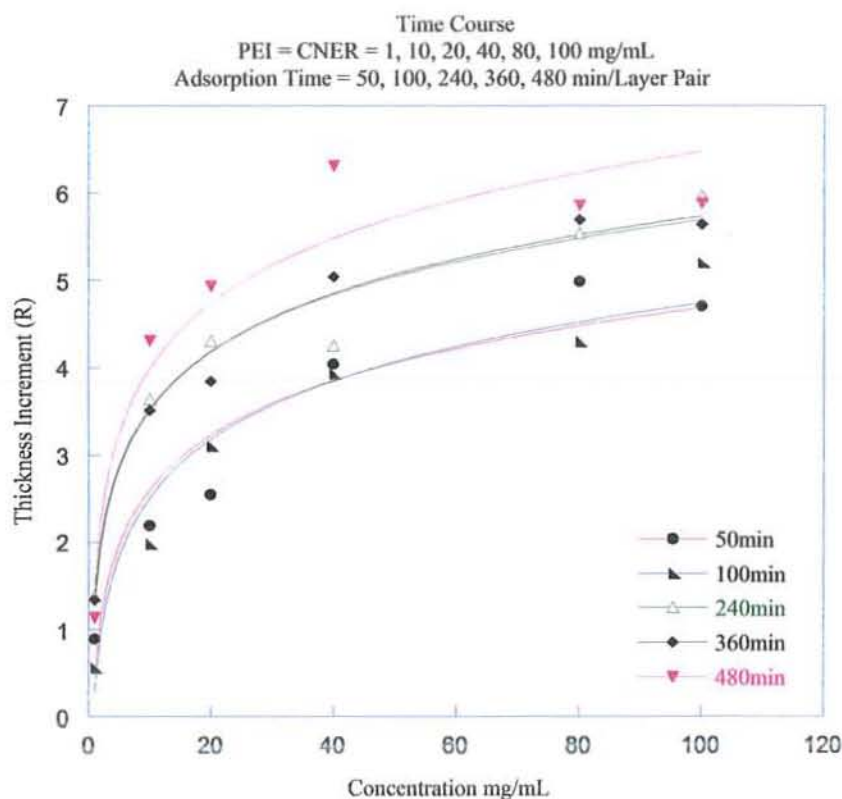

Figure 3.3: Variation of the single layer pair increment of (PEI/CNER)$_n$ films at different adsorption times as a function of polymer concentrations.

Slope coefficients (R) of these experiments were calculated and a matrix was constructed between slope coefficients (called single layer pair increment) against polymer concentrations for different dipping time (Figure 3.3) and secondly against adsorption time for different polymer concentrations (Figure 3.4). Thus, the matrix obtained from about 30 different experiments for (PEI/CNER)$_{10}$, it was observed that the single layer thickness increment increases exponentially in the beginning up to 40 mg mL^{-1} polymer concentrations.

When the concentrations of PEI and CNER were increased from 1.0 to 40 mg mL^{-1}, the single layer pair film increment increased eight folds (0.55 nm for 1.0 mg mL^{-1} polymer solutions to 4 nm for 40 mg mL^{-1}), while for 100 mg mL^{-1} concentration, it

increases ten folds (5.2 nm) as shown in Table 3.1. This means there was no proportionate increase in layer pair increment on raising polymer concentration from 40 to 100 mg mL^{-1}. It was further noted that the higher concentrations of polymers were not only difficult to handle but after a certain number of layer pairs, the optical homogeneity of the multilayer was also deteriorated. Based on these observations, 40 mg mL^{-1} polymer concentration was selected as optimum concentration for further work.

Table 3.1: Single layer pair increment (R) for (PEI/CNER)$_1$ film build-up for different polymer concentrations, as determined from Figure 3.2.

Concentration of Polymers (mg mL^{-1})	Single layer pair increment (nm)
1	0.5
10	2.5
40	3.9
100	5.2

An appreciable increase in single layer pair increment was observed for adsorption time up to 100 min per layer pair for various polymer concentrations (Figure 3.4). Variation of the single layer pair increment with adsorption time for different polymer concentration also show that the longer dipping times do not give a proportionate increase in thickness rather steady thickness increment was obtained. The longer dipping times are practically difficult to carry out with optical non-homogeneity of the films. So 100 min per layer pair adsorption time was optimised for dipping mode covalent LbL assembly of epoxy-amine multilayers.
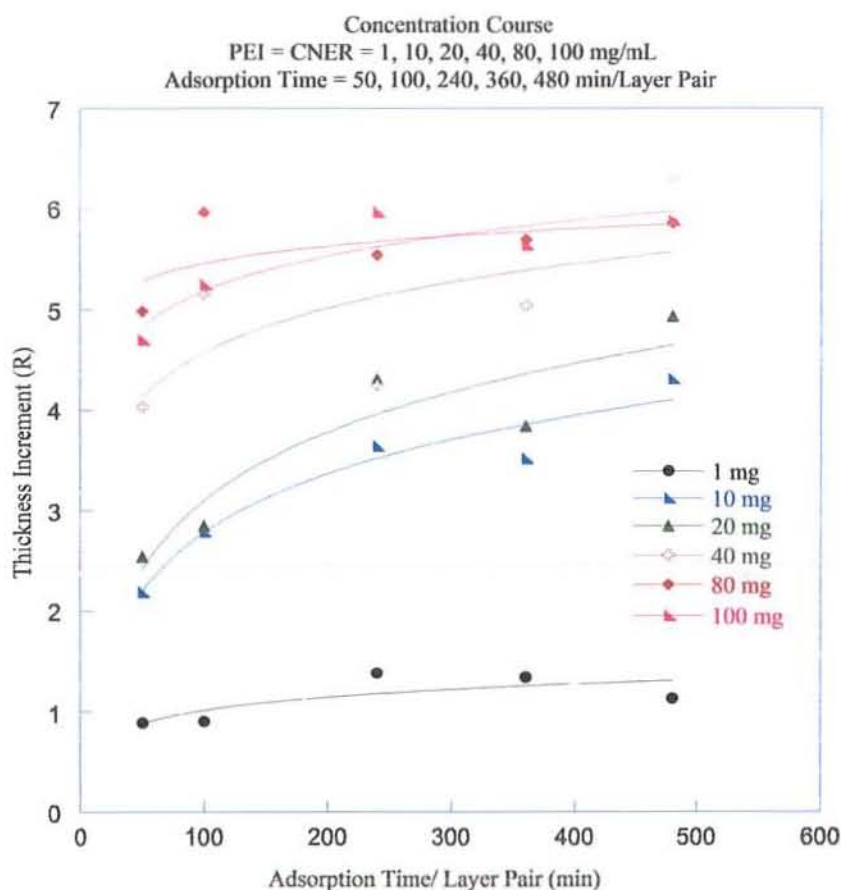
Figure 3.4: Variation of the single layer pair increment of (PEI/CNER)$_n$ films at different polymer concentrations as a function of adsorption times.

UV-Visible spectroscopic measurements also confirmed the linear growth of (PEI/CNER)$_{10}$ multilayer films. The multilayers for this purpose were deposited onto the quartz substrate by dipping process. The pre-cleaned quartz substrate was dipped into PEI and CNER epoxy solution for 50 min each followed by washing and drying. UV-Visible spectra were recorded after every layer pair. Figure 3.5 (A-D) shows that for different polymer concentration absorbance increases at 202 and 280 nm wavelength with increase in number of layer pairs, thus complementing the presence of UV active aromatic chromophores in CNER epoxy. As concentration of the two polymer solutions increases from 1.0 to 100 mg mL^{-1}, there is an increase in absorbance maximum. The absorption at around 280 nm corresponds to the aromatic group of CNER.
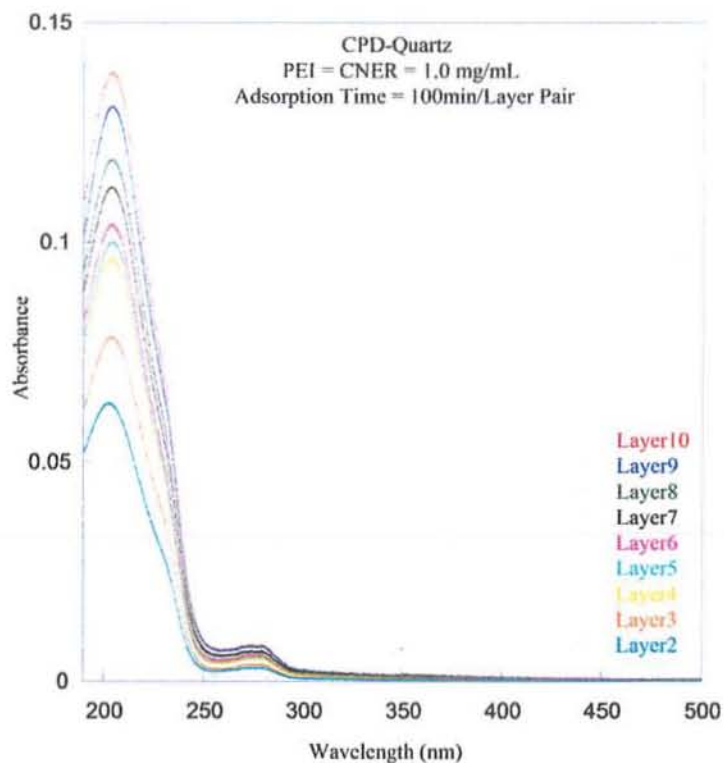
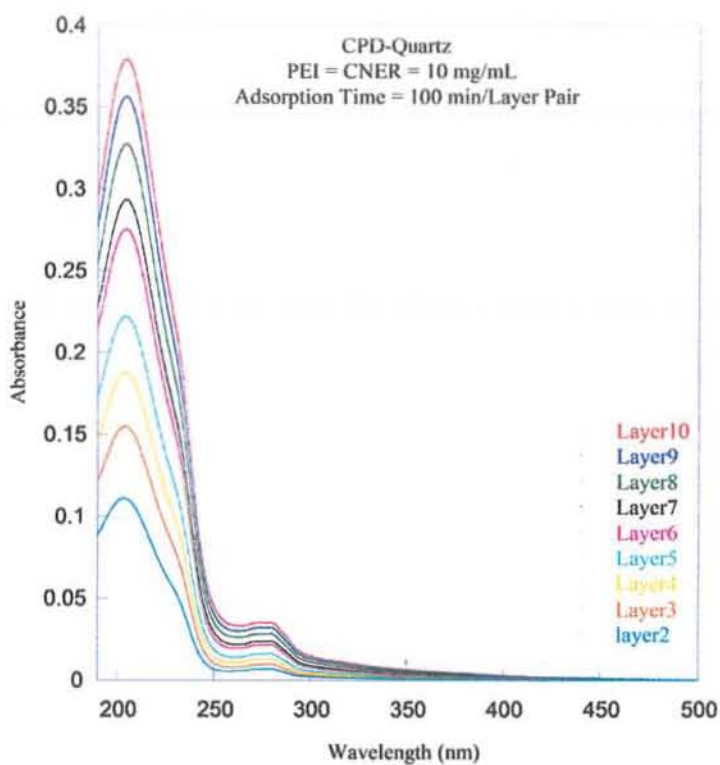**Figure 3.5A:** UV-Visible spectra of (PEI/CNER)$_{10}$ for polymer conc. 1.0 mg mL^{-1}.

Figure 3.5B: UV-Visible spectra of (PEI/CNER)$_{10}$ for polymer conc. 10 mg mL^{-1}.
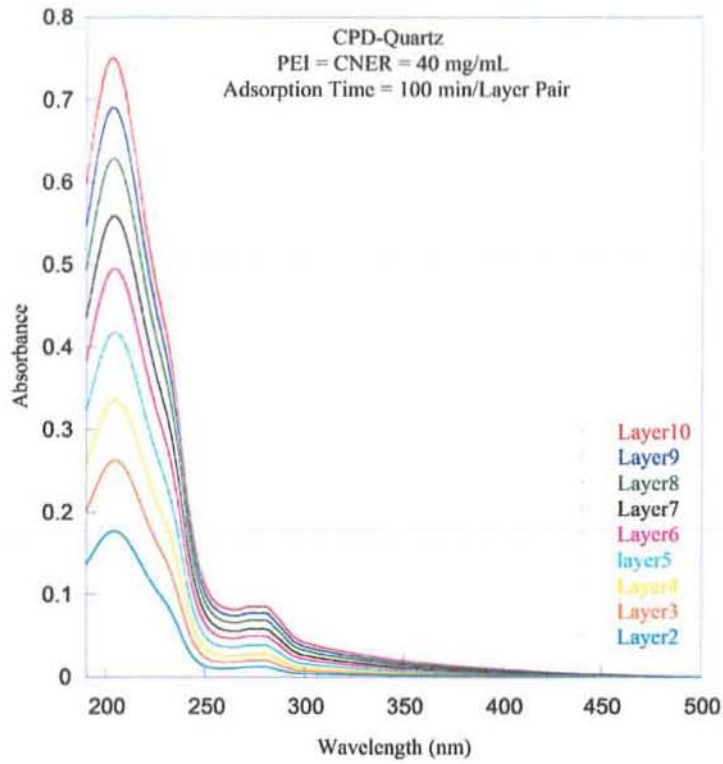
Figure 3.5C: UV-Visible spectra of (PEI/CNER)$_{10}$ for polymer conc. 40 mg mL^{-1}.
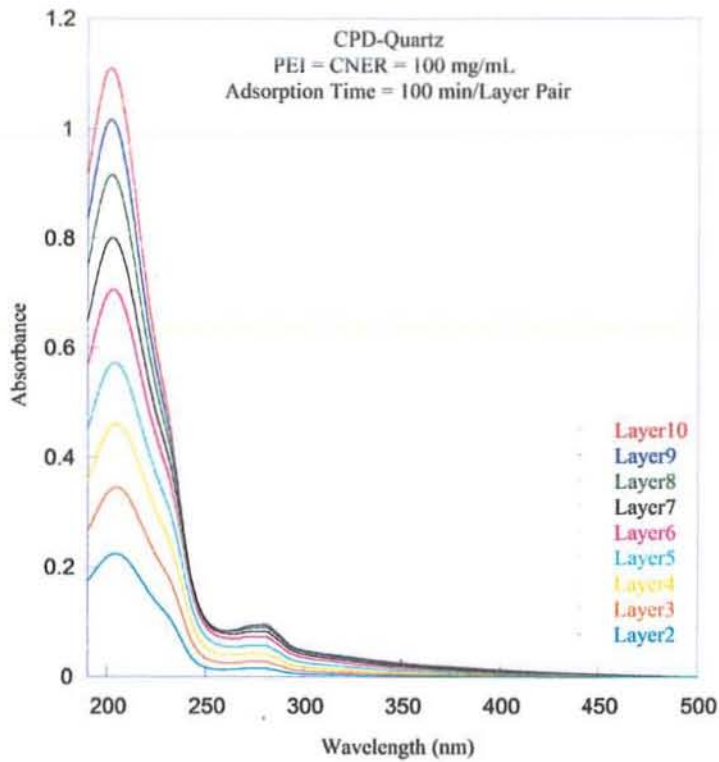

Figure 3.5D: UV-Visible spectra of (PEI/CNER)$_{10}$ for polymer conc. 100 mg mL^{-1}.

So, UV-Visible spectroscopy results also verified the linear growth of the epoxy-amine layer by layer covalent assemblies. The absorbance maximum as a function of number of layer pair shows a linear rise for all the four polymer concentrations. With increase in polymer concentration, there was a steady increase in absorbance maximum indicating a linear increase in thickness of these covalently bonded LbL assemblies (Figure 3.5). These results also strongly support the linear growth of the $(PEI/CNER)_{10}$ films as shown by ellipsometric measurements in Figure 3.2.
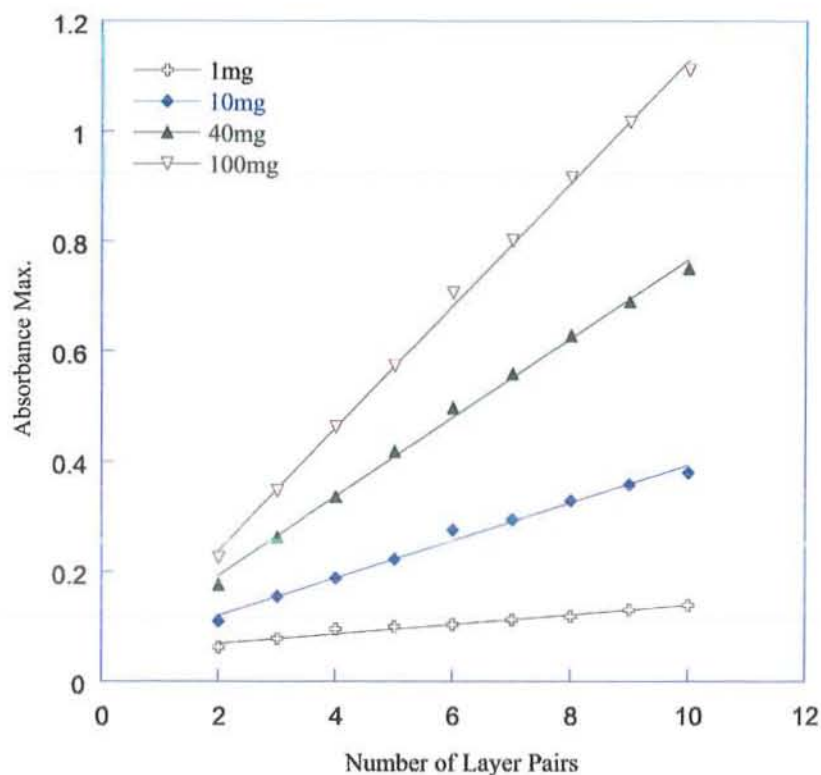

Figure 3.6: Absorbance maximum as a function of number of layer pairs for different concentrations of $(PEI/CNER)_{10}$ system.

AFM images of $(PEI/CNER)n$, where n= 1 for polymer concentrations 1, 40 and 100 mg mL^{-1} were taken in the tapping mode to substantiate our choice of 40 mg mL^{-1} as optimised polymer concentration for further protection work (Figure 3.7). The rms roughness values for the three samples increases with increase in concentrations of polymers (Table 3.2).

Table 3.2: Thickness of one layer pair and rms roughness of (PEI/CNER)$_1$ films.

Sample Code	Thickness 1 LP (nm)	rms roughness (nm)
CPD-1/100	2.67	5.3
CPD-40/100	5.00	29.0
CPD-100/100	6.02	40.4

All the AFM images presented in Figure 3.7 (A-C) were the result of 1 μm^2 surface area scan for this particular study. An important point to be mentioned for the AFM images presented below and elsewhere is that out of every set of three images, the one on left is always a 2-D surface image, the middle one is 3-D image indicating the surface roughness while rms surface roughness is presented as line profile on right side.

The surface morphology of 1.0 mg mL^{-1} sample (Figure 3.7A) shows that the polymer chains especially epoxy resin chemisorbs onto PEI horizontally. This may be due to very dilute polymer solutions where the individual polymer chains have ample space to lie down flattened on the underlying polymer or substrate. The AFM image of 40 mg mL^{-1} sample shows a very homogeneous surface morphology with uniform hills and valleys in the 3-D image. The epoxy chains adsorb vertically onto the polyamine (Figure 3.7B) due to higher concentrations of polymers as compared to 1.0 mg mL^{-1} concentration (Figure 3.7A).

The surface morphology of 100 mg mL^{-1} sample was even less homogeneous (Figure 3.7C) due to higher concentrations of the two polymers, so the density of vertical chains was quite thick. The rms roughness value for the 100 mg mL^{-1} concentration samples was 40 nm as compared to 20 nm for 40 mg mL^{-1} sample. So based on this and many other previously stated observations, 40 mg mL^{-1} polymer solution was chosen for the further protection of weak multilayers.
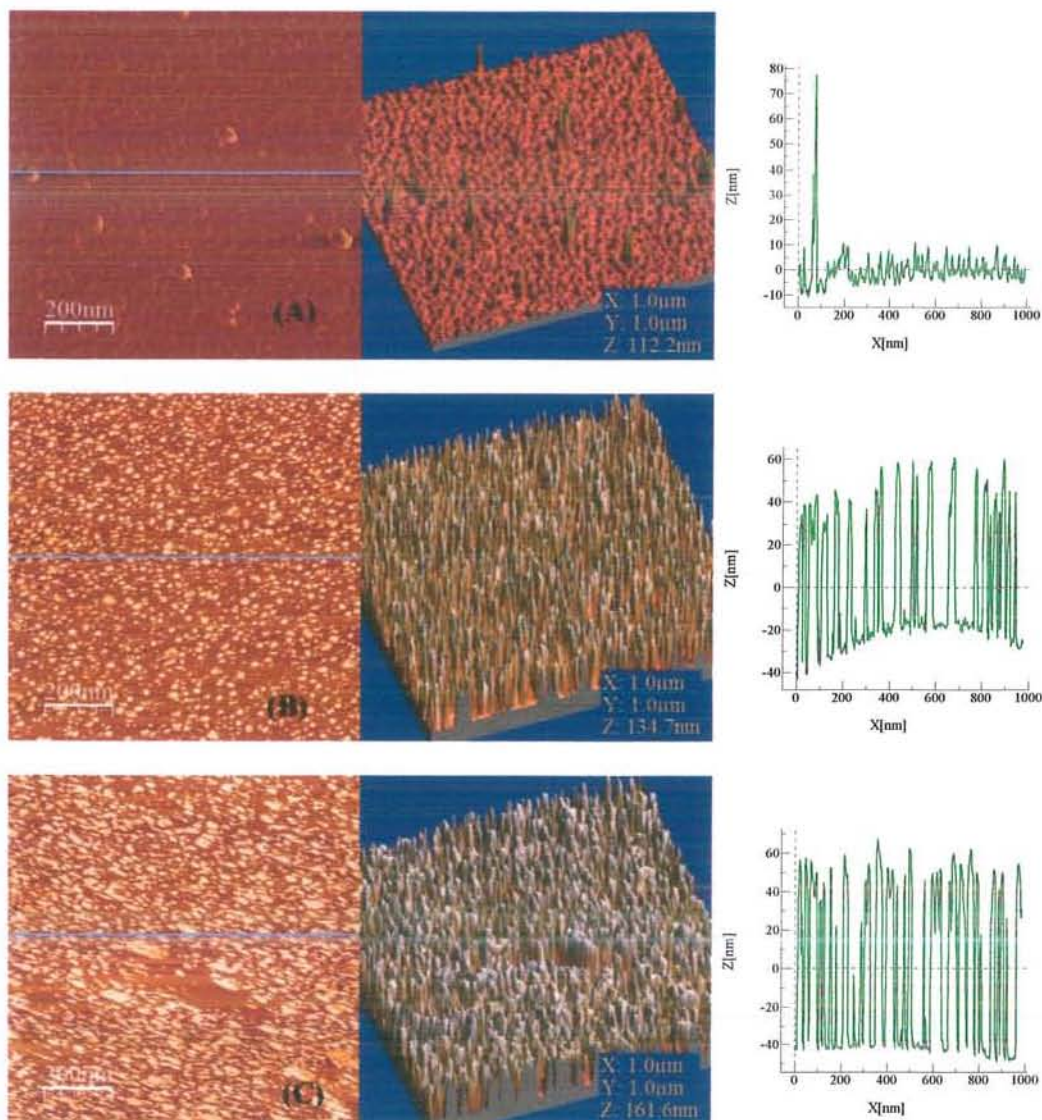
100

Figure 3.7: Surface morphological studies of (PEI/CNER)$_1$ for 1.0 mg mL^{-1} (A), 40 mg mL^{-1} (B), 100 mg mL^{-1} (C) polymer concentrations. 2-D image (L), 3-D image (Middle), (R) rms surface roughness (line profile).

3.1.2 Optimisation of Concentration and Adsorption Time for (PEI/PNER)$_n$ System

For the construction of (PEI/PNER)$_n$ dipped films, the concentration for polymer solutions PEI and PNER were kept the same. The dipping times for both polymer solutions were kept at 50, 100, 240, 360 and 480 min per layer pair. The concentrations of the polymers used were 5, 10, 20, 40, 60, 100 mg mL^{-1}. Ellipsometry data indicates a linear film growth for all the (PEI/PNER)$_n$ films (Figure 3.8). The film thickness

101

increases with increase in the polymer concentration from 5 to 100 mg mL^{-1}. Because at low concentration, polymer chains may have a linear extended state and they adsorb horizontally to give a very little increase in thickness of the layer pairs. When the concentration increases further, more and more polymer chains are adsorbed on the surface. Due to electro-repulsion among the adjacent polymer chains, they began to adsorb vertically creating more free space on the surface. As the molecular mass of PNER polymer (n = 1.6) is lesser as compared to CNER polymer (n = 3), a PNER polymer chain is more capable to enter and occupy any free available space as compared to CNER. As a consequence, a surface can easily be saturated by a long polymer chain instead of a short polymer chain. That is why the film thickness increment for (PEI/PNER)$_n$ are less as compared to (PEI/CNER)$_n$ multilayer systems.
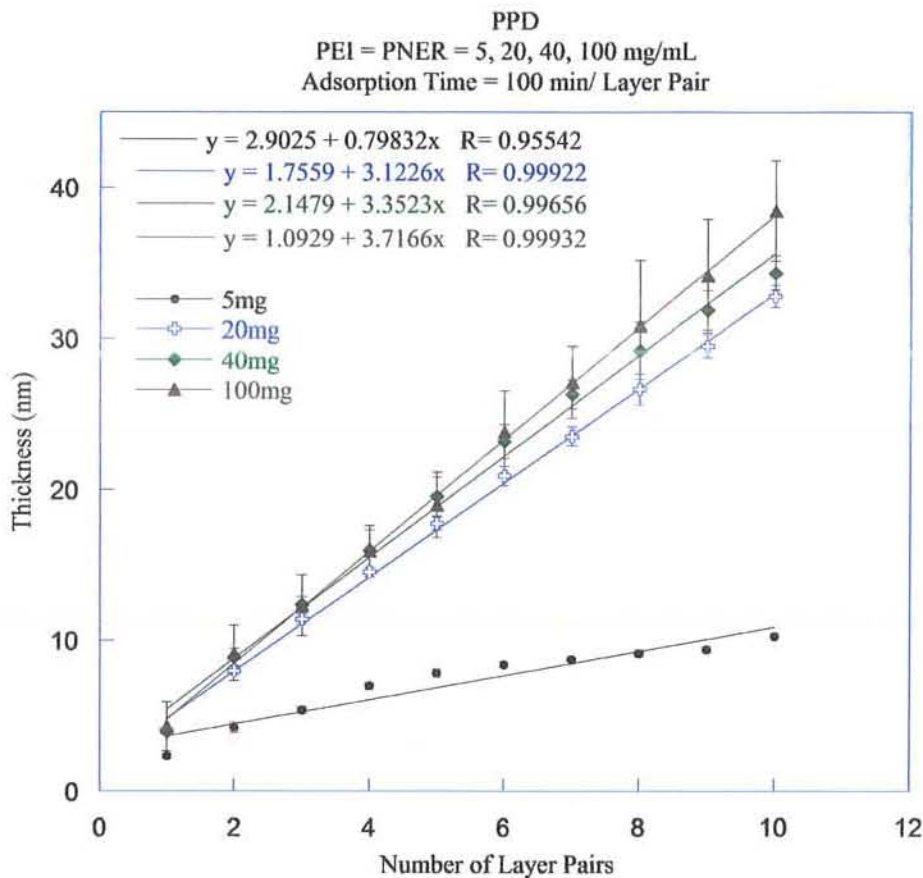

Figure 3.8: Thickness of (PEI/PNER)$_n$ films for different polymers concentrations as a function of the number of layer pairs at 100 min per layer pair adsorption time.

The plot of thickness as a function of number of layer pairs shows a regular increase with increase in concentration of polymer. But for the higher concentrations of polymers, the thickness increase was not proportional rather for 20, 40, 100 mg mL^{-1} concentrations, there appear similar thickness regime (Table 3.3).

Table 3.3: Single layer pair increment (R) for (PEI/PNER)$_n$ film build-up for different polymer concentrations, as determined from Figure 3.8.

Conc. of Polymers (mg mL^{-1})	Single Layer Pair Increment (nm)
5	0.8
20	3.1
40	3.35
100	3.72

The single layer pair increment obtained by plotting layer pair thickness vs number of layer pairs for various concentrations and adsorption times was then plotted against various polymer concentrations and for all the adsorption times are shown in the Figure 3.9. This matrix was obtained as a result of conducting about 25 different experiments for (PEI/PNER)$_n$, elaborates that the thickness increases exponentially in the beginning up to 40 mg mL^{-1} polymer concentrations. When the polymer concentrations were increased from 5 to 40 mg mL^{-1}, the thickness per layer pair increases four folds (0.8 nm for 5 mg mL^{-1} polymer solutions to 3.3 nm for 40 mg mL^{-1}), while for 100 mg mL^{-1} concentration, it increases 4.5 folds (3.7 nm) as given in Table 3.3.

This means there was no proportionate increase in layer pair increment on raising polymer concentration from 40 to 100 mg mL^{-1} (Figure 3.9). Thus 40 mg mL^{-1} concentration was selected as optimised polymer concentration for further work as it gives very smooth, homogeneous and optically good quality film with good layer pair growth.
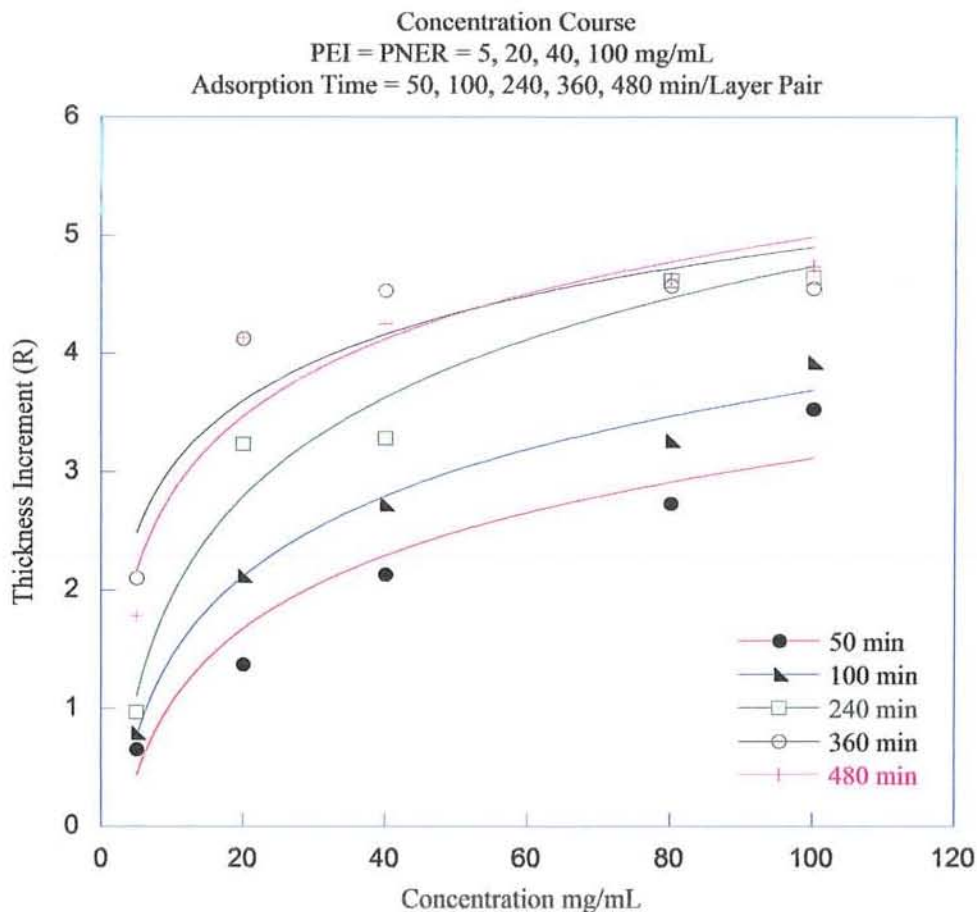
Concentration Course
PEI = PNER = 5, 20, 40, 100 mg/mL
Adsorption Time = 50, 100, 240, 360, 480 min/Layer Pair

Figure 3.9: Variation of the single layer pair increment of (PEI/CNER)$_n$ films at different adsorption times as a function of polymer concentrations.

For (PEI/PNER)$_n$ multilayer film, the polymer chain reorganization increases the slope coefficient as a function of dipping time upto a certain concentration (Figure 3.10). But as PNER is short chain prepolymer as compared to the CNER, they can adopt the optimal conformation more rapidly. Thus, 480 min per layer pair dipping time overlaps with 360 min per layer pair dipping time, because the PNER has already adopted its optimal conformation with 360 min per layer pair dipping time. As there was a sharp increase in thickness per layer pair at adsorption time 100 min per layer pair, therefore, this may be an optimum dipping time for both the polymers. The optimised polymer concentration for PEI and PNER was 40 mg mL^{-1} for the protection of underlying weak colloidal layers as revealed in Figure 3.10.
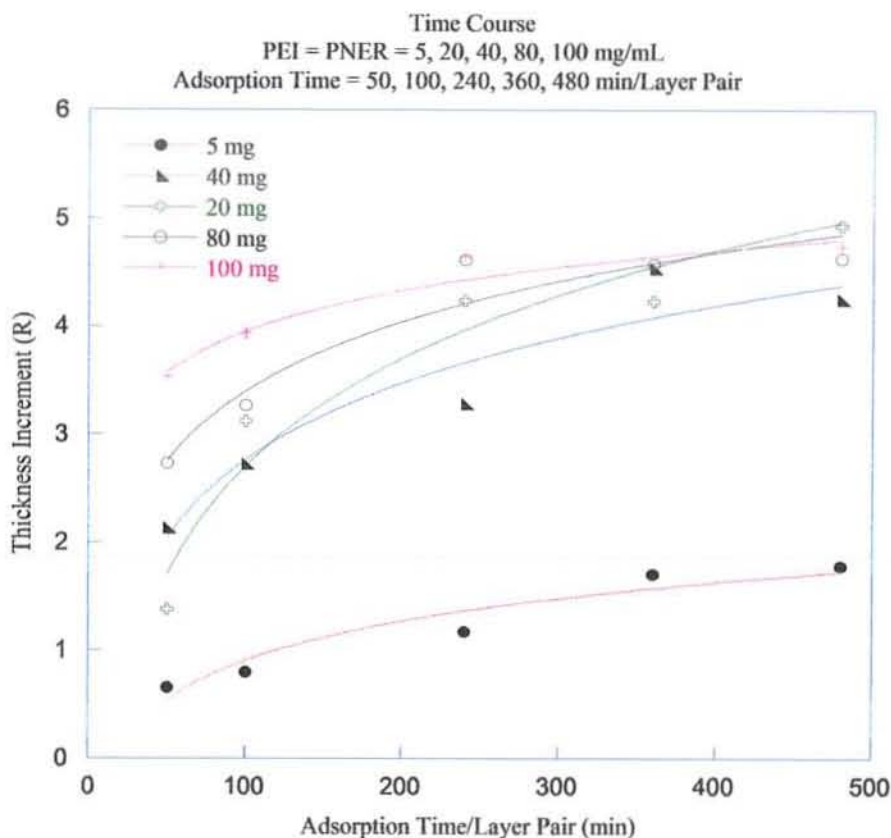
Figure 3.10: Variation of the single layer pair increment of $(PEI/PNER)_n$ films at different polymer concentrations as a function of adsorption times.

This linear growth of $(PEI/PNER)_{10}$ multilayer films was also validated by conducting UV-Visible spectroscopic measurements. The multilayers for this purpose were deposited onto the pre-cleaned quartz substrate and UV spectra were taken after every layer pair. Four different polymer concentrations were employed including 1, 10, 40 and 100 mg mL^{-1} for the two polymers. Figure 3.11 (A-D) shows that with increase in number of layer pairs, absorbance increases at around 280 nm wavelength.

It was also observed that as concentration of the two polymer solutions increased from 1.0 to 100 mg mL^{-1}, there was an increase in the intensity of absorbance maximum. The absorption at around 280 nm was due to the aromatic group present in PNER.
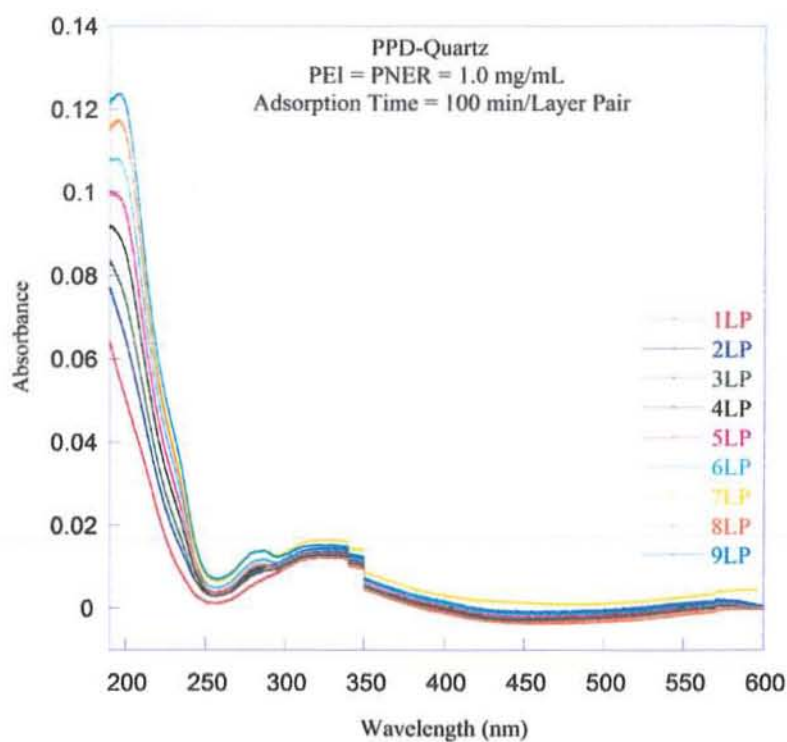
Figure 3.11A: UV-Visible spectra of (PEI/PNER)$_{10}$ for polymer conc. 1.0 mg mL^{-1}.
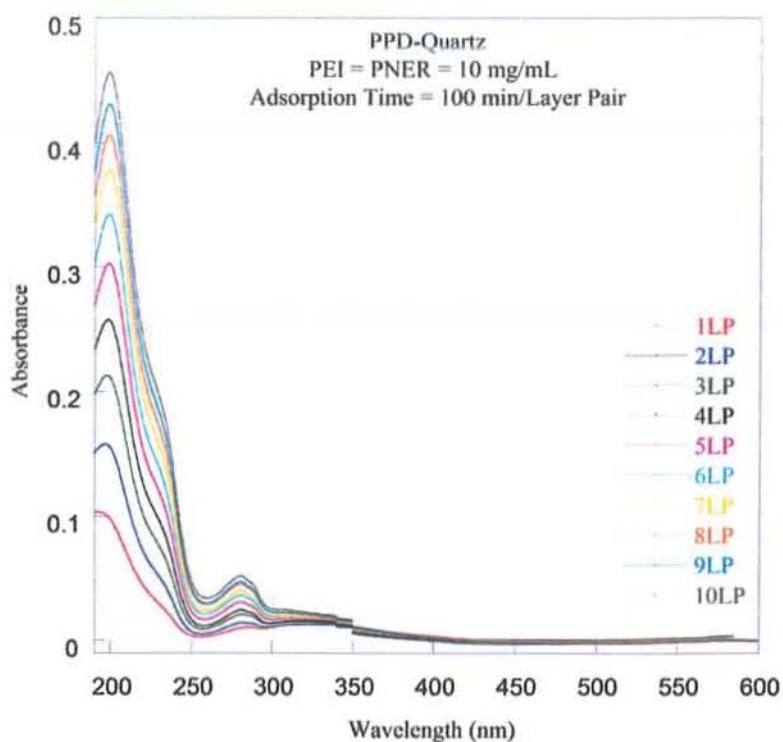
Figure 3.11B: UV-Visible spectra of (PEI/PNER)$_{10}$ for polymer conc. 10 mg mL^{-1}.

106
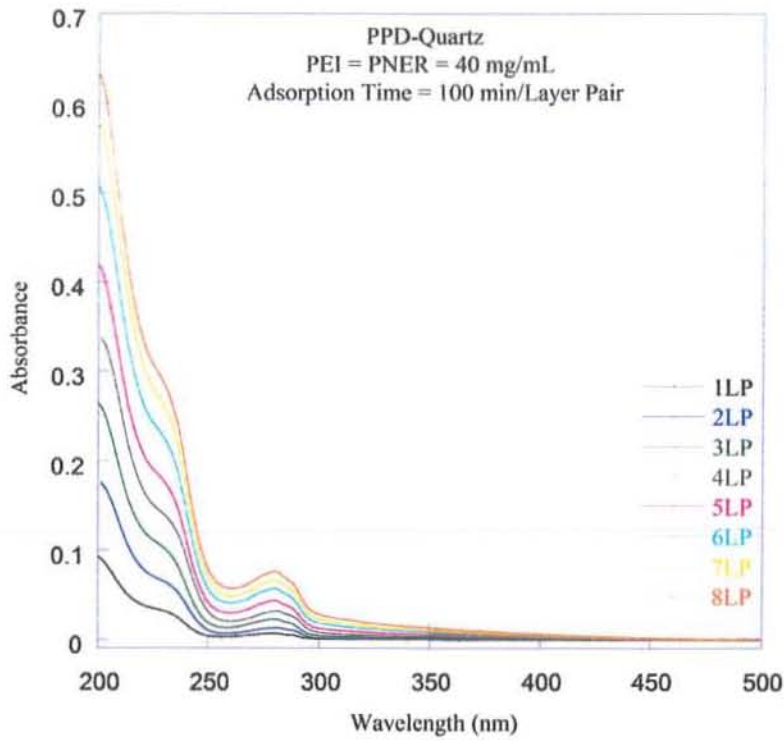
Figure 3.11C: UV-Visible spectra of (PEI/PNER)$_{10}$ for polymer conc. 40 mg mL^{-1}.
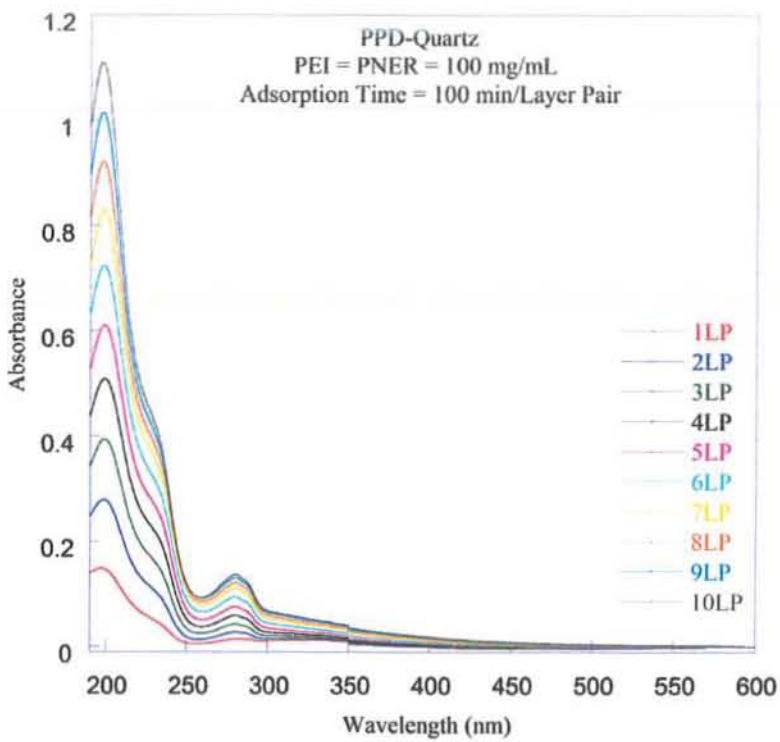

Figure 3.11D: UV-Visible spectra of (PEI/PNER)$_{10}$ for polymer conc. 100 mg mL^{-1}.

107

The absorbance maximum as a function of number of layer pair indicates a linear relationship for 10, 40 and 100 mg mL^{-1} polymer concentrations. With increase in polymer concentration, there is a steady increase in absorbance maximum which shows a linear increase in thickness for these covalently bonded LbL assemblies. The absorbance maximum for 1.0 mg mL^{-1} polymer concentration was below the threshold limit of the instrument, so it is missing here (Figure 3.12).
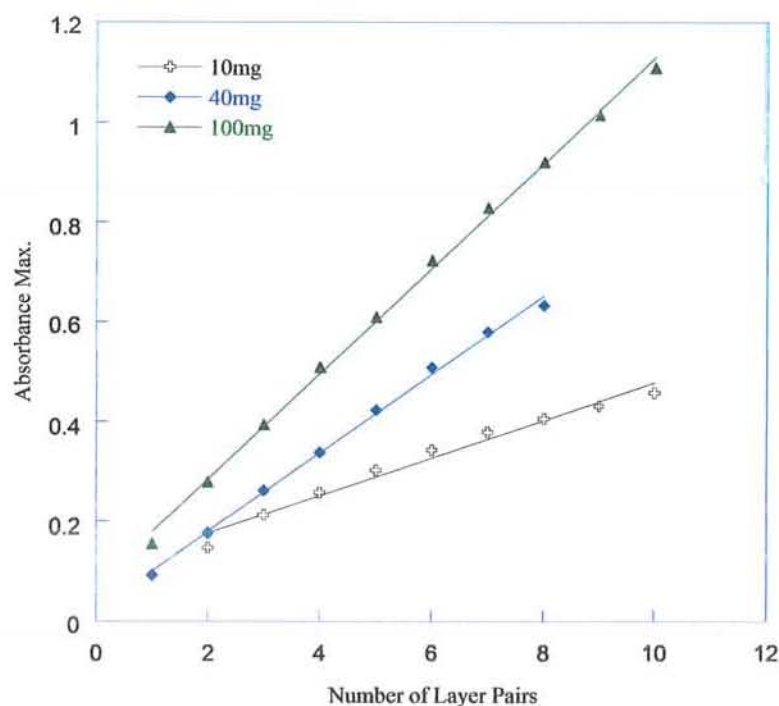

Figure 3.12: Absorbance maximum as a function of number of layer pairs for different concentrations of (PEI/PNER)$_{10}$ system.

Therefore, it may be concluded that for (PEI/CNER)$_{10}$ and (PEI/PNER)$_{10}$ systems, the dipping time was optimised at 100 min per layer pair with polymer concentration as 40 mg mL^{-1}.

3.2 Mechanical Robustness Studies of Optimised Systems

Mechanical stability is one of the key parameter that controls the general stability of the ultrathin film devices and thus its further applications. Therefore, mechanical robustness of all these films was tested by a rubbing machine. This machine gives qualitative information about the wear-tear behaviour of a polymeric material in

addition to molecular alignment. The film thickness before rubbing test was measured with ellipsometer. After a definite number of rubbing cycles, the substrate was washed with acetone to remove any loose material, dried with a stream of compressed air and then its thickness was once again measured with the help of ellipsometer. Any change in the film thickness before and after rubbing test was noted. It is important to mention that rubbing machine works with a constant pressure of 2 bars using cotton velvet cloth wrapped around a cylinder as shown in the Figure 2.10. The surface morphology of the rubbed and un-rubbed film was then studied with AFM. Whether the epoxy films withstand hostile environment of the rubbings test? The ellipsometry along with AFM provides answer to such questions. The AFM image of the $(PEI/CNER)_{10}$ film before rubbing test shows a homogeneous surface morphology with rms roughness value 8.9 nm. The 3-D image shows the presence of very smooth hill-valley view (Figure 3.13).
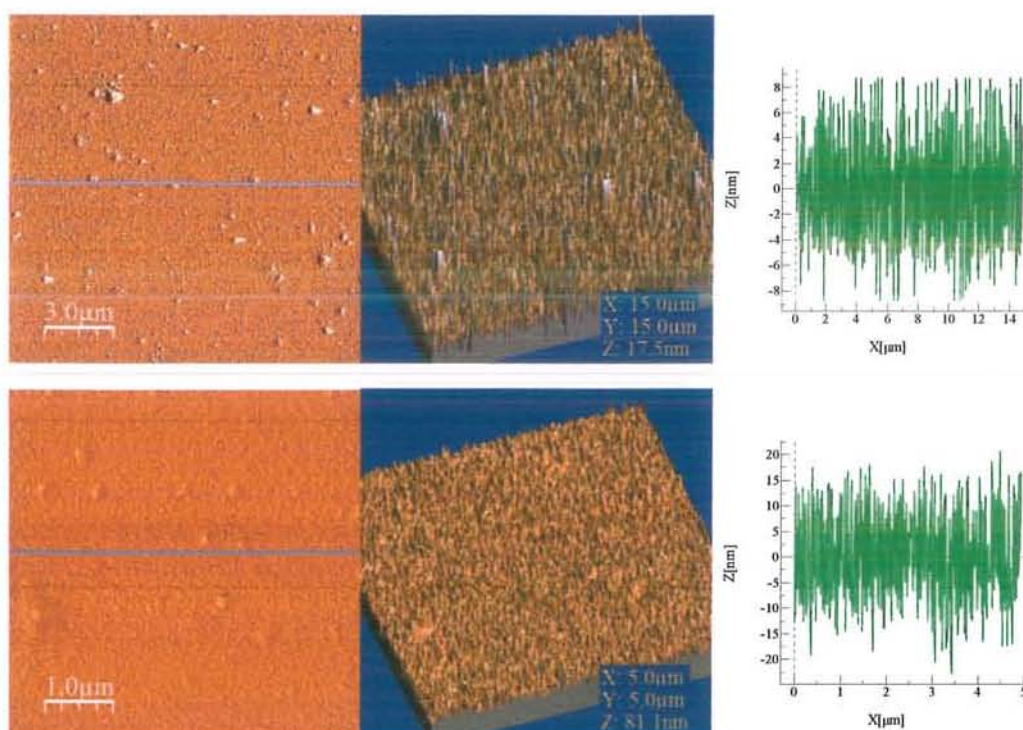

Figure 3.13: Surface morphology and roughness profile of un-rubbed $(PEI/CNER)_{10}$.

The sample was subjected to 60 consecutive rubbing cycles with rubbing machine. Thickness of the sample before and after the rubbing test was measured with ellipsometer. After rubbing cycles, the thickness loss was only around 2% of the whole film thickness (Table 3.4).

Table 3.4: Thickness and rms roughness of (PEI/CNER)$_{10}$ before and after rubbing.

Film Architecture	Thickness (nm)		rms Roughness (nm)		Percentage
	Before Rubbing	After 60 Rubbings	Before Rubbing	After 60 Rubbings	Loss after 60 Rubbings
(PEI/CNER)$_{10}$	31.65	31.05	8.9	3.99	1.8

The tapping mode AFM image indicates that there is no dramatic change in surface morphology of the film before and after rubbing test. However, the appearance of certain grooves was observed on the surface of 60 rubbed epoxy-amine film while ellipsometry results show that whole of the film adhered onto the substrate (Table 3.4 & Figure 3.14). These grooves appeared in vertical direction of the film as shown by the 3-D image suggesting that the whole epoxy film sticks on the substrate. Surface roughness analysis indicates a slight decrease of rms roughness from 8.9 nm to 3.99 nm indicating the possibility of film compression due to cylinder of rubbing machine. This also rules out any loss in film thickness as a result of rubbing test. These observations also confirmed the excellent mechanical properties of ultrathin LbL assemblies made with amine curing of epoxy, as mentioned in literature review.
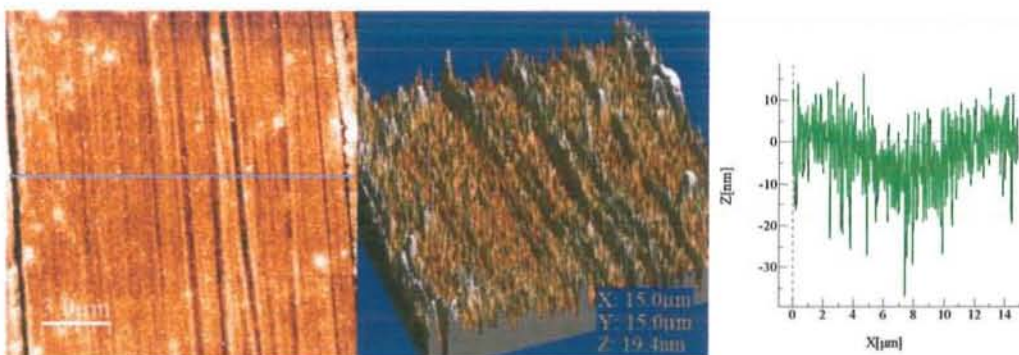
Figure 3.14: Surface morphology of 60 rubbed (PEI/CNER)$_{10}$ film.

In another interesting study, the inner morphology of the same (PEI/CNER)$_{10}$ film was studied in the contact mode. It was noted that the cantilever was not able to pierce the outer portion of hard epoxy-amine film, although the cantilever force was successively increased to 400 nN. However, the cantilever marked a square compression on the

sample (Figure 3.15). The rms roughness value for this sample was 2.99 nm indicating a very smooth surface even after the implication of 400 nN cantilever force.
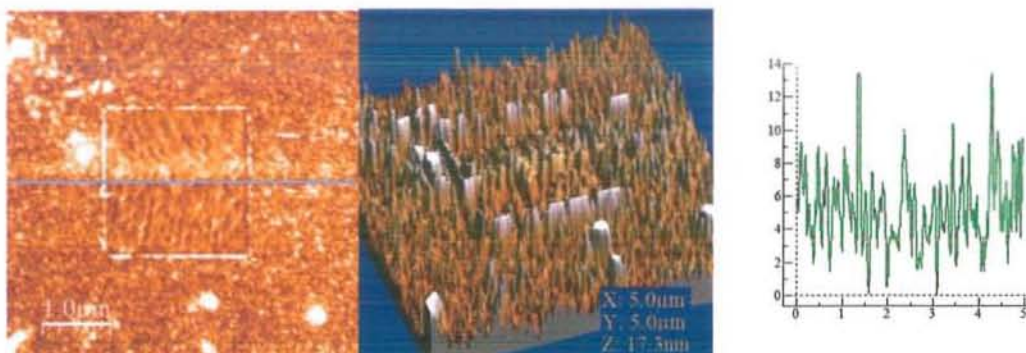

Figure 3.15: Contact mode image of (PEI/CNER)$_{10}$ with cantilever force of 400 nN.

Surface morphology of (PEI/PNER)$_{10}$ ultrathin film is given in Figure 3.16 (A, B) in the tapping mode for the two concentrations i.e. 20 mg mL^{-1} (3.16-A) and 40 mg mL^{-1} (3.16-B) of the polymers with 100 min per layer pair adsorption time. It was observed that rms roughness value increase from 4.83 nm to 7.47 nm with increase in polymer concentration.
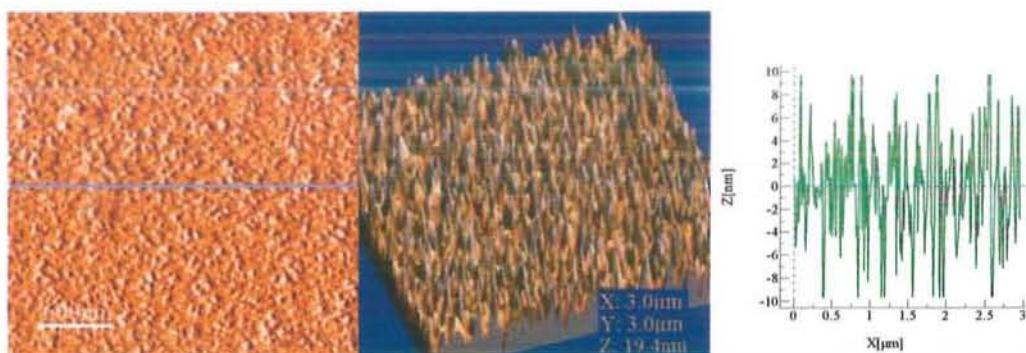

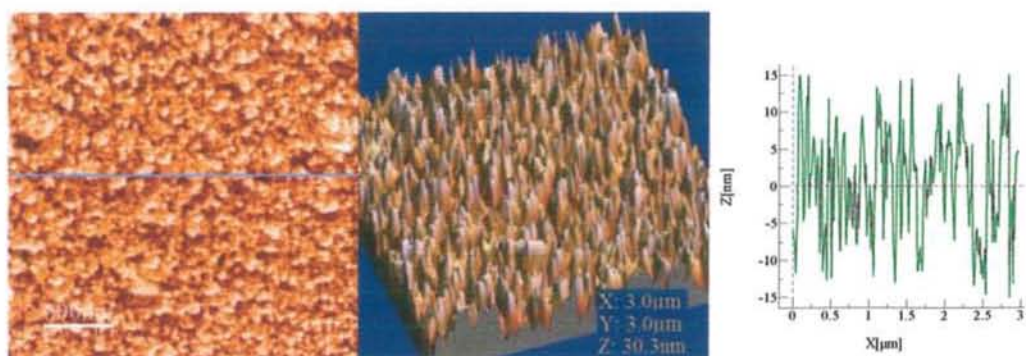**Figure 3.16A:** Surface morphology images of (PEI/PNER)$_{10}$ for 20 mg mL^{-1}.

Figure 3.16B: Surface morphology images of (PEI/PNER)$_{10}$ for 40 mg mL^{-1}.

3.2.1 Minimum Thickness Required to Attain Mechanical Robustness

Now the question arises, how much of the epoxy-amine film thickness is required to endure the harsh environment of rubbings test. The minimum thickness of the epoxy-amine network required to protect the underlying weak Au-NPs film has to be ascertained.

To answer such questions, apart from the $(PEI/CNER)_{10}$ and $(PEI/PNER)_{10}$ systems, another particularly important system was tried using Araldite MY-720 epoxy with PEI obtained from Aldrich and BASF respectively. Araldite MY-720 was used to prepare high performance structural adhesives and showed best properties when cured at high temperatures[1].

Araldite MY-720 was used to prepare covalent multilayers of the architecture $(PEI/MY-720)_{10}$ for adsorption times of 50 and 100 min per layer pair (Figure 3.17). The overall film thickness obtained after 10 layer pairs for 50 and 100 min per layer pair adsorption time was less than 5 and 10 nm respectively with large error bars. Therefore, 20 min per layer pair sample was not prepared as the expected overall growth was much less to be used for further applications. The $(PEI/MY-720)_{10}$ samples prepared were then cut to two parts. One part was subjected to thermal cure at $100°C$ for 1 hr and the other to time cure for 3 days at room temperature. Both the films were then subjected to rubbings test. The thickness of the films was measured before and after the rubbing test.

The effect of accelerators on growth of the LbL films and also on mechanical strength of the prepared films was also studied (Table 3.5). After 20 rubbing cycles there was no loss in thickness of the thermally cured films. So thermal curing improves the mechanical strength of the $(PEI/MY-720)_{10}$ films which was also indicated in the TDS of Araldite MY-720. The rubbing data obtained after 20 rubbing cycles show good mechanical strength for particularly longer dipping time samples (Table 3.5). Epoxy embedding medium accelerator gives comparatively good mechanical strength for the longer as well as shorter dipping time for both thermally and time cured samples.
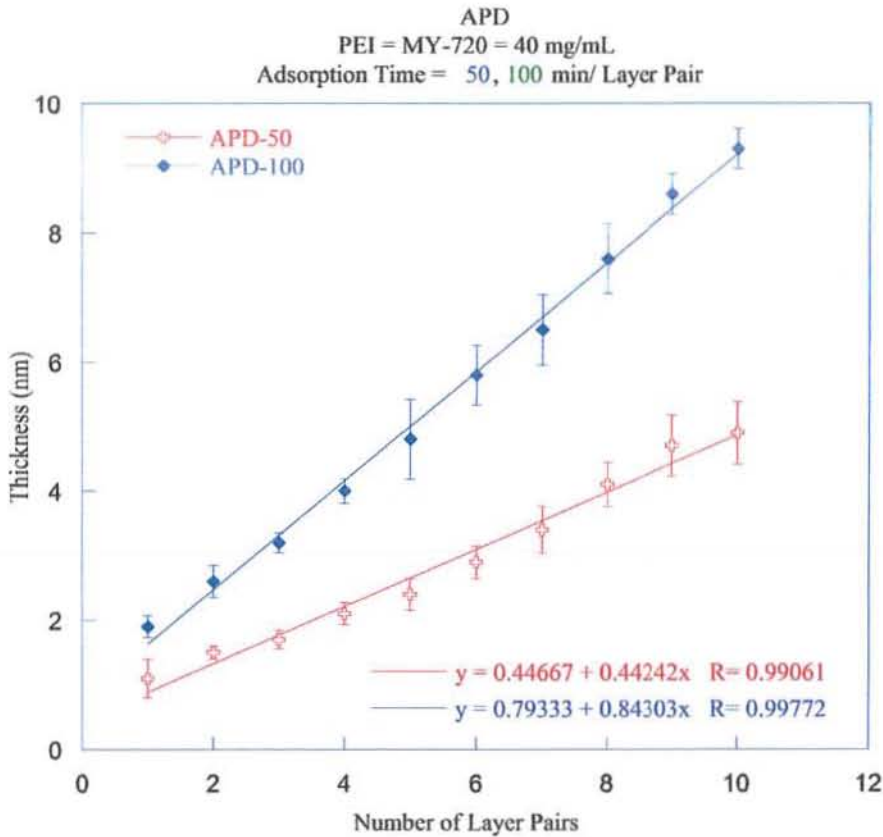
Figure 3.17: Thickness as a function of number of layer pairs (PEI/MY-720)$_{10}$.

Table 3.5: Mechanical robustness of (PEI/MY-720)$_{10}$ for different curing modes.

System	Thickness 50 min/lp (nm)	Percent loss cured film	Percent Loss Time cured film	Thickness 100 min/lp (nm)	Percent loss temp. cured film	Percent loss time cured film
APD	4.9	No Loss	29.0	9.2	No Loss	6.5
APDA	5.6	No Loss	24.0	9.8	No Loss	15.0
APDP	4.95	No Loss	4.2	9.2	No Loss	13.0
APDE	4.6	No Loss	4.4	8.3	No Loss	4.2
APDC	4.4	9.0	22.0	8.0	No Loss	30.0

In another interesting study, minimum thickness of the $(PEI/CNER)_n$ and $(PEI/PNER)_n$ films required for maximum mechanical robustness was determined (where $n = 2$ and 4 layer pairs). High concentrations of all the polymers (100 mg mL^{-1}) were used to get maximum thickness for lesser number of layer pairs chemisorbed. The samples were then subjected to time and thermal cure process as stated earlier. The results are summarised in Table 3.6.

Table 3.6: Mechanical robustness as a function of thickness for time and thermal cure.

System	Number of layer pairs	Thickness (nm)	Percent Loss after 20 rubs (Thermal cure)	Percent Loss after 20 rubs (Time cure)
CPD-100-20	2	8.0	6.5	92.0
CPD-100-20	4	15.8	2.6	74.0
CPD-100-100	2	11.2	73.0	92.0
CPD-100-100	4	22.6	24.5	81.0
PPD-100-20	2	6.0	26.0	90.0
PPD-100-20	4	12.8	No Loss	94.0
PPD-100-100	2	8.4	51.0	72.0
PPD-100-100	4	16.0	1.0	29.0

It was interesting to note that irrespective of the dipping time, $(PEI/CNER)_4$ and $(PEI/PNER)_4$ films demonstrated good mechanical strength for both the time and thermal cured systems as compared to the samples with two layer pairs. Thermal curing greatly affects the mechanical strength of four layer pair samples. This means 15 nm of $(PEI/CNER)_n$ while 10 nm of $(PEI/PNER)_n$ films may be sufficient to withstand rubbings by rubbing machine (Table 3.6).

3.3 Preparation of Au-colloid Nanofilms

The research work reported in this section was conducted in collaboration with Zhiqiang Zheng, a doctorate student working under the supervision of Dr. Gero Decher, in Institut Charles Sadron, Université de Strasbourg, Strasbourg, France.

A gold nano-particle film of the (PAH/Au-NPs)$_n$ architecture on silicon wafer or quartz slide was built-up by spray method. The spray deposition technique was discovered by Schlenoff and his team[2]. This technique allows fabrication of a layer pair in 1 or 2 min, an acceleration of 50-150[3] times in terms of working time compared to the traditional LbL dipping technique.

For the construction of Au-NPs film, PAH was chosen as polycation and its concentration was kept as 3 mM. The procedure for the spray deposition of Au-NPs onto the substrate follow the sequence described below;

Precursor PEI layer was deposited onto the substrate by dipping followed by a PSS layer deposited by spray. This was followed by the consecutive PAH and Au-NPs adsorption by spray technique. At first the polymer was sprayed onto the substrate for t_1 = 5 s followed by adsorption (wait) time t_2 = 15 s. Then the wash solution (0.5 M NaCl) was sprayed onto the substrate for t_3 = 5 s followed by waiting time t_4 = 15 s. Same procedure was carried out for the deposition of Au-NPs except that washing was done with Milli-Q water instead of aqueous NaCl solution. In order to ensure a full surface coverage by Au-NPs layer, the spray and rinse cycle for Au-NPs were repeated 5 times. In this way the total processing time for the deposition of one PAH layer, was 40 s, as compared to 200 s for a Au-NPs layer. After the (PAH/Au-NPs)$_n$ colloid film deposition, an additional (PAH/PSS) layer was sprayed on the colloid film to make a connection to the next sequential PEI/CNER film deposition. Concentrations of both PSS and PAH were kept the same. The complete architecture of this Au colloid film was Si/PEI/PSS/(PAH/Au-NPs)$_n$, generally called (PAH/Au-NPs)$_n$ film.

In this system, there was no interlayer diffusion of Au-NPs in PAH layers because Au-NPs were separated by only one PAH layer with a thickness less than 1.5 nm, (according to neutron reflectometry measurement). This value was much less than Au-NPs mean size, 13.6 nm in diameter, which avoids any particles inter-diffusion and

leads to a linear film growth mechanism. LbL film construction of (PAH/Au-NPs)$_5$ was monitored by ellipsometry (Table 3.7 Figure 3.17) and UV-Visible spectroscopy (Figure 3.18).

Table 3.7: Thickness of (PAH/Au-NPs)$_n$ film as a function of number of layer pairs.

Film architecture	Film thickness (nm)
(PAH/Au-NPs)$_1$	14.1 ± 0.2
(PAH/Au-NPs)$_2$	24.4 ± 0.3
(PAH/Au-NPs)$_3$	32.8 ± 0.3
(PAH/Au-NPs)$_4$	40.4 ± 1.0
(PAH/Au-NPs)$_5$	44.8 ± 0.9

Film thickness and UV-Visible absorption were measured after each layer pair deposition. Both ellipsometry and UV-Visible data indicate a linear film growth for (PAH/Au-NPs)$_5$ films as depicted in Figure 3.18.
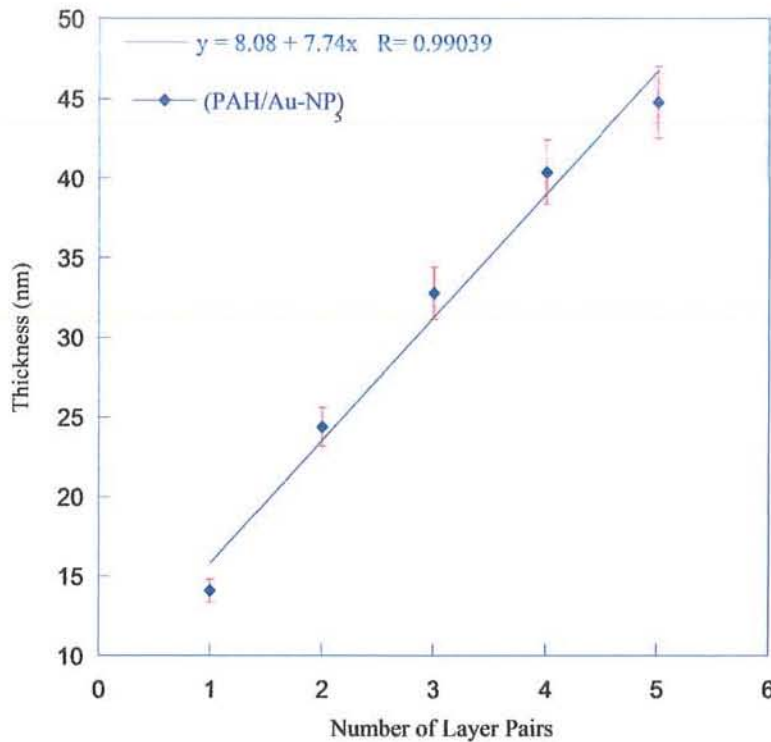

Figure 3.18: Thickness of Au-NPs layer as a function of number of layer pairs.

116

The ellipsometric measurement for Au-NPs film may not give the true thickness of the film[4]. This lack of precision is due to the Kramers-Kronig effect linked to the optical absorption of Au-NPs at the measuring laser wavelength 632.8 nm of the ellipsometer[5]. For these qualitative experiments, the true thickness of the films was not an important issue, it was sufficient to determine the relative growth increments without applying the Kramers-Kronig correction.

The UV-Visible absorption spectrum for the formation of (PAH/Au-NPs)$_5$ (Figure 3.19 Right) shows that the first gold nanoparticle layer deposited onto the surface leads to an absorption peak around 520-550 nm corresponding to the plasmon absorption of "individual" Au-NPs. The absorption peak shifts to 640 ~ 680 nm by adding more Au-NPs layers onto the substrate surface. This red shift in wavelength of absorption is due to the strong plasmon interactions between two adjacent Au-NPs layers[6]. The linear growth of the (PAH/Au-NPs)$_5$ nanoparticle multilayer film was demonstrated by plotting absorbance maximum as a function of number of layer pairs (Figure 3.19 Left).
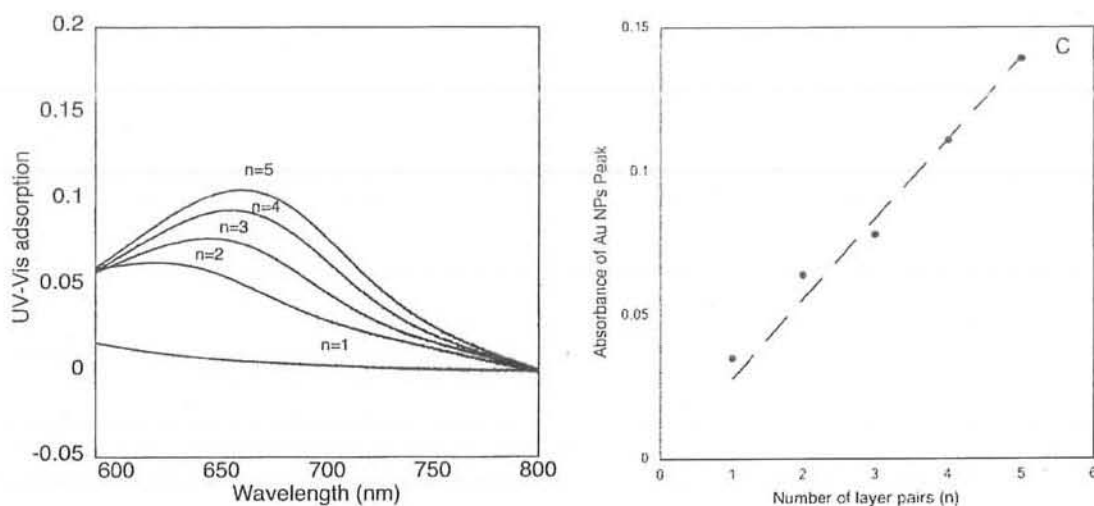

Figure 3.19: UV-Visible absorption of (PAH/Au-NPs)$_5$ film (L) and absorbance maximum vs number of layer pairs (R)[7].

3.4 Mechanical Robustness of Epoxy-Amine Protected Au-NPs Films

The research work reported in this section was also conducted in collaboration with Zhiqiang Zheng, a doctorate student working under the supervision of Dr Gero DECHER, Institut Charles Sadron, Université de Strasbourg, Strasbourg, France.

The potential applications of an ultrathin device depend on its wear resistance in addition to its physical and chemical stability. Several research groups are working on gold colloid nanoparticle films for their potential applications in catalysis[8], nanoelectronic[9], optical devices[10] and a tremendous horizon of applications in biological and biomedical areas. As a noble metal, Au-NPs have an excellent chemical and physical stability. Particularly, the mechanical properties of colloid films have been studied[11].

The main emphasis in the present work was to improve the mechanical resistance of functional LbL films. First of all, the mechanical strength of virgin sprayed Au colloid films was tested using a simple rubbing machine described in chapter 2. After few rubbing cycles, nearly whole of the sprayed, virgin $(PAH/Au-NP)_5$ film was removed from the substrate (Table 3.8). The un-protected Au colloid film has lost more than 88% of the original film thickness after 15 rubbing cycles of this 3 month old film.

Table 3.8: Thickness of Au colloid film as a function of different rubbing cycles.

Number of rubbing cycles	Sprayed film thickness (nm)
0	41.2±0.4
1	36.4±0.5
5	8.8±2.4
15	5.0±1.0

The sprayed $(PAH/Au-NPs)_5$ films prepared were quite homogeneous as indicated by a very small error in thickness. After one rubbing cycle, the loss in film thickness was only 10%. However, after 15 rubbing cycles, the loss in thickness of film was 90%.

Very low mechanical strength of the Au colloid films may be due to the weak interactions between PAH and Au-NPs. In the Au colloid films, spherical gold nanoparticle are connected with PAH polymer chains via negatively charged citrate which in turn was weakly bound to the Au-NPs. When a strong shear force was applied in the form of rubbing test, the weak interactions between Au-NPs and PAH layer are disturbed with decrease in film thickness. However, with the same architecture, the reason why dipped colloid films had weaker mechanical resistance than sprayed colloid films is still unknown. But apparently, sprayed films are robust than dipped films, for this reason, investigation on sprayed colloid films was focused on in order to have stronger mechanical resistance film.

The surface morphology of sprayed Si/PEI/PSS/(PAH/Au-NPs)$_5$/PAH colloid film before and after rubbing test was studied by AFM analysis. The AFM image of the virgin Au colloid film (Figure 3.20A), shows quite homogeneous surface morphology with rms roughness of 6.7 nm in a scan area of 15 μm. After only one rubbing cycle (Figure 3.20B), a big crack in addition to some grooves appear under the shearing force. Section analysis indicates a vertical distance of 16.1 nm and a horizontal distance of 1.9 μm for the trench on the surface. The vertical distance of the trench represents already ~ 40% of the initial thickness of the colloid film.
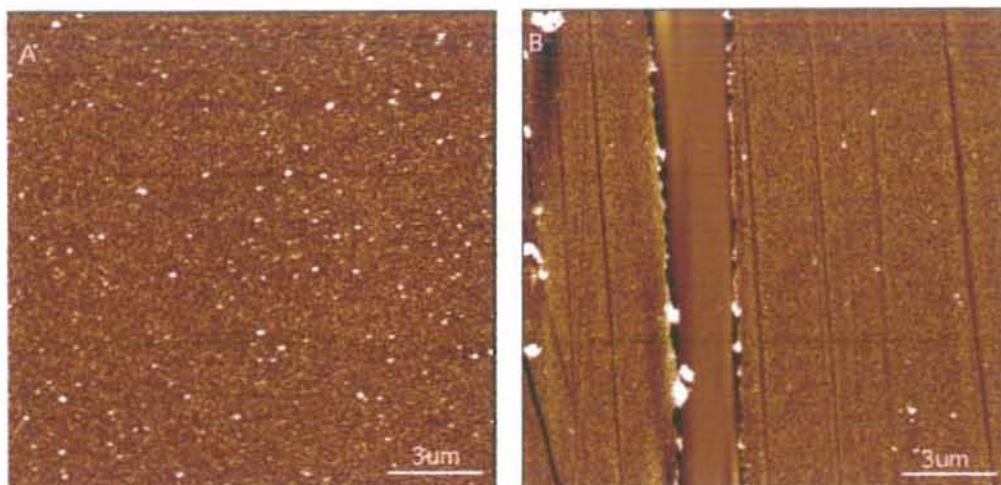

Figure 3.20: AFM images of virgin Au-NPs film (A) and 1 rub Au-NPs film (B)

Furthermore, the surface roughness analysis in Figure 3.20B reveals rms roughness value of 5.2 nm. During the rubbing test, the colloid film surface was progressively

eroded by forming a trench. However, the slight decrease of surface roughness of rubbed film was probably due to the palette-knife effect, which may make film smoother.

The mechanical strength of Au colloid films prepared *via* dipping process was even less than sprayed films. Therefore, a protective film was necessary for potential applications of these colloid films. The protective layer was coated on the otherwise very weak Au colloid layers in the same manner as was followed in the classical LbL assemblies. Out of many possible candidates, a $(PSS/PAH)_n$ film was selected as the first candidate for the protection of Au colloid film because such films were easy to prepare. The Au colloid films protected with $(PSS/PAH)_n$ layers had a slight improvement in mechanical resistance as compared to virgin Au-NPs. The multilayer films prepared by the electrostatic attractions of oppositely charged polyelectrolytes proved to be much weaker as protective layers. In order to overcome this problem, very fast curing reaction between the components of epoxy adhesive was chosen to construct the covalent LbL assemblies. This covalent reaction was first optimised to construct covalent LbL assemblies in nanoscale on Si and quartz surface and then applied onto the Au colloid films for their protection against hostile environment of the rubbing machine.

For this purpose, very fast room temperature covalent reaction between the two components of epoxy adhesive was studied. Epoxy adhesives are chemical compounds used to join components by providing a bond between two surfaces. The epoxy resins are widely used in many applications including automobiles, electrical and electronic industry, construction, medical, aircraft industry etc. The epoxy resins have a number of peculiar characteristics that promote their use in industry including;

- Nearly infinite number of ways to engineer an adhesive to provide the required application properties and end-use properties in a joint.
- A variety of forms and curing methods to optimize the assembly process.
- No evolution of volatiles and low shrinkage during cure.
- Good wetting properties resulting in excellent adhesion to most substrates.
- Excellent cohesive strength and mechanical properties.
- Good moisture, humidity, chemical, and temperature resistance.

120

For the protection of Au colloid nanoparticle films, CNER, PNER and Araldite MY-720[1] were selected as epoxy component while a branched PEI and TEPA as polyamine curing agent were used. Previously optimised polymer concentration and adsorption times were employed to prepare epoxy-amine multilayers for the protection of Au-NPs films. So epoxy resin and polyamine concentration of 40 mg mL^{-1} each and adsorption time as 100 min per layer pair were used initially.

In order to establish a minimum thickness of epoxy-amine network required to protect the Au-NPs film, the thickness of Au colloid film was kept almost constant while epoxy-amine protective layer thickness was varied. This depends on number of epoxy-amine layer pairs deposited on the Au colloid film. This means the improved mechanical resistance of the Au colloid film will depend on the thickness of epoxy-amine film. After the epoxy-amine film construction on top of (PAH/Au-NPs)$_5$ films, the mechanical resistance of these films were tested with the help of rubbing machine. In order to optimise the minimum thickness of epoxy-amine multilayers needed to protect the Au-NPs layers, two film architectures were initially followed;

[PEI/PSS/(PAH/Au)$_5$/PAH/PSS]/[PEI/CNER]$_3$ coded as (PAH/Au-NPs)$_5$/(PEI/CNER)$_6$

[PEI/PSS/(PAH/Au)$_5$/PAH/PSS]/[PEI/CNER]$_6$ coded as (PAH/Au-NPs)$_5$/(PEI/CNER)$_3$

The film thickness changes before and after rubbing test was measured by ellipsometry after washing the rubbed film with acetone (Table 3.9). Surface morphology before and after rubbing test was studied by AFM in the taping mode and the images were recorded as height images. The mechanical resistance test of these epoxy-amine protected Au colloid films revealed a great improvement as a function of the epoxy film thickness.

As compared to the ellipsometric data of Au colloid film with no epoxy protection, (Table 3.8 after 15 rubbing cycles, only 5 nm left, 12.15%), data in the Table 3.9 indicates very clearly that the presence of an epoxy layer had greatly improved the mechanical resistance of the colloid film. This mechanical robustness may be due to a specific thickness of epoxy-amine film coated on the Au colloids. After 25 rubbing cycles, the thickness of (PAH/Au-NPs)$_5$/(PEI/CNER)$_6$ film does not change too much

as less than 1 nm film have been wiped off during the rubbing test as compared to 30 nm of the (PAH/Au-NPs)$_5$/(PEI/CNER)$_3$.

Table 3.9: Evaluation of film thickness for epoxy protected colloid film as a function of various number of rubbing cycles.

Rubbing cycles	Film thickness (nm)	
	(PAH/Au-NPs)$_5$/(PEI/CNER)$_6$	(PAH/Au-NPs)$_5$/(PEI/CNER)$_3$
0	55.48	48.72
1	54.97	47.61
5	54.69	38.53
15	55.16	28.76
25	54.63	17.76

This means that more than 98% of the film still remains intact, as compared to 36.45% of (PAH/Au-NPs)$_5$/(PEI/CNER)$_3$ after 25 rubbing cycles. Loss of 1 nm in the thickness of (PAH/Au-NPs)$_5$/(PEI/CNER)$_6$ film may be due to the filling of interstices among the Au-NPs by the compression of rubbing machine. So, (PEI/CNER)$_n$ film has successfully protected the underlying weak Au colloid film. It also showed that certain thickness of the epoxy-amine film may be required to protect the underlying film as 3 layer pairs of (PAH/Au-NPs)$_5$/(PEI/CNER)$_3$ were not sufficient for protection purpose.

AFM surface morphological analysis confirmed the improvement in mechanical resistance of the epoxy coated Au-NPs film as a function of epoxy film thickness. This was evident from the difference in the surface morphology of (PAH/Au-NPs)$_5$/(PEI/CNER)$_3$ film (Figure 3.21 C-1) and (PAH/Au-NPs)$_5$/(PEI/CNER)$_6$ film (Figure 3.21 D-1). AFM surface roughness analysis indicates a rms roughness value of 3.38 nm for (PAH/Au-NPs)$_5$/(PEI/CNER)$_3$ film before the rubbing test, which was very similar to the rms roughness value (2.91 nm) for pure epoxy film. It was important to note that the outer most layer was always an epoxy layer.
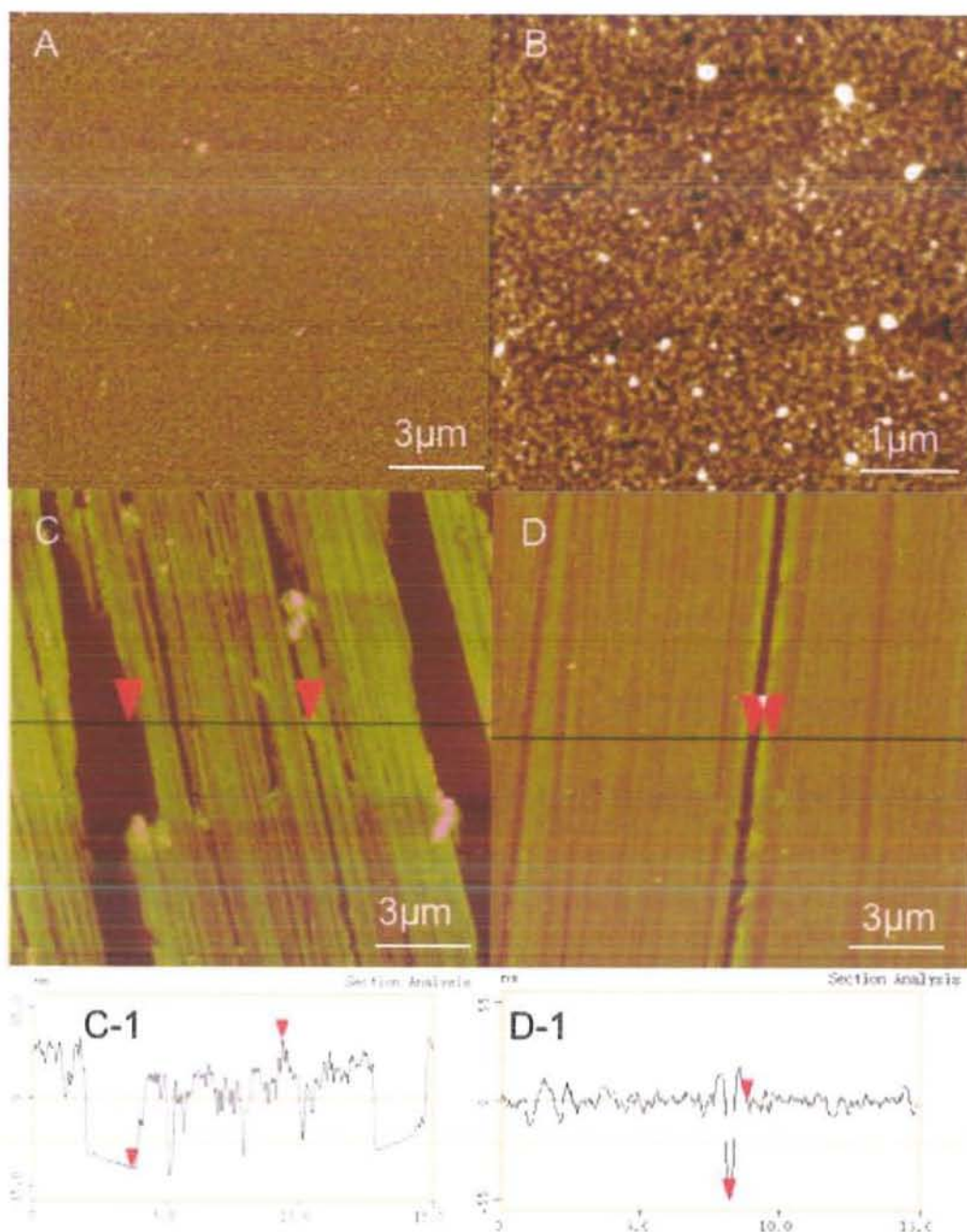
Figure 3.21: Surface morphological images of samples before and after rub test (A) Virgin (PAH/Au-NPs)$_5$/(PEI/CNER)$_3$ film (B) Virgin (PAH/Au-NPs)$_5$/(PEI/CNER)$_6$ film (C) (PAH/Au-NPs)$_5$/(PEI/CNER)$_3$ film after 5 rubbing cycles and (D) (PAH/Au-NPs)$_5$/(PEI/CNER)$_6$ film after 25 rubbing cycles.

The (PAH/Au-NPs)$_5$/(PEI/CNER)$_3$ film was completely torn off after 5 rubbing cycles, indicated by the dark part in the AFM images. The surface roughness analysis shows an increase in rms value to 10.65 nm (Figure 3.21 C), and the vertical distance

50.70 nm (Figure 3.21 C-1). AFM image presented in Figure 3.21 C was probably the PEI layer on the silicon substrate.

As for (PAH/Au-NPs)$_5$/(PEI/CNER)$_6$ film, a déjà vu AFM image was obtained. There are some small compressions and a groove on the surface (Figure 3.21 D) shown by the AFM image taken after 60 rubbing cycles at a stretch of this particular sample. The friction force causes an enlarged crack (Figure 3.21 D-1) with an increase in rms roughness from 3.40 nm to 24.68 nm, and a vertical distance of 55.45 nm of this big groove. Except this compression, rest of the film shows quite homogeneous surface morphology and it was also supported by the ellipsometric data.

This tremendous difference in rms roughness values i.e. between the (PAH/Au-NPs)$_5$/(PEI/CNER)$_3$ and (PAH/Au-NPs)$_5$/(PEI/CNER)$_6$ films may also be observed from the surface morphological images. As a large part of film has been wiped off after only 5 rubbing cycles in the case of (PAH/Au-NPs)$_5$/(PEI/CNER)$_3$ film, the silicon substrate or the PEI layer has been exposed. Surface morphology of both substrate surface and PEI was very smooth. In case of (PAH/Au-NPs)$_5$/(PEI/CNER)$_6$ film, after 60 rubbing cycles, almost all of the film was still on the substrate (Table 3.10). The mechanical friction caused by the rubbing machine has developed only one deep crack on the surface in addition to some slight compressions.

Table 3.10: Percent loss of thickness after 60 rubbing cycles for (PEI/CNER)$_{10}$ and (PAH/Au-NPs)$_5$/(PEI/CNER)$_6$ films.

Film Architecture	Thickness (nm)		Percentage
	Before Rubbing	After 60 Rubbings	Loss after 60 Rubbings
(PEI/CNER)$_{10}$	31.65	31.05	1.8
(PAH/Au-NPs)$_5$/(PEI/CNER)$_6$	55.48	52.34	6.3

These compressions may be due to the 2 bar pressure exerted by the cylinder of the rubbing machine. Both ellipsometry and AFM surface analysis confirmed that the deposition of epoxy layer over Au colloid film can improve the mechanical resistance

of the whole film and this improvement changes as a function of the epoxy film thickness. Therefore, it may be concluded that a 6 layer pair epoxy-amine film provides an optimal protection to the underlying weak Au-NPs film because after 25 rubbing cycles, ~97% of the film was still on the surface as compared to 36% for 3 layer pairs epoxy-amine film for the same number of rubbings and 12% for virgin Au nanoparticle film after only 15 rubbing cycles.

3.5 Speed up of Film Deposition *via* Dipping

In order to increase the speed of deposition process and to reduce the processing time for covalent LbL film formation, smaller adsorption times than the previously optimised 100 min per layer pair adsorption time were employed. It should be important to know that PEI supplied by Aldrich was employed for this particular study. The adsorption times of 20, 50 and 100 min per layer pair were used with polymer concentration 40 mg mL^{-1} for both the polymers. The thickness per layer pair increases linearly for (PEI/CNER)$_{10}$ system as a function of number of layer pairs but as expected the longer dipping times yield more thickness increment (Figure 3.22). Data correlation was high with low error for each measurement.
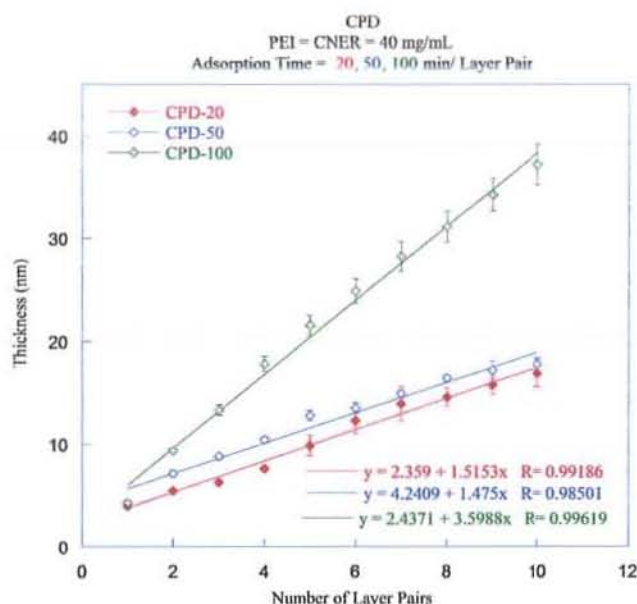

Figure 3.22: Thickness vs number of layer pairs (PEI/CNER)$_{10}$.

For the DEN$^{®}$-438 epoxy resin, thickness per layer pair increases linearly as a function of number of layer pairs. Here again, longer dipping times yield more thickness

increment but data scatter was more as compared to smaller dipping times (Figure 3.23). Also data correlation for longer dipping times was less with relatively more error for each measurement.
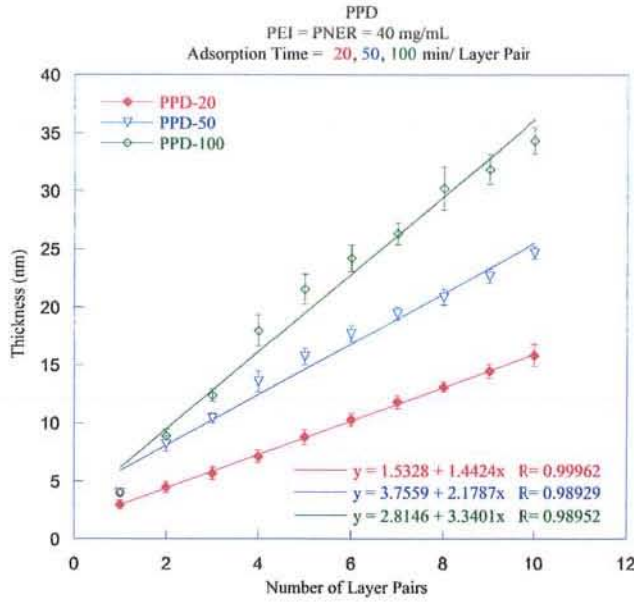

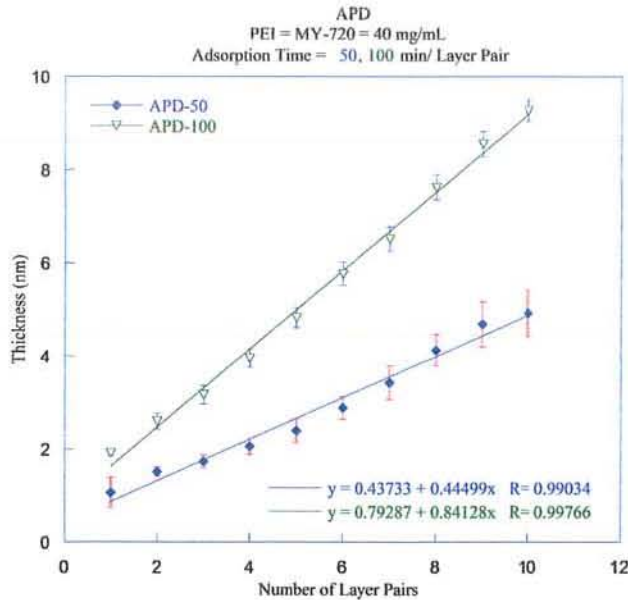**Figure 3.23:** Thickness vs number of layer pairs $(PEI/PNER)_{10}$.

Figure 3.24: Thickness vs number of layer pairs $(PEI/MY-720)_{10}$.

The thickness per layer pair increases linearly for $(PEI/MY-720)_{10}$ as a function of number of layer pairs (Figure 3.24). Longer dipping times yield more layer pair thickness films with low data scatter as compared to smaller dipping times (Figure

126

3.24). Data correlation for longer dipping times was less with relatively low error for each measurement. As compared to (PEI/CNER)$_{10}$ and (PEI/PNER)$_{10}$ systems, the overall thickness for (PEI/MY-720)$_{10}$ was quite less for the same number of layer pairs which was also obvious as molecular size and molecular weight of Araldite MY-720 is smaller as compared to the other two epoxy resins.

Same set of experiments was carried out using TEPA in place of PEI with all the three epoxy resins. In all the experiments where TEPA was used as curing agent, first layer pair used was always of the architecture (PEI/ER) followed by replacing PEI with TEPA to get the film architecture PEI(ER/TEPA)$_9$ER. The overall thickness of these systems was also less due to low molecular weight and small size of TEPA as compared to PEI. Data correlation and error was quite high for the smaller deposition times (Figure 3.25).
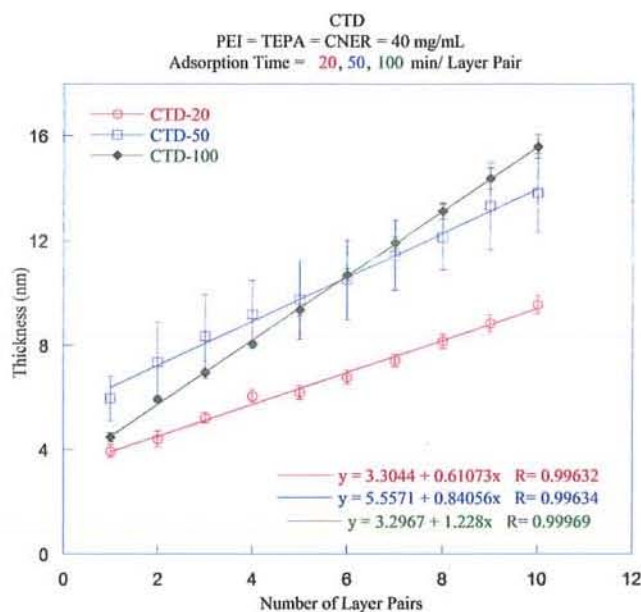

Figure 3.25: Thickness vs number of layer pairs PEI(CNER/TEPA)$_9$CNER.

There was a regular increase in film thickness as a function of number of layer pairs for the PEI(PNER/TEPA)$_9$PNER system with low error values and high data correlation (Figure 3.26). Longer dipping times yield more film thickness as compared to smaller. Longer dipping times yield identical growth per layer pair.
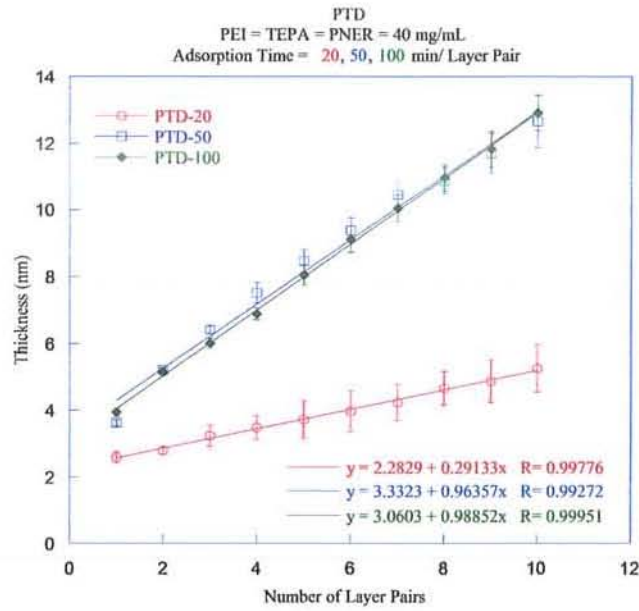
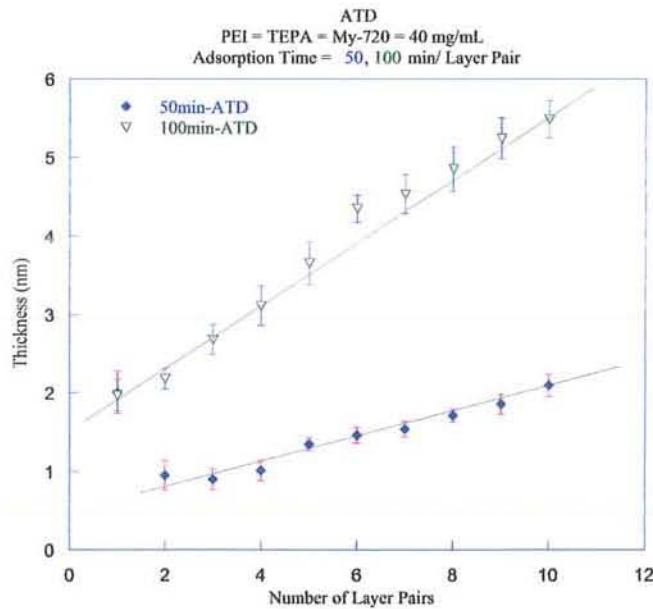**Figure 3.26:** Thickness vs number of layer pairs PEI(PNER/TEPA)$_9$PNER.

Figure 3.27: Thickness vs number of layer pairs PEI(MY-720/TEPA)$_9$MY-720.

Figure 3.27 shows highly irregular and scattered data for the deposition times of 50 and 100 min per layer pair. The overall film thickness was also quite low due to the low molecular weight of both TEPA and Araldite MY-720. So, 20 min per layer pair dipping time was not employed in this case.

So, it may be concluded that the longer dipping times always yielded more film growth and overall film thickness as compared to smaller ones. This may be due to the provision of ample time to polymer chains to arrange themselves in the vertical configuration.

3.6 Effect of Various Accelerators on Curing

Some catalysts/accelerators were also used during the optimisation of fast curing process of epoxy-amine. It was ensured that accelerators selected were in solution form and completely miscible with polyamine solution in Milli-Q water. In addition the accelerators should decrease the curing time and increase the thickness of the epoxy-amine layer pair. So four accelerator systems were selected which include;

1- Piperazine (P)

2- A-399 (A)

3- Epoxy embedding medium accelerator (E) and

4- A combination of P, E and triethanolamine (C).

These accelerators were always added in the polyamine solution and not in epoxy solution to avoid self polymerisation of epoxy. As a control, a parallel set of un-catalysed system was also carried out in order to make a comparison between the catalysed and un-catalysed curing of the epoxy-amine network under similar processing conditions.

As Araldite MY-720, gives less growth even for the longer dipping times, so it was not used to construct multilayers for shorter dipping time of 20 min per layer pair. The catalysts increased the overall thickness of the $(PEI/CNER)_{10}$ and $(PEI/PNER)_{10}$ systems as compared to un-catalysed system for 20 min per layer pair adsorption time (Figure 3.28 A, B, C, D, E). Data scatter for the catalysed and un-catalysed $(PEI/CNER)_{10}$ system was more as compared to the other systems prepared. As expected, the overall thickness of the $(PEI/CNER)_{10}$ was always more than $(PEI/PNER)_{10}$ system due to difference in molar mass of the CNER and PNER epoxy resins. As for as mechanical robustness of the multilayer was concerned, the catalysts has no dramatic effect on 20 min per layer pair systems as compared to un-catalysed system (Table 3.11).

The overall thickness of the catalysed systems prepared with the 50 min per layer pair dipping time was more than the un-catalysed systems. Data scatter was high for the $(PEI/MY-720)_{10}$ and $PEI(MY-720/TEPA)_9MY-720$ systems with lesser overall growth (Figure 3.29 A, B, C, D, E). Multilayer systems base on CNER epoxy give more overall growth for 10 layer pairs as compared to other epoxy resin based multilayers. Data correlation was high for the catalysed systems, so catalyst has a positive effect on the reduction of data scatter. The epoxy-amine multilayer prepared with 50 min per layer pair dipping time shows more mechanical robustness as compared to samples prepared with lesser dipping time (Table 3.11).

Table 3.11: Mechanical robustness of catalysed and un-catalysed epoxy-amine curing for various adsorption times. Polymer concentration used was 40 mg mL^{-1} and adsorption times of 20, 50, 100 min per layer pair.

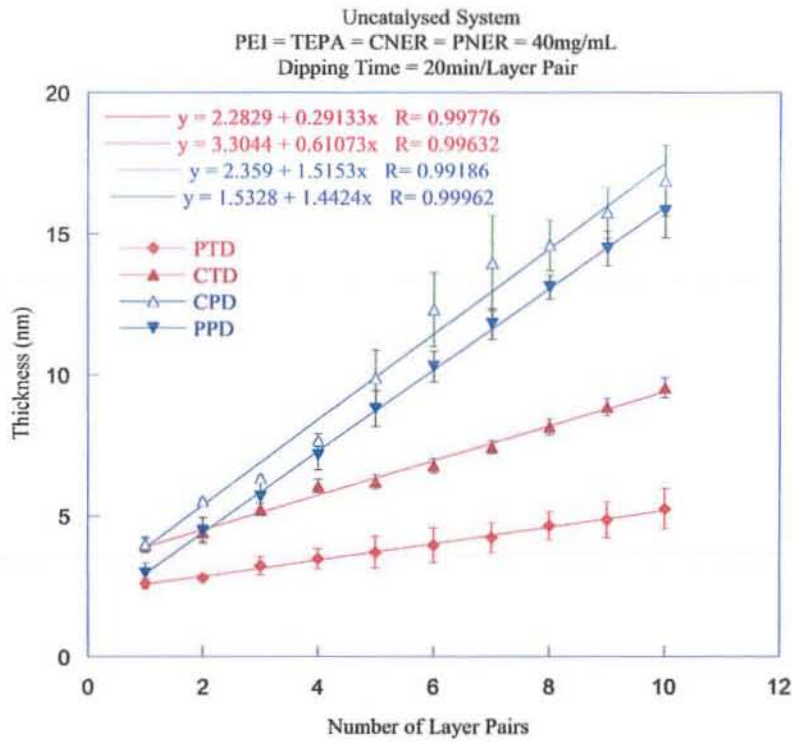| Sample Code	Percent loss after 20 Rubbing (-40-20)	Percent loss after 20 Rubbing (-40-50)	Percent loss after 20 Rubbing (-40-100)
CPD	9.9	4.4	1.8
CPDA	6.8	2.5	5.3
CPDP	No Loss	No Loss	5.8
CPDE	18.5	7.5	4.7
CPDC	No Loss	10.5	13.6
PPD	No Loss	2.0	1.4
PPDA	No Loss	4.2	1.6
PPDP	7.3	14.9	1.2
PPDE	11.6	4.2	2.0
PPDC	13.8	6.6	2.75

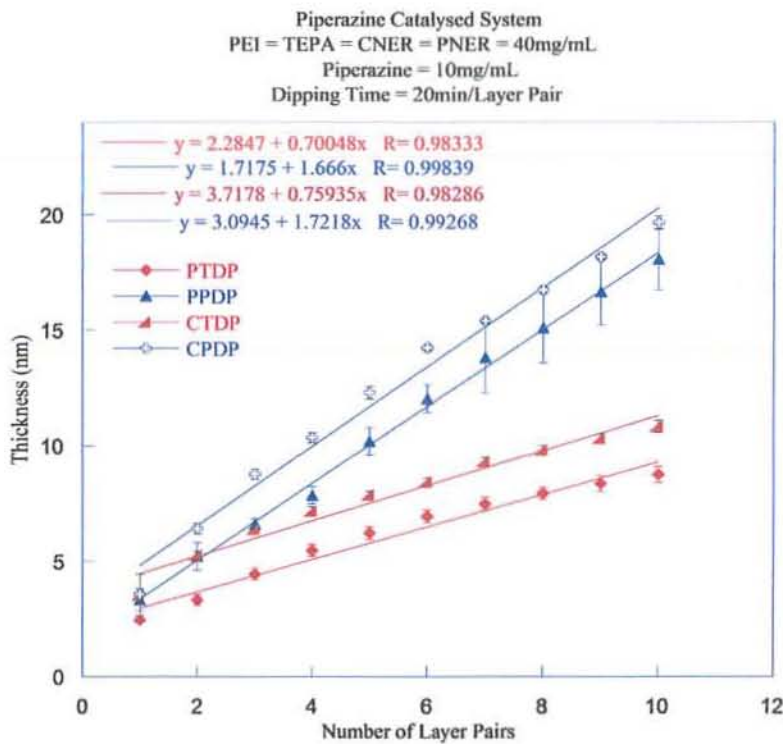**Figure 3.28A:** Un-catalysed epoxy-amine curing for 20 min/LP adsorption time.

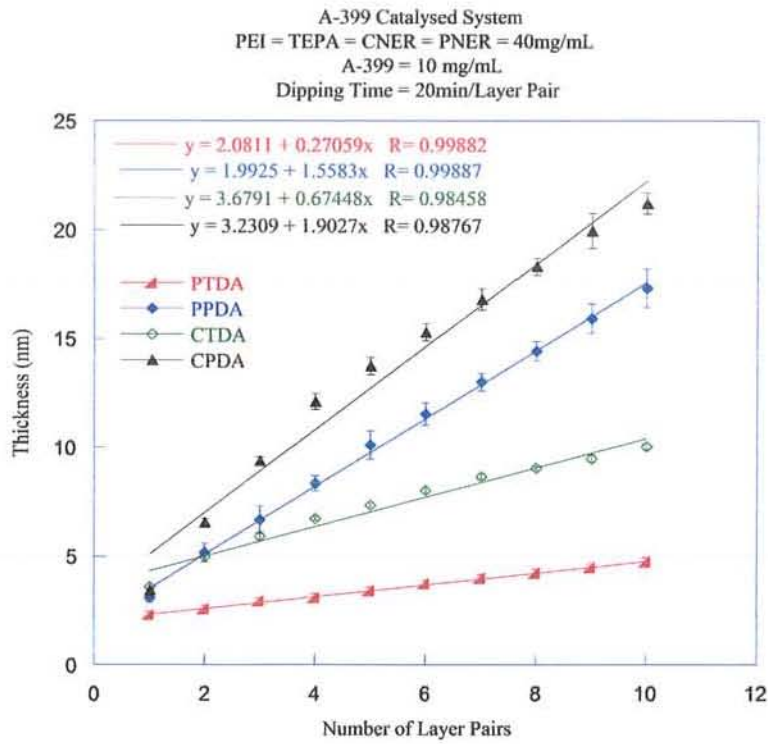**Figure 3.28B:** Piperazine catalysed epoxy-amine curing for 20 min/LP ads. time.

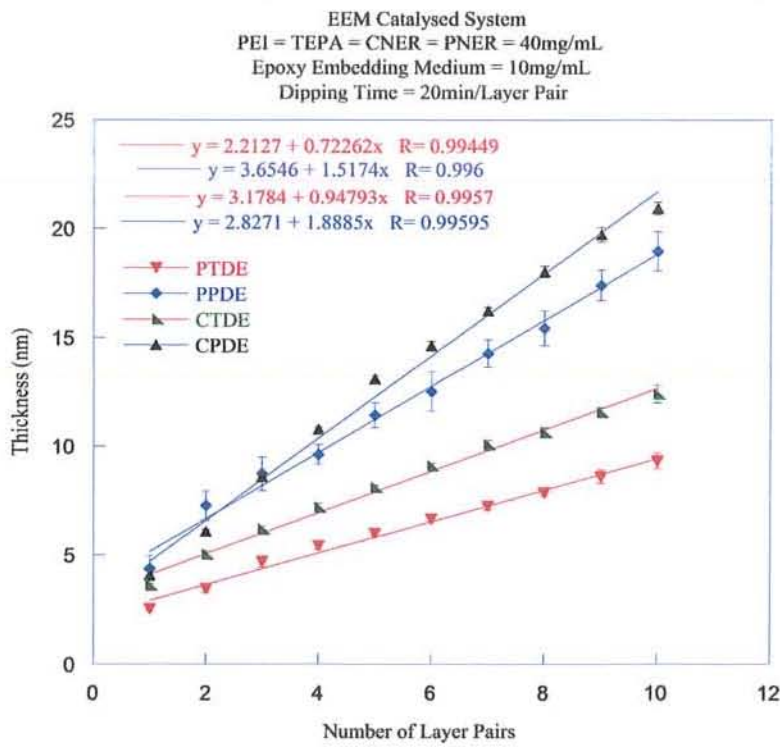**Figure 3.28C:** A-399 catalysed epoxy-amine curing for 20 min/LP adsorption time.

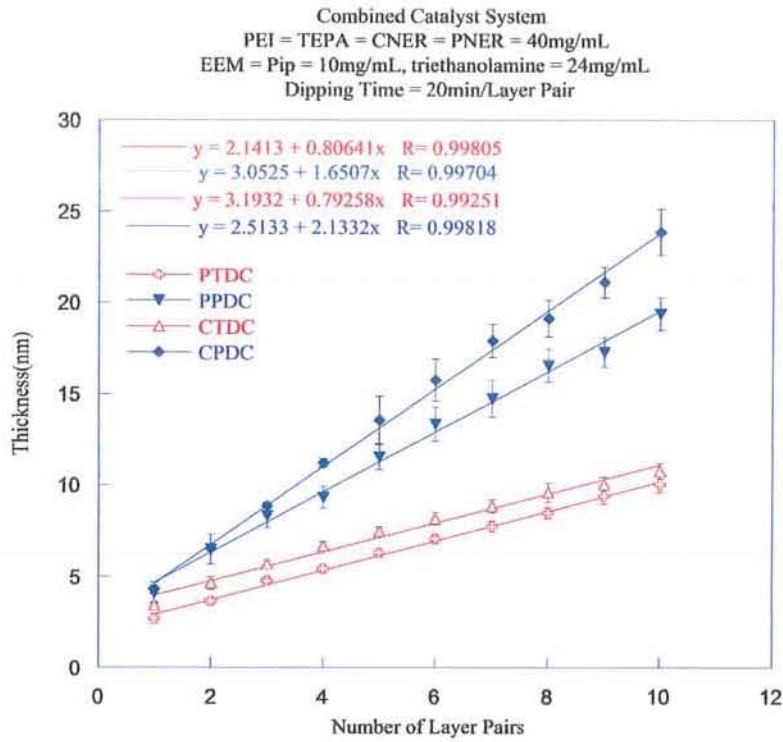**Figure 3.28D:** EEM catalysed epoxy-amine curing for 20 min/LP adsorption time.

132

Figure 3.28E: Combined catalysed epoxy-amine curing for 20 min/LP adsorption time.
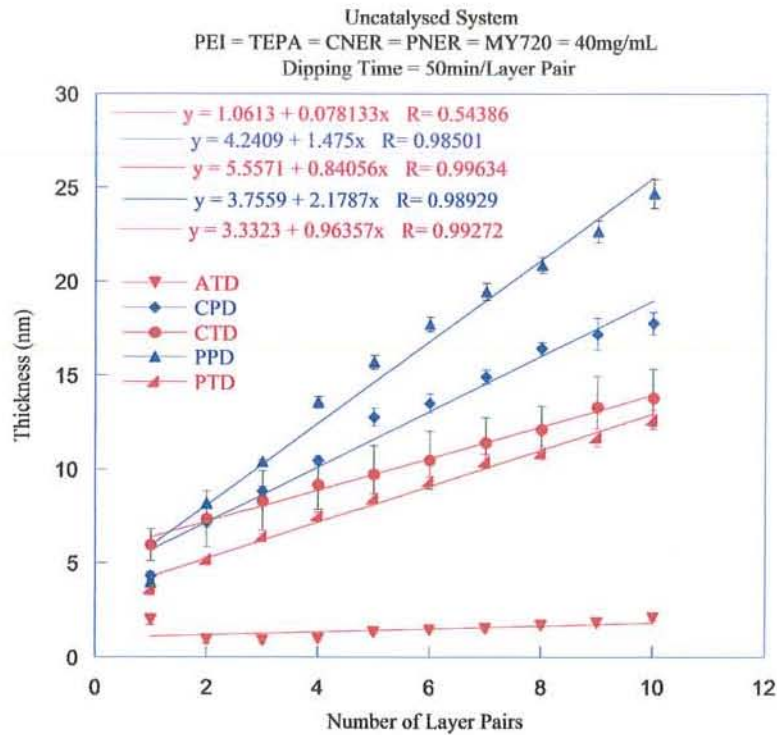

Figure 3.29A: Un-catalysed epoxy-amine curing for 50 min/LP adsorption time.
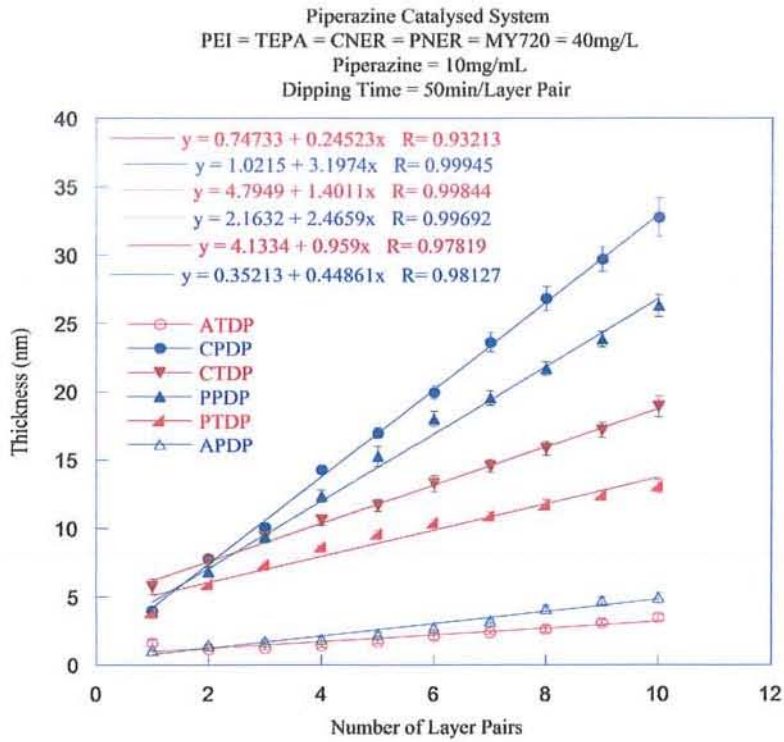
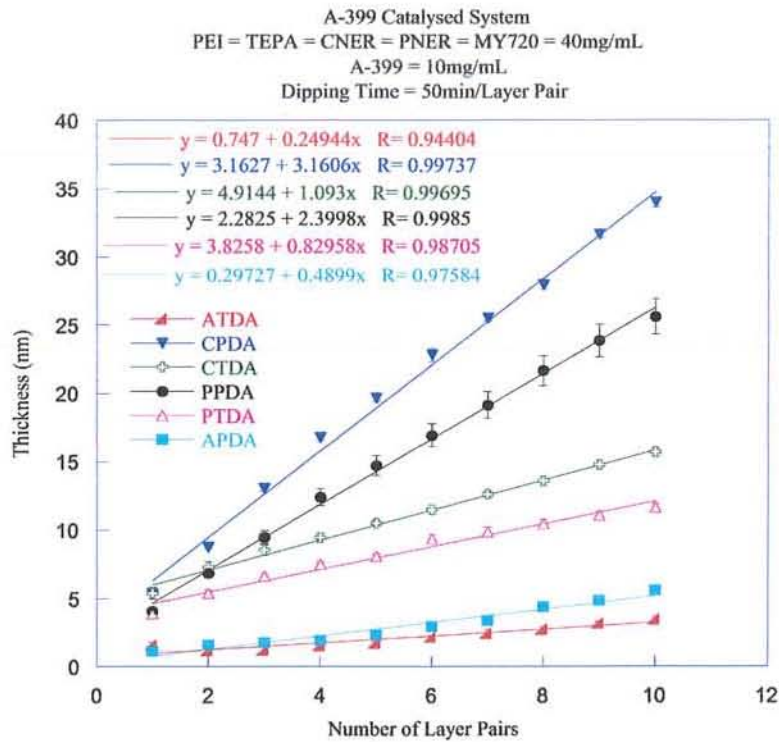**Figure 3.29B:** Piperazine catalysed epoxy-amine curing for 50 min/LP ads. time.

Figure 3.29C: A-399 catalysed epoxy-amine curing for 50 min/LP adsorption time.
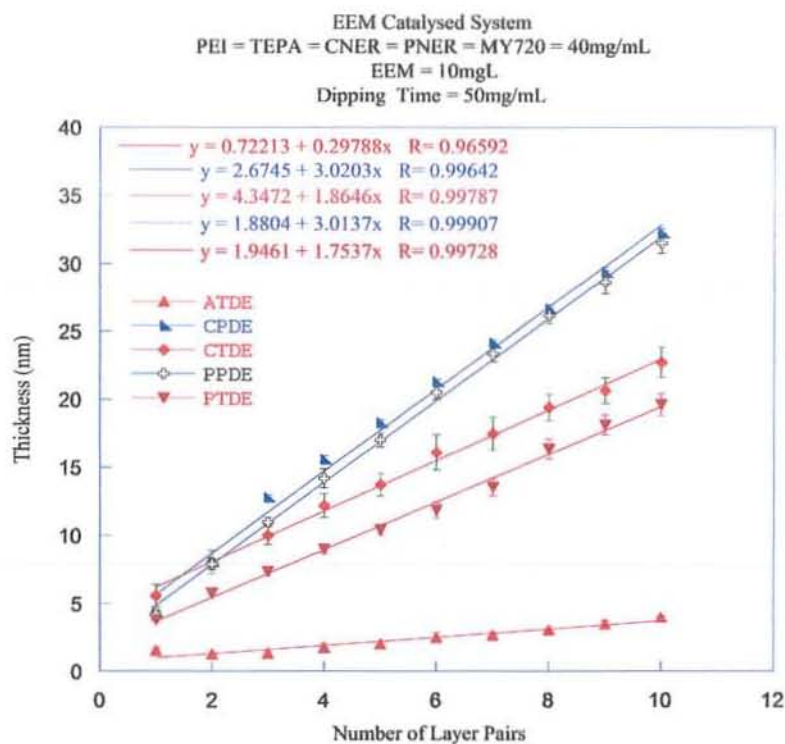
Figure 3.29D: EEM catalysed epoxy-amine curing for 50 min/LP adsorption time.

Figure 3.29E: Combined catalysed epoxy-amine curing for 50 min/LP adsorption time.

Figure 3.30A: Un-catalysed epoxy-amine curing for 100 min/LP adsorption time.

Figure 3.30B: Piperazine catalysed epoxy-amine curing for 100min/LP ads. time.

Figure 3.30C: A-399 catalysed epoxy-amine curing for 100 min/LP adsorption time.

Figure 3.30D: EEM catalysed epoxy-amine curing for 100 min/LP adsorption time.
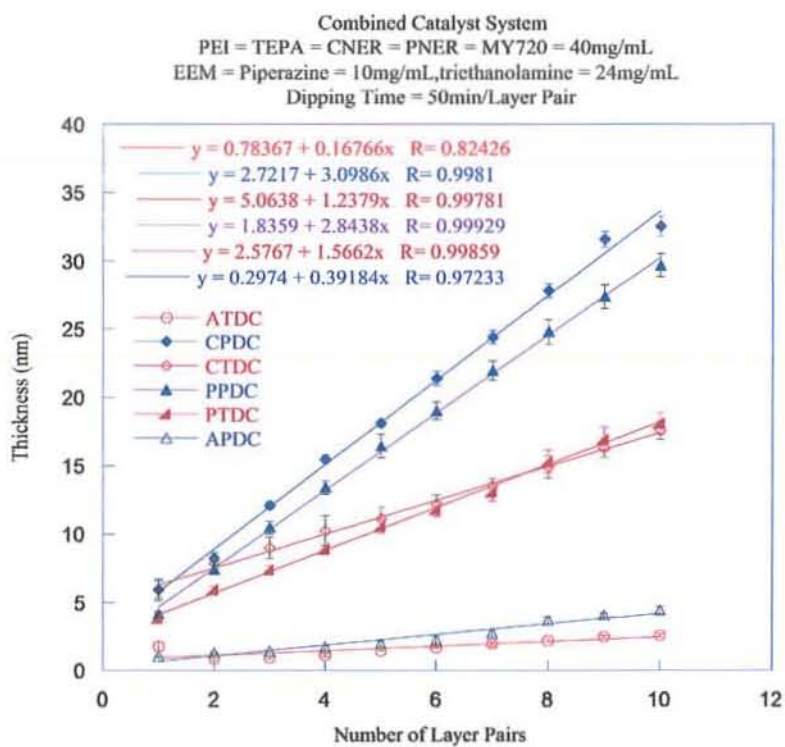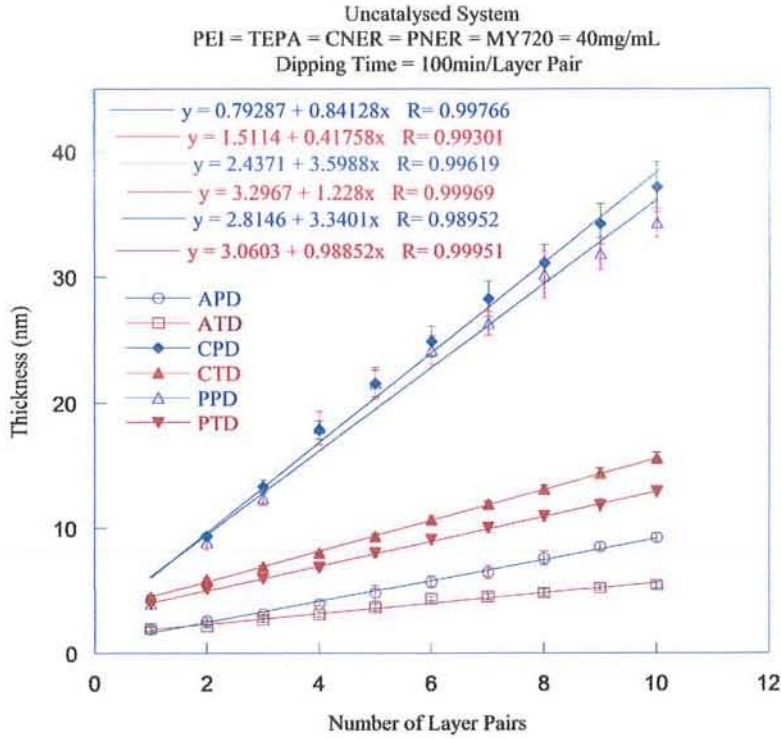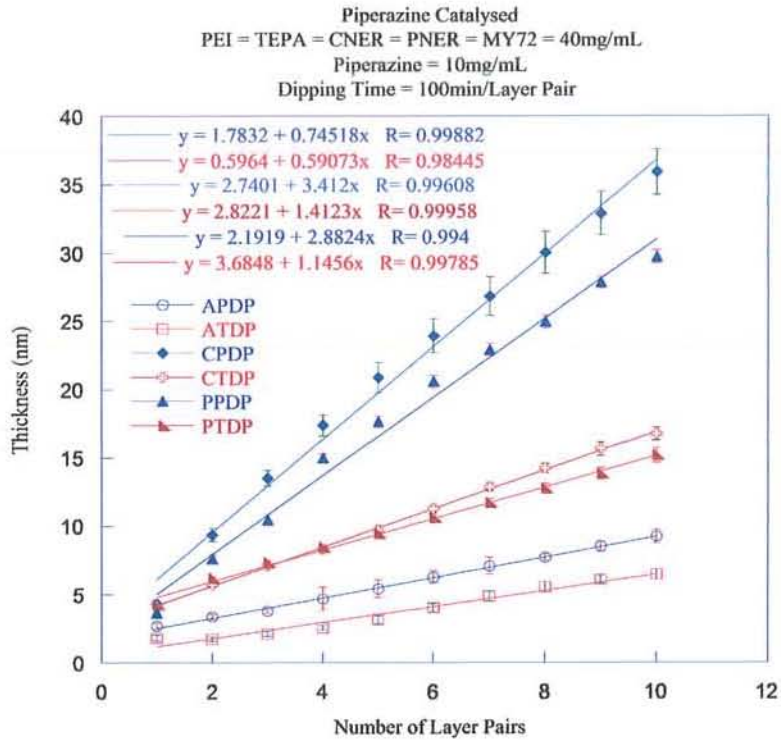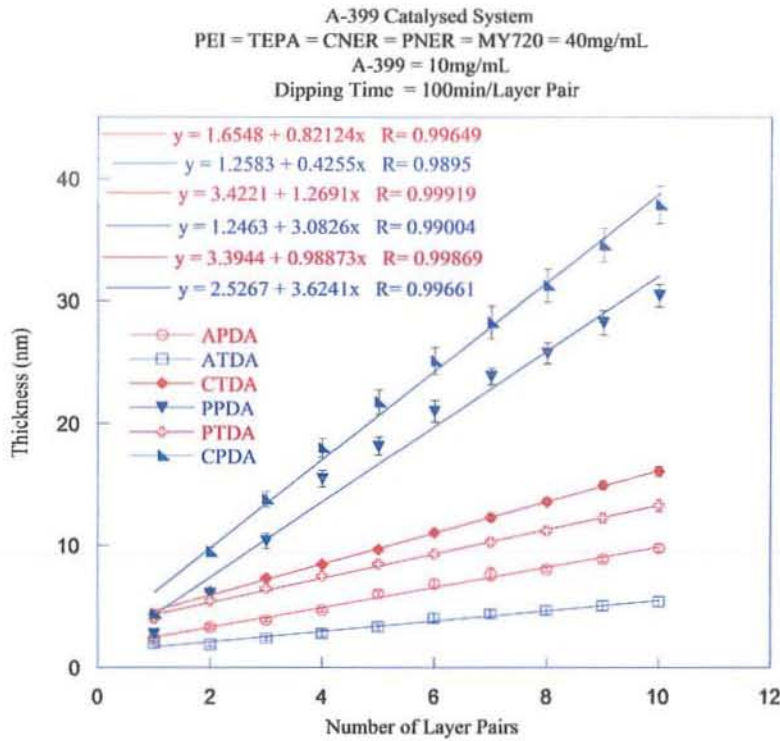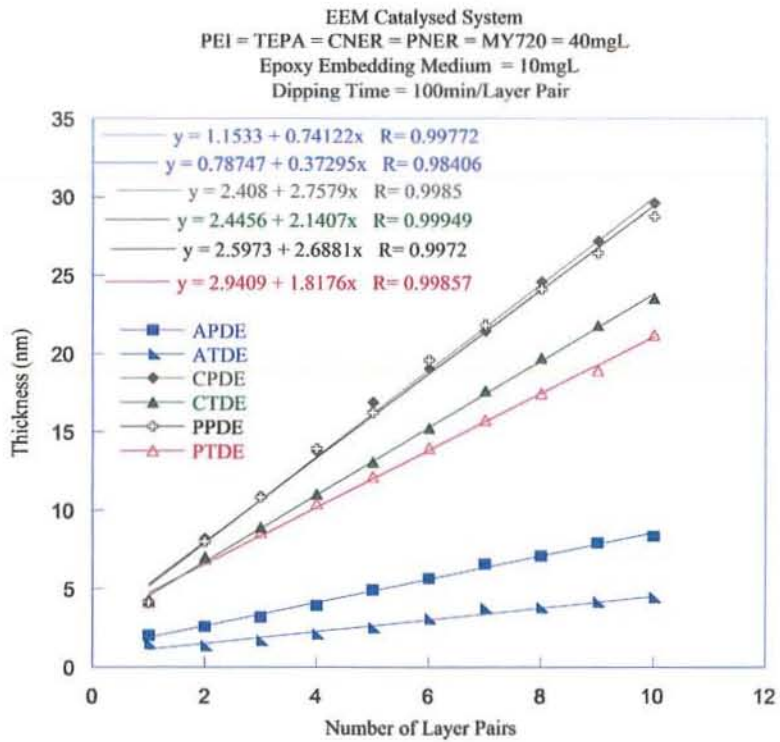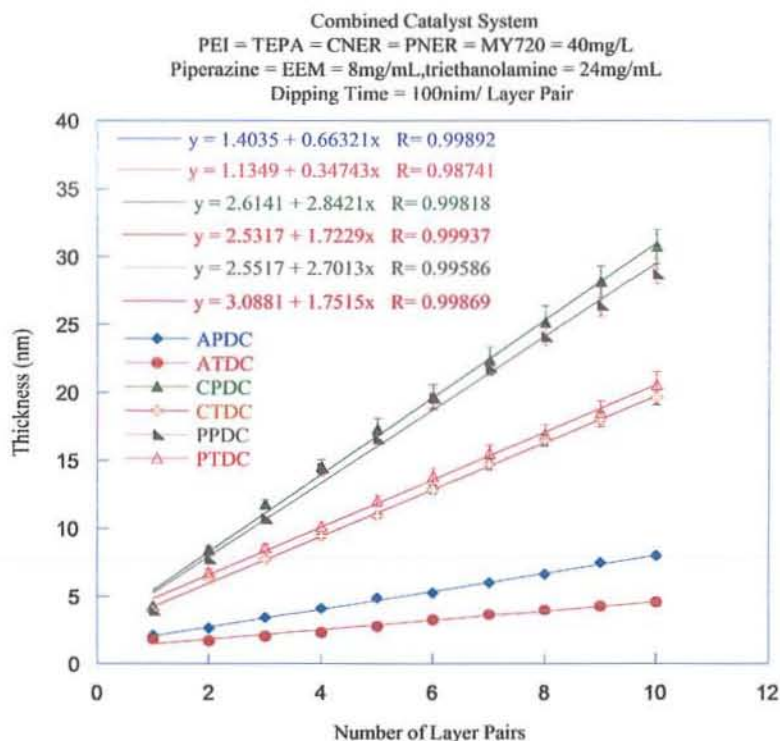
Figure 3.30E: Combined catalyst epoxy-amine curing for 100 min/LP adsorption time.

Un-catalysed, piperazine and A-399 catalysed systems prepared with adsorption time of 100 min per layer pair show more overall film thickness as compared to samples prepared with EEM and combined catalyst system (Figure 3.30 A, B, C, D, E). Data correlation was less and high error in measurement for the (PEI/MY-720)$_{10}$ and PEI(MY-720/TEPA)$_9$MY-720 systems. As expected the multilayer prepared with MY-720 epoxy resin show lesser overall growth due to low molecular weight. For other systems studied the errors in measurement were less and data correlation was high due to longer dipping times.

The mechanical robustness studies performed with rubbing machine revealed that the longer dipping times helps in improving the mechanical strength of the epoxy-amine films irrespective of the use of catalysts (Table 3.11). Although A-399 system supplied by Huntsman provides more mechanical strength against the harsh environment of the rubbing machine, yet the system with no catalyst also show good mechanical strength.

In a nutshell the catalysts and accelerators used here have no dramatic increase in the overall thickness of the epoxy-amine multilayer film as a function of shorter dipping

times. There was a small increase in thickness of the catalysed systems as compared to un-catalysed. But an important finding was that the data correlation becomes high with less error when catalysts and accelerators were employed.

3.7 Epoxy Curing with Dialysed (PEI$_{dia}$) and Un-dialysed PEI

One of the curing agent used was PEI obtained from Aldrich which is a 20% solution of PEI in water. BASF is the supplier of PEI to Aldrich by trade name LUPASOL in two concentrations. LUPASOL-HF is 50% aqueous solution of PEI while LUPASOL-WF is 100% pure PEI with no moisture in it. Lupasol-HF is highly branched polymer with molar ratios of primary to secondary to tertiary amino groups of 34:40:26[12,13] respectively. The polydispersity of BASF Lupasol-HF having $\overline{M_w} = 25,000$ is very high as it contains polymer chains of varying molecular weight along with traces of ammonia. All the different molecular weight chains contribute towards the epoxy resin curing process. Whether the low molecular weight amine molecule cure the epoxy resins or not? And does it also contribute towards the enhancement of mechanical strength of the cured epoxy-amine film? In order to answer these questions, an experiment was carried out to prepare epoxy-amine LbL assemblies using very low molecular weight amine i.e. ammonia (as ammonium hydroxide). After ten layer pairs of epoxy-ammonia multilayer formation, total thickness obtained was less than 10 nm (Figure 3.31). This means ammonia can cure epoxy resins.

The prepared PEI(CNER/Ammonia)$_9$/CNER sample was cut to two parts; one part was cured at 100°C for 1 hr while the other was time cured for 72 hrs at room temperature. Both the thermally cured and time cured samples gave no mechanical strength as after only 5 rubbing cycles more than 80% of the overall film thickness was lost. It means that the low molecular weight polymer chains contribute towards decrease in mechanical robustness of epoxy-amine network although there was increase in multilayer film growth as a function of number of layer pairs chemisorbed.

So in order to speed up the curing process, highly purified PEI was required which have narrow molecular weight distribution. For this purpose, the LUPASOL-HF was subjected to dialysis to remove the low molecular weight polymer chains. This was achieved with the help of SPECTRA PRO DIALYSIS MEMBRANE with molecular

weight cut at 3500. After dialysis, all the PEI_{dia} polymer chains should have more than 3500 molecular weight.

As is evident from the Figure 3.31, that there was appreciable increase in film thickness as a function of number of layer pairs for the curing of CNER with PEI_{dia}. The Figure also showed a good comparison for the curing of PEI_{dia} and un-dialysed PEI using an A-399 and EEM accelerator. The multilayers prepared with PEI_{dia} not only demonstrated larger growth increment as compared to un-dialysed PEI based systems with less value of error bars. The mechanical strength of the samples prepared with PEI_{dia} was also much high as there was no loss in film thickness after 20 rubbing cycles (Table 3.12).

So it can be inferred that the mechanical robustness of the epoxy-amine films was greatly affected by the presence of small molecular weight chains in the un-dialysed PEI. The dialysis of the BASF Lupasol-HF results in complete curing of the epoxy and thus greatly enhancing the mechanical strength of the films in short span of curing time at room temperature which may also be the shelf life of the product.
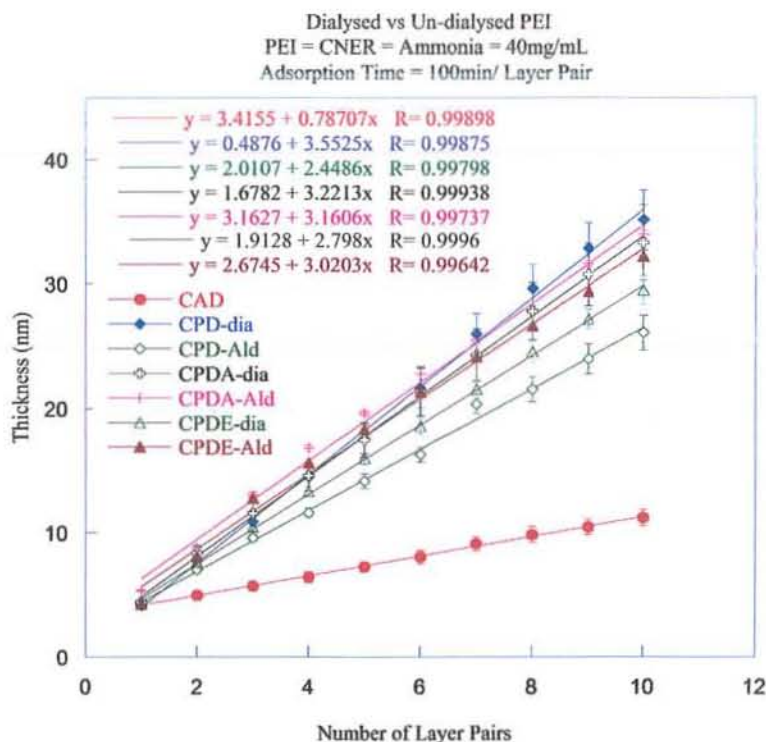

Figure 3.31: Thickness of epoxy-amine films as a function of PEI_{dia}, un-dialysed PEI and ammonia.

Table 3.12: Mechanical robustness of epoxy-amine LbL films cured with catalysed and un-catalysed PEI_{dia} and un-dialysed PEI.

System	Percent loss after 20 rubs thermal Cured (%)	Percent Loss after 20 rubs time cured (%)
CAD	74.0	93.0
CPD-Dia	No Loss	No Loss
CPD-Ald	4.5	30.4
CPDA-Dia	No Loss	No Loss
CPDA-Ald	2.8	9.3
CPDE-Dia	No Loss	No Loss
CPDE-Ald	3.47	12.56

3.8 Use of Paint Brush Spray System to Get Fast Adsorption Process

In dipping deposition process, it is very difficult to agitate solutions in such a way that immersed substrates experience the same flow conditions on their whole surface, especially when substrates have complex shapes. "Dipping" experiments were, therefore, carried out in the absence of agitation. Deposition of polymer multilayers by spraying was tested as a way of agitation. It is safe to assume that a fine spray jet arriving on a substrate surface provides much more homogeneous flow conditions on macroscopic surfaces than immersion *via* "dipping" in solutions. These flow conditions like local concentrations of adsorbing compounds close to the surface and adsorption times of polymers strongly influence diffusion of molecules onto the substrate surface. It has already been demonstrated for electrostatic LbL assembly that spraying can accelerate the deposition process by a factor of 250^3 or more with respect to dipping.

As the dialysed PEI shows considerable increase in thickness as a function of number of layer pairs and at the same time enhances the mechanical robustness of the epoxy-amine films at room temperature time cure process. So in the next stage, the deposition time was further reduced to speed up the curing process. The previously optimised dipping time was 20 min per layer pair with very good mechanical strength. As the PEI_{dia} solution was prepared in Milli-Q water, so it can be sprayed onto the substrate with the help of a paint brush spray system obtained from PASCHE MILLINIUM WOOD. The paint brush spray system was very economical in terms of solvent and

141

polymer consumption. In addition very fine jets of the paint brush spray system made a very fine aerosol with a controlled droplet size. During the time of flight of the polymer solution from paint brush spray system nozzle to the substrate, some of the solvent of the polymer solution might evaporates away, thus more concentrated polymer solution was deposited onto the substrate. The paint brush spray system was not recommended to spray the epoxy solution prepared in organic solvent due to health and environmental issues.

PEI_{dia} was sprayed onto the substrate for $(t_1) = 10$ s, followed by a wait period of 30 s. The substrate was then given three repeated wash with Milli-Q with AIR-BOY spray bottles followed by drying the substrate with a stream of compressed air. The dried substrate was then put in the ER solution in acetone for 10 min followed by three equal time wash with acetone solvent. It is important to note that to ensure the complete removal of loosely bound polymers, the substrates were again washed with the solvents using wash bottles.
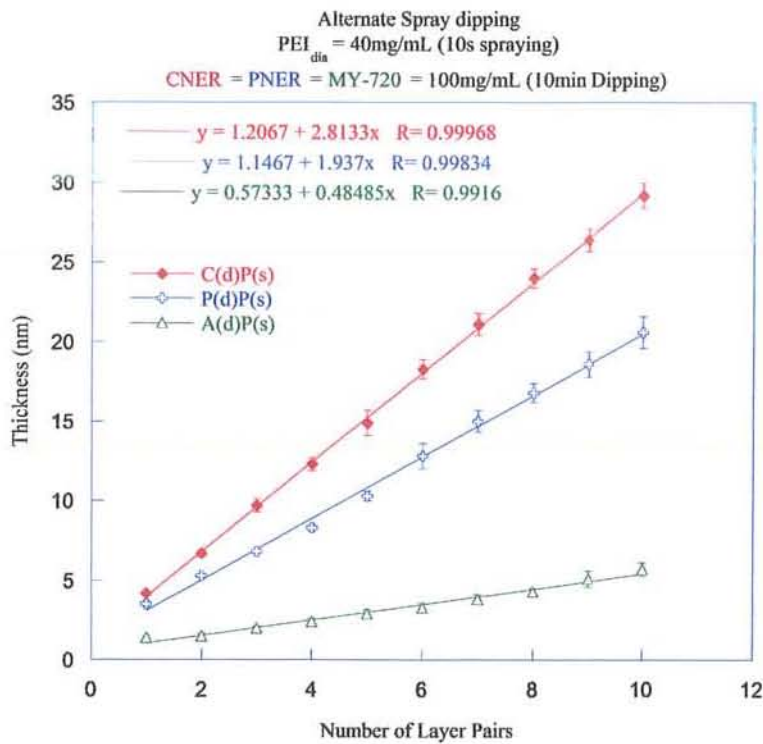

Figure 3.32: Thickness vs number of layer pairs for alternate spray-dipping process.

So, in this way we get a layer pair of epoxy-amine in a practical time of 10 min and 10 s, a great enhancement in the deposition speed using alternate spray and dipping with

epoxy and amine solutions respectively. The ellipsometric data in the Figure 3.32 demonstrate a linear rise in thickness of this fast speed adsorption process as a function of number of layer pairs. For the curing of all the three epoxy resins with PEI_{dia}, the data correlation coefficient was also quite high with quite low value of error bars.

The mechanical robustness of the prepared epoxy-amine films was quite high in case of time cure process. After 72 hrs curing at room temperature, both the films show good mechanical strength as there was no loss in thickness after 20 rubbing cycles. After 10 day time cure, both the system shows great robustness because there was no decrease in thickness of the two films after 20 rubbing cycles. Time curing has a positive effect on the mechanical strength of epoxy-amine LbL assemblies at nanoscale, as shown below in the tabulated data (Table 3.13).

Table 3.13: Thickness of epoxy as a function of number of rubbing cycles and time curing at ambient temperature.

System	Thickness before Rubbing (nm)	Thickness after 20 Rubbings (nm)	Thickness after 60 Rubbings (nm)	Loss of after 60 Rubbings (%)
$(PEI_{dia}/CNER)_{10}$	29.4	30.8	27.2	7.0
$(PEI_{dia}/PNER)_{10}$	20.2	20.2	18.8	7.0

After 60 consecutive rubbing cycles, there was only 7.0% decrease in thickness of both the $(PEI_{dia}/PNER)_{10}$ and $(PEI_{dia}/CNER)_{10}$ multilayer films. This means that the PEI_{dia} has improved the mechanical strength of the epoxy-amine LbL assemblies and it can be used to protect weak electrostatic multilayers particularly of Au colloid.

UV-Visible spectra for the deposition of $(PEI_{dia}/CNER)_{10}$ and $(PEI_{dia}/PNER)_{10}$ using PEI_{dia} as amine component is shown in the Figure 3.33 (A, B). PEI_{dia} was sprayed onto the quartz substrate with the help of paint spray brush for 10 s followed by 30 s wait period and washings using Milli-Q water.

The quartz substrate was dipped in the epoxy solution for 10 min after drying with compressed air. The substrate was washed with acetone and dried under a stream of
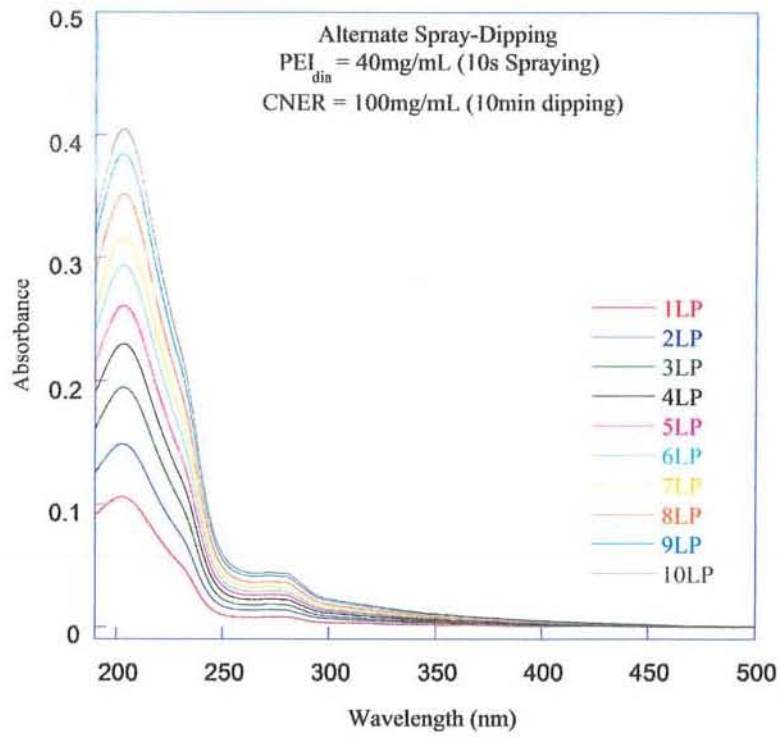
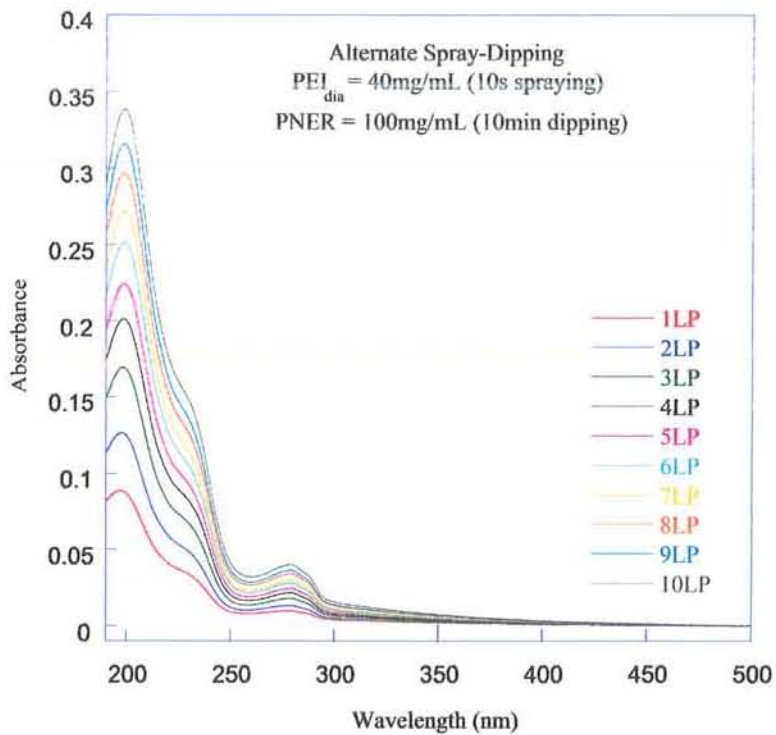**Figure 3.33A:** UV-Visible data of fast speed adsorption process $(PEI_{dia}/CNER)_{10}$.

Figure 3.33B: UV-Visible data of fast speed adsorption process $(PEI_{dia}/PNER)_{10}$.

144

compressed air. UV-Visible spectrum was recorded for each layer pair. Both the epoxy system shows an increase in absorbance (at wavelength maximum 280 nm) as a function of number of layer pairs chemisorbed.

The absorbance maximum at 280 nm was plotted against number of layer pairs which shows a linear increase thus complementing the linear growth of these films as shown by ellipsometer data (Figure 3.34).
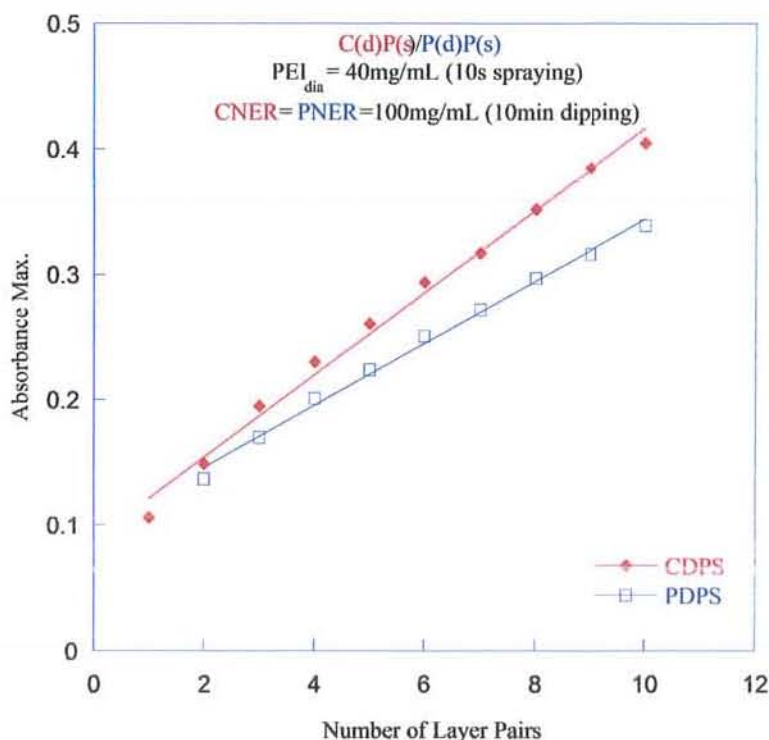

Figure 3.34: Plot of absorbance maximum vs number of layer pairs.

So, an epoxy-amine network layer can be deposited in 10 min and 10 s, a great enhancement in deposition speed of these covalent LbL assemblies with great mechanical robustness to be applied for the protection of weak multilayers.

3.8.1 Protection of Au-NPs Films *via* Fast Adsorption Process

After the optimisation of alternate spray dipping process for the covalent LbL assembly of commercially available amine epoxy compounds, it was applied to protect the already prepared (PAH/Au-NPs)$_5$ films. Before epoxy-amine protection, the surface morphology of the virgin Au-NPs was recorded with the help of AFM in the tapping

mode. The AFM images show a very homogeneous morphology with rms roughness values of 12.04 nm at 6 and 12 μm length scales (Figure 3.35).
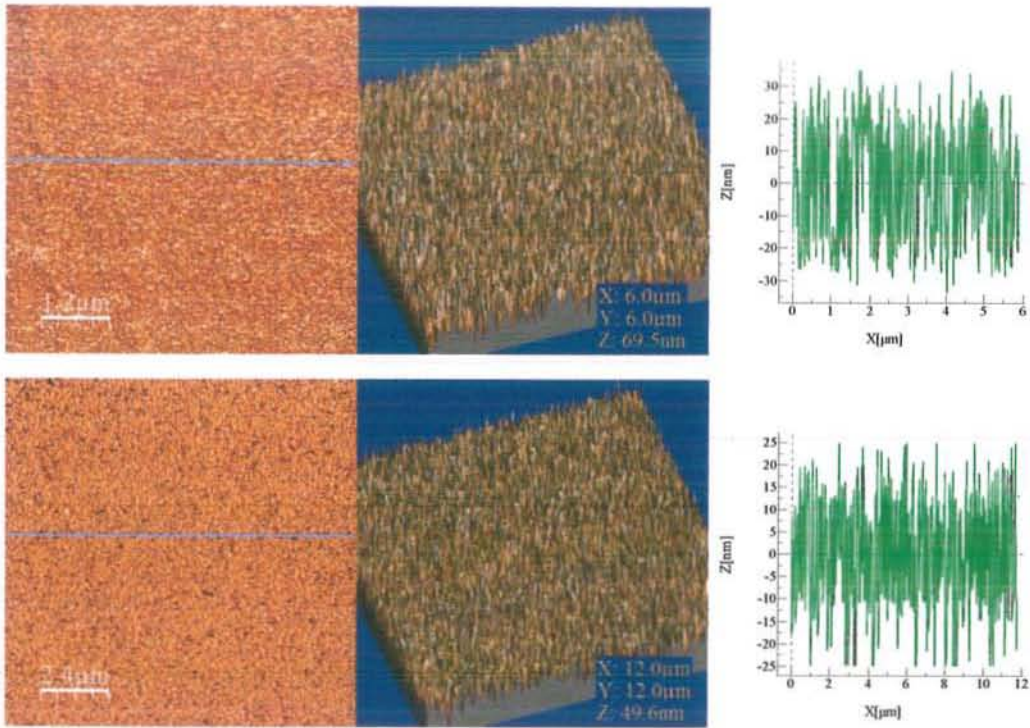

Figure 3.35: AFM images of virgin (PAH/Au-NPs)$_5$

PEI_{dia} layer was first deposited using paint brush spray system onto the Au-NPs layers of the architecture (PAH/Au-NPs)$_5$. This was achieved by spraying the PEI_{dia} for 10 s followed by 30 s wait time to ensure maximum adsorption of PEI_{dia}. The substrate was then washed with Milli-Q water in three equal wash (each 10 s sprays) and then dried with the help of compressed air. The substrate was then put into epoxy solution in acetone for 10 min followed by three 1 min washings with pure acetone solvent to remove any un-adsorbed material especially epoxy at this stage. After drying the sample with compressed air, the thickness of the epoxy-amine layer was determined with ellipsometer. Increase in thickness of the epoxy-amine film onto Au colloid film was not regular. So thickness was measured after each half layer. It was interesting to note that after every PEI_{dia} layer adsorption there was slight decrease followed by an increase in thickness after epoxy layer adsorption for both the (PAH/Au-NPs)$_5$/(PEI$_{dia}$/CNER)$_n$ (Table 3.14) and (PAH/Au-NPs)$_5$/(PEI$_{dia}$/PNER)$_n$ (Table 3.15) systems.

146

Table 3.14: Thickness variations of PEI and CNER on (PAH/Au-NPs)$_5$ substrate.

Architecture	Thickness (nm)	Architecture	Thickness (nm)
(PAH/AuNPs)$_5$	47.7		
(PAH/AuNPs)$_5$/PEI	46.94	(PAH/AuNPs)$_5$/PEI/CNER	47.7
(PAH/AuNPs)$_5$/PEI/CNER/PEI	47.53	(PAH/AuNPs)$_5$/(PEI/CNER)$_2$	48.52
(PAH/AuNPs)$_5$/(PEI/CNER)$_2$/PEI	48.6	(PAH/AuNPs)$_5$/(PEI/CNER)$_3$	49.55
(PAH/AuNPs)$_5$/(PEI/CNER)$_3$/PEI	50.2	(PAH/AuNPs)$_5$/(PEI/CNER)$_4$	51.66
(PAH/AuNPs)$_5$/(PEI/CNER)$_4$/PEI	52.37	(PAH/AuNPs)$_5$/(PEI/CNER)$_5$	53.83
(PAH/AuNPs)$_5$/(PEI/CNER)$_5$/PEI	55.58	(PAH/AuNPs)$_5$/(PEI/CNER)$_6$	56.53
(PAH/AuNPs)$_5$/(PEI/CNER)$_6$/PEI	57.23	(PAH/AuNPs)$_5$/(PEI/CNER)$_7$	59.62
(PAH/AuNPs)$_5$/(PEI/CNER)$_7$/PEI	60.13	(PAH/AuNPs)$_5$/(PEI/CNER)$_8$	62.16
(PAH/AuNPs)$_5$/(PEI/CNER)$_8$/PEI	63.2	(PAH/AuNPs)$_5$/(PEI/CNER)$_9$	64.77
(PAH/AuNPs)$_5$/(PEI/CNER)$_9$/PEI	65.33	(PAH/AuNPs)$_5$/(PEI/CNER)$_{10}$	67.7

To know why and how the thickness showed an irregular trend for the adsorption of epoxy-amine network onto Au colloid film, the sample was cut after the adsorption of only one layer pair of epoxy-amine on Au-NPs layer and subjected to AFM analysis (Figure 3.36 and 3.37).

The AFM images showed the penetration of epoxy-amine polymers among the interstices created due to the close packing of spherical Au colloid particles. This means initially there was no increase in thickness of epoxy-amine layers rather sometime a little decrease was observed in thickness which may be due to solvent interchange effect between epoxy and amine part of the layer pairs and the rearrangement of Au nanoparticles in the interstices[14]. The rms roughness values for the one layer pair (PEI$_{dia}$/CNER) film was also quite high showing that some of the epoxy might have penetrated while some settles down onto the Au particles as can be seen in the AFM images shown in Figure 3.36.
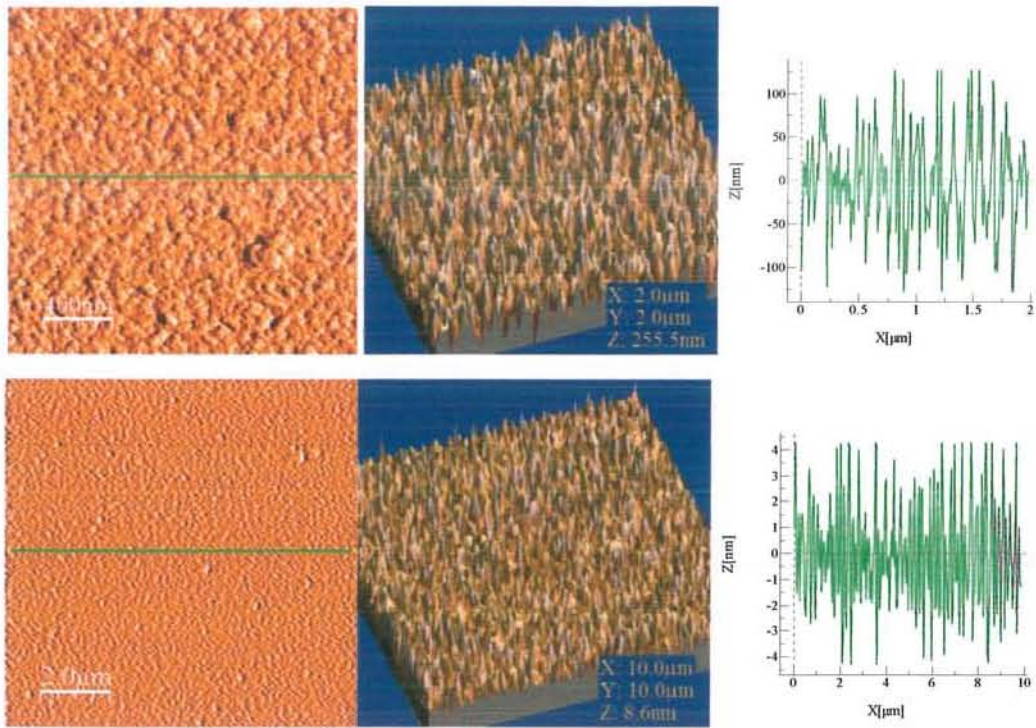
147

Figure 3.36: AFM images and rms data of CNER protected Au-NPs film (1LP Epoxy).

Similar trend was also observed for the deposition of PEI and PNER layer on (PAH/Au-NPs)$_5$ as reported in Table 3.15. However, as expected, thickness increments were much less for (PEI/PNER)$_n$ as compared to (PEI/CNER)$_n$ system due to smaller size of PNER epoxy.

Table 3.15: Thickness variations of PEI and PNER on (PAH/Au-NPs)$_5$ substrate.

Architecture	Thickness (nm)	Architecture	Thickness (nm)
(PAH/AuNPs)$_5$	52.2		
(PAH/AuNPs)$_5$/PEI	51.69	(PAH/AuNPs)$_5$/PEI/PNER	51.68
(PAH/AuNPs)$_5$/PEI/PNER/PEI	51.71	(PAH/AuNPs)$_5$/(PEI/PNER)$_2$	51.6
(PAH/AuNPs)$_5$/(PEI/PNER)$_2$/PEI	51.4	(PAH/AuNPs)$_5$/(PEI/PNER)$_3$	51.5
(PAH/AuNPs)$_5$/(PEI/PNER)$_3$/PEI	51.44	(PAH/AuNPs)$_5$/(PEI/PNER)$_4$	51.3
(PAH/AuNPs)$_5$/(PEI/PNER)$_4$/PEI	51.5	(PAH/AuNPs)$_5$/(PEI/PNER)$_5$	51.92
(PAH/AuNPs)$_5$/(PEI/PNER)$_5$/PEI	51.96	(PAH/AuNPs)$_5$/(PEI/PNER)$_6$	52.83
(PAH/AuNPs)$_5$/(PEI/PNER)$_6$/PEI	53.26	(PAH/AuNPs)$_5$/(PEI/PNER)$_7$	54.2
(PAH/AuNPs)$_5$/(PEI/PNER)$_7$/PEI	54.65	(PAH/AuNPs)$_5$/(PEI/PNER)$_8$	56.04
(PAH/AuNPs)$_5$/(PEI/PNER)$_8$/PEI	56.08	(PAH/AuNPs)$_5$/(PEI/PNER)$_9$	57.43
(PAH/AuNPs)$_5$/(PEI/PNER)$_9$/PEI	57.53	(PAH/AuNPs)$_5$/(PEI/PNER)$_{10}$	59.4

AFM images taken in tapping mode show epoxy-amine covered homogeneous Au-NPs. The rms roughness values for the PNER protected films were also quite high for the adsorption of one layer pair of (PEI$_{dia}$/PNER) (Figure 3.37).
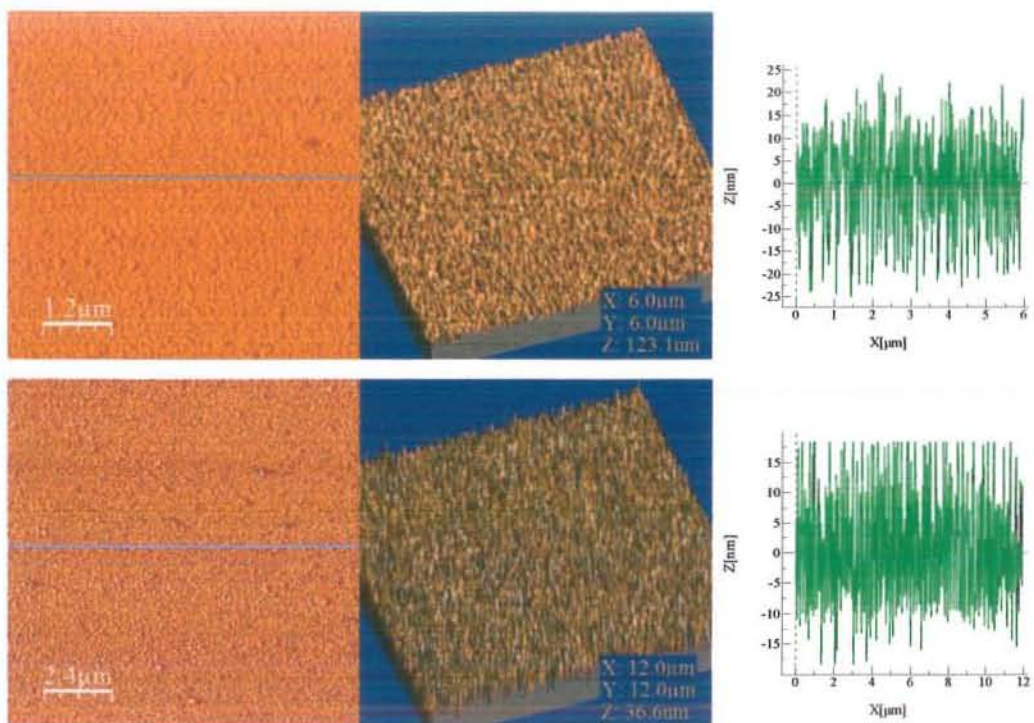
Figure 3.37: AFM images and rms data of PNER protected Au-NPs film (1LP Epoxy).

After the adsorption of 10 layer pairs of epoxy-amine onto (PAH/Au-NPs)$_5$ film, the substrates were put to time curing process in a tightly capped polystyrene bottles at ambient temperature. The 72 hrs time cured samples were subjected to AFM analysis in the tapping mode (Figure 3.38 A, B). AFM images show quite homogeneous surface morphology for these un-rubbed epoxy-amine protected Au colloid samples.
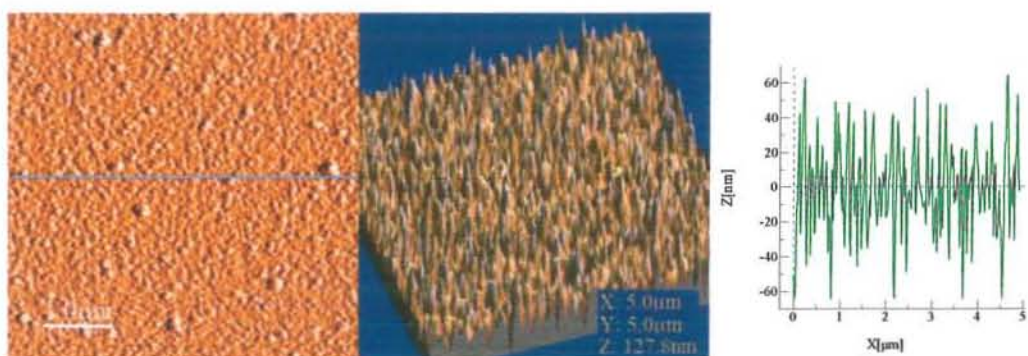
Figure 3.38A: Surface morphology of virgin (PAH/Au-NPs)$_5$/(PEI$_{dia}$/CNER)$_{10}$ film.
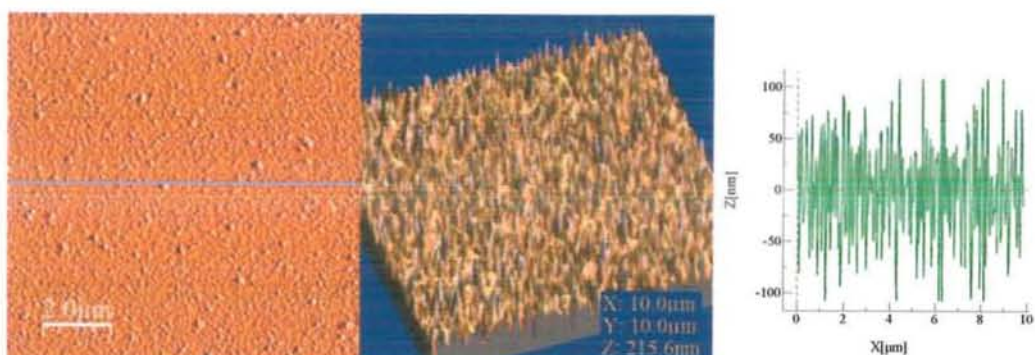
Figure 3.38B: Surface morphology of virgin (PAH/Au-NPs)$_5$/(PEI$_{dia}$/CNER)$_{10}$ film.

The rms roughness value of 32 nm for the (PAH/Au-NPs)$_5$/(PEI$_{dia}$/CNER)$_{10}$ protected Au colloid film confirms their homogeneous morphology in two different scan sizes of 5 and 10 μm (Figure 3.38 A, B).

Tapping mode surface morphology study of the PNER protected film (PAH/Au-NPs)$_5$/(PEI$_{dia}$/PNER)$_{10}$ shows surface roughness as compared to CNER protected Au colloid film with less rms roughness value less than 15 nm (Figure 3.39). Some large particles may be seen may be due to in-sufficient washing for this particular sample.

Figure 3.39: AFM images of virgin (PAH/Au-NPs)$_5$/(PEI/PNER)$_{10}$ film.

150

Both the CNER and PNER protected Au colloid films were then subjected to rubbing test. After 60 rubbing cycles, the thickness of the films was measured using ellipsometer. Before thickness measurement, the samples were washed with acetone solvent to remove any inhomogeneity caused by the threads of rubbing cloth or any scratched material what so ever. The 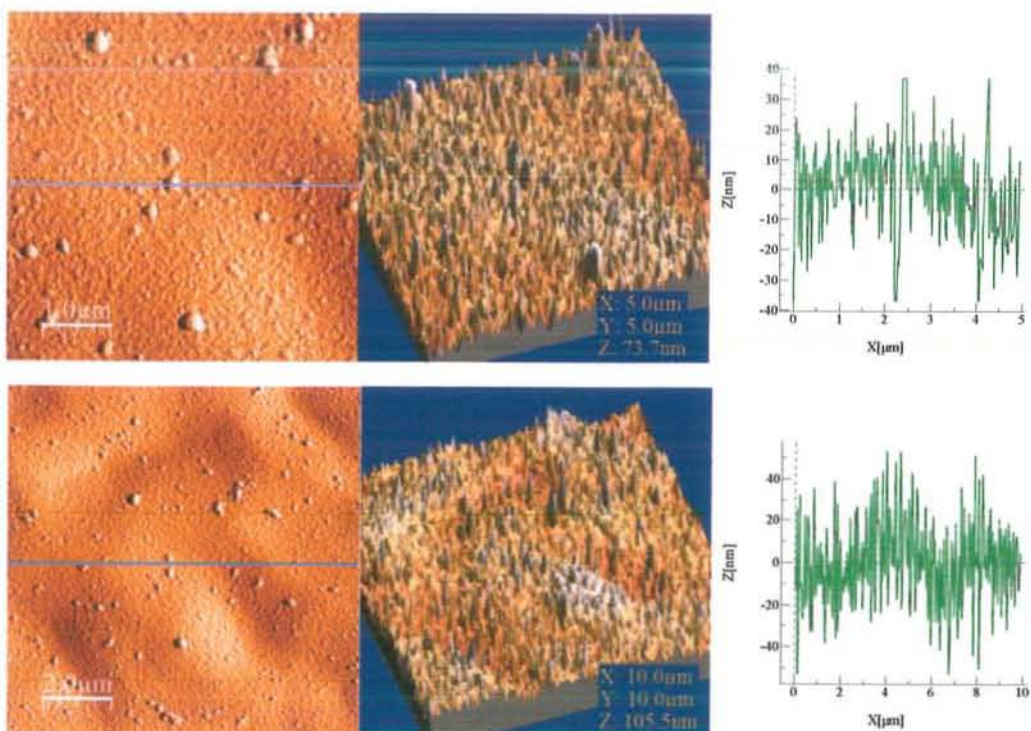ellipsometric data shows that there was very little change in the thickness of both the samples protected with the different epoxy compounds (Table 3.16). This loss in thickness may be due to the filling of the spherical Au colloid particles into the interstices among themselves by the compression caused by rolling rubbing cloth. There was less than 4% decrease in thickness of the epoxy protected gold colloid films after 60 rubbing cycles. Thus, the covalently bonded epoxy-amine network using the dialysed PEI_{dia} (Lupasol HF) has successfully protected the underlying weak Au colloid film using the alternate spray-dipping process.

Table 3.16: Loss in CNER and PNER protected Au colloid film thickness after 60 rubbing cycles.

Film Architecture	Thickness before rubbing (nm)	Thickness after 60 rubbing (nm)	Thickness of epoxy layer over Au colloid	Percent loss after 60 rubbings
$PEI(Au/PAH)_5Au(PEI_{dia}/CNER)_{10}$	69.1	65.6	20.0	3.6
$PEI(Au/PAH)_5Au(PEI_{dia}/PNER)_{10}$	59.8	58.4	7.2	2.3

As the rubbing analysis is a macroscopic property of such protected films, therefore, AFM analysis was carried out at 5 and 10 μm magnifications. After 60 consecutive rubbing cycles, the AFM tapping image showed that all of the film was intact and ellipsometry data also confirmed that there was no dramatic change in the overall film thickness. However, some compressions appeared in the direction of the rubbing cloth movement. Especially one big groove was observed with a depth of 20 nm which may be due to the inhomogeneous compression at that particular part of the film (Figure 3.40). Low rms roughness (15.6 to 25.5 nm) value also confirmed the absence of cracks in the film evident also from the AFM image (Figure 3.40).
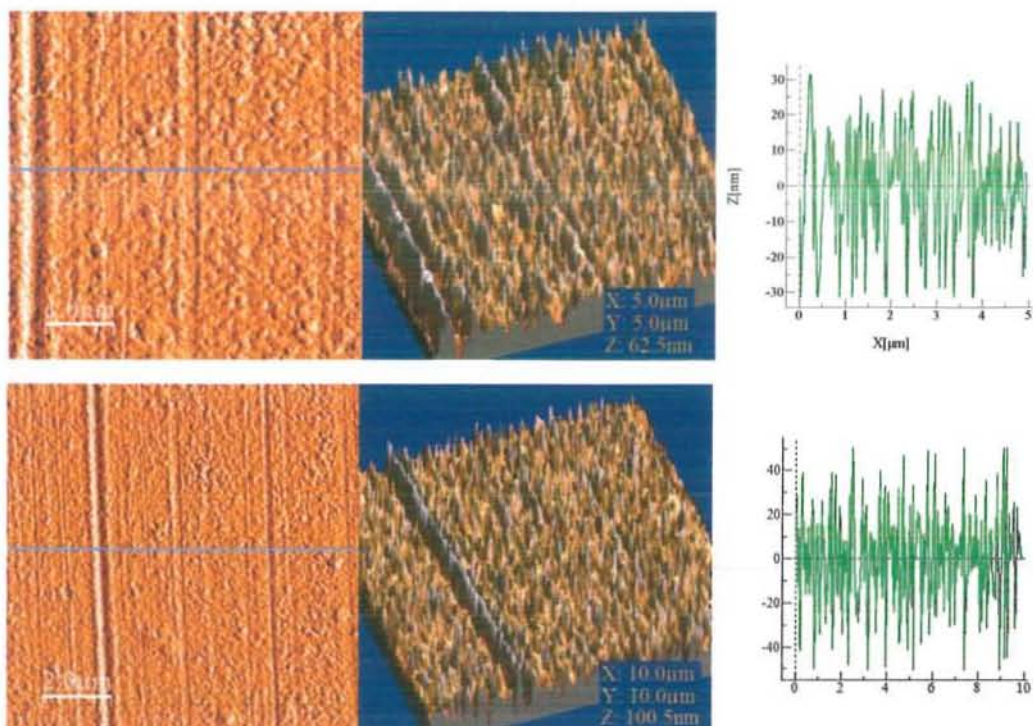
Figure 3.40: Surface morphology and rms surface analysis of (PAH/Au-NPs)$_5$/ (PEI/ CNER)$_{10}$ film after 60 rubbing cycles.

The AFM image of the (PAH/Au-NPs)$_5$/(PEI$_{dia}$/PNER)$_{10}$ showed more apparent inhomogeneity as compared to (PAH/Au-NPs)$_5$/(PEI$_{dia}$/CNER)$_{10}$ (Figure 3.41). But there was no overall significant decrease in thickness of this film as confirmed by the ellipsometric data (only 2.3% loss in thickness after 60 rubbing cycles). The depth of these grooves was 10 nm, so this inhomogeneity may be due to the compression of rubbing cloth on one side of the film. The force exerted by the roller of rubbing machine have compressed the spherical Au-NPs in the interstices present among the Au-NPs as shown also by the photographic image in the Figure 3.43. The overall morphology of the rubbed sample shows rms surface roughness value of 10 nm. This means that the PNER epoxy has successfully protected the weak Au-NPs present underneath. It is worth mentioning that PNER epoxy layer on the Au-NPs film was only 7.2 nm thick which is almost three times less as compared to CNER epoxy coating (20 nm) over the same Au-NPs film.
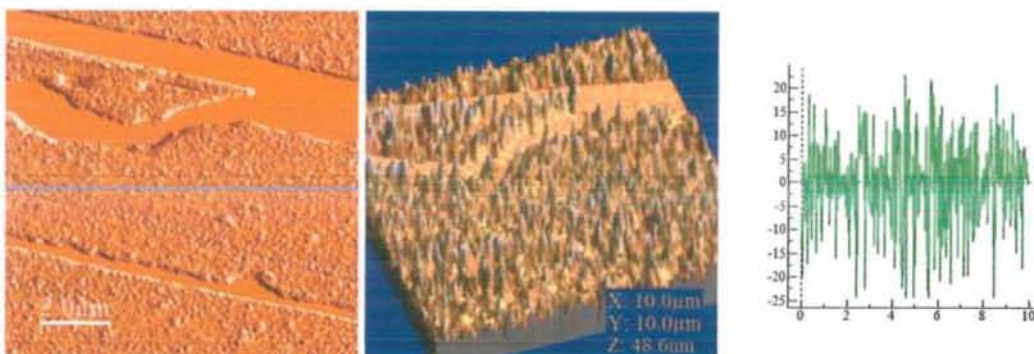
Figure 3.41: Surface morphology and rms surface analysis of (PAH/Au-NPs)$_5$/ (PEI/PNER)$_{10}$ film after 60 rubbing cycles.

A very homogeneous photographic image of the virgin (PAH/Au-NPs)$_5$ with no rubbing (R) and after only one rub (L) is shown in Figure 3.42. It is important to note that after only one rub, whole of the (PAH/Au-NPs)$_5$ film has been wiped off leaving the grey silicon wafer. The same film was protected with the PNER having film architecture (PAH/Au-NPs)$_5$/(PEI$_{dia}$/PNER)$_{10}$ and stored for time cure process at ambient temperature. The time cured film on the silicon wafer was cut to two parts. One portion of the film was subjected to 60 continuous rubbing cycles (R) while other part was stored as such un-rubbed (L) for reference to study change in surface morphology. The photographic image clearly shows quite homogeneous surface of un-rubbed film (L) while the there are many vertical grooves seen on the rubbed film (R) (Figure 3.43).

Figure 3.42: Photograph of virgin (PAH/Au-NPs)$_5$ (L) 1 rub film (R) No rub film

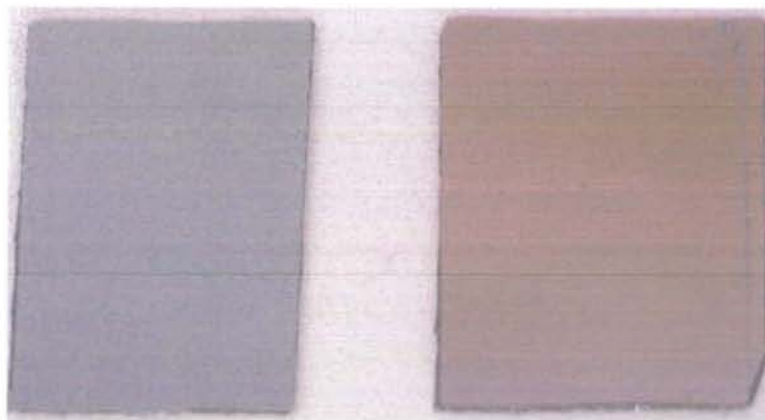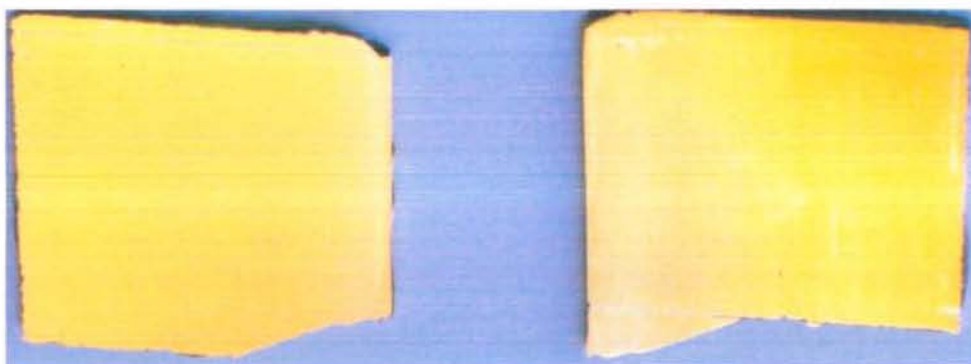**Figure 3.43:** Photographic image of un-rubbed (L) and 60 rubbing (PAH/Au-NPs)$_5$/(PEI/PNER)$_{10}$ films (R).

Therefore, CNER and PNER epoxy systems proved to be excellent in protecting gold colloid films from the hostile environment of the rubbing machine. The minimum layer needed to protect the underlying weak Au-NPs was 20 nm for the CNER while 7 nm for the PNER epoxy while using (dialysed Lupasol HF) PEI$_{dia}$ as curing agent.

3.9 Effect of Thermal and Time Curing

In the classical method of curing, epoxy-amine film was subjected to elevated temperature for a specified time period. The film may be treated with still higher temperature to bring about post curing where all the remaining functional groups react to give a mechanically strong film. The epoxy-amine films prepared *via* LbL process were also subjected to elevated temperature curing process (100°C for 1 hr). The cured films were then tested for their mechanical strength with the help of rubbing machine. As expected the thermally cured epoxy-amine LbL films show extreme robustness and resist in any loss of material after 20 rubbing cycles. In the time cure process, samples were stored in well capped polystyrene bottles for a specific time which may range from 72 hrs to several days. While the time cured samples especially those prepared with Aldrich PEI shows varying degree of loss in thickness after the same number of rubbing cycles.

One of the objectives of this research work was to devise a mechanism for the development of ultra-thin protective films onto otherwise weak electrostatic and nanoparticle LbL films. Secondly the products so prepared must not involve any heat

treatment during their processing as heating may destroy the delicate nanoparticles and electrostatically assembled multilayers present underneath. To achieve these objectives two modifications were suggested.

First highly purified polymers with narrow molecular weight distribution were selected. This was achieved with dialysis of Lupasol-HF obtained from BASF. Dialysis was carried out using dialysis Pro-membrane with molecular weight cut at 3500. As mentioned earlier the epoxy-amine LbL films prepared with PEI_{dia} show a greater improvement in the mechanical strength as compared to the films prepared with un-dialysed PEI obtained from Aldrich.

Secondly the prepared epoxy-amine films using PEI_{dia} were kept in the laboratory shelves for a specified time period for curing. During curing process, the reactive functional groups of both epoxy and amine react to form chemical linkages which enhance the robustness of the multilayers. Maximum functional groups of epoxy and amine react during prolong time cure and thermal curing process to yield toughened coatings. The motive behind the time curing process was to complete the curing of epoxy and amine functional groups during the shelf life of the synthesized product before its delivery to the end user. Here two time periods were selected for the curing of epoxy-amine and epoxy-amine protected gold colloid films i.e. three days and seven days time curing.

For this purpose the samples were prepared by spraying the 40 mg mL^{-1} aqueous solution of PEI_{dia} (10 s) onto the substrate followed by dipping the substrate in 100 mg mL^{-1} epoxy solution (10 min) prepared in acetone.

The results shown in Figure 3.44 for the two systems $(PEI_{dia}/CNER)_{10}$ abbreviated as C(d)P(s) and $(PEI_{dia}/PNER)_{10}$ abbreviated as P(d)P(s) showed that samples cured for 3 days at ambient temperature lost a bit of thickness after 20 and 40 rubbings cycles as shown by red and green bars respectively (Figure 3.44). While part of the same two samples which were subjected to 7 days time curing has not lost any thickness after 20 rubbing cycles (blue and black bars in Figure 3.44). So 7 days time cured samples are robust enough to withstand the harsh environment of the rubbing test.
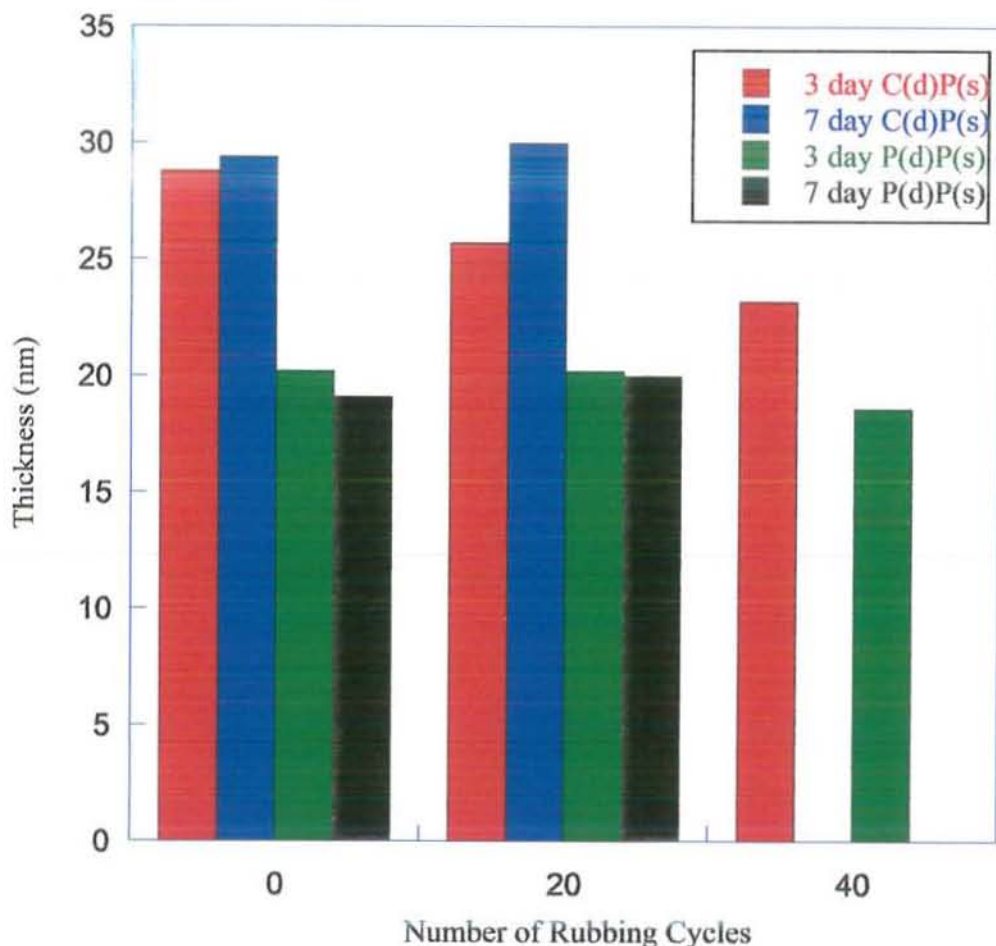
Figure 3.44: Effect of time curing on the mechanical strength of epoxy-amine films.

As the time for the curing of the epoxy-amine LbL film was optimised as 7 days, the next step was to use this for the protection of Au-NPs film. For this purpose the above mentioned epoxy-amine films were constructed onto the $(PAH/Au-NPs)_5$ films. The samples prepared were stored in the laboratory for time curing process at ambient temperature. These samples were then subjected to rubbing test. Rubbing data for 7 days time cured $(PAH/Au-NPs)_5/(PEI_{dia}/CNER)_{10}$ sample show a loss of less than 5% in overall film thickness while $(PAH/Au-NPs)_5/(PEI_{dia}/PNER)_{10}$ lose only about 3% thickness after three days time curing when subjected to 60 rubbing cycles (Figure 3.45).

So there was great improvement in the mechanical robustness of the epoxy-amine LbL films prepared with PEI_{dia} subjected to time cure process at room temperature. This

seems to be promising process for the protection of underlying heat sensitive polymeric and nanoparticles films.
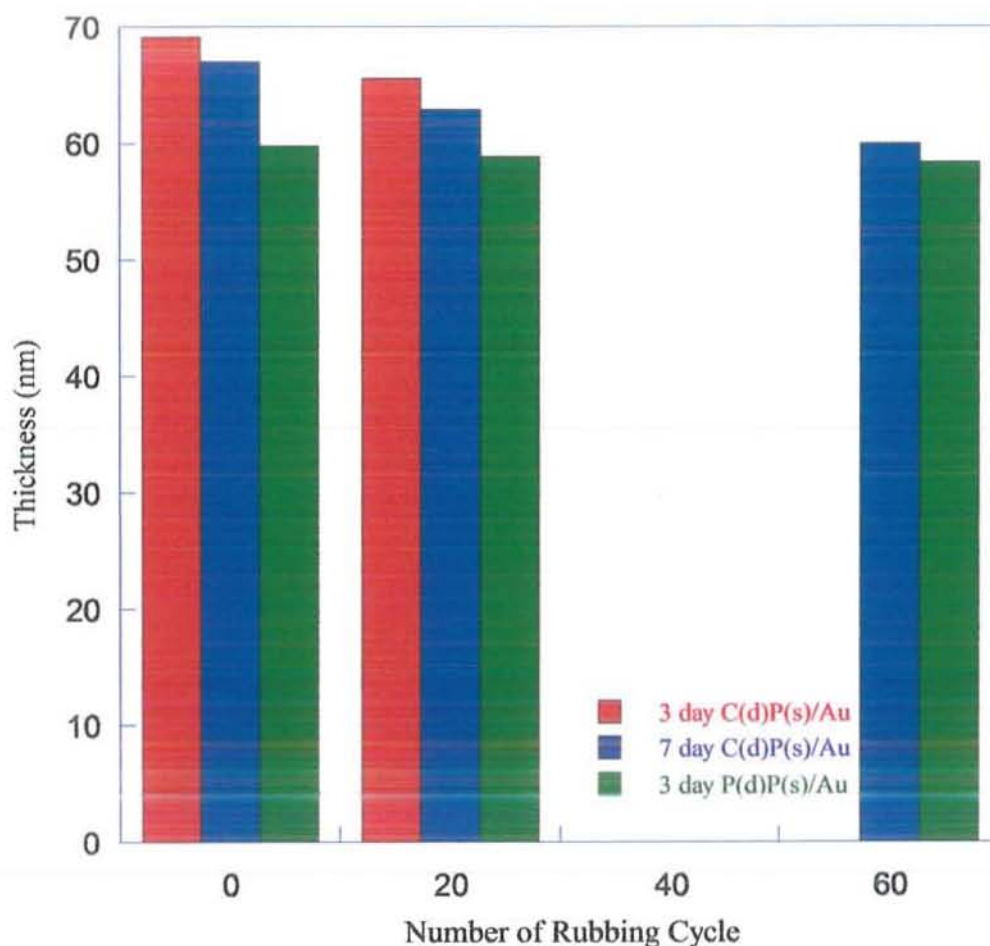
Figure 3.45: Effect of time curing on the mechanical strength of epoxy-amine protected Au-NPs films.

3.10 Study of TEPA as Curing Agent

For the construction of PEI_{dia} $(CNER/TEPA)_n/CNER$ and PEI_{dia} $(PNER/TEPA)_n/PNER$ covalent multilayers, the pre-activated substrate (silicon wafer or quartz slide) was dipped in aqueous solution of PEI_{dia} for a specific time (t_1) followed by subsequent 2 min washing in Milli-Q water in three equal wash baths (t_2). During each washing sequence, substrate was given slight manual agitation to ensure the removal of un-adsorbed polymers. The substrate was dried with a stream of nitrogen or compressed air. The substrate with precursor PEI_{dia} layer was then put in epoxy solution in acetone

157

for the same time (t_3) as it was dipped previously in PEI_{dia} solution so that $t_1 = t_3 = 10$, 25, 50 min. The substrate was then washed with pure acetone for 2 min in three equal wash (t_4). The substrate was then put in aqueous solution of TEPA for the same time (t_1) as it was dipped previously in PEI_{dia} solution and after wash and drying process; it was put in epoxy solution. This means for a single layer pair, the total processing time was $T = t_1 + t_2 + t_3 + t_4$.

During the formation of multilayers using TEPA as curing agent, accelerators/catalysts were also used in the amounts as reported in literature. These include piperazine (P), A-399 (A), epoxy embedding medium accelerator (E) and a combination of Piperazine, Epoxy embedding medium accelerator and triethanolamine (C) taken in aqueous polyamine solution.

TEPA is a straight chain polyamine with a combination of primary and secondary amine hydrogen atoms to cure oxirane ring of epoxy resins. Based on the molecular dimensions of the epoxy and TEPA compounds, it was expected that the layer pair increment for these (TEPA/ER) multilayer might be less than (PEI_{dia}/ER) layer pair thickness. The ellipsometric data for the formation of catalysed and un-catalysed PEI_{dia} (CNER/TEPA)$_n$/CNER multilayers termed generally as CTD shows a linear increase in thickness as a function of number of layer pairs for the three adsorption times used 20, 50, 100 min per layer pair. It has also been observed that the epoxy embedding medium accelerator (E) gives larger growth increment as compared to other catalysed and un-catalysed systems as shown in the Figure 3.46. The data correlation coefficient is quite high with very low error in measurement.

The prepared samples were subjected to rubbing machine test to evaluate their mechanical strength. For this purpose, the samples were cut to two pieces. One piece was subjected to curing at $100°C$ for 1 hr in an oven while the other one was placed in the caped polystyrene bottle for time curing for 72 hrs (Table 3.17). Cured and un-cured low deposition time samples (20 min per layer pair) showed negligible mechanical strength. The un-catalysed samples show no mechanical strength while longer dipping time samples (100 min per layer pair) using combined catalyst system show appreciable mechanical robustness (Table 3.17).

PEI = TEPA = CNER = PNER = 40mg/mL
Adsorption Time = 20 min/ Layer Pair
A = P = E = 10 mg/mL, triethanolamine = 24 mg/mL
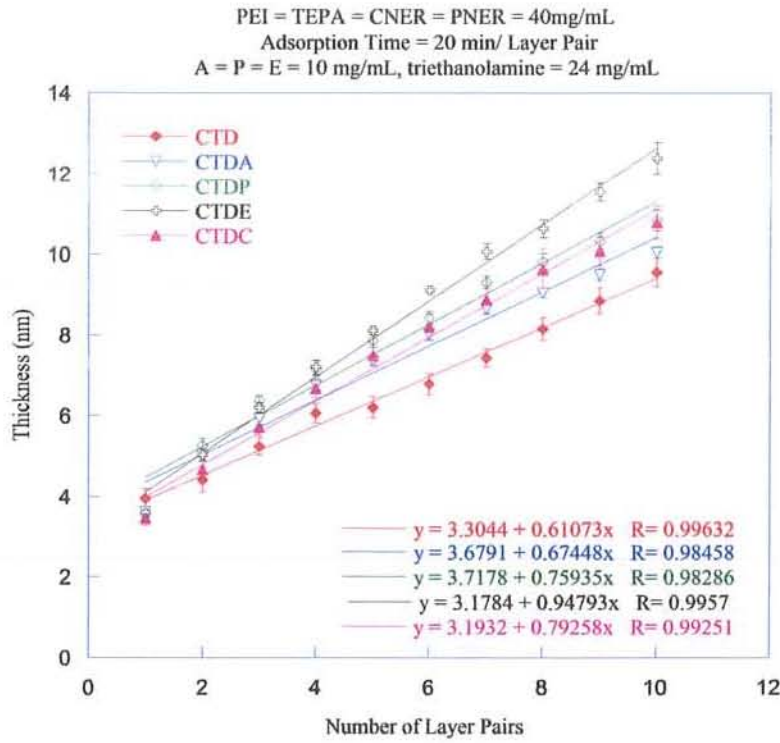
Figure 3.46A: LbL build up for 20 min/Layer Pair for $PEI_{dia}/(CNER/TEPA)_9/CNER$

PEI = TEPA = CNER = PNER = 40mg/mL
Adsorption Time = 50min Layer Pair
A = P= E = 10 mg/mL, triethanolamine = 24 mg/mL
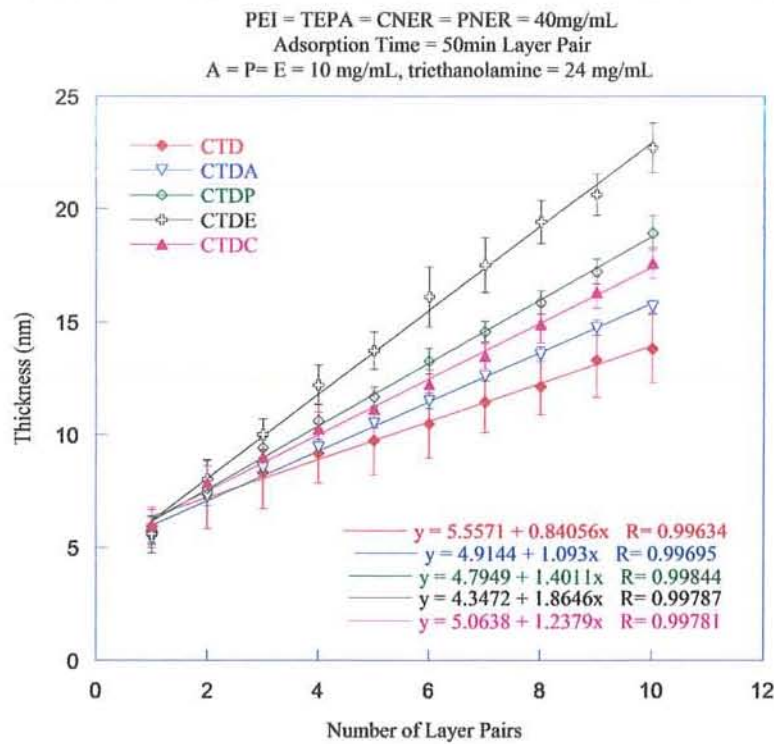
Figure 3.46B: LbL build up for 50 min/Layer Pair for $PEI_{dia}/(CNER/TEPA)_9/CNER$

PEI = TEPA = CNER = PNER = 40mg/mL
Adsorption Time = 100 min/Layer Pair
A = P = C = 10mg/mL.,triethanolamine = 24 mg/mL

$y = 3.2967 + 1.228x$ R= 0.99969
$y = 3.4221 + 1.2691x$ R= 0.99919
$y = 2.8221 + 1.4123x$ R= 0.99958
$y = 2.4456 + 2.1407x$ R= 0.99949
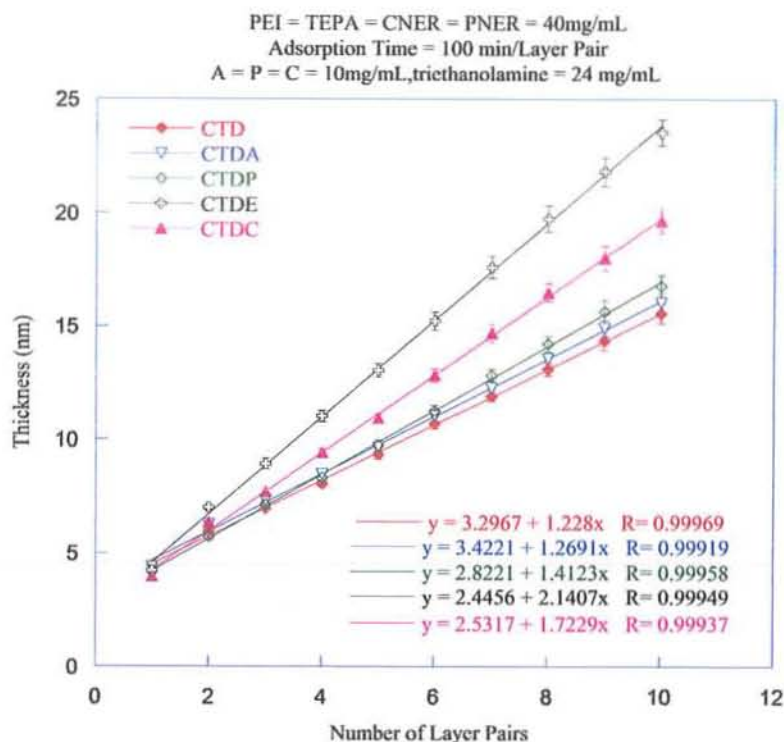$y = 2.5317 + 1.7229x$ R= 0.99937

Figure 3.46C: LbL build up for 100 min/Layer Pair for $PEI_{dia}/(CNER/TEPA)_9/CNER$.

Table 3.17: Thickness before rubbing and percent loss in thickness of cured $PEI_{dia}/(CNER/TEPA)_9/CNER$ system after 20 rubbings.

System	Thickness and percent loss of thermal and time cured samples (20 rubbing cycles)								
	% loss 20 min/LP			% loss 50 min/LP			% loss 100 min/LP		
	Thick-ness (nm)	Temp. Cured (%)	Time cured (%)	Thick-ness (nm)	Temp. Cured (%)	Time Cured (%)	Thick-ness (nm)	Temp. Cured (%)	Time Cured (%)
CTD	9.5	97.0	98.0	13.8	95.0	88.0	15.6	98.0	98.0
CTDA	10.0	97.0	96.0	15.7	88.0	88.0	16.0	98.0	98.0
CTDP	10.8	98.0	98.0	22.7	23.0	37.0	23.5	62.0	77.0
CTDE	12.4	94.0	95.0	18.9	66.0	27.0	16.8	99.0	87.0
CTDC	10.8	63.0	98.0	17.6	21.0	35.0	19.6	16.0	17.0

The ellipsometric data for the formation of catalysed and un-catalysed PEI_{dia} $(PNER/TEPA)_n/PNER$ multilayers termed generally as PTD shows a linear increase in thickness as a function of number of layer pairs for the three adsorption times used 20, 50, 100 min per layer pair. As the adsorption time increases, the thickness per layer pair also increases. It was also been observed that piperazine (P) and combined catalyst system (C) gave more growth increment as compared to other catalysed and un-catalysed systems as shown in the Figure 3.47 (A, B, C). The data correlation coefficient was quite high with very low error in data values.

However, the thickness increment per layer pair obtained with TEPA was much less as compared to same number of layer pairs formed by PEI cured samples. Another important observation from the Figure 3.47 (A, B, C) was the larger thickness (2 to 3 nm) obtained for the first layer pair (PEI/ER) deposited as precursor layer.
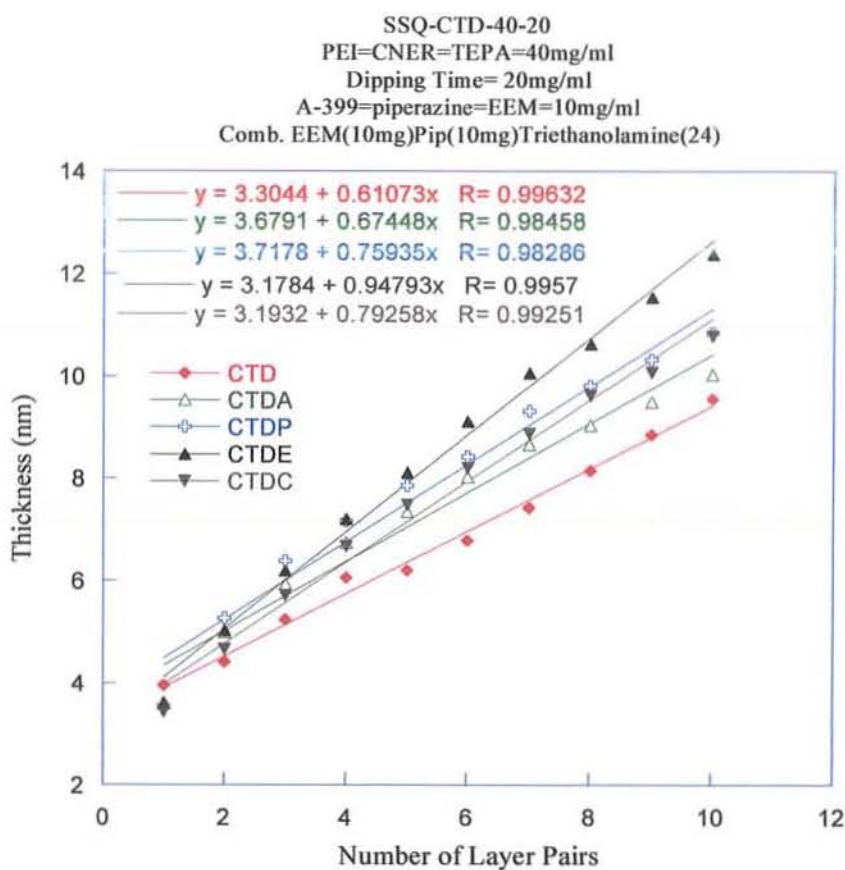

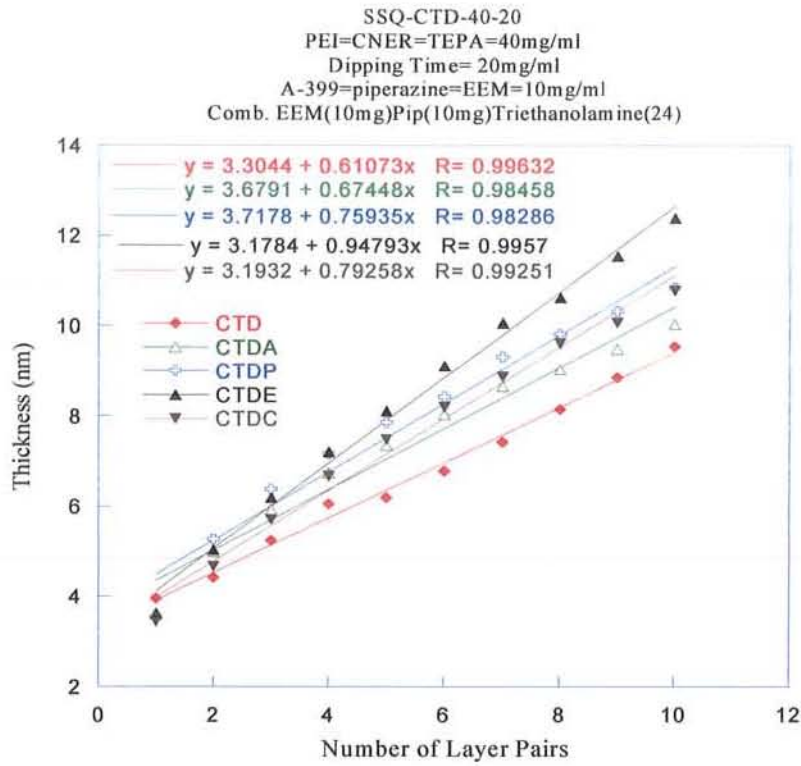**Figure 3.47A:** LbL build up for 20 min/Layer Pair for $PEI_{dia}/(PNER/TEPA)_9/PNER$

SSQ-CTD-40-20
PEI=CNER=TEPA=40mg/ml
Dipping Time= 20mg/ml
A-399=piperazine=EEM=10mg/ml
Comb. EEM(10mg)Pip(10mg)Triethanolamine(24)

$y = 3.3044 + 0.61073x$ R= 0.99632
$y = 3.6791 + 0.67448x$ R= 0.98458
$y = 3.7178 + 0.75935x$ R= 0.98286
$y = 3.1784 + 0.94793x$ R= 0.9957
$y = 3.1932 + 0.79258x$ R= 0.99251

CTD
CTDA
CTDP
CTDE
CTDC

Figure 3.47B: LbL build up for 50 min/Layer Pair for $PEI_{dia}/(PNER/TEPA)_9/PNER$

SSQ-CTD-40-20
PEI=CNER=TEPA=40mg/ml
Dipping Time= 20mg/ml
A-399=piperazine=EEM=10mg/ml
Comb. EEM(10mg)Pip(10mg)Triethanolamine(24)

$y = 3.3044 + 0.61073x$ R= 0.99632
$y = 3.6791 + 0.67448x$ R= 0.98458
$y = 3.7178 + 0.75935x$ R= 0.98286
$y = 3.1784 + 0.94793x$ R= 0.9957
$y = 3.1932 + 0.79258x$ R= 0.99251
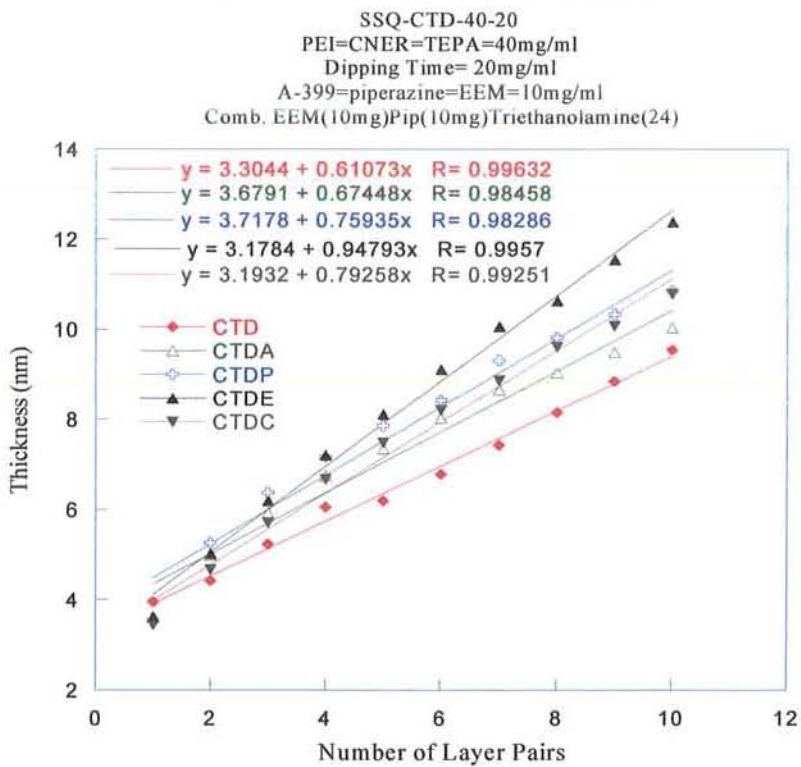
CTD
CTDA
CTDP
CTDE
CTDC

Figure 3.47C: LbL build up for 100 min/Layer Pair for $PEI_{dia}/(PNER/TEPA)_9/PNER$

162

The rubbing data shows much interesting results that the time cured systems show more robustness as compared to thermally cured for larger dipping times (Table 3.18). Low deposition time samples show no mechanical strength. Piperazine and combined catalyst samples show more mechanical resistance when subjected to rubbing machine test. Another important observation was that the longer dipping time samples i.e. 100 min per layer pair shows more strength in both the cured and uncured samples. This means that the catalysts do not show a drastic increase in mechanical robustness as a function of increased deposition speed. Data correlation coefficient was quite high with low error value of bars.

Table 3.18: Thickness before rubbing and percent loss in thickness of cured $PEI_{dia}/(PNER/TEPA)_9/PNER$ system after 20 rubbings.

System	Thickness and percent loss of thermal and time cured samples (20 rubbing cycles)								
	% loss 20 min/LP			% loss 50 min/LP			% loss 100 min/LP		
	Thick-ness (nm)	Temp. Cured (%)	Time cured (%)	Thick-ness (nm)	Temp. Cured (%)	Time Cured (%)	Thick-ness (nm)	Temp. Cured (%)	Time Cured (%)
PTD	8.9	62.0	93.0	12.6	91.0	8.0	12.9	53.0	31.0
PTDA	8.2	93.0	93.0	13.0	86.0	7.0	13.2	31.0	56.0
PTDP	9.3	98.0	89.0	19.6	18.0	12.0	21.2	14.0	3.0
PTDE	10.7	36.0	91.0	11.6	46.0	43.0	15.1	7.0	18.0
PTD	8.9	62.0	93.0	12.6	91.0	8.0	12.9	53.0	31.0

The UV-Visible analysis of $PEI_{dia}/(CNER/TEPA)_9/CNER$ and $PEI_{dia}/(PNER/TEPA)_9/PNER$ was also carried out using higher concentrations of epoxy and amine components. Polyamine and epoxy concentrations were taken as 100 mg mL^{-1} as lower concentrations of the polymer do not give a peak above threshold due to low molecular weight particularly of TEPA. As the chromophore groups for the two epoxy resins were same, therefore, both systems show a linear increase in absorbance as a function of number of layer pairs at the same absorbance maximum respectively (Figure 3.48 A, B).
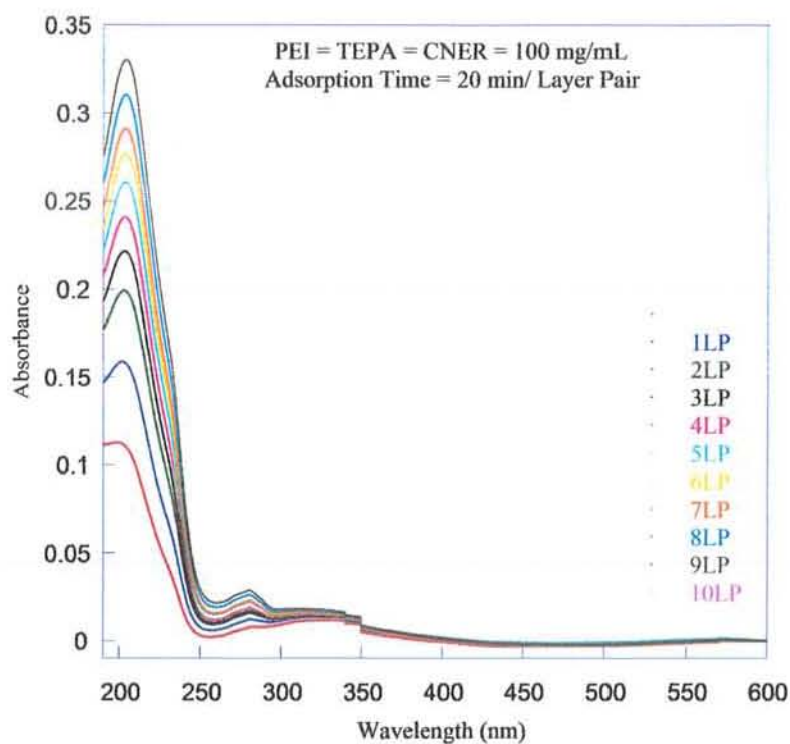
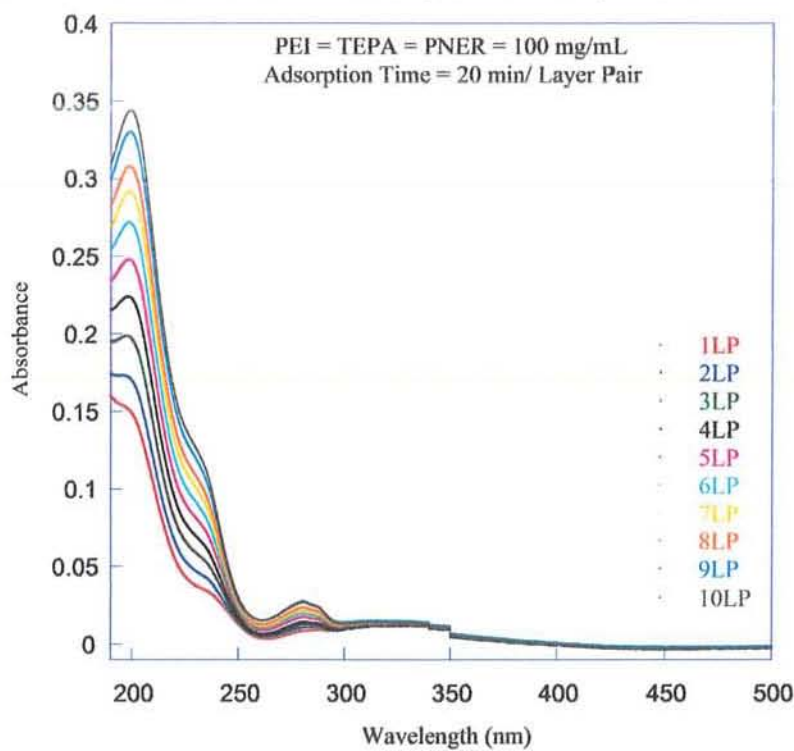**Figure 3.48A:** UV-Visible data of $PEI_{dia}/(CNER/TEPA)_9/CNER$ film build-up.

Figure 3.48B: UV-Visible data of $PEI_{dia}/(PNER/TEPA)_9/PNER$ film build-up.

164

The linear growth of the PEI$_{dia}$/(CNER/TEPA)$_9$/CNER and PEI$_{dia}$/(PNER/TEPA)$_9$/PNER films was also confirmed by absorbance maximum of the respective systems as a function of number of layer pairs at wavelength maximum of 280 nm. A linear increase in absorbance maximum was observed as depicted in Figure 3.49. For PEI$_{dia}$/(PNER/TEPA)$_9$/PNER system few points are missing due to the fact that their absorption was below threshold limits of the instrument.
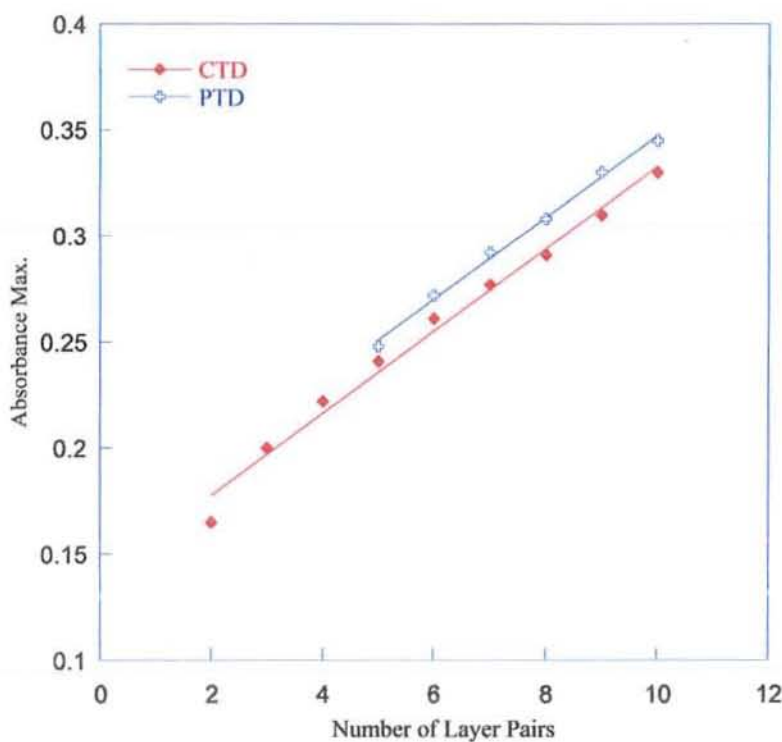

Figure 3.49: Absorbance maximum vs number of layer pairs for PEI$_{dia}$/(CNER/TEPA)$_9$/CNER and PEI$_{dia}$/(PNER/TEPA)$_9$/PNER.

As UV-Visible data for both the systems PEI$_{dia}$/(CNER/TEPA)$_9$/CNER and PEI$_{dia}$/(PNER/TEPA)$_9$/PNER shows linear behaviour, therefore, it also complements the linear growth shown by the ellipsometric data for the same systems.

In a nutshell, successful covalent LbL methodology for the construction of epoxy-amine network has been developed and successfully applied to protect the underlying Au-NPs film. The conditions for the build-up of LbL assemblies were primarily optimised using different epoxy resins and curing agents. The curing reaction between epoxy and polyamine resulted in linear growth as a function of number of layer pairs chemisorbed as shown in the following figures for $(PEI/CNER)_{10}$ and $(PEI/PNER)_{10}$ for various concentrations;
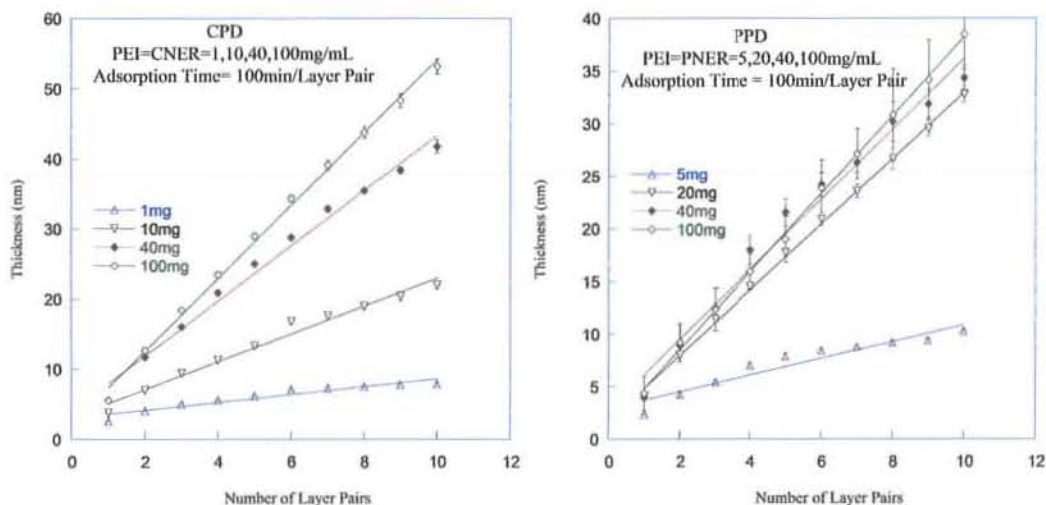
Thickness as a function of number of layer pairs, $(PEI/CNER)_{10}$ (L) and $(PEI/PNER)_{10}$ (R).

UV-Visible spectroscopy measurement confirmed that absorption of chromophore groups increases linearly with increase in number of layer pairs.
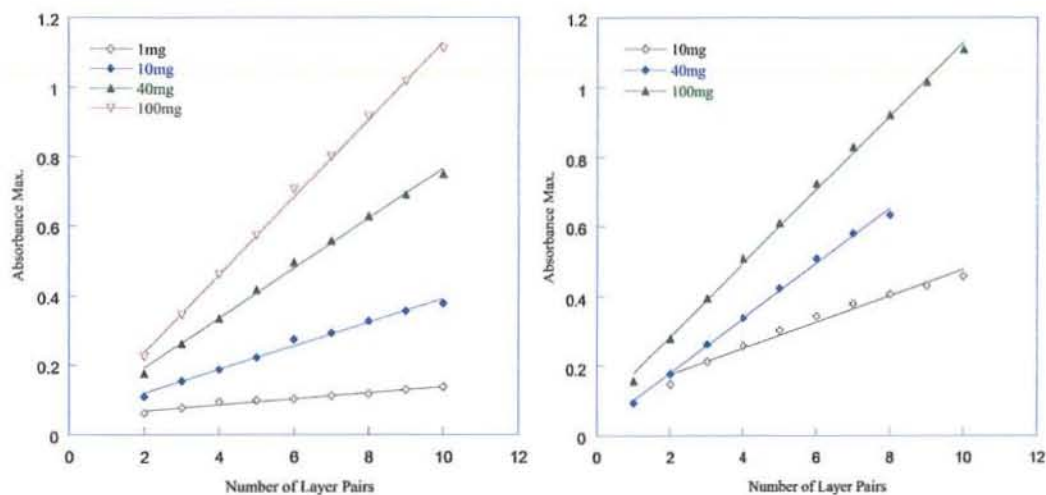

Absorbance max. vs number of layer pairs, $(PEI/CNER)_{10}$ (L) and $(PEI/PNER)_{10}$ (L).

166

Absorbance maximum increased linearly as a function of number of layer pairs, thus complementing the ellipsometric data as shown in above the Figure.

The optimised polymer concentration of 40 mg mL^{-1} and adsorption time 100 min per layer pair was then applied onto the Au-NPs film to successfully protect it after time curing at ambient temperature. The surface morphology of the rubbed and un-rubbed epoxy-amine protected Au-NPs film showed homogeneity with low rms surface roughness value. Although, there appear some grooves due to the compression of rubbing cloth, the ellipsometric data showed that almost 6.3% of the overall film thickness was lost after 60 rubbing cycles. So, the covalent LbL dipping technique using epoxy-amine had successfully protected the Au-NPs films to endure the aggressive environment of the rubbing machine.

Percent loss of overall thickness as a function of number of rubbing cycles.

Film Architecture	Thickness (nm)		Percentage
	Before Rubbing	**After 60 Rubbings**	**Loss after 60 Rubbings**
(PEI/CNER)$_{10}$	31.65	31.59	1.8
(PAH/Au)$_5$/(PEI/CNER)$_6$	55.48	52.34	6.3
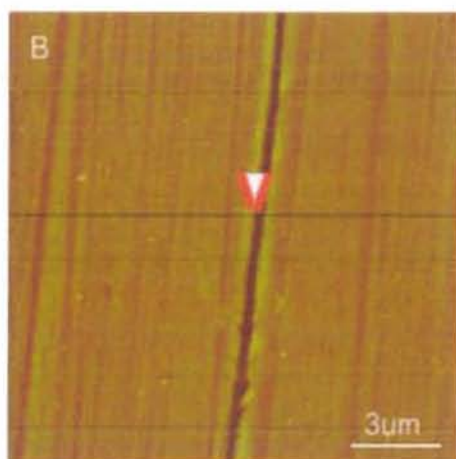
AFM image of CNER epoxy protected Au-NPs sample prepared by dipping deposition after 60 consecutive rubbing cycles.

In the next step, the method was modified by using dialysed PEI and spray brush system for the adsorption of PEI_{dia}. Therefore, PEI_{dia} (40 mg mL^{-1}) was sprayed onto the substrate for 10 s followed by dipping adsorption of epoxy resin (100 mg mL^{-1}) for 10 min to get a layer pair in 10 min and 10 s. There was a tremendous decrease in the adsorption time for the covalently assembled multilayers with linear increase in thickness without compromising on mechanical robustness of the samples cured at ambient temperature.
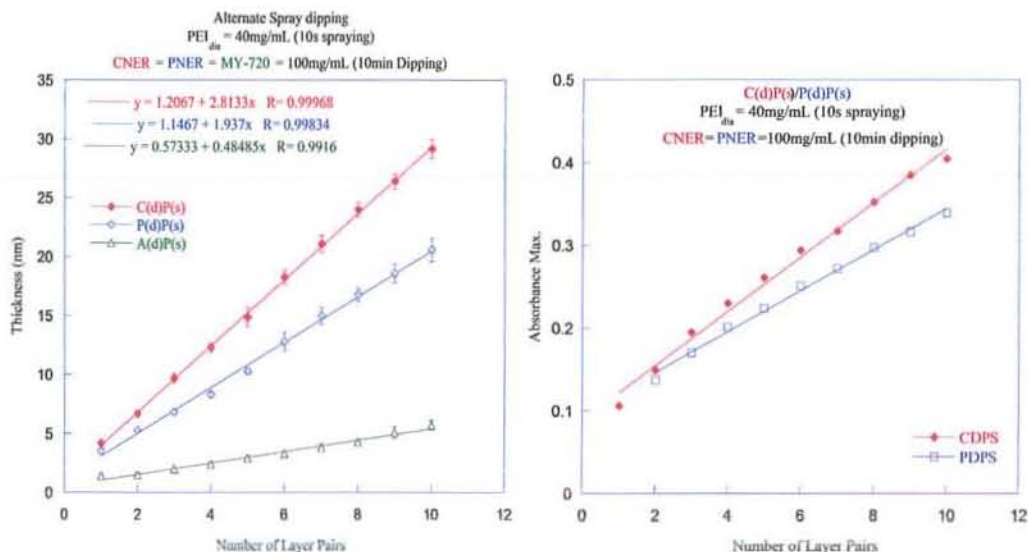
Ellipsometric (L) and UV-Visible data (A_{max} vs number of layer pairs) (R).

The covalently bonded LbL samples prepared with epoxy resins and PEI_{dia} showed that after 20 rubbing cycles, there was no loss of thickness. After 60 rubbing cycles, the films showed a loss of approximately 7% as shown below;

Loss in thickness of epoxy-amine films after 20 and 60 rubbing cycles.

| System	Thickness before rubbing (nm)	Thickness after 20 Rubbings (nm)	Thickness after 60 Rubbings (nm)	Loss of after 60 Rubbings (%)
$(PEI_{dia}/CNER)_{10}$	29.4	30.8	27.2	7.0
$(PEI_{dia}/PNER)_{10}$	20.2	20.2	18.8	7.0

The epoxy protected Au-NPs of the architecture PEI(Au/PAH)$_5$Au(PEI$_{dia}$/CNER)$_{10}$ and PEI(Au/PAH)$_5$Au(PEI$_{dia}$/PNER)$_{10}$ showed excellent mechanical robustness even after 60 rubbing cycles (Table below);

Loss in thickness of epoxy-amine protected Au-NPs film after 60 rubbing cycles.

Film Architecture	Thickness before rubbing (nm)	Thickness after 60 rubbing (nm)	Thickness of epoxy layer over Au colloid	Percent loss after 60 rubbings
PEI(Au/PAH)$_5$Au(PEI$_{dia}$/CNER)$_{10}$	69.1	65.6	20.0	3.6
PEI(Au/PAH)$_5$Au(PEI$_{dia}$/PNER)$_{10}$	59.8	58.4	7.2	2.3

The photographic and AFM images taken before and after 60 rubbing cycles, show quite homogeneous morphology, with the appearance of certain grooves. The ellipsometric data taken before and after rubbing cycles confirmed that generally there is quite low decrease in overall thickness of these films cured at ambient temperature for a specific time.
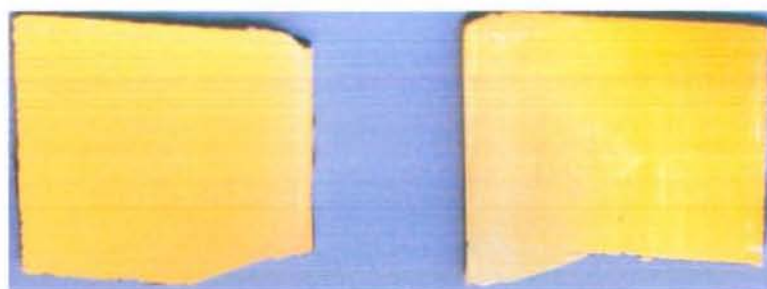
Photographic image of un-rubbed epoxy protected (L) and 60 rubbed sample (R).
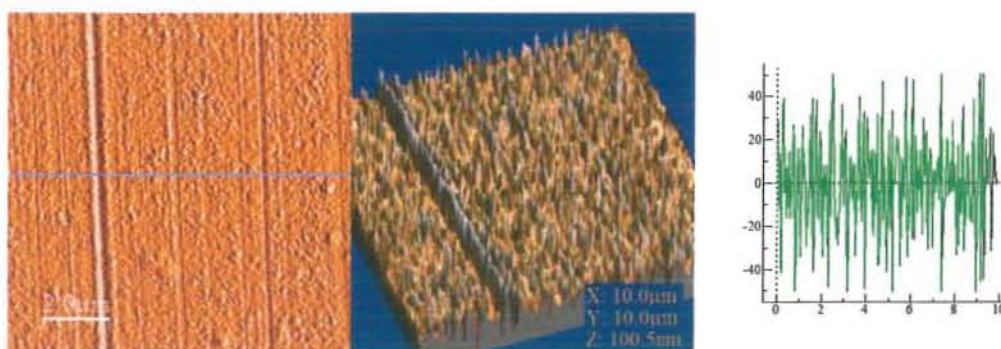
AFM images of (PAH/Au)$_5$/(PEI/CNER)$_{10}$ film after 60 rubbing cycles.
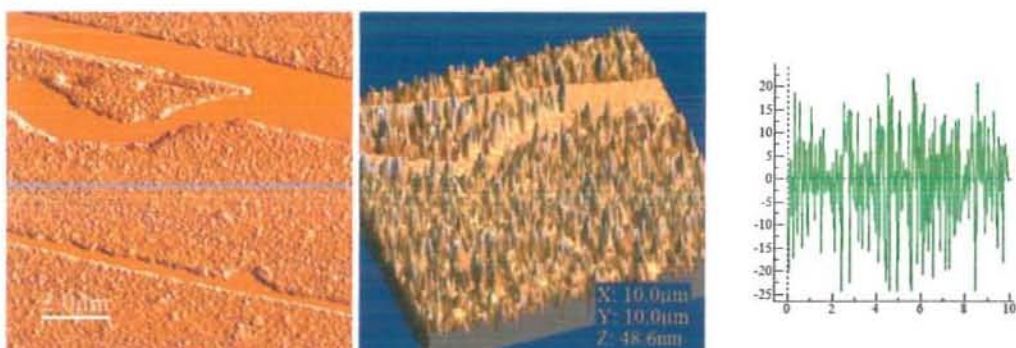
AFM images of (PAH/Au)₅/(PEI/PNER)₁₀ film after 60 rubbing cycles.

The time cured samples at room temperature demonstrated that longer the curing time, the better is the overall mechanical strength of the epoxy-amine protected Au-NPs film as illustrated below;
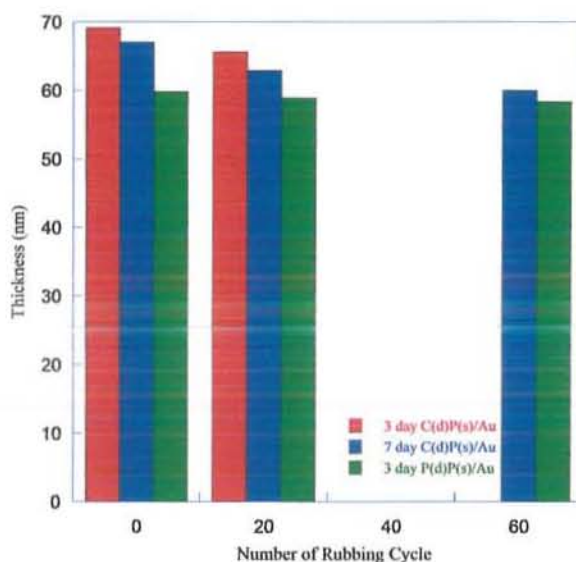
Effect of time cure on mechanical robustness of epoxy-amine protected Au-NPs film.

Thus, various epoxy resins cured by polyamine proved to be excellent in protecting otherwise weak polyelectrolyte and nanoparticles layers. Longer time curing at ambient temperature results in better mechanical strength.

3.11 References:

1- TDS of Araldite MY-720 by Huntsman

2- Schlenoff, J. B.; Dubas, S. T.; Farhat, T., *Langmuir,* **2000**, 16, 9968.

3 -Izquierdo, A.; Ono, S. S.; Voegel, J. C.; Schaaff, P.; Decher, G. *Langmuir,* **2005**, 21, 7558.

4- Ellipsométrie: Théorie, Bernoux, F.; Piel, J. P.; Castellon, B.; Lecat, J. H.; Boher, P.; Stehle, J. L., R6490, **2003**, Edit. Techniques de l'Ingénieur.

5- Kramers-Kronig Relations in Optical materials Research, Series: Springer Series in Optical Sciences, Vol. 110 Lucarini, V.; Saarinen, J. J.; Peiponen, K. E.; Vartiainen, E. M., **2005**, Edit. Springer.

6- Schmitt, J.; Decher, G.; Dressick, W. J.; Brandow, S. L.; Geer, R. E.; Shashidhar, R.; Calvert. J. M., *Adv. Mater.,* **1997**, 9, 61.

7- Thesis Zhiqiang Zheng, Institut Charles Sadron, Universite de Strasbourg, Strasbourg, France.

8- Porcel, C. H.; Izquierdo, A.; Ball, V.; Decher, G.; Voegel, J. C.; Schaaf. P., *Langmuir,* **2005**, 21, 800.

9- Zhong, C. J.; Mayer, M. M., *Adv. Mater.,* **2001**, 13, 1507.

10- Katz, E.; Willner, I., *Ang. Chem. Int. Ed.,* **2004**, 43, 6042.

11- Shipway, A. N.; Lahav, M.; Willner, I., *Adv. Mater.,* **2000**, 12, 993.

12- Thunemann, A. F.; Beyermann, J., *Macromolecules,* **2003**, 33, 6878.

13- Information supplied by manufacturer BASF, specialty chemicals, Ludwigshafen, Germany.

14 - Gill, R.; Mazhar, M.; Felix, O.; Decher, G., *Ang. Chem. Intl. Ed.,* **2010**, 35, 6116.

Conclusions

Conclusions

Epoxy-amine reactions are well reported in the adhesive formulations especially in two component epoxy systems to strongly bind two surfaces. The present study was focused on establishing covalent LbL reaction between various multifunctional epoxy resins and polyamines like PEI and TEPA at the nanoscale level under ambient conditions. These films proved to be quite robust in protecting the otherwise weak gold colloid films.

This was achieved by the optimisation of covalent LbL methodology for various epoxy resins and polyamines at room temperature. The multilayer films showed regular increase in thickness as a function of number of layer pairs for various concentrations of polymers as well as for different adsorption times studied. The linear growth of these films was monitored with the help of ellipsometry as well as UV-Visible spectrometry. For various concentrations of polymers and adsorption times, all the multilayer films showed high degree of reproducibility along with optical homogeneity. The multilayer films prepared with adsorption times of two hrs or longer showed optical inhomogeneity after a few layer pairs. Also with polymer concentration higher than 100 mg mL^{-1}, the multilayer film quality was deteriorated after a few layer pairs. Longer adsorption times and higher concentrations of polymer solutions did not yield good reproducible results and were difficult to carry out. Therefore, 40 mg mL^{-1} polymer concentration for the two polymers and 100 min per layer pair adsorption time was optimised for further studies and applications for the protection of Au-NPs film, in particular. Atomic force microscopy studies in the tapping mode also showed very homogeneous morphology of these films. AFM studies were also performed in the contact mode to study the inner morphology of these films. The cantilever force was successively increased up to 400 nN but could not pierce the outer most epoxy-amine layer showing the high strength of these films.

Thermally cured epoxy-amine multilayer samples showed high degree of mechanical robustness for many rubbing cycles at room temperature. The thermal curing reaction between various epoxy resins and amines was carried out by placing the multilayer samples in an oven for 1 hr at 100°C. But in order to avoid any detrimental effects of thermal curing to the samples, time-cured samples at room temperature were also prepared and studied for their mechanical robustness. The time-cured samples showed good robustness to the external deforming forces. The epoxy-amine network was then

172

applied to the weak gold colloid films. The epoxy protected Au-NPs films showed excellent robustness against the deforming forces created by rubbing machine. AFM analysis showed that the rubbed samples have certain deformations in these films which may be due to the inhomogeneity of the rubbing cotton velvet cloth.

In order to further speed up the curing process between epoxy and amines, PEI (Lupasol-HF, BASF) after appropriately dialysis was used instead of the one purchased from Aldrich. The dialysed PEI was then sprayed (10 s) onto the substrate by using the paint spray brush system (Paasche Millennium Wood), while dipping time in epoxy solution of higher concentrations was reduced to 10 min. In this way, we obtained an epoxy-amine layer pair in 10 min and 10 s, a considerable increase in processing speed of adsorption. The alternate spray-dipping technique gave highly reproducible results as confirmed by ellipsometry and UV-Visible spectroscopy. The time-cured samples of this fast adsorption process showed excellent mechanical robustness. The epoxy-amine network so produced was then applied onto the Au-NPs films. Mechanical robustness studies confirmed excellent protection of the Au-NPs film using time curing for 7 days. The epoxy protected Au-NPs film endured more than 60 rubbing cycles with less than 7% loss in overall thickness of the film. Therefore, BASF dialysed PEI proved to be an exceptional curing agent for epoxy to protect underlying weak NPs and a future protection candidate for further weak polymers. The atomic force microscopic analysis also confirmed homogeneous morphology of the virgin and protected films without rubbing, but showed the presence of certain compressions after rubbing the films for more than 60 consecutive rubbing cycles.

Effect of various accelerators/ catalysts on the curing behaviour of the epoxy-amine LbL films was also a part of the present study. The presence/absence of the accelerators/catalysts showed no marked difference in the film thickness per layer pair. Although ellipsometric results showed a decrease in film roughness, yet the mechanical robustness of the catalysed and un-catalysed samples was almost the same.

The covalent LbL films prepared using TEPA as amine component with all the three epoxies showed regular but less growth as compared to PEI cured films. Araldite MY-720 gave much little film growth for the same number of layer pairs as compared to CNER and PNER epoxy resins and film growth was also quite irregular. Thickness of 10

173

nm was obtained for the covalent LbL assemblies of $(PEI/MY-720)_{10}$. There was absolutely no loss in film thickness after several rubbing cycles for the elevated temperature cured samples while time cured samples had comparatively low mechanical strength.

The findings of the present study showed that the essential thickness of the protecting network required for the underlying weak layers such as Au-NPs was just around 10 nm and 6 nm for CNER epoxy and PNER epoxy, respectively. Moreover, the study has proved an economical preparation of more effective covalent LbL assemblies, both in terms of cost and time.

Future Plans

Future Plan

Protection of gold nanoparticles films using epoxy-amine LbL assembly has paved the way for future research in the area of protection films. This will enable the use of otherwise weak multilayers of polyelectrolytes and nanoparticles to withstand hostile environment in a number of fields including nanotechnology, bio-nanotechnology, and material science.

Since their discovery, Au-NPs are finding increased utility as hybrid organic-inorganic and bio-inoganic applications in various fields as diverse as opto-electronics, magnetic, catalytic and bio-medical. Particularly their extra-ordinary stability, complete bio-compatibilization, variety in modes of synthesis (like bio and template synthesis), and a number of benign properties paved the way for their future role in nanoscience, nanotechnology, bio-sensing, bio-nanotechnology and material science. Due to increased demand of Au-NPs in nanotechnology, there is ample space to incorporate such polymers as protective materials having bio-compatibility and inertness.

Many polyelectrolytes, polymers, drugs and other materials may be protected with bio-compatible polymers to use them in bio-medical applications. Another field of immense interest may be to devise ultra-thin devices based on such protective coating for a number of applications in material science and nanotechnology.